**Competitive IgG Adsorption on Protein A Chromatography Resins
and Improving Resin Performance with PEGylated Ligands**

Submitted in partial fulfillment of the requirements for

the degree of

Doctor of Philosophy

in

Chemical Engineering

Justin B. Weinberg

B.E., Chemical Engineering, The Cooper Union for the Advancement of Science and Art

Carnegie Mellon University

Pittsburgh, PA

December, 2017

Acknowledgements

This thesis and research would not have been possible without the help and support of many people along the way.

First and foremost, I would like to thank my advisor, Professor Todd Przybycien, for not only making this research possible but also for supporting my career in more ways than I ever could have asked for. Todd, thank you for connecting me into the bioprocessing community, for giving me to the opportunity to share my research in so many wonderful venues and locations, allowing me to freely explore my own ideas, always being there if I ever had a question, encouraging me to apply for the NSF GRFP, allowing me to incorporate outreach activities into my time as a Ph.D. student, and so much more. I am a better person in many ways because of your guidance and I can't thank you enough. I sincerely hope for and look forward to opportunities of working together in the future.

I would like to thank Professor Giorgio Carta of the University of Virginia for not only opening his laboratory to my research projects and serving on my committee, but for also taking such an active role in my Ph.D. work. Giorgio, your careful and consistent methodologies were a great inspiration to me as I learned the ropes of chromatography and gave me something to strive for in my own results. Working with you and your students was definitely the highlight of my Ph.D. and I have no doubt that this thesis would look the same without your involvement.

I would like to thank Shaojie Zhang for working closely with me during my time at the University of Virginia and for sharing his expertise in confocal microscopy to help us generate so many important results. I would also like to thank other members of the Carta lab including Arch Creasy, Jason Reck, Preston Fuks, Yiran Wang, Mimi Zhu, and Andreas Alberti for their advice

First, from Carnegie Mellon:

Anirudh Subramanyam, thank you for being such a close and loyal friend over the years. I am so glad we met and have been able to share so many memories and "classic times". Thank you for being there during the good times and bad; these years haven't been easy. I look forward to many more adventures with you, Saransh, Lisa, Javier, and Sundar in the future.

The lunch crew: Nikos Lappas, Chris Hanselman, and Anirudh. Thank you for the great times and adding some much needed consistency in my life. I don't know what I'm going to do without Tepper salads.

Qin Gu, thank you for being my groupmate and supporting me whenever you could. Sorry if I was a little intimidating in the beginning!

All the other great friends who I met during my time here: Javier Lanauze, Jake Boes, Nick Austin, Lisa D'Costa, Saransh Singh, Ross Cunningham, Annia Maisa, Ankit Gupta, Irem Sen, Burcu Karagoz, Brittany Nordmark, Yun-Ru Huang, Alex Bertuccio, Randy Gamble, Akang Wang, Natalie Isenberg, Devin Griffith, John Eason, Steve Iasella, Khalid Hajj, Amy Stetten, Brad Johnson, Ben Sauk, Dana McGuffin, Cristiana Lara, Zach Wilson, Ningxin Wang, Antonis Tasoglou, Sarah Nelson, Markus Drouven, Svena Drouven, and Pablo Garcia. Thank you for all the great adventures!

From New York and beyond:

Igor Belyayev, the best co-founder I could have asked for. Thank you for being my partner in crime, sticking it out, and believing in me. We are building something great together and I can't wait to see where it's going next.

Dj Das and Jason Zeng, your close friendship and support mean so much. Thank you for being there and I look forward to our future travels, get-togethers, and more in the years to come.

Professor Ruben Savizky, thank you for inspiring me to start doing research and for continuing to support me in many ways during my career.

To the many others who have built and maintained friendships with me over the years: Shay Khan, Marc Lim, Cindy Tsui, Ang Li, Gabe Kooreman, Muneeb Hai, Sergey Kolchinsky, Alex Gerofsky, Eric Lo, and Michael Benoit. Thank you!

Last but certainly not least, I would like to thank my family. My mother, Jacqueline Chait, who instilled the drive and passion for excellence that makes me who I am today. My grandparents, Betty and Morty Chait, who gave me such a loving upbringing and always believed in me even when I was a child.

Abstract

Protein A (ProA) chromatography is a bioseparations technique employed throughout the biopharmaceutical industry for the selective capture and purification of IgG-class monoclonal antibodies (mAbs) and Fc-fusion proteins. The rapid growth of mAbs as commercial therapeutics has motivated the need for improved, efficient, and high-throughput purification processes during manufacturing. In direct response, the work presented in thesis aims to 1) increase the scientific community's understanding of IgG adsorption behavior on ProA chromatography resins and 2) improve the performance of ProA chromatography with ligands that are chemically modified using polyethylene glycol (PEGylated).

The results of this thesis suggest that IgG molecules of varying binding strength, or varying elution pH, are capable of competing for binding sites on ProA chromatography resins in simultaneous or sequential adsorption. The competitive phenomenon derives from variance in IgG binding strength, or IgG elution pH, due to differences in sub-class behavior as well as secondary IgG binding interactions with the ProA ligand. Competition is readily apparent in the adsorption of human polyclonal IgG, which has a wide variety of IgG sub-classes and binding epitopes.

Additionally, the results presented in this thesis suggest that ProA chromatography resins with PEGylated ligands are a viable path to increase resin robustness and real-world chromatographic selectivity. It is demonstrated that ligand PEGylation can increase resistance to proteolytic digestion, mitigate impurity interactions with mAbs that are bound to ProA, and increase process selectivity against Chinese Hamster Ovary host cell proteins by up to 37%. However, resins with large volumes of conjugated PEG significantly decrease IgG static binding capacity and decrease the available pore space for diffusion, resulting in losses in dynamic binding capacity and productivity. Lighter modifications appear to avoid losses in dynamic binding

capacity, however, they do not appear to be effective at mitigating impurity interactions with mAbs that are bound to ProA, which is key to increasing process selectivity. PEGylation of ProA also universally increases the elution pH of IgG molecules by weakening the binding interaction. This last result opens another path of viability for PEGylated ProA ligands for purification of mAbs of Fc-fusion proteins that are sensitive to low pH environments.

Table of Contents

List of Tables

List of Figures

1

Background and Motivation

1.1. Background

1.1.1. Affinity chromatography

Affinity chromatography is a powerful bioseparations technique with a wide variety of commercial uses and applications. The method takes advantage of the selective binding capabilities of certain biological molecules in order to purify and separate target proteins within solutions of interest. Affinity chromatography is currently being used in industry to purify enzymes, plasma proteins, monoclonal antibodies, hormones, vaccines, and other genetic materials produced by microorganisms [1].

During typical operation, a liquid feed containing a target protein of interest is passed through a packed bed of a porous particles or gel, commonly referred to as a resin, that contains an immobilized, high affinity ligand for the target. The high affinity ligand in the solid phase could, for example, be an immobilized antibody that is specific for the desired target molecule [1]. As the target of interest in the feed comes into contact with the solid phase, it diffuses into the pores of the resin particles and adsorbs to the affinity ligand. Once the column has been loaded with a satisfactory concentration of target, it is washed to remove any contaminating materials that are non-specifically adsorbed. The wash step is followed by an elution process, which disrupts the specific interactions between the affinity ligand and target, resulting in the

1

collection of purified product. Affinity chromatography resins and processes are typically designed so that they may be regenerated and reused for multiple process cycles [2].

1.1.2. IgG antibodies

One class of biomolecules that will be heavily discussed in this thesis are antibodies, which are a member of the immunoglobulin family of molecules. Antibodies are proteins that are produced as a defense mechanism in response to foreign agents in a host organism. Immunoglobulins have a common monomeric structure, which is illustrated in Figure 1.1a. A corresponding three-dimensional structure of an immunoglobulin class G (IgG) molecule is shown in Figure 1.1b. A seen in Figure 1.1a, the immunoglobulin structure consists of four polypeptide chains: two identical heavy chains and two identical light chains. Disulfide bonds join the heavy chains together as well as each heavy chain to one of the light chains. The two heavy chains are joined together in a flexible region known as the hinge, which is susceptible to enzymatic or chemical cleavage. Both the heavy chain and light chain chains contain constant (C) and variable (V) regions. Heavy chains contain three constant regions while light chains contain a single constant region. The variable regions of the heavy and light chains combine to form two antigen binding sites on either side of the molecule, which determines the specificity of the antibody. Together, the regions above the hinge form two identical regions known as the Fab-regions, while the region below the hinge is known as the Fc-region. For IgG antibodies, which will be exclusively discussed in this thesis, the Fc fragment is ~50 kDa while each Fab fragment is ~50 kDa, which forms a molecule with a total molecular weight of ~150 kDa. Human IgG antibodies can be even further divided into subclasses that result from minor differences in their amino acid sequences. In humans, there are four IgG subclasses: IgG_1, IgG_2,

IgG$_3$, and IgG$_4$ [3]. It should be noted that human IgG antibodies belonging to the same subclass have been shown to have >95% homology in the amino acid sequences of their Fc-regions [4].
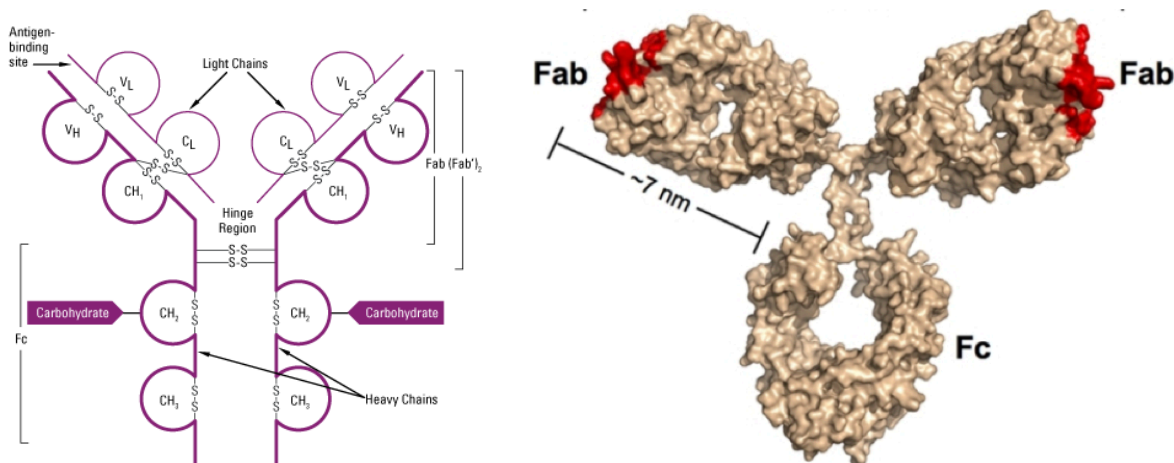
Figure 1.1. (a) Structural map of an immunoglobulin molecule adapted from ThermoFisher Scientific [5] and (b) three-dimensional structure of a IgG-class antibody adapted from Klein and Bjorkman [6].

1.1.3. IgG-class monoclonal antibodies

Monoclonal antibodies (mAbs) are highly specific antibodies that comprise only one antibody type (binds to one antigen). The high binding specificity of mAbs for their cognate antigens has enabled this class of biomolecules to be used as therapeutic agents in humans by targeting certain diseases in the body [3]. Over the past several decades, the development of genetically engineered mAbs has overcome problems such as immunogenicity in humans and has widely expanded their range of potential disease targets [7]. Currently, mAbs are the fastest growing class of therapeutic proteins [8] and are expected to command a $140 billion global market in 2017 [9]; as of November 2014, there have been 47 mAbs and antibody-derived products approved by for human therapeutic use within the United States and Europe [10]. The tremendous growth of mAbs as therapeutics has been, in part, due to the ability of these

molecules to successfully treat a variety of diseases including several forms of cancer, immunological disorders, and even elevated cholesterol [7].

1.1.4. Staphylococcal Protein A

Staphylococcal Protein A (SPA) is a cell wall associated protein that is exposed on the surface of the Gram-positive bacterium *Staphylococcus aureus*. The SPA structure consists of three regions, which are illustrated in Figure 1.2: S, a signal sequence processed during secretion; five homologous IgG binding domains, E, D, A, B, and C; and an anchoring region XM [11]. Flexible, random coil sequences link each region together, which gives the SPA molecule a fair degree of mobility. The linking sequences have also been shown to be very susceptible to proteolytic cleavage. Each of the binding domains in SPA is roughly cylindrical with individual molecular weights of ~6.6 kDa. The total molecular weight of the native intact molecule is ~54 kDa [12].
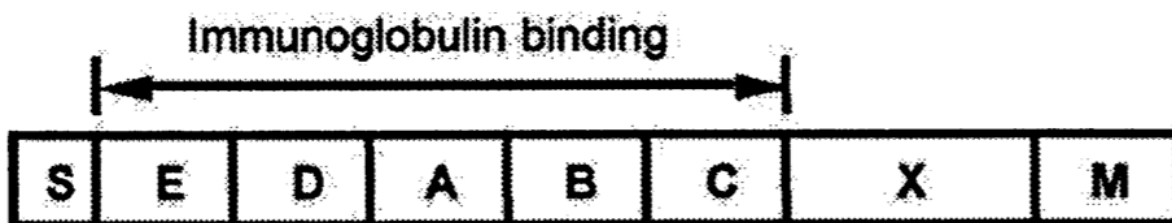
Figure 1.2. Structure map of Staphylococcal Protein A showing independent binding, signal, and anchoring domains. Adapted from Hober et al. [11].

All five binding domains in SPA have been individually shown to have high, and roughly equivalent, binding affinity to IgG molecules from various species including human, rabbit, and guinea pig as well as variable affinity for other species. For human IgG, SPA has high affinity

4

for the IgG$_1$, IgG$_2$, and IgG$_4$ subclass molecules, with very weak affinity for the IgG$_3$ subclass

[11]. The affinity constant of the individual SPA binding domains to IgG$_1$, IgG$_2$, and IgG$_4$ has

been determined to be on the order of 10^8 M^{-1} [13]. The range of affinities for SPA to antibody

subclasses is summarized in Figure 1.3.

Species	Subclasses	Protein A
Human	IgG1	++
	IgG2	++
	IgG3	−
	IgG4	++
	IgA	Variable
	IgD	−
	IgM	Variable
Rabbit	No distinction	++
Guinea pig	IgG1	++
	IgG2	++
Bovine		+
Mouse	IgG1	+
	IgG2a	++
	IgG2b	+
	IgG3	+
	IgGM	Variable
Chicken	IgY	−

Strong binding ++, medium interaction +, weak or no interaction −.

Figure 1.3. Summary of SPA binding affinity for antibody subclasses. Adapted from Hober et al.
[11].

The primary IgG binding site, which is also referred to as the classical binding site, for

SPA is on the Fc region of the molecule at the junctures of the C$_H$2 and C$_H$3 domains [11]. Since

there are two of these junctures on either site of the Fc region, there are two SPA binding sites

per IgG molecule. Figure 1.4 is an excellent illustration showing the binding of SPA to an IgG

molecule via its classical binding site. Studies have shown that the binding interaction is mostly

hydrophobic with additional stabilization from hydrogen bonding. Since the interaction is

hydrophobic, the binding is weakened at low salt concentrations [12]. The binding is also pH

sensitive: histidine residues in both the SPA and IgG binding sites become positively charged at

low pHs, causing mutual charge repulsions and the disruption of the protein-protein binding

5

interaction [12]. In addition to the classical binding site, studies have shown that SPA has secondary interactions, via the D and E binding domains, with the Fab region of the IgG structure for antibodies that belong to the V_H3 gene family [14].
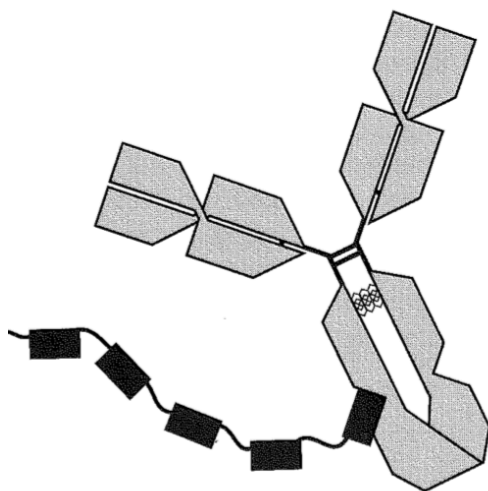
Figure 1.4. Illustration of SPA-IgG classical binding. Adapted from Gagnon [12].

1.1.5 Protein A chromatography

One application of affinity chromatography, namely Protein A (ProA) chromatography, utilizes immobilized SPA ligands on porous resin beads (typically a form of cross-linked agarose or synthetic polymer) for the purification of IgG-class mAbs. This process exploits SPA's binding interactions with the Fc portion of the antibody structure for the highly selective capture and purification of mAbs [15]. ProA chromatography is also routinely used for purification of Fc-fusion proteins, which are a class of biotherapeutics that chemically bond a therapeutic protein to an IgG Fc fragment for use as a purification handle [16]. In the case of ProA chromatography, SPA ligands are often recombinantly produced with modified anchoring domains, amongst other modifications, to enable attachment to the resin backbone of choice [11,12].

For industrial purposes, mAbs are produced recombinantly in mammalian cell culture, often in Chinese hamster ovary (CHO) cells, creating, along with the drug, a slew of contaminants such as host cell proteins (HCPs), mAb aggregates and fragments, host cell DNA, and virus particles that must be removed from the final pharmaceutical product. Due to its high specificity and generic applicability to IgG molecules, ProA chromatography has been established as the key step of the "platform" or general industrial process for mAb downstream production [7]. Along these lines, ProA chromatography typically achieves ≥98% mAb purity by mass from the initial cell culture in a single step purification step [17].

During typical operation of ProA chromatography, harvested CHO cell culture fluid (CHO HCCF) containing mAbs and impurities is first loaded onto ProA chromatography resin packed in a column at pH ~7. In the column, the mAbs diffuse into pores of the resin particles and eventually bind to the immobilized ProA on the resin surface. Loading is followed by a series of wash steps, which can vary in pH and composition amongst use cases, that remove impurities from the column. Finally, the pH is adjusted to 3-4 to dissociate the mAbs from the ProA ligands resulting in elution of the purified antibody [7,12]. In reality, a small level of non-specific binding occurs due to impurities that either bind to the ProA or associate with the mAbs, which results in co-elution of impurities; studies have shown impurity binding to the resin particles is negligibly small [18,19]. These remaining impurities require orthogonal purification steps following ProA chromatography, known as polishing steps, that bring the product up to pharmaceutical purity standards [7,15]. ProA chromatography is set within in the context of the overall downstream purification process for mAbs in the next section.

1.1.6 Monoclonal antibody downstream platform process

As discussed in section 1.1.5, ProA chromatography is the key step of the "platform" or general industrial process for mAb downstream production. For this thesis, it is important to also understand ProA chromatography in the context of the entire platform process. Figure 1.5 illustrates the steps of a typical mAb downstream platform process. After production of the mAb in mammalian cell culture, the crude culture undergoes a harvest process that removes cells and cell debris. The harvested cell culture fluid is then loaded and purified by ProA chromatography as discussed in section 1.1.5. This initial separation of the target protein from the cell culture fluids is known as the capture step. Subsequent polishing steps mainly focus on removing product-related impurities such as HCPs, host DNA, mAb aggregates, and virus particles. Additionally, leached ProA ligands and fragments are a focus of the polishing steps. Viral clearance is typically achieved by a low-pH viral inactivation hold step and then a second, orthogonal removal step via filtration conducted near the end of the process. Two or three additional chromatography steps typically follow ProA chromatography, which usually comprise forms of ion-exchange chromatography and/or hydrophobic interaction chromatography, to remove the remaining host proteins, leached ProA ligands, and host DNA. The process ends with an ultrafiltration/diafiltration (UF/DF) step, which concentrates the mAb and exchanges it into formulation buffer for use in humans [7,15]. Given the numerous additional steps required after ProA chromatography, and the fact that these additional steps focus on product-related impurities, the majority of downstream process development effort and time is spent on removing less than 2% of the initial impurities [20-22].
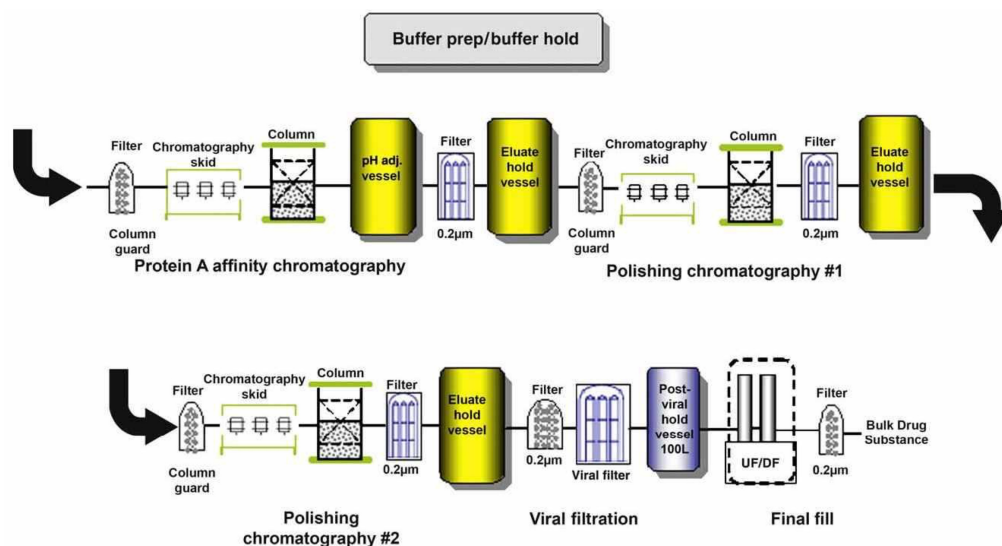
Figure 1.5. mAb downstream platform process. Adapted from Shukla and Thommes [7].

1.1.7 Protein A chromatography resins

ProA was first reported for use as chromatography ligand to purify IgG by Hjelm and Sjöquist [23] in 1972. In this original paper, the authors covalently linked native SPA from *Staphylococcus aureus* to Sepharose 4B, which is a commercial, 4% cross-linked agarose resin backbone produced at the time byPharmacia Fine Chemicals (now GE Healthcare) [23]. Since then, multiple generations of ProA chromatography resins have entered the market that have improved various aspects of resin and process performance. These resins, now sold by a variety of competing manufacturers, have novel modifications to the resin base matrix and pore structure as well as to the ligand density, attachment chemistry, and engineering of the ProA ligand itself [11]. Repligen pioneered the recombinant production of ProA ligands in 1985, which removed the need to source SPA from the *Staphylococcus aureus* bacterium [24]. Two decades later, GE Healthcare developed the engineered ProA ligand, SuRe, via selective substitution of asparagine residues in the protein structure in order to increase ligand stability under harsh, alkaline clean-n-place (CIP) conditions [11,25]. Improvements to the ligand attachment chemistry have included

a multi-point covalent attachment chemistry that reduces ProA leaching during processing [26], as well as a single-point directed attachment of the ligand in GE Healthcare's MabSelect family that increases ProA accessibility and efficiency [27]. Cross-linked agarose is a common base matrix material used for protein chromatography resins, however, entrants from Life Technologies and EMD Millipore using more rigid cross-linked poly(styrene-divinylbenzene) or controlled pore glass have enabled increased stability against higher pressures and faster flow rates for higher productivity [28]. GE Healthcare's MabSelect Xtra and MabSelect SuRe LX variants have met industry demands for faster mass transport and increased binding capacities by decreasing particle sizes and increasing ligand densities, respectively [29,30].

Given that an entire recombinant protein production and purification process must be completed just to generate the ProA ligand itself, the associated chromatography resins are expensive. Currently, market leading ProA chromatography resins are sold for on the order of $5,000-$10,000/L [31]. For mAb purification, industrial ProA column sizes are up to 1000 L [32,33], thus representing a significant cost in downstream processing.

1.1.8 Polyethylene glycol (PEG) and PEGylated proteins

Another molecule that will be heavily discussed in this thesis is polyethylene glycol (PEG). PEG is a neutral hydrophilic polymer with the structure and repeating monomer unit shown in Figure 1.6. The polymer has many industrial uses and appears as a chemical component in many commercial products. A short list of applications of PEG include: surface coating, chemical precipitant, dispersant, lubricant, ink solvent, anti-foaming agent, and insulator [34]. PEG itself is also biocompatible and generally regarded as safe by the FDA; medical use cases include PEG as a pharmaceutical excipient and as a laxative [34,35].
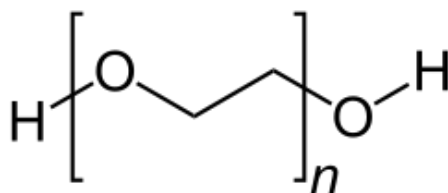
Figure 1.6. Chemical structure of polyethylene glycol (PEG).

The most relevant application of the polymer to this thesis is the covalent attachment of PEG (PEGylation) to proteins in order to enhance native protein properties. PEGylation of proteins was first reported by Davies and Abuchowsky [36,37] in the 1970s when they demonstrated the modification of bovine serum albumin and catalase. Since then, PEGylation chemistries, modification strategies, and applications have proliferated. PEGylation has been used to reduce the fouling of surfaces, shown to enhance protein folding stability, and to enhance the delivery of therapeutic proteins [38-42]. PEG itself is inert and unreactive, however, activated derivatives of the polymer, such as those listed and shown in Figure 1.7, are capable of reacting with amino acid residues on proteins. As seen in Figure 1.7, there are a large variety of activated PEG derivatives available that are specific to certain residues, maintain overall protein charge, and mask positive charges on the protein [35]. PEG molecular weights may also be controlled to fine tune the size of the protein-polymer conjugate. A particular PEGylation chemistry that is relevant to this thesis is the PEG-aldehyde chemistry, which reacts with accessible primary amine groups on proteins in the presence of sodium cyanoborohydride ($NaCNBH_3$, reducing agent) by reductive amination to form a higher order amine bond. At low pHs, this chemistry has been shown to be selective towards the free amine group on the N-terminus of the target protein, which typically has a pKa that is lower than that of lysine side chains [35,43,44].

PEG derivatives that maintain the charge of the native protein in the final conjugate

Structure	Alkylating PEGs	Properties
PEG–CH$_2$CH$_2$–CHO (PEG with propionaldehyde group)	PEG–aldehyde (also in the form of more stable acetale)	A two steps reaction; the first product (a Shiff base) is reduced by NaCNBH$_3$. When the coupling reaction is carried out at low pH = 4.5–5, it labels only the α-amino group.
PEG$-$O$-$SO$_2$$-CH_2CF_3$	PEG–tresyl or tosyl	Not much used because the chemistry leads to a mixture of products.
PEG$-$O–dichlorotriazine and bis-PEG-O–monochlorotriazine structures	PEG–dichlorotriazine or chlorotriazine	Now they are abandoned for therapeutic application because of their toxicity.
PEG$-$O$-$CH$_2$–epoxide	PEG–epoxide	Slowly reactive, rarely used.

PEG derivatives that, after amino coupling, lead to a loss of positive charge in the final conjugate with respect to starting protein

Structure	PEG-carboxilates	Properties
PEG$-$O$+$CH$_2$$)_n$C(=O)OSu	Several PEG derivatives with one or more CH$_2$ groups between the PEG and the carboxylic group	The carboxylic group is activated as N-hydroxy succinimidyl ester, imidazole or benzotriazole. The kinetic rate of conjugation depends on the numbers, and eventual ramification of CH$_2$ groups linked to the carboxyl group.
PEG$-$O$-$C(=O)$-$CH$_2$CH$_2$$-$C(=O)$-$OSu	PEG–succinimidyl succinate	The ester bond between succinic acid and PEG is easily hydrolyzed.
PEG$-$X$-$C(=O)$-$OSu	PEG–amino acid–succinimidyl ester	Nle or βAla as amino acid moiety allows an easy quantification of the number of linked PEG chains by amino acid analysis.
PEG$+$X$)_n$C(=O)$-$OSu	PEG–peptide–succinimidyl ester	The Met-Nle or Met-βAla allows the removal of PEG by CNBr treatment for an easy localization of PEGylation site. Lysosomal cleavable sequences, as H-Gly-Phe-Lue-Gly-OH, allow the release of the bound drug inside the cell.

Structure	PEG-carbonates	Properties
PEG$-$O$-$C(=O)$-$O$-$C$_6$H$_4$$-NO_2$	PEG–p-nitrophenyl carbonate	Slowly reactive, yield a urethane linkage with amine.
PEG$-$O$-$C(=O)$-$O$-$N-benzotriazolyl	PEG–benzotriazolyl carbonate	Slowly reactive, yield a urethane linkage with amine.
PEG$-$O$-$C(=O)$-$O$-$2,3,5-trichlorophenyl	PEG–2,3,5-trichlorophenyl carbonate	Slowly reactive, yield a urethane linkage with amine.
PEG$-$O$-$C(=O)$-$OSu	PEG–succinimidyl carbonate	Slowly reactive, yield a urethane linkage with amine.

Key: Su, succinimide; X, amino acid linker.

12
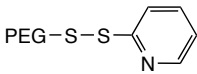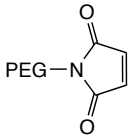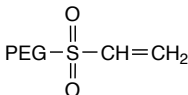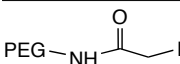
PEGs reactive towards a thiol group		
Structure	**Thioreactive PEGs**	**Properties**
PEG−S−S−⟨pyridine⟩	PEG–pyridildisulphide	The most specific towards thiol but yields a cleavable linkage by a reducing agent also *in vivo*.
PEG−N⟨maleimide⟩	PEG–maleimide	Gives stable linkage by double bond addition but can also react with amines at pH >8.
PEG−S(=O)(=O)−CH=CH$_2$	PEG–vinylsulfone	
PEG−NH−C(=O)−CH$_2$−I	PEG–iodo acetamide	Less reactive, not much used

Figure 1.7. Summary of available PEGylation chemistries. Adapted from Veronese and Pasut [35].

PEGylation of therapeutic proteins has been shown to increase drug retention time (half-life) in the body, reduce immunogenicity, and increase resistance against metabolic enzymes. This is accomplished by two main mechanisms. First, the attachment of one or more PEG chains to a therapeutic protein significantly increases the hydrodynamic size of the drug, which reduces the glomerular filtration rate by the kidneys and thus increases the drug half-life. Second, the PEG chains act as a steric barrier that reduces attack (non-specific binding) from immune proteins and proteolytic enzymes, thus also increasing the persistence of the drug in the body. As a side note, the hydrophilic nature of PEG has also been used to increase the solubility small (organic) molecule drugs in the body. Figure 1.8 illustrates the benefits of PEGylating drugs for enhanced delivery. It should be noted that PEGylation of therapeutic proteins has also been shown to accompany a loss in biological activity. An example of this is PEGylated α-interferon (Pegasys®), which retains only 7% of the activity of the native protein. However, the increased half-life of the PEGylated variant overcomes this loss in activity and demonstrates significantly

13

improved effectiveness *in vivo* [35]. As of 2017, 15 PEGylated drugs have been approved by the FDA for human therapeutic use [45].
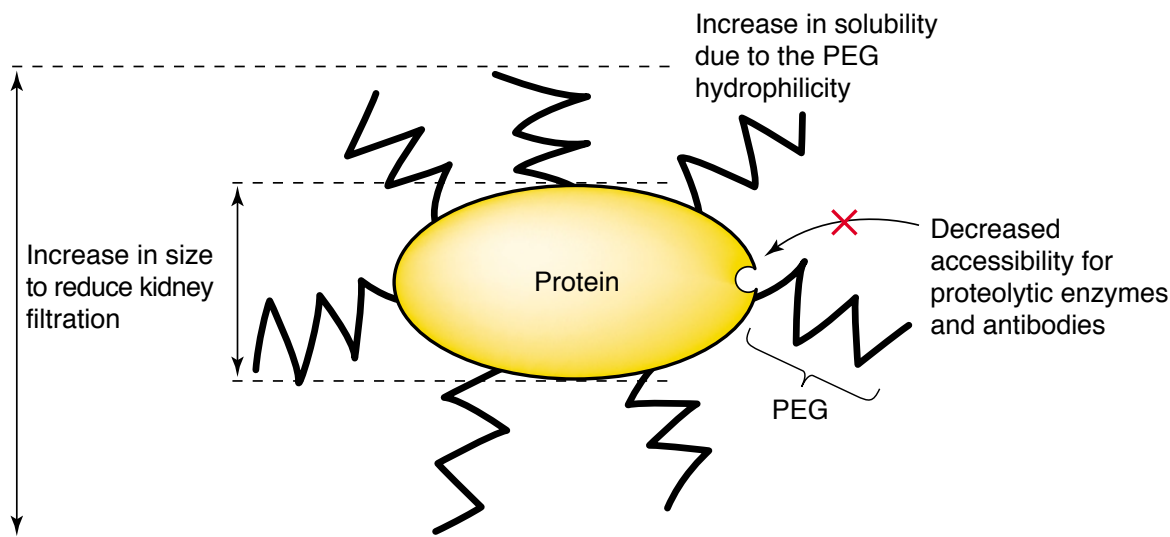
Figure 1.8. PEGylation of therapeutics for enhanced drug delivery. Adapted from Veronese and Pasut [35].

1.2. Motivation and thesis aims

As discussed in section 1.1, ProA chromatography is a central unit operation in the purification of mAbs, which command a rapidly growing, $100B+ industry. As such, significant effort and resources are devoted to fully understanding the highly complex biomolecular interactions that occur within the ProA chromatography as well to continually improve the performance of the process. The work presented in this thesis aims to do both.

In recent years, advancements in cell culture technology (upstream production) have dramatically increased the titers (concentration in culture) of mAbs and the levels of impurities that are co-expressed with the product, while advancements in the downstream platform process have been modest [7]. As a result, downstream processing is often the bottleneck in the production of mAbs. ProA chromatography, in particular, has been identified as a bottleneck due

to its limited binding capacity compared to other modes of chromatography. The limited capacity of ProA chromatography resins becomes challenging when dealing with high titer feeds since additional or larger columns are necessary to meet throughput needs. The aforementioned solutions create significant economic challenges due to the highly expensive cost of additional resin [46]. At the same time, since both the number of mAb drugs in development and the demand for the drug quantities has increased, companies in the biopharmaceutical industry continue to look to and rely upon platform processes to optimize the speed to market of drug candidates [7]. Although several attempts have been made to create alternatives to processes including ProA chromatography, no other process has yet proven to be commercially viable and simultaneously rival the excellent selectivity and ease of generic 'platformability' that ProA offers for mAb purification [47-49]. Additionally, there is significant regulatory burden associated with deviation from the platform process, which further discourages companies from venturing outside of it [21,22]. Thus, there has been a drive to innovate within the platform process by improving existing unit operations including ProA chromatography.

A multitude of literature studies have been performed by both academic and industrial labs that have greatly expanded the scientific community's understanding of the ProA chromatography process. Often times these studies lay the foundation for future improvements to process performance. Published studies have included the analysis and modeling of IgG mass transport and binding kinetics in resins [50-52], the identification of fouling mechanisms over resin lifetime [53,54], the biophysical characterization of HCP impurity interactions with ProA during chromatography [55], the characterization of secondary binding interactions of IgG with ProA via the Fab region with respect to elution pH [14], and the characterization of differences in binding capacity for different IgG molecules and Fc-fusion proteins on ProA resins [16]. In

this thesis, the relatively unexplored topic of multi-component IgG adsorption on ProA chromatography resins is investigated. As will be discussed in Chapter 3, this results in the significant discovery that IgG molecules of different binding strengths compete for binding sites on ProA resins upon simultaneous adsorption.

Section 1.1.7 discusses the generational improvements to ProA chromatography resins by commercial manufacturers. Additionally, there has been a history of literature studies that have focused on optimizing the ProA chromatography process and modifying ProA resins for increased performance. Published studies have included optimizing binding capacity with dual flow rate strategies [46], engineering the ProA ligand to produce milder elution pH conditions for IgG [56], optimizing wash conditions to mitigate impurity interactions with mAbs during chromatography [18], and optimizing process conditions to extend resin lifetime over multiple process cycles [57].

In this thesis, the PEGylation of ProA chromatography ligands for purposes of increasing process selectivity and improving resin robustness is explored. The concept of PEGylating affinity chromatography ligands is not novel. In fact, Wen and Niemeyer [58] demonstrated improved ligand thermal and organic solvent stability when PEGylating the affinity chromatography ligand concanavalin A. This study provided initial inspiration for PEGylation as a viable route to improve the intrinsic properties of affinity ligands and is consistent with literature demonstrating PEGylation's ability to increase the stability of proteins [59-61]. In the case of PEGylated ProA, it is hypothesized that PEGylation of the ligand provides a steric barrier against non-specific binding of process impurities akin to the *in vivo* "stealth" characteristics that PEGylation of therapeutic proteins enables in drug delivery [35]. A significant increase in ProA chromatography selectivity would reduce the burden on the downstream mAb platform process

16

or possibly remove the need for one polishing step, which would produce tremendous benefits in terms of reduced process development costs and validation times [62,63]. Increasing resin robustness (reducing resin fouling, ProA denaturation, or degradation from host cell proteinases) would also enable the resin to withstand more chromatography process cycles, which would in turn reduce the need for resin replacement and further save on costs. Figure 1.9 is a cartoon that illustrates the hypothesized mechanism for improving ProA chromatography selectivity and robustness via ligand PEGylation.
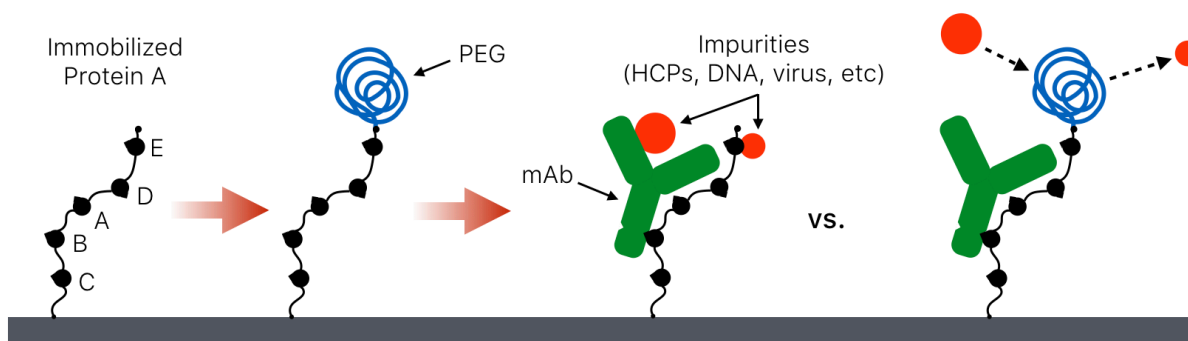
Figure 1.9. Illustration of hypothesized mechanism for improving ProA chromatography selectivity and robustness via ligand PEGylation.

Initial exploratory work on PEGylated ProA resins conducted at Carnegie Mellon University was published by Gonzalez-Valdez et al. [64] in the journal of *Biotechnology Progress* in 2014. This work investigated the selectivity of the ProA resin, Repligen CaptivA PriMAB, which was modified with 5.0 and 20.7 kDa PEG chains, respectively. PEGylation of the immobilized ligands was conducted by reductive amination of accessible amines on the protein with aldehyde–activated mono–methoxy PEGs in the presence of sodium cyanoborohydride at pH 5.1. Selectivities of the unmodified and resins with PEGylated ligands were evaluated by monitoring product recovery and contaminant clearance after 0.5 mL analytical injections of 1.0 mg/mL polyclonal rabbit IgG (rIgG) spiked with solutions of 0.33-30

mg/mL yeast extract (YE) and 1.0-10.0 %vol/vol fetal bovine serum (FBS) (mock contaminants). Figures 1.10a and 1.10b display plots of the selectivities that were determined as a function of contaminant concentration for the unmodified, 5.0 kDa PEG, and 20.7 kDa PEG modified resins. As shown in Figure 1.10a, the 5.0 kDa PEG modified resin was about five to ten times more selective on average than the unmodified resin and the 20.7 kDa PEG modified resin was about ten to thirty times more selective than the unmodified resin for the YE spiking experiments. Selectivity gains were smaller, but still significant for the FBS spiking experiments as shown in Figure 1.10b. These results also suggested a direct correlation between selectivity and the molecular weight of the PEG modification.
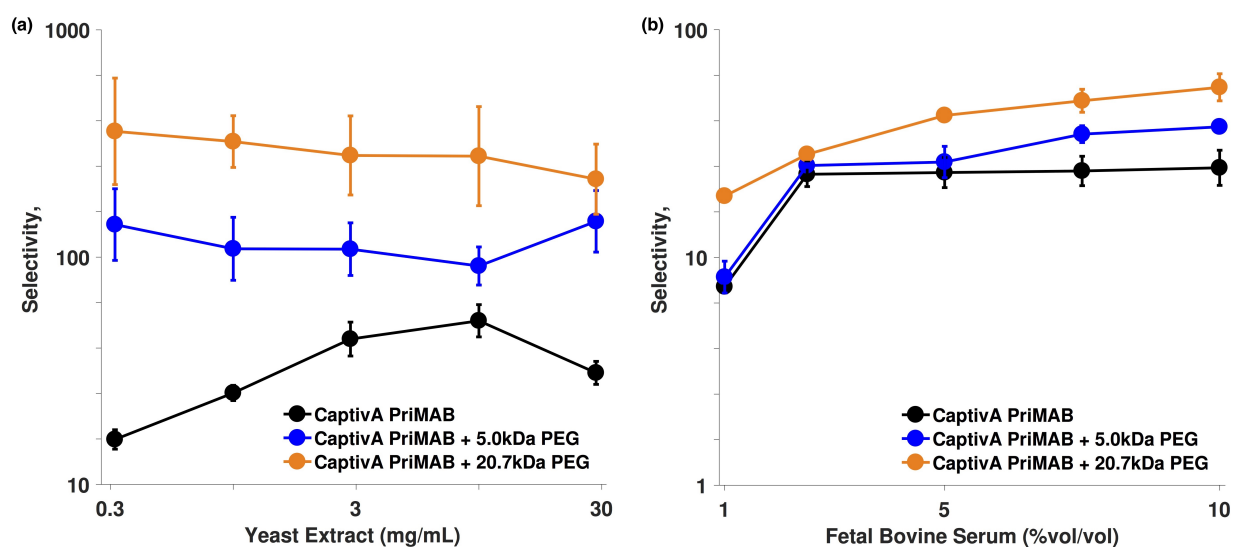
Figure 1.10. Chromatographic process selectivity as a function of (a) yeast extract contaminant concentration and (b) fetal bovine serum contaminant concentration for analytical-scale injections of rabbit IgGs purified unmodified CaptivA PriMAB, 5.0 kDa PEG modified, and 20.7 kDa PEG modified resins. Adapted from Gonzalez-Valdez et al. [64].

The YE and FBS used in the exploratory work were mock contaminants and thus not representative of impurities present in the typical industrial CHO HCCF feed. Additionally, the analytical injections (0.5 mL) used for loading were not representative of typical loading

conditions where the column is loaded to ~10% breakthrough capacity (140-160 mL for the particular column and IgG concentration used in the exploratory work). However, the results of the exploratory work were a promising indication that the PEGylation of ProA ligands should be further investigated with a more rigorous and realistic set of experiments and materials. This thesis goes beyond the work of Gonzalez-Valdez et al. [64] with a comprehensive study of IgG adsorption, process selectivity, and resin robustness for ProA chromatography resins with PEGylated ligands.

1.3 Thesis outline

Chapter 2 of this thesis discusses the underlying theory describing transport in affinity chromatography systems. In particular, the derivation of the predictive height equivalent to a theoretical plate (HETP) equation is described. Additionally, the chapter describes how the predictive HETP equation is used in conjunction with van Deemter analysis to experimentally determine mass transfer properties in affinity chromatography systems. The aforementioned is utilized several times in subsequent chapters to gain insights into mass transfer resistances in ProA chromatography resin variants.

Chapter 3 of this thesis reports a study that compares the adsorption of an IgG mAb (single-component system) and human polyclonal IgG (multi-component system) on various ProA chromatography resins. The study concludes with the significant discovery that IgG molecules of different binding strengths compete for binding sites on ProA resins upon simultaneous adsorption. This chapter was adapted as appropriate from the article, "Polyclonal and monoclonal IgG binding on protein A resins—Evidence of competitive binding effects", authored by Justin Weinberg, Shaojie Zhang, Gillian Crews, Edward Healy, Giorgio Carta, and

Todd Przybycien and published in the journal of *Biotechnology and Bioengineering* on June 6th, 2017.

Chapter 4 of this thesis is a comprehensive study of IgG adsorption equilibrium, kinetics, and transport in ProA chromatography resins with PEGylated ligands. Aspects of modified resin performance including binding capacities, elution pHs, pore structure, binding kinetics, and mass transport with respect to PEGylation molecular weight and reaction extent are discussed in detail. This chapter was adapted as appropriate from the manuscript, "Chemical Modification of Protein A Chromatography Ligands with Polyethylene Glycol. I: Effects on IgG Adsorption Equilibrium, Kinetics, and Transport", authored by Justin Weinberg, Shaojie Zhang, Gillian Crews, Giorgio Carta, and Todd Przybycien. The manuscript was submitted for review to the *Journal of Chromatography A* on September 5th, 2017.

Chapter 5 of this thesis is a continuation of the study reported in Chapter 4 that investigates the selectivity and robustness properties of ProA chromatography resins with PEGylated ligands. Modified resin resistance to proteolytic digestion, fouling, and selectivity against HCPs present in CHO HCCF are discussed in detail. This chapter of the thesis was adapted as appropriate from the manuscript, "Chemical Modification of Protein A Chromatography Ligands with Polyethylene Glycol. II: Effects on Resin Robustness and Process Selectivity", authored by Justin Weinberg, Shaojie Zhang, Allison Kirkby, Enosh Shachar, Giorgio Carta, and Todd Przybycien. The manuscript was submitted for review to the *Journal of Chromatography A* on September 5th, 2017.

Chapter 6 of this thesis summarizes the results of additional research that was conducted within the scope of Chapters 3-5, which but was not included in publications for the sake of brevity or because it was tangential to the main conclusions of the articles.

Finally, Chapter 7 of this thesis presents a summary of conclusions, original contributions of this work, broader impacts, and future directions.

1.4. References

[1] Arnold, F. H., Blanch, H. W., & Wilke, C. R., "Analysis of affinity separations I: predicting the performance of affinity adsorbers" *The Chemical Engineering Journal*. 30 (1985): B9-B23.

[2] A. Jungbauer, Chromatographic media for bioseparation, J Chromatogr A. 1065 (2005) 3-12.

[3] GE Healthcare, Antibody Purification Handbook, Handbook 18-1037-46 AD 1, 2007.

[4] Hamilton RG, The Human IgG Subclasses, Calbiochem-Novabiochem Corporation, Textas. 1987.

[5] ThermoFisher Scientific, Immunoglobulin Structure and Classes, https://www.thermofisher.com/us/en/home/life-science/antibodies/antibodies-learning-center/antibodies-resource-library/antibody-methods/immunoglobulin-structure-classes.html

[6] J.S. Klein, P.J. Bjorkman, Few and Far Between: How HIV May Be Evading Antibody Avidity, PLoS Pathog 6. (2010) 908.

[7] A. Shukla, J. Thommes, Recent advances in large-scale production of monoclonal antibodies and related proteins, Trends Biotechnol. 28 (2010) 253-261.

[8] J. Li, Z. Zhu, Research and development of next generation of antibody-based therapeutics, Acta Pharmacologica Sinica. 31 (2010) 1198-1207.

[9] RnR Market Research, Global and China Monoclonal Antibody Industry Report, 2013.

[10] J. Reichert, Marketed therapeutic antibodies compendium, mAbs. 4 (2012) 413-415.

[11] S. Hober, K. Nord, M. Linhult, Protein A chromatography for antibody purification, Chromatogr B. 848 (2007) 40-47.

[12] P. Gagnon, Purification Tools for Monoclonal Antibodies, Validated Biosystems Inc.*,* Tucson, 1996.

[13] L. Jendeberg, P. Nilsson, A. Larsson, P. Denker, M. Uhlén, B. Nilsson, P.Å. Nygren, Engineering of Fc(1) and Fc(3) from human immunoglobulin G to analyse subclass specificity for staphylococcal protein A, J Immunol Methods. 201 (1997) 25-34.

[14] S. Ghose, M. Allen, B. Hubbard, C. Brooks, S.M Cramer, Antibody variable region interactions with Protein A: Implications for the development of generic purification processes, Biotechnol Bioeng. 92 (2005) 665-673.

[15] A.A. Shukla, B. Hubbard, T. Tressel, S. Guhan, D. Low, Downstream processing of monoclonal antibodies-Application of platform approaches, J Chromatogr A. 848 (2007) 28-39.

[16] S. Ghose, B. Hubbard, S.M. Cramer, Binding capacity differences for antibodies and Fc-fusion proteins on protein A chromatographic materials, Biotechnol Bioeng. 96 (2007) 768-779.

[17] R.D.R. Tarrant, M.L. Velez-Suberbie, A.S. Tait, C.M. Smales, D.G. Bracewell, Host cell protein adsorption characteristics during protein a chromatography, Biotechnol Prog. 28 (2012) 1037-1044.

[18] A.A. Shukla, P. Hinckley, Host cell protein clearance during protein A chromatography: development of an improved column wash step, Biotechnol Prog. 24 (2008) 1115-1121.

[19] B. Nogal, K. Chhiba, J.C. Emery, Select host cell proteins coelute with monoclonal antibodies in protein a chromatography, Biotechnol Prog. 28 (2012) 454-458.

[20] K. Eriksson, A. Ljunglöf, G. Rodrigo, E. Brekkan, MAb Contaminant removal with a multimodal anion exchanger, BioProcess International, 2009.

[21] B. Kelley, Very large scale monoclonal antibody purification: The case for conventional unit operations, Biotechnol Prog. 23 (2007) 995-1008.

[22] G. Jagschies, A. Gronberg, T. Bjorkman, K.M. Lacki, H.J. Johansson HJ, Technical and Economical Evaluation of Downstream Processing Options for Monoclonal Antibody (Mab) Production, BioPharm International, 2006.

[23] H. Hjelm, K. Hjelm, J. Sjöquist. Protein a from Staphylococcus aureus. Its isolation by affinity chromatography and its use as an immunosorbent for isolation of immunoglobulins, FEBS Lett. 28 (1972) 73-76.

[24] Z. Liu, S. Mostafa, A. Shukla, A comparison of Protein A chromatographic stationary phases: Performance characteristics for monoclonal antibody purification, Biotechnol Appl Biochem. 62 (2014) 37-47.

[25] GE Healthcare Life Sciences, MabSelect SuRe, Data File 11-0011-65 AC, 2011.

[26] Repligen, Captiva Primab—Protein A affinity resin—Regulatory Support File RSF-1003201, 2010.

[27] GE Healthcare Life Sciences, MabSelect, Data File 18-1149-94 AF, 2011.

[28] Z. Liu, S. Mostafa, A. Shukla, A comparison of Protein A chromatographic stationary phases: Performance characteristics for monoclonal antibody purification, Biotechnol Appl Biochem. 62 (2014) 37-47.

[29] GE Healthcare Life Sciences, MabSelect Xtra, Data File 11-0011-57 AC , 2011.

[30] GE Healthcare Life Sciences, MabSelect SuRe LX, Data File 28-9870-62 AA , 2011.

[31] J.R. Ryland, Process Development, Manufacturing Strategies and Costs, Recovery of Biological Products XIV, 2010.

[32] C. Jiang C, J. Liu, M. Rubacha, A.A. Shukla, A mechanistic study of Protein A chromatography resin lifetime, J Chromatogr A. 1216 (2009) 5849-5855.

[33] B. Kelley, Very large scale monoclonal antibody purification: The case for conventional unit operations, Biotechnol Prog. 23 (2007) 995-1008.

[34] Polyethylene glycol, Uses, https://en.wikipedia.org/wiki/Polyethylene_glycol

[35] F.M. Veronese, G. Pasut, PEGylation, successful approach to drug delivery, Drug Discovery Today, 10 (2005) 1451-1458.

[36] A. Abuchowski, T van Es, N.C. Palczuk, F.F. Davis, Alteration of immunological properties of bovine serum albumin by covalent attachment of polyethylene glycol, J Biol Chem. 252 (1977) 3578–3581.

[37] A. Abuchowski, J.R. McCoy, N.C. Palczuk, T. van Es, F.F. Davis, Effect of covalent attachment of polyethylene glycol on immunogenicity and circulating life of bovine liver catalase, J Biol Chem. 252 (1977) 3582–3586.

[38] M. Michaelis, J. Cinatl, J. Cinatl, P. Pouckova, K. Langer, J. Kreuler, J. Matousek, Coupling of the antitumoral enzyme bovine seminal ribonuclease to polyethylene glycol chains increases its systemic efficacy in mice, Anti-cancer Drugs. 13 (2002) 149-154.

[39] J.M. Harris, N.E. Martin, N. Modi, Pegylation: a novel process for modifying pharmacokinetics, Clinical Pharmacokinetics, 40 (2001) 539-551.

[40] R. Gref, A. Domb, P. Quellec, T. Blunk, R.H. Muller, J.M Verbavatz, R. Langer, The Controlled Intravenous Delivery of Drugs using PEG-Coated Sterically Stabilized Nanospheres, Advanced Drug Delivery Reviews. 16 (1995) 215-233.

[41] I. Szleifer, M.A. Carignano, Tethered polymer layers: phase transitions and reduction of protein adsorption, Macromolecular Rapid Communications. 21 (2000) 423-448.

[42] J. Wei, D.B. Ravn, L. Gram, P. Kingshott, Stainless steel modified with poly(ethylene glycol) can prevent protein adsorption but not bacterial adhesion, Colloids and Surfaces B: Biointerfaces. 32 (2003) 275-291.

[43] O. Kinstler, N. Gabriel, C. Farrar, R. DePrince, N-terminally chemically modified protein compositions and methods, US Patent no. 5,824,784 A, 1998.

[44] D.R. Lide, Handbook of Chemistry and Physics, 72nd Edition, CRC Press, Boca Raton, FL, 1991.

[45] U.S. Food & Drug Administration, FDA Approved, Drug Products, https://www.accessdata.fda.gov/scripts/cder/daf/

[46] S. Ghose, J. Zhang, L. Conley, R. Caple, K. Williams, D. Cecchini, Maximizing binding capacity for protein A chromatography, Biotechnol Progr. 30 (2014) 1335-1340.

[47] D.K. Follman, R.L. Fahrner, Factorial screening of antibody purification processes using three chromatography steps without protein A, J Chromatogr A. 1024 (2004) 79–85.

[48] S. Ghose, B. Hubbard, S.M. Cramer, Protein interactions in hydrophobic charge induction chromatography (HCIC), Biotechnol Prog. 21 (2005) 498–508.

[49] S. Ghose, B. Hubbard, S.M Cramer, Evaluation and comparison of alternatives to protein A chromatography: mimetic and hydrophobic charge induction chromatographic stationary phases, J Chromatogr A. 1122 (2006) 144–152.

[50] E.X. Perez-Almodovar, G. Carta, IgG adsorption on a new protein A adsorbent based on macroporous hydrophilic polymers. I. Adsorption equilibrium and kinetics, J Chromatogr A 1216 (2009) 8339-8347.

[51] R. Hahn, P. Bauerhansl, K. Shimahara, C. Wizniewski, A. Tscheliessnig, A. Jungbauer, Comparison of protein A affinity sorbents II. Mass transfer properties, J Chromatogr A. 1093 (2005) 98-110.

[52] J.T. McCue, G. Kemp, D. Low, I. Quinones-Garcia, Evaluation of pro- tein-A chromatography media, J Chromatogr A. 2003989 (2003) 139–153.

[53] S. Zhang, K. Xu, W. Daniels, J. Salm, J. Glynn, J. Martin, C. Gallo, R. Godavarti, G. Carta, Structural and functional characteristics of virgin and fouled Protein A MabSelect resin cycled in a monoclonal antibody purification process, Biotechnol Bioeng. 113 (2016) 367-375.

[54] S. Zhang, W. Daniels, J. Salm, J. Glynn, J. Martin, C. Gallo, R. Godavarti, G. Carta, Nature of foulants and fouling mechanism in the Protein A MabSelect resin cycled in a monoclonal antibody purification process, Biotechnol Bioeng. 113 (2016) 141-149.

[55] N. Levy, K. Valente, L. Choe, K. Lee, A. Lenhoff, Identification and characterization of host cell protein product-associated impurities in monoclonal antibody bioprocessing, Biotechnol Bioeng. 111 (2013) 904-912.

[56] T. Pabst, R. Palmgren, A. Forss, J. Vasic, M. Fonseca, C. Thompson, W.K. Wang, X. Wang, A.K. Hunter, Engineering of novel Staphylococcal Protein A ligands to enable milder elution pH and high dynamic binding capacity, J Chromatogr A. 1362 (2014) 180-185.

[57] L. Yanga, J.D. Hardinga, A.V. Ivanovb, N. Ramasubramanyana, D.D. Donga, Effect of cleaning agents and additives on Protein A ligand degradation and chromatography performance, J Chromatogr A. 1385 (2015) 63-68

[58] Z. Wen, B. Niemeyer, Preparation and characterization of PEGylated Concanavalin A for affinity chromatography with improved stability, J Chromatogr B. 879 (2011) 1732–1740.

[59] Z. Yang, M. Domach, R. Auger, F.X. Yang, A.J. Russell, Polyethylene glycol-induced stabilization of subtilisin, Enzyme and Microbial Technology. 18 (1996) 82-89.

[60] H. Garcia-Arellano, B. Valderrama, G. Saab-Rincon, R. Vazquez-Duhalt, High temperature biocatalysis by chemically modified cytochrome C, Bioconjugate Chemistry. 13 (2002) 1366-1344.

[61] I.J. Castellanos, W. Al-Azzam, K. Griebenow, Effect of the covalent modification with poly(ethylene glycol) on alpha-chymotrypsin stability upon encapsulation in poly(lactic-co-glycolic) microspheres, Journal of Pharmaceutical Sciences. 94 (2005) 327-340.

[62] B.K. Nfor, P.D.E.M. Verhaert, L.A.M. van der Weilen, J. Hubbuch, M. Ottens, Rational and systematic protein purification process development: the next generation, Trends in Biotechnology. 27 (2009) 673-679.

[63] A. Rajapakse, N.J. Tichener-Hooker, S.S. Farid, Modeling of the biopharmaceutical pathway and portfolio management, Computers in Chemical Engineering. 29 (2005) 1357-1368.

[64] J. González-Valdez, A. Yoshikawa, J. Weinberg, J. Benavides, M. Rito-Palomares, T. Przybycien, Toward improving selectivity in affinity chromatography with PEGylated affinity ligands: The performance of PEGylated protein A, Biotechnol Prog. 30 (2014) 1364-1379.

2

Theory: Band Broadening, General Rate Model, and Height Equivalent to a Theoretical Plate (HETP)

2.1. Band broadening in chromatography

As discussed in Chapter 1, affinity chromatography is a core industrial technique for the purification of biological molecules. Thus, there is an impetus to understand the underlying theory to be able to model affinity chromatography such that these systems can be properly optimized and utilized to their fullest potential.

This chapter of the thesis describes the connection between theory and experiment for pulse analysis in affinity chromatography columns. Pulse analysis concerns the effect of peak spreading (also known as band broadening) when a short injection of solute (a pulse) is loaded onto a chromatography column containing a packed bed of porous media. The concentration profile of a pulse entering the column is rectangular, however, the concentration profile of the pulse exiting the column (typically read by a detector) is a Gaussian or semi-Gaussian shape due to band broadening. The effect of peak spreading/band broadening is roughly illustrated in Figure 2.1.

Figure 2.1. Cartoon showing the band broadening of a pule injection in a packed bed column.

Band broadening of a pulse injection is due to the contribution of mass transfer and binding resistances in the column, which are illustrated in Figure 2.2. As seen from Figure 2.2 (A), molecules (denoted by small cross marks) enter the packed bed of porous media in a pulse. The first effect of band broadening is due to eddy diffusion, as shown in Figure 2.2 (B), which is due to the multitude of possible paths that the molecules in the pulse can travel between the particles in the column. Since some of these paths are bound to be longer than others, molecules that take longer paths will exit the column at a later time. The second effect is due to convection and molecular diffusion, as shown in Figure 2.2 (C). In liquid chromatography systems, flow is typically in the laminar region such that the pulse spreads in the flow direction by convective transport. Furthermore, concentration gradients between the pulse and the mobile phase cause additional spreading due to molecular diffusion. The combination of effects from eddy diffusion and molecular diffusion is commonly referred to as axial dispersion. The third and fourth effects, which are illustrated in Figure 2.2 (D), are film mass transfer and pore diffusion. Each of the porous particles in the column is surrounded by a stagnant fluid film, which creates a mass transfer resistance to molecules that attempt to enter the pores of the particle. After entering the pores of the particle, the molecules diffuse at a slower rate due to the restriction of space available to them within the pores. In order to exit the column, the molecules that diffuse into the pores must diffuse back out of them, causing them to elute at a later time than molecules that do not enter the pores.

27

Finally, the fifth effect, illustrated in Figure 2.2 (E), is kinetic binding resistance of the solute to any ligand immobilized on the solid phase. If the solute molecule of interest were to have an affinity for the ligand, it would be retained on the column and thus elute at a later time [1].

Understanding the contributions of each mass transfer resistance to overall band broadening is the purpose of pulse analysis. This chapter will describe the development of predictive equations that can be used to determine the contribution of the mass transfer effects discussed above. This information can be used, for example, to assist the scale-up of chromatographic processes from a lab scale to an industrial scale. After developing the predictive equations, this chapter will also describe how the predictive equations are used in conjunction with experimental data to determine the mass transfer characteristics of affinity chromatography systems.
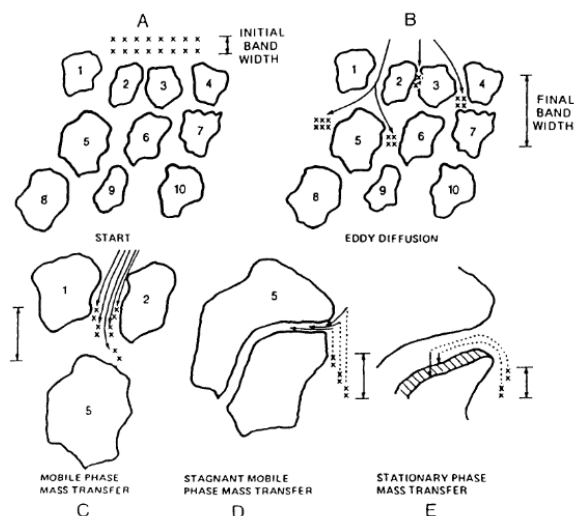
Figure 2.2. Contributions to band broadening in chromatography. Adapted from Blanch and Clark [1].

2.2. General Rate Model (GRM)

To develop the theory that governs pulse analysis, the General Rate Model (GRM) of chromatography must be fully described. The model is based on the isothermal adsorption of a single solute through a packed bed of monodisperse porous particles. This system is illustrated in Figure 2.3. Although terms will be defined throughout the chapter, a quick summary of relevant variables and parameters is as follows:

$c(z,t)$ - the solute concentration in the bulk liquid

Q - the volumetric flowrate

L - length of bed

A - cross sectional area of bed

ε – interstitial porosity (between particles)

R - radius of particles

β - porosity of particles (within particles)

ρ_p - density of particles

$q(r,z,t)$ – sorbate concentration in the particle

$c_i(r,z,t)$ - solute concentration in the pores of the particles
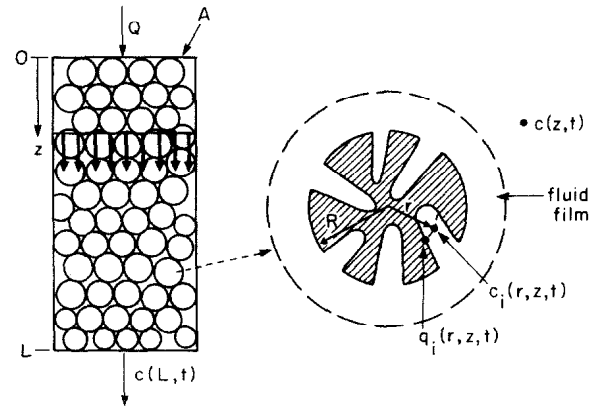
Figure 2.3. Model of the affinity column. Adapted from Arnold et al. [2].

2.2.1. Mass balance on column

The GRM consists of four differential mass balances, the first of which is an overall mass balance on the column described by [1]:

$$\frac{\partial(V_0 c)}{\partial t} + u_s \frac{\partial(V_C c)}{\partial z} + \frac{\partial(V_S \bar{s})}{\partial t} = D_L \frac{\partial^2(V_C c)}{\partial z^2} \tag{2.1}$$

where:

$V_C = V_0 + V_S$ - total column volume

V_0 - interstitial volume

V_S - solid phase volume (solid + pore volume)

$u_s = Q/A$ - superficial velocity (volumetric flow rate/column cross-sectional area)

$\bar{s} = \beta \bar{c}_i + \rho_p \bar{q}$ - the average concentration in the particles, including the solute in the pores and solute adsorbed to the surface

D_L - axial dispersion coefficient

The terms of the mass balance (from left to right) account for accumulation of the solute in the liquid, convective flow, accumulation of solute in the solid phase, and axial dispersion, respectively.

The average concentration of solute in the pores ($\bar{c}_i$) and average concentration of solute adsorbed to the particles ($\bar{q}$) are defined by volume averages over the spherical particles [1].

$$\bar{c}_i = \frac{\int_0^R c_i(t,r,z) 4\pi r^2 dr}{\frac{4}{3}\pi R^3} = \frac{3}{R^3} \int_0^R r^2 c_i dr \tag{2.2}$$

Similarly,

$$\bar{q} = \frac{3}{R^3} \int_0^R r^2 q dr \tag{2.3}$$

Equation (2.1) is divided by column volume (V_c) to give:

$$\varepsilon \frac{\partial c}{\partial t} + u_s \frac{\partial c}{\partial z} + (1-\varepsilon) \frac{\partial \bar{s}}{\partial t} = D_L \frac{\partial^2 c}{\partial z^2} \tag{2.4}$$

where:

$$\frac{V_0}{V_C} = \varepsilon \quad \frac{V_s}{V_C} = \frac{V_C - V_0}{V_C} = 1 - \varepsilon \tag{2.5}$$

Equation (2.4) is divided by interstitial porosity (ε) to give:

$$\frac{\partial c}{\partial t} + \frac{u_s}{\varepsilon} \frac{\partial c}{\partial z} + \frac{1-\varepsilon}{\varepsilon} \frac{\partial \bar{s}}{\partial t} = \frac{D_L}{\varepsilon} \frac{\partial^2 c}{\partial z^2} \tag{2.6}$$

The interstitial fluid velocity is defined as:

$$u_i = \frac{u_s}{\varepsilon} \tag{2.7}$$

Equation (2.6) becomes:

$$\frac{\partial c}{\partial t} + u_i \frac{\partial c}{\partial z} + \frac{1-\varepsilon}{\varepsilon} \frac{\partial \bar{s}}{\partial t} = \frac{D_L}{\varepsilon} \frac{\partial^2 c}{\partial z^2} \tag{2.8}$$

The average concentration of solute in the particles is differentiated with respect to time to give:

$$\frac{\partial \bar{s}}{\partial t} = \beta \frac{\partial \bar{c}_i}{\partial t} + \rho_p \frac{\partial \bar{q}}{\partial t} \tag{2.9}$$

It is assumed that the accumulation of solute in the pores is negligible because in practice the concentration of solute adsorbed to the surface is much greater than that in the pores [1]. Thus,

$$\frac{\partial \bar{c}_i}{\partial t} \approx 0 \tag{2.10}$$

$$\frac{\partial \bar{s}}{\partial t} = \rho_p \frac{\partial \bar{q}}{\partial t} \tag{2.11}$$

Substituting equation (2.11) into (2.8) produces:

$$\frac{\partial c}{\partial t} + u_i \frac{\partial c}{\partial z} + \rho_p \frac{1-\varepsilon}{\varepsilon} \frac{\partial \bar{q}}{\partial t} = \frac{D_L}{\varepsilon} \frac{\partial^2 c}{\partial z^2} \tag{2.12}$$

2.2.2. Mass balance on a single particle

Focusing on a single particle in the packed bed, the mass balance of solute in the particle is determined by Fick's 2nd law.

$$\frac{\partial s}{\partial t} = \beta \frac{\partial c_i}{\partial t} + \rho_p \frac{\partial q}{\partial t} = D_p \nabla^2 c_i \tag{2.13}$$

where D_p is the pore diffusivity.

In spherical coordinates and assuming no change in c_i with respect to θ or ϕ:

$$\nabla^2 c_i = \frac{1}{r^2} \frac{\partial}{\partial r}\left(r^2 \frac{\partial c_i}{\partial r}\right) = \frac{1}{r^2}\left(2r \frac{\partial c_i}{\partial r} + r^2 \frac{\partial^2 c_i}{\partial r^2}\right) = \frac{2}{r} \frac{\partial c_i}{\partial r} + \frac{\partial^2 c_i}{\partial r^2} \tag{2.14}$$

32

Substituting (2.14) into (2.13) gives:

$$\beta \frac{\partial c_i}{\partial t} + \rho_p \frac{\partial q}{\partial t} = D_p \left(\frac{2}{r} \frac{\partial c_i}{\partial r} + \frac{\partial^2 c_i}{\partial r^2} \right) \tag{2.15}$$

Rearranging (2.15) gives:

$$D_p \left(\frac{2}{r} \frac{\partial c_i}{\partial r} + \frac{\partial^2 c_i}{\partial r^2} \right) - \beta \frac{\partial c_i}{\partial t} - \rho_p \frac{\partial q}{\partial t} = 0 \tag{2.16}$$

2.2.3. Flux balance on solute entering the solid phase

The average concentration of solute entering the solid is related to the flux of molecules entering through the pores of the particle by [1]:

$$\frac{\partial \bar{s}}{\partial t} \approx \rho_p \frac{\partial \bar{q}}{\partial t} = \left[\frac{Surface\ Area}{Volume} \right] D_p \frac{\partial c_i}{\partial r} \bigg|_{r=R} = \left[\frac{4\pi R^2}{\frac{4}{3}\pi R^3} \right] D_p \frac{\partial c_i}{\partial r} \bigg|_{r=R} = \left(\frac{3}{R} \right) D_p \frac{\partial c_i}{\partial r} \bigg|_{r=R} \tag{2.17}$$

The flux across the fluid film of the particle must also equal the flux entering the pores [1]. Thus,

$$k_f (c - c_i|_{r=R}) = D_p \frac{\partial c_i}{\partial r} \bigg|_{r=R} \tag{2.18}$$

where k_f is the film mass transfer coefficient.

Combining (2.17) and (2.18) gives:

$$\frac{\partial \bar{q}}{\partial t} = \left(\frac{3}{R}\right) \frac{D_p}{\rho_p} \frac{\partial c_i}{\partial r}\Big|_{r=R} = \left(\frac{3}{R}\right) \frac{k_f}{\rho_p} (c - c_i|_{r=R}) \tag{2.19}$$

2.2.4. Mass balance on surface

Affinity systems are commonly modeled using Langmuir binding kinetics, consisting of a 2nd order adsorption process and 1st order desorption process described by [1]:

$$\frac{\partial q}{\partial t} = \mu_f c_i (q_{max} - q) - \mu_r q \tag{2.20}$$

where μ_f and μ_r are the forward and reverse rate constants, respectively, and q_{max} is the maximum allowable adsorbed concentration of solute on the particle.

At steady state, (2.20) produces the Langmuir isotherm:

$$0 = \mu_f c_i (q_{max} - q^*) - \mu_r q^* \tag{2.21}$$

$$q^* = \frac{\mu_f q_{max} c_i}{\mu_f c_i + \mu_r} = \frac{q_{max} K c_i}{1 + K c_i} \tag{2.22}$$

$$K = \frac{\mu_f}{\mu_r} \tag{2.23}$$

Expanding (2.20) gives:

$$\frac{\partial q}{\partial t} = \mu_f q_{max} c_i - \mu_r q c_i - \mu_r q \tag{2.24}$$

$$\frac{\partial q}{\partial t} = \mu_f q_{max} \left(c_i - \left(\frac{\mu_f c_i + \mu_r}{\mu_f q_{max}} \right) q \right) \qquad (2.25)$$

$$\frac{\partial q}{\partial t} = \mu_f q_{max} \left(c_i - \left(\frac{c_i}{q_{max}} + \frac{1}{K q_{max}} \right) q \right) \qquad (2.26)$$

It is assumed that $q \ll q_{max}$ since the number of binding sites on the particle is typically large compared to the loading conditions. Thus, (2.25) becomes:

$$\frac{\partial q}{\partial t} = \mu_f q_{max} \left(c_i - \left(\frac{1}{K q_{max}} \right) q \right) \qquad (2.27)$$

2.2.5. Boundary conditions

The GRM for a pulse injection comprises four boundary conditions. The pulse is a finite injection of solute onto the front of the column at concentration c_0 for a short time t_0 [1]. Thus,

$$c = c_0 \ at \ z = 0 \ for \ 0 \ \leq t \ \leq t_0 \qquad (2.28)$$

The column and bed are initially free of solute. Thus,

$$c = 0 \ at \ z \ > 0 \ for \ t = 0 \qquad (2.29)$$

$$c_i = 0 \ at \ r \ \geq 0 \ for \ t = 0 \qquad (2.30)$$

Finally, at the center of each particle there is an internal diffusion boundary condition due to the radial symmetry of the particle.

$$\frac{\partial c_i}{\partial r} = 0 \ at \ r = 0 \ for \ t > 0 \tag{2.31}$$

2.2.6. Summary

Equations (2.12), (2.16), (2.19), and (2.27) coupled with boundary conditions (2.28) – (2.31) comprise the GRM. The equations and conditions are summarized below.

$$\frac{\partial c}{\partial t} + u_i \frac{\partial c}{\partial z} + \rho_p \frac{1-\varepsilon}{\varepsilon} \frac{\partial \bar{q}}{\partial t} = \frac{D_L}{\varepsilon} \frac{\partial^2 c}{\partial z^2}$$

$$D_p \left(\frac{2}{r} \frac{\partial c_i}{\partial r} + \frac{\partial^2 c_i}{\partial r^2} \right) - \beta \frac{\partial c_i}{\partial t} - \rho_p \frac{\partial q}{\partial t} = 0$$

$$\frac{\partial \bar{q}}{\partial t} = \left(\frac{3}{R} \right) \frac{D_p}{\rho_p} \frac{\partial c_i}{\partial r} \bigg|_{r=R} = \left(\frac{3}{R} \right) \frac{k_f}{\rho_p} (c - c_i|_{r=R})$$

$$\frac{\partial q}{\partial t} = \mu_f q_{max} \left(c_i - \left(\frac{1}{Kq_{max}} \right) q \right)$$

$$c = c_0 \ at \ z = 0 \ for \ 0 \leq t \leq t_0$$

$$c = 0 \ at \ z > 0 \ for \ t = 0$$

$$c_i = 0 \ at \ r \geq 0 \ for \ t = 0$$

$$\frac{\partial c_i}{\partial r} = 0 \ at \ r = 0 \ for \ t > 0$$

2.3. Moment analysis of the GRM

The GRM as described in section 2.2 cannot be solved analytically. However, simplifying assumptions can be made to reduce the system to one that can be solved analytically. One example that allows for an analytical solution is the assumption of a linear adsorption isotherm, or:

$$q = Kc_i \tag{2.32}$$

Instead of an analytical solution that describes the concentration of the solute as a function of position and time through the column, it is possible to gain considerable information on axial dispersion, film resistance, pore diffusion, and binding kinetics from a statistical moment analysis of the peak that is produced by the pulse.

In practice, we are only interested in three statistical moments of a peak, although an infinite number of moments can be theoretically calculated. They are [3]:

The zeroth moment, or the area of the peak:

$$\mu_0 = \int_0^\infty c(L,t)dt = Peak\ area \tag{2.33}$$

The normalized first absolute moment, or the average retention/residence time of the peak [3]:

$$\mu_1 = \frac{\int_0^\infty c(L,t)t\,dt}{\int_0^\infty c(L,t)dt} = \frac{\int_0^\infty c(L,t)t\,dt}{\mu_0} = t_r \tag{2.34}$$

The normalized second central moment, or the variance of the peak [3]:

$$\mu_2' = \frac{\int_0^\infty (t-\mu_1)^2 c(L,t)dt}{\int_0^\infty c(L,t)dt} = \frac{\int_0^\infty (t-\mu_1)^2 c(L,t)dt}{\mu_0} = \sigma^2 \tag{2.35}$$

A visual representation of how these moments relate to a typical chromatography peak is shown in Figure 2.4.
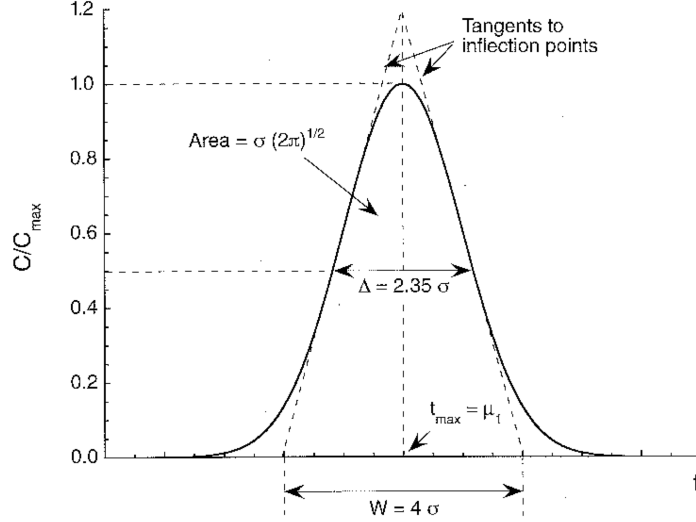
Figure 2.4. Properties of a typical (Gaussian) chromatography peak. Adapted from Carta and Jungbauer [3].

The normalized n^{th} moment of the peak is defined by [3]:

$$\mu_n = \frac{\int_0^{\infty} c(L,t)t^n dt}{\int_0^{\infty} c(L,t)dt} = \frac{\int_0^{\infty} c(L,t)t^n dt}{\mu_0} \tag{2.36}$$

Using this definition, it is possible to express the normalized second central moment in terms of the first and second normalized absolute moments.

$$\mu_2' = \frac{\int_0^{\infty}(t-\mu_1)^2 c(L,t)dt}{\int_0^{\infty} c(L,t)dt} = \frac{\int_0^{\infty}(t-\mu_1)^2 c(L,t)dt}{\mu_0} = \frac{\int_0^{\infty}(t^2-2\mu_1 t+\mu_1^2)c(L,t)dt}{\mu_0} \tag{2.37}$$

$$\mu_2' = \frac{\int_0^{\infty} t^2 c(L,t)dt}{\mu_0} - 2\mu_1 \frac{\int_0^{\infty} tc(L,t)dt}{\mu_0} + \mu_1^2 \frac{\int_0^{\infty} c(L,t)dt}{\mu_0} = \mu_2^2 - 2\mu_1\mu_1 + \mu_1^2 = (\mu_2 - \mu_1)^2$$

$$\tag{2.38}$$

Kubin and Kucera [4] determined analytical expressions for the first absolute and second central moments of the solution to the GRM via a Laplace-Carson transform and applying the van der Laan theorem. The full work that was performed to reach these expressions is extremely complex, however, the most important steps of the solution are described below.

The Laplace-Carson transform of the concentration of solute in the bed is defined as [4]:

$$C(z,s) = s \int_0^\infty c(z,t)e^{-st}dt \tag{2.39}$$

This transform was applied to the system of PDEs and boundary conditions in the GRM. After applying the transforms, the concentration of solute in the bed in the Laplace-Carson domain was determined to be [4]:

$$C(z,s) = c_o[1 - e^{-st_0}]e^{-\gamma z} \tag{2.40}$$

where:

$$\gamma = -\frac{u_i \varepsilon}{2D_L} + \sqrt{\left(\frac{u_i \varepsilon}{2D_L}\right)^2 + \frac{s\varepsilon}{D_L}[1 + h(s)]} \tag{2.41}$$

$$h(s) = \frac{3k_f}{R}\frac{1-\varepsilon}{\varepsilon}\left[\frac{1}{s} - \frac{\sinh(R\sqrt{\lambda})}{\left(\frac{sD_p}{k_f}\right)\sqrt{\lambda}\cosh(R\sqrt{\lambda})+s\left[1-\left(\frac{D_p}{Rk_f}\right)\right]\sinh(R\sqrt{\lambda})}\right] \tag{2.42}$$

$$\lambda = \frac{s\beta}{D_p}\left[1 + \frac{\left(\frac{\rho_p}{\beta}\right)K\mu_f}{Ks+\mu_f}\right] \tag{2.43}$$

It is not possible to take the inverse Laplace-Carson transform of the above expression, however, using the van der Laan theorem, the nth normalized absolute moment of the peak can be determined by [3]:

$$\mu_n = \frac{\int_0^\infty c(L,t)t^n dt}{\int_0^\infty c(L,t)dt} = (-1)^n \lim_{s \to 0} \frac{d^n}{ds^n}[C(z,s)] \qquad (2.44)$$

Using the van der Laan theorem, the normalized first absolute and second central moments of the peak were determined to be [1]:

$$\mu_1 = \frac{L}{u_i}[1 + \delta_0] + \frac{t_0}{2} \qquad (2.45)$$

$$\mu_2' = \frac{2L}{u_i}\left[\delta_1 + \frac{D_L}{\varepsilon}(1 + \delta_0)^2 \frac{1}{u_i^2}\right] + \frac{t_0^2}{12} \qquad (2.46)$$

where:

$$\delta_0 = \frac{1 - \varepsilon}{\varepsilon}\beta\left[1 + \frac{\rho_p}{\beta}(Kq_{max})\right] \qquad (2.47)$$

and

$$\delta_1 = \frac{1 - \varepsilon}{\varepsilon}\beta\left[\frac{\rho_p}{\beta}\frac{(Kq_{max})^2}{\mu_f} + \frac{R^2\beta}{15}\left(1 + \frac{\rho_p}{\beta}Kq_{max}\right)^2\left(\frac{1}{D_p} + \frac{5}{k_f R}\right)\right] \qquad (2.48)$$

Rearranging (2.46), it is seen that the normalized second central moment is a sum of contributions due to adsorption, intraparticle diffusion, film mass transfer, axial dispersion and injected pulse width.

$$\frac{\mu_2' - \frac{t_0^2}{12}}{\frac{2L}{u_i}} = \delta_{Ad} + \delta_D + \delta_f + \delta_L \frac{1}{u_i^2} \tag{2.49}$$

Adsorption:

$$\delta_{Ad} = \frac{1-\varepsilon}{\varepsilon} \beta \frac{\rho_p}{\beta} \frac{(Kq_{max})^2}{k_f} \tag{2.50}$$

Intraparticle diffusion:

$$\delta_D = \delta_0 \frac{R^2 \beta}{15} \left(1 + \frac{\rho_p}{\beta} Kq_{max}\right) \frac{1}{D_p} \tag{2.51}$$

Film mass transfer:

$$\delta_f = \delta_0 \frac{R^2 \beta}{15} \left(1 + \frac{\rho_p}{\beta} Kq_{max}\right) \frac{5}{k_f R} \tag{2.52}$$

Axial dispersion:

$$\delta_L = \frac{D_L}{\varepsilon} (1 + \delta_0)^2 \tag{2.53}$$

Injected pulse width $t_o^2/12$

These analytical solutions for the normalized first and second central moments as well as the idea of additive variances will be revisited in a section 2.6 in order to develop the predictive equation.

2.4. Plate theory

Previous sections of this chapter have described the equations and boundary conditions that define the GRM as well as how a moment analysis can be applied to derive analytical expressions for the normalized first absolute and second central moments of a peak produced by a pulse injection. In this section, the concept of height equivalent to a theoretical plate (HETP) will be introduced.

The plate theory of chromatography, originally developed by Martin and Synge [5], treats the chromatography column as a series of N theoretical equilibrium stages or plates. In this model, the solid phase in the column is distributed equally among the plates while the liquid phase containing the solute of interest flows from stage to stage at a constant flow rate. Thus, the theoretical height of each plate is simply the entire length of the column (L) divided by the number of plates (N) or:

$$HETP = \frac{L}{N} \tag{2.54}$$

In order to determine an expression for the number of plates for a pulse injection, the column is treated as a series of N perfectly mixed continuously stirred tank reactors (CSTRs) as shown in Figure 2.4. It is assumed that adsorption equilibrium is achieved in each reactor.
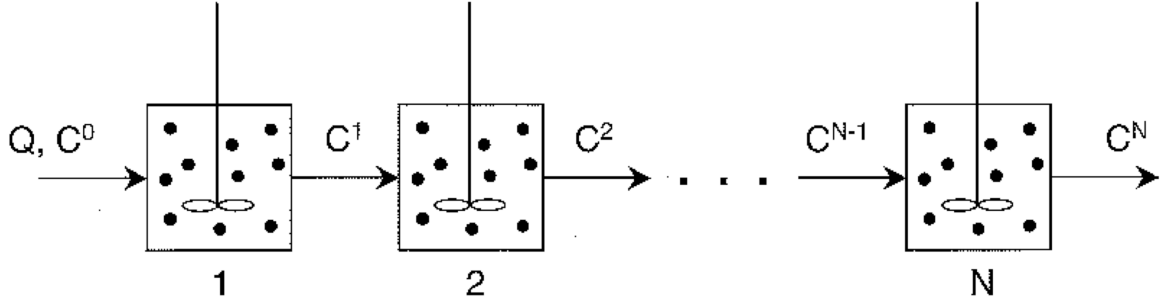
Figure 2.5. Treatment of a chromatography column as a series of N CSTRs. Adapted from Carta and Jungbauer [3].

From Figure 2.5, Q is the volumetric flow rate of liquid through the system, which as stated above, is assumed to be constant over all stages, C^0 is the initial concentration of solute in the pulse, C^j is the concentration of solute exiting the jth reactor, and C^{j-1} is the concentration of solute entering the jth reactor. Figure 2.6 focuses on one of these reactors in series, or the jth reactor.
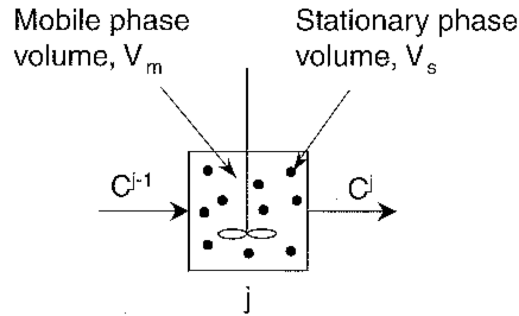
Figure 2.6. Flow diagram of the jth CSTR in series. Adapted from Carta and Jungbauer [3].

In Figure 2.6, V_m is the mobile phase volume in the jth reactor, and V_s is the solid phase volume in the jth reactor. Performing a mass balance on the jth reactor[6]:

$$QC^{j-1} - QC^j = V_m \frac{dC^j}{dt} + V_s \frac{dq^j}{dt} \qquad (2.55a)$$

$$Input - Output = Accumulation \qquad (2.55b)$$

If V_c is defined to be the total column volume, V_m can be expressed as:

$$V_m = \frac{\varepsilon V_c}{N} \tag{2.56}$$

$$V_s = \frac{(1-\varepsilon)V_c}{N} \tag{2.57}$$

Additionally, it is assumed that a linear isotherm governs adsorption within each stage. Thus,

$$q^j = KC^j \tag{2.58}$$

$$\frac{dq^j}{dt} = K\frac{dC^j}{dt} \tag{2.59}$$

Substituting (2.59) into (2.55) yields:

$$QC^{j-1} = QC^j + V_m\frac{dC^j}{dt} + KV_s\frac{dC^j}{dt} \tag{2.60}$$

$$QC^{j-1} = QC^j + (V_m + KV_s)\frac{dC^j}{dt} \tag{2.61}$$

Substituting (2.56) and (2.57) into (2.61) yields:

$$QC^{j-1} = QC^j + \left(\frac{\varepsilon V_c}{N} + \frac{(1-\varepsilon)KV_c}{N}\right)\frac{dC^j}{dt} \tag{2.62}$$

$$QC^{j-1} = QC^j + \frac{\varepsilon V_c}{N}\left(1 + \frac{(1-\varepsilon)K}{\varepsilon}\right)\frac{dC^j}{dt} \tag{2.63}$$

$$C^{j-1} = C^j + \frac{1}{N}\frac{\varepsilon V_c}{Q}\left(1 + \frac{(1-\varepsilon)K}{\varepsilon}\right)\frac{dC^j}{dt} \tag{2.64}$$

where:

$$\frac{\varepsilon V_c}{Q}\left(1 + \frac{(1-\varepsilon)K}{\varepsilon}\right) = t_r \tag{2.65}$$

Thus,

$$C^{j-1} = C^j + \frac{t_r}{N}\frac{dC^j}{dt} \tag{2.66}$$

Taking the Laplace transform of (2.66) yields:

$$\bar{C}^{j-1} = \bar{C}^j + \frac{t_r}{N}\left(s\bar{C}^j - C^j(t=0)\right) \tag{2.67}$$

Since the concentration exiting the jth reactor at time zero is zero, (2.66) becomes:

$$\bar{C}^{j-1} = \bar{C}^j + \frac{t_r}{N}s\bar{C}^j \tag{2.68}$$

$$\bar{C}^{j-1} = \bar{C}^j\left(1 + \frac{st_r}{N}\right) \tag{2.69}$$

$$\frac{\bar{C}^j}{\bar{C}^{j-1}} = \left(1 + \frac{st_r}{N}\right)^{-1} \tag{2.70}$$

45

Applying (2.70) to the last reactor in the series ($j = N$):

$$\frac{\bar{C}^N}{\bar{C}^{N-1}} = \left(1 + \frac{st_r}{N}\right)^{-1} \tag{2.71}$$

Applying (2.70) to the second to last reactor in the series ($j = N - 1$):

$$\frac{\bar{C}^{N-1}}{\bar{C}^{N-2}} = \left(1 + \frac{st_r}{N}\right)^{-1} \tag{2.72}$$

$$\bar{C}^{N-1} = \bar{C}^{N-2} \left(1 + \frac{st_r}{N}\right)^{-1} \tag{2.73}$$

Substituting (2.73) into (2.71) yields:

$$\frac{\bar{C}^N}{\bar{C}^{N-2}} = \left(1 + \frac{st_r}{N}\right)^{-2} \tag{2.74}$$

Following the pattern,

$$\frac{\bar{C}^N}{\bar{C}^0} = \left(1 + \frac{st_r}{N}\right)^{-N} = G(s) \tag{2.75}$$

Applying the van der Laan theorem to the transfer function in order to the determine the nth normalized absolute moment [3]:

$$\mu_n = \frac{\int_0^\infty C^N(t)t^n dt}{\int_0^\infty C^N(t)dt} = (-1)^n \lim_{s\to 0} \frac{d^n}{ds^n}[G(s)] \tag{2.76}$$

The normalized first absolute moment is determined by:

$$\mu_1 = (-1)\lim_{s\to 0}\left[\frac{dG(s)}{ds}\right] \tag{2.77}$$

$$\frac{dG(s)}{ds} = -t_r\left(\frac{st_r}{N}+1\right)^{-N-1} \tag{2.78}$$

$$\mu_1 = (-1)\lim_{s\to 0}\left[\frac{dG(s)}{ds}\right] = t_r \tag{2.79}$$

This result is expected since the normalized first absolute moment is defined as the mean residence time of the peak.

The normalized second absolute moment is determined by:

$$\mu_2 = \lim_{s\to 0}\left[\frac{d^2 G(s)}{ds^2}\right] \tag{2.80}$$

$$\frac{d^2 G(s)}{ds^2} = \frac{t_r^2 N(N+1)\left(\frac{st_r}{N}+1\right)^{-N}}{(st_r+N)^2} \tag{2.81}$$

$$\mu_2 = \lim_{s\to 0}\left[\frac{d^2 G(s)}{ds^2}\right] = \frac{t_r^2 N(N+1)(1)^{-N}}{N^2} = \frac{t_r^2(N+1)}{N} \tag{2.82}$$

Applying the definition of the normalized second central moment:

47

$$\mu_2' = \mu_2 - \mu_1^2 = \frac{t_r^2(N+1)}{N} - t_r^2 = \frac{t_r^2}{N} \tag{2.83}$$

Thus, an expression for the number of theoretical plates can be written in terms of the normalized first absolute and second central moments of the peak:

$$N = \frac{t_r^2}{\mu_2'} = \frac{\mu_1^2}{\mu_2'} \tag{2.84}$$

The height equivalent to a theoretical plate is therefore:

$$HETP = \frac{L}{N} = \frac{L\mu_2'}{\mu_1^2} = \frac{L\sigma^2}{t_r^2} \tag{2.85}$$

With this definition of HETP, the analytical moment solutions from the GRM can now be substituted into (2.85) to derive the predictive HETP equation for a pulse injection.

2.5. Predictive equation for HETP

Equations (2.45) – (2.48) describe the analytical solutions for the normalized first absolute and second central moments of a peak produced by a pulse injection on an affinity chromatography column. Equation (2.48) shows that the normalized second central moment (variance) is a sum of contributions from adsorption, intraparticle diffusion, film mass transfer, axial dispersion and injected pulse width. It should be noted from equations (2.50) and (2.51) that the contributions from intraparticle diffusion and film mass transfer are coupled with effects of binding resistance.

It is therefore of interest to describe these moments under binding and non-binding conditions such that the effects of the film mass transfer coefficient and pore diffusivity can be isolated. The derivation of the predictive HETP equation under non-binding conditions will be described in detail below, as it is most common for experimental analysis to be performed under these conditions.

Under non-binding conditions, the binding equilibrium constant (K) is set to zero. Thus, (2.46) and (2.47) become:

$$\delta_0 = \frac{1-\varepsilon}{\varepsilon}\beta \tag{2.86}$$

$$\delta_1 = \frac{1-\varepsilon}{\varepsilon}\beta\left[\frac{R^2\beta}{15}\left(\frac{1}{D_p} + \frac{5}{k_f R}\right)\right] \tag{2.87}$$

Since pulse injections are typically very short (small volume), it can be assumed that the time of the pulse injection (t_0) is insignificant compared to the time it takes for the pulse to reach the end of the column [1]. Thus, t_0 can be eliminated from the expressions for the first and second central moments. Equations (2.44) and (2.45) become:

$$\mu_1 = \frac{L}{u_i}[1 + \delta_0] \tag{2.88}$$

$$\mu_2' = \frac{2L}{u_i}\left[\delta_1 + \frac{D_L}{\varepsilon}(1 + \delta_0)^2\frac{1}{u_i^2}\right] \tag{2.89}$$

Substituting (2.87) and (2.88) into the definition of HETP from plate theory results in:

$$HETP = \frac{L\mu_2'}{\mu_1^2} = \frac{\frac{2L^2}{u_i}\left[\delta_1 + \frac{D_L}{\varepsilon}(1+\delta_0)^2 \frac{1}{u_i^2}\right]}{\left(\frac{L}{u_i^2}\right)[1+\delta_0]^2} = \frac{\left(\frac{u_i}{L}\right)^2\left[\frac{2L^2 D_L}{u_i^3}(1+\delta_0)^2 + \frac{2L^2\delta_1}{u_i}\right]}{[1+\delta_0]^2} \qquad (2.90)$$

Equation (2.90) reduces to:

$$HETP = \frac{2D_L}{\varepsilon u_i} + \frac{2u_i\delta_1}{(1+\delta_0)^2} \qquad (2.91)$$

Substituting (2.88) and (2.89) into (2.91) yields:

$$HETP = \frac{2D_L}{\varepsilon u_i} + \frac{\frac{2(1-\varepsilon)\beta}{\varepsilon}\left[R^2\beta\left(\frac{1}{15}\frac{1}{D_p} + \frac{5}{k_f R}\right)\right]u_i}{\left[1+\left(\frac{1-\varepsilon}{\varepsilon}\right)\beta\right]^2} \qquad (2.92)$$

To make the plate height dependent on superficial velocity instead of interstitial velocity, which is a more practical parameter, $u_i = u_s/\varepsilon$ is substituted into (2.92) to yield:

$$HETP = \frac{2D_L}{u_s} + \frac{2(1-\varepsilon)\beta^2\left[\frac{R^2}{15}\left(\frac{1}{D_p} + \frac{5}{k_f R}\right)\right]u_i}{[\varepsilon+(1-\varepsilon)\beta]^2} \qquad (2.93)$$

To simplify (2.99), α, which is defined to be the total porosity of the column (fraction of entire column volume that is porous) is introduced.

$$\alpha = \varepsilon + (1-\varepsilon)\beta \qquad (2.94)$$

50

Thus,

$$HETP = \frac{2D_L}{u_s} + \frac{2(\alpha - \varepsilon)\beta \left[\frac{R^2}{15}\left(\frac{1}{D_p} + \frac{5}{k_f R} \right) \right] u_i}{\alpha^2} \tag{2.95}$$

Axial dispersion is the combination of effects due to eddy diffusion and molecular diffusion in the axial/longitudinal directions from concentration gradients between the pulse and the liquid/mobile phase. Thus, the axial dispersion coefficient can be expressed as [1]:

$$D_L = \eta' D_{mol} + l u_s \tag{2.96}$$

where η' is the diffusibility of the solute, D_{mol} is the molecular diffusion coefficient, and l is the scale of dispersion. Substituting (2.96) into (2.95) yields:

$$HETP = 2l + \frac{2\eta D_{mol}}{u_s} + \frac{2(\alpha - \varepsilon)\beta}{\alpha^2} R^2 \left(\frac{1}{15 D_p} + \frac{1}{3 k_f R} \right) u_s \tag{2.97}$$

Substituting $R = d_p/2$ into (2.97), where d_p is the average particle diameter in the bed yields the predictive HETP equation under non-binding conditions.

$$HETP = 2l + \frac{2\eta D_{mol}}{u_s} + \frac{(\alpha - \varepsilon)\beta}{\alpha^2} \frac{d_p^2}{2} \left(\frac{1}{15 D_p} + \frac{2}{3 k_f d_p} \right) u_s \tag{2.98}$$

Equation (2.98) assumes the form of:

$$HETP = A + \frac{B}{u_s} + C u_s \tag{2.99}$$

51

where *A* represents the contributions to plate height from eddy diffusion, *B* represents the contributions from molecular diffusion, and *C* represents the contributions due to pore diffusion and film mass transfer. This is the same form as the van Deemter equation, which was developed from empirical results before the work to derive the predictive HETP equation was first published [6]. Figure 2.7 displays a plot of plate height versus superficial velocity for a gas chromatography system carrying n-butane through a sterchamol column as determined by van Deemter. As seen from Figure 2.7, the form of the hyperbolic-linear equation is apparent from the plotted data.
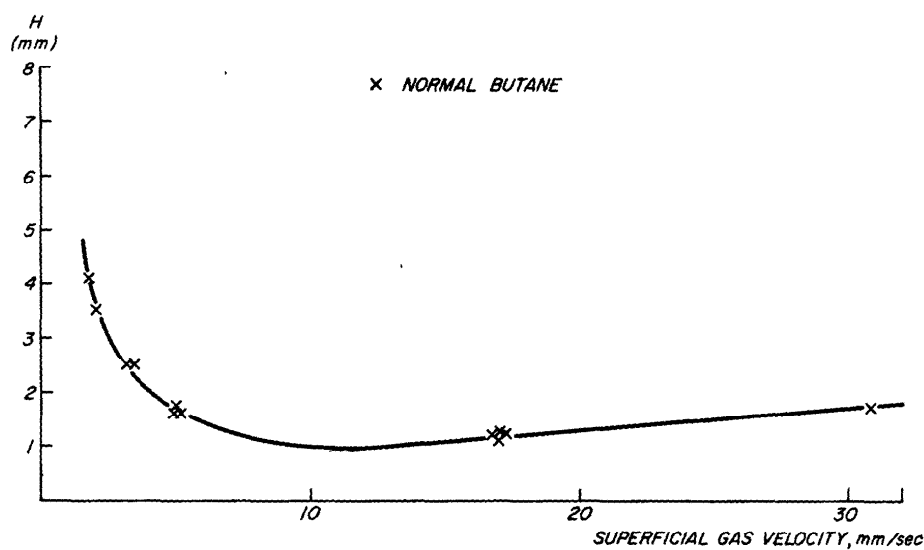
Figure 2.7. HETP versus superficial velocity of n-butane on a sterchamol column as determined by van Deemter [6].

There is an abundance of evidence from the literature that the form of the predictive HETP equation aligns with experimental data. It is for this reason that pulse analysis is a commonly used technique to obtain information on the mass transfer parameters of chromatography systems.

In liquid chromatography systems, such as those used to purify proteins, the effect of molecular diffusion (*B*) on plate height is typically negligible [1]. Thus, the hyperbolic term of the predictive equation is eliminated from the expression.

$$HETP = 2l + \frac{(\alpha-\varepsilon)\beta}{\alpha^2} \frac{d_p^2}{2} \left(\frac{1}{15D_p} + \frac{2}{3k_f d_p} \right) u_s \qquad (2.100)$$

The form of (2.100) is a linear equation, with a slope of C and a y-intercept of A. Figure 2.8 displays a typical plate height versus superficial velocity plots for various liquid chromatography columns as determined by Yamamoto et al. [7]. As seen from Figure 2.8, plate height versus superficial velocity in liquid chromatography takes on a purely linear relationship as opposed to gas chromatography where a hyperbolic relationship exists at low velocities. This is expected since gaseous molecules diffuse much faster compared to molecules in a liquid medium.
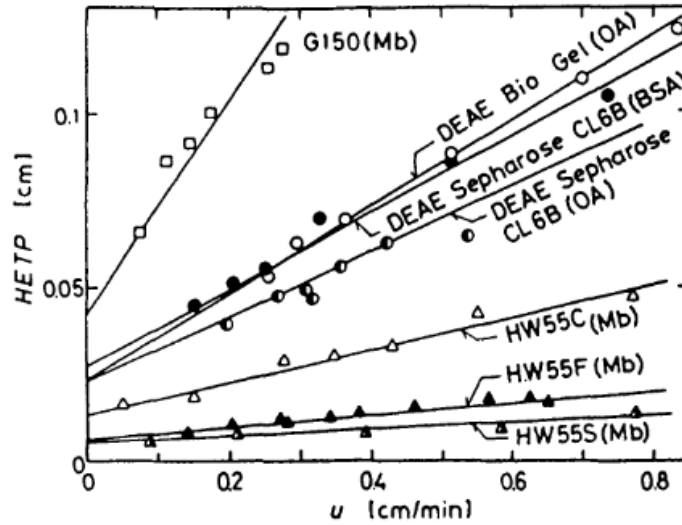
Figure 2.8. HETP versus superficial mobile phase velocity for various liquid chromatography columns as determined by Yamamoto et al. [7]

Neglecting the effect of molecular diffusion also allows for the intercept of the equation to be expressed in terms of the axial Peclet number (Pe_{axial}) [1].

$$D_L = \eta' D_{mol} + l u_s \approx l u_s \qquad (2.101)$$

$$Pe_{axial} = \frac{d_p u_s}{D_L} = \frac{d_p}{l} \qquad (2.102)$$

$$HETP = \frac{2d_p}{Pe_{axial}} + \frac{(\alpha - \varepsilon)\beta}{\alpha^2} \frac{d_p^2}{2} \left(\frac{1}{15D_p} + \frac{2}{3k_f d_p} \right) u_s \qquad (2.103)$$

2.6. Experimental analysis

The predictive HETP equation described in the previous section 2.7 can be utilized in conjunction with experimental data to determine the contributions of axial dispersion, film mass transfer, pore diffusion, and equilibrium binding to the variance (spreading) of the peak produced by a pulse injection. It is therefore possible to quantitatively determine factors such as the film mass transfer coefficient, pore diffusivity, and tortuosity of the bed. This section describes how these values are determined from an experimental plot of plate height versus superficial velocity for pulse injections, as shown in Figure 2.8.

It is first important to note that in practice, pulses are not directly loaded onto the front of the column. In a liquid chromatography system, a pulse is typically injected by a syringe into a series of tubing, connectors, valves, and mixers that feed into the column. When exiting the column, the pulse goes through another series of tubing and connectors that feed into a detector (UV, fluorescence, etc.). The detector ultimately provides the feedback on the pulse that allows for plate height analysis to occur. Due to the laminar velocity profile of the pulse in the tubing, the pulse experiences additional spreading in the flow direction by convective transport and molecular diffusion [2]. Additionally, some backmixing may occur in the tubing, valves, and detector cells.

This effect can be exacerbated by unnecessarily long tubing or poorly fitted connectors. For these reasons, it is always good practice to have the shortest and simplest route between the injector and detector. These effects produce a small but significant 'extra-column variance' (a.k.a. peak spreading) that is not accounted for in the theoretical predictive HETP equation but must be accounted for in experiment.

Extra-column variance and plate height is evaluated by performing pulse injections without the presence of a column but with the same tubing set-up. Figure 2.9 provides an excellent illustration of the effects of extra-column variance and how it is evaluated.
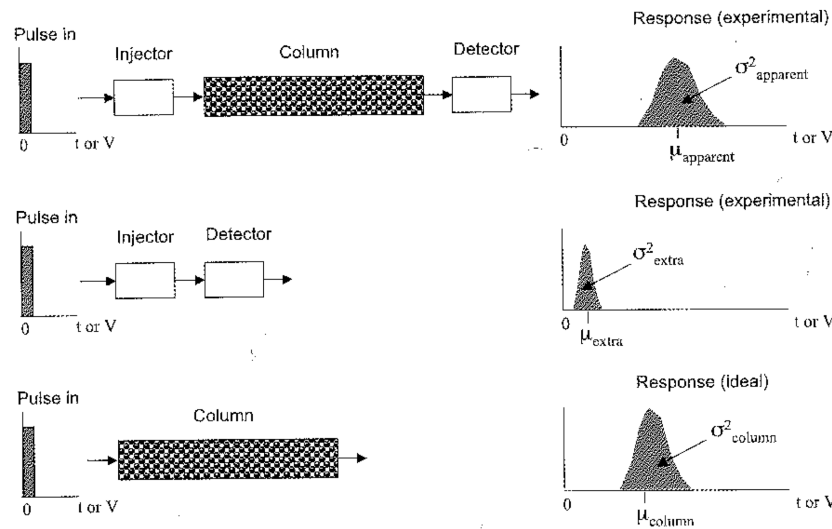
Figure 2.9. Corrections for extra-column effects to apparent peak first moments and variance. Adapted from Carta and Jungbauer [3].

Based on the assumption that the variance of the peak exiting the column is a sum of the variance from extra-column effects and from column effects (mass transfer, adsorption, dispersion, etc.) [2]:

$$\sigma_{total}^2 = \sigma_{column}^2 + \sigma_{ec}^2 \tag{2.104}$$

55

It follows that the plate height is a sum of column and extra column effects [8]:

$$H_{total} = H_{column} + H_{ec}$$

(2.105)

The total plate height and plate height for extra-column effects are determined by [2,8]:

$$H_{total} = \frac{L\mu'_{2,column}}{\mu_{1,column}^2}$$

(2.106)

$$H_{ec} = \frac{L\mu'_{2,no\ column}}{\left(\mu_{1,column} - \mu_{1,no\ column}\right)^2}$$

(2.107)

where the subscripts 'column' and 'no column' refer to the experimentally determined normalized first absolute and second central moments of the pulse with the column attached and without the column attached, respectively.

Returning to equation (2.49), it was shown that the second central moment, or variance, of the pulse was the summation of contributions due to axial dispersion, film mass transfer, pore diffusion, and adsorption. It thus follows that the plate height due to column effects can be expressed as:

$$H_{column} = H_{total} - H_{ec} = H_{Ad} + H_D + H_f + H_L = \frac{2d_p}{Pe_{axial}} + \frac{2\left[\frac{K'}{k_d} + \frac{(\alpha - \varepsilon + K')^2}{K_{OL}a_p}\right]u_s}{(\alpha + K')^2}$$

(2.108)

Under non-binding conditions ($H_{Ad} = 0$):

$$H_{column} = H_{total} - H_{ec} = H_D + H_f + H_L = \frac{2d_p}{Pe_{axial}} + \frac{(\alpha-\varepsilon)\beta}{\alpha^2} \frac{d_p^2}{2} \left(\frac{1}{15D_p} + \frac{2}{3k_f d_p} \right) u_s \qquad (2.109)$$

As discussed in the section 2.7, the predictive HETP equation for liquid chromatography systems has the form $H = A + Cu_s$, where A is the contribution due to axial dispersion and C is the contribution due to pore diffusion and film mass transfer. Thus,

$$H_L = \frac{2d_p}{Pe_{axial}} = 2l \qquad (2.110)$$

$$H_D = \frac{(\alpha-\varepsilon)\beta}{\alpha^2} \frac{d_p^2}{2} \frac{1}{15D_p} u_s \qquad (2.111)$$

$$H_f = \frac{(\alpha-\varepsilon)\beta d_p}{\alpha^2} \frac{1}{3k_f} u_s \qquad (2.112)$$

The superficial velocity (u_s) is determined from the experimentally chosen volumetric flow rate (Q), which is then divided by the column cross-sectional area (A). The column bed length and diameter are typically known values from associated documentation. The bed porosities $(\alpha, \varepsilon, \beta)$ can either be listed in column documentation or can be experimentally determined from pressure drop or inverse-size exclusion chromatography experiments [3]. The average particle diameter in the bed (d_p) is typically listed in column documentation. The film mass transfer coefficient is determined from the dimensionless Sherwood number (Sh), which relates convective to diffusive mass transfer.

$$Sh = \frac{k_f d_p}{D_{mol}} \qquad (2.113)$$

The molecular diffusion coefficient (D_{mol}) can be experimentally determined or calculated from semi-empirical correlations such as the following correlation for globular proteins developed by Tyn and Gusek [9]:

$$D_{mol} = \frac{9.2 \times 10^{-8} T}{M^{1/3} \eta} \qquad (2.114)$$

where T is the operating temperature, M is the molecular weight of the solute molecule, and η is the mobile phase viscosity at the operating temperature. For IgG monoclonal antibodies ($M = 150,000\ Da$) at room temperature in water, the molecular diffusion coefficient is determined to be 3.7×10^{-7} cm^2/s.

For packed beds, the Sherwood number is a function of the dimensionless particle Reynolds number (Re_p) and the dimensionless Schmidt number (Sc) [3].

$$Sh = f(Re_p, Sc) \qquad (2.115)$$

$$Re_p = \frac{u w_s d_p \rho_f}{\mu} = \frac{intertial\ forces}{viscous\ forces} \qquad (2.116)$$

$$Sc = \frac{\mu}{\rho_f D_{mol}} = \frac{viscous\ diffusion}{molecular\ diffusion} \qquad (2.117)$$

The following correlations are available for the Sherwood number, although the best correlation is dependent on system parameters such as Reynolds number and average particle size [3,8] .

$$Sh = 2 + 1.45Re_p^{1/2}Sc^{1/3} \tag{2.118}$$

$$Sh = \left(\frac{1.09}{\varepsilon}\right)Re_p^{1/3}Sc^{1/3} \tag{2.119}$$

$$Sh = 1.85\left(\frac{1-\varepsilon}{\varepsilon}\right)^{1/2}Re_p^{1/2}Sc^{1/3} \tag{2.120}$$

With the above correlations and known constants, it is possible to determine the film mass transfer coefficient and the contributions of plate height due to film mass transfer as a function of superficial velocity. Subtracting film plate height from the total column plate height results in a new linear equation:

$$H_{column} - H_f = H_D + H_L = \frac{2d_p}{Pe_{axial}} + \frac{(\alpha-\varepsilon)\beta}{\alpha^2}\frac{d_p^2}{2}\frac{1}{15D_p}u_s = A + C'u_s \tag{2.121}$$

Plotting the modified experimental data versus superficial velocity produces a line with slope C' that can be used to determine the pore diffusivity:

$$D_p = \frac{(\alpha-\varepsilon)\beta}{\alpha^2}\frac{d_p^2}{2}\frac{1}{15C'} \tag{2.122}$$

The pore diffusivity is related to the bed tortuosity (τ_p) by [8,9]:

$$D_p = \frac{\beta D_{mol}}{\tau_p} \quad \rightarrow \quad \tau_p = \frac{\beta D_{mol}}{D_p} \tag{2.123}$$

The intercept of this plot also allows the axial dispersion coefficient (D_L) to be determined [2]:

$$A = \frac{2d_p}{Pe_{axial}} = 2l \tag{2.124}$$

$$D_L = \eta D_{mol} + lu_s \approx lu_s = \frac{Au_s}{2} \tag{2.125}$$

It should be noted that equation (2.109) is also written in dimensionless form in some literature as [9]:

$$h = a + \frac{1}{30}\left(\frac{\varepsilon}{1-\varepsilon}\right)\left(\frac{\mu_1 - V_0}{\mu_1}\right)^2 \left(\frac{10}{Sh} + \frac{D_{mol}}{D_p}\right)v' \tag{2.126}$$

where $h = HETP/d_p$ is the reduced $HETP$, $v' = u_s d_p / D_0$ is the reduced velocity, and a is a constant that represents the plate height contributions from axial dispersion. Non-dimensionalizing the plate height and velocity facilitates comparisons across multiple columns and systems with different particle sizes and solutes with different rates of diffusion.

Figure 2.10a displays experimentally generated non-binding pulse injections of polyclonal human IgG antibody on a Bio-Rad UNOsphere SUPrA chromatography column by Perez-Almodovar and Carta [10]. As seen in the figure, the effects of peak spreading can be visually

observed as the volumetric flow rate (and superficial velocity) is increased in the column. Figure 2.10b displays a plot of h versus v' for the same pulse injections. Using values of $\varepsilon = 0.35$, $\beta = 0.62$, $D_{mol} = 3.7 \times 10^{-7}\ cm^2/s$, and $d_p = 57\ \mu m$ as well as equation (2.119) for the Sherwood number, values of pore diffusivity $D_p = 8.0 \times 10^{-8}\ cm^2/s$ and tortuosity $\tau_p = 2.8$ were determined for the system.
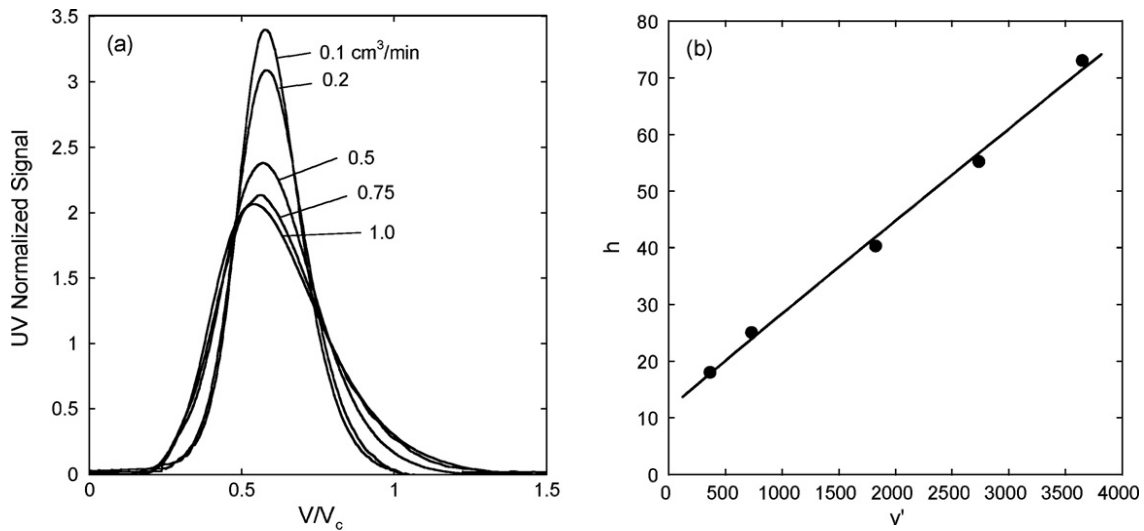
Figure 2.10. (a) Peaks produced by non-binding pulse injections of human polyclonal IgG at various volumetric flow rates on a Bio-Rad UNOsphere SUPrA chromatography column. (b) Reduced plate height (h) versus reduced velocity determined from the pulse injections in (a). Adapted from Perez-Almodovar and Carta [10].

2.7. References

[1] D.S. Clark, H.W. Blanch HW, Biochemical Engineering, Second Edition, CRC Press, 1997.

[2] Arnold, F. H., Blanch, H. W., & Wilke, C. R., "Analysis of affinity separations I: predicting the performance of affinity adsorbers" *The Chemical Engineering Journal*. 30 (1985): B9-B23.

[3] G. Carta, A. Jungbauer A, Protein Chromatography, Process Development and Scale-Up, John Wiley & Sons, 2010.

[4] O. Pazdernik, P. Schneider, Peak moments for gas chromatographic columns with a pressure drop, J Chromatogr A. 208 (1981) 181-191.

[5] R.L. Synge, Experiments on animo-acids: The partition of acetamino-acids between immiscible solvents, Biochem J. 33 (1939) 1913–1917.

[6] J. van Deemter, F. Zuiderweg, A. Klinkenberg, Longitudinal diffusion and resistance to mass transfer as causes of nonideality in chromatography, Chemical Engineering Science. 5 (1957) 271-289.

[7] S. Yamamoto, K. Nakanishi, R. Matsuno, Ion Exchange Chromatography of Proteins, Marcel Dekker, Inc., New York, 1988.

[8] V. Natarajan, S. Cramer, A Methodology for the Characterization of Ion-Exchange Resins, Separation Science and Technology. 35 (2000)1719-1742.

[9] M.Y. Tyn, T.W. Gusek, Prediction of diffusion coefficients of proteins, Biotechnol Bioeng. 35 (1990) 327-328.

[10] E.X. Perez-Almodovar, G. Carta, IgG adsorption on a new protein A adsorbent based on macroporous hydrophilic polymers. I. Adsorption equilibrium and kinetics, J Chromatogr A 1216 (2009) 8339-8347.

3

Competitive Binding Behavior of IgG Antibodies on Protein A Chromatography Resins

This chapter of the thesis was adapted from the article, "Polyclonal and monoclonal IgG binding on protein A resins—Evidence of competitive binding effects," which was published in the journal of Biotechnology and Bioengineering on June 6th, 2017.

3.1. Chapter abstract

Protein A (ProA) chromatography is used extensively in the biopharmaceutical industry for the selective capture of both polyclonal and monoclonal antibodies (mAbs). This work provides a comparison of the adsorptive behavior of a highly heterogeneous polyclonal hIgG with that of a mAb as well as the behavior of their mixtures on representative ProA resins. Both pH gradient elution and frontal loading experiments using human polyclonal IgG (hIgG) reveal a distribution of IgG-ProA binding strengths likely associated with multiple IgG subclasses and the heterogeneity of the variable region. pH gradient analysis of fractions collected along the breakthrough curve demonstrate a clear progression from weaker binding (higher pH eluting) to stronger binding (lower pH eluting) IgG species leaving the column suggesting the possibility of stronger binding species displacing the weaker binding ones. Displacement is directly observed by visualizing the adsorption of fluorescently labeled mAb and hIgG using confocal laser scanning microscopy (CLSM). Here, the displacement behavior of hIgG results in a broad

adsorption front compared to the sharp, 'shrinking core' behavior typically observed with mAbs. Sequential CLSM adsorption experiments with a mAb and hIgG confirm that stronger or equivalent-binding hIgG species are able to displace and desorb bound mAb molecules. These phenomena are examined using a variety of ProA resins including CaptivA PriMAB, MabSelect, and MabSelect SuRe to understand the effect of different ligand properties on binding strength and competition among different IgG species. The results of these comparisons suggest that the competition kinetics are slower with ligands that have a single-point covalent attachment to the base matrix compared to a multi-point attachment.

3.2. Introduction

Protein A (ProA) chromatography is used extensively for the selective capture of antibodies and Fc-fusion proteins [1]. Due to its general applicability, ProA has been widely adopted as the "platform" capture step for mAb manufacturing [2]. The growing market for mAbs and the increasing titers attained by cell culture have driven the development of improved ProA chromatography resins in recent years [3], including modifications to the resin base matrix and pore structure, increased ligand density, enhanced ligand attachment chemistry, and increased alkaline stability.

Regardless of ligand and base matrix chemistry, however, the broad applicability of ProA resins is a result of highly specific interactions between the ligand and the C_H2-C_H3 cleft in the Fc region of the antibody molecule [4]. Since this region is highly conserved, the interactions of different antibodies within the same class are generally thought to be very similar. More recently, however, evidence has also surfaced that different mAbs in the same sub-class can also have significantly different binding and/or elution behaviors. For example, Ghose et al. [5]

demonstrated that a variety of mAbs and Fc-fusion proteins have different static and dynamic binding capacities, and different binding stoichiometries. In another article, Ghose et al. [6] demonstrated that different mAbs and Fc-fusion proteins elute at different pH values, suggesting that the binding strength varies for different mAbs. The reason for these differences has been attributed to secondary IgG variable region (Fab) binding of the heavy chain of antibodies belonging to the V_H3 gene family to wildtype ProA binding domains. Ghose et al. [6] demonstrated that removing these secondary interactions via use of the SuRe ligand, an engineered version of the wildtype B-domain that does not bind to the IgG heavy chain, results in more consistent elution pHs among the same group of antibodies. However, a more recent study by Bach et al. [7] has shown that binding to the Z-domain of the SuRe ligand is still possible among Fab fragments of antibodies from the V_H3 family. Additional studies have suggested that ProA modifications have a direct effect on the elution pH and binding strength of IgG to ProA [8-10].

While the above examples demonstrate that individual mAbs can exhibit different binding and elution behaviors, to our knowledge the behavior of mixtures of antibodies has not been investigated in this regard. An outstanding question is whether a mixture of antibodies can exhibit competitive binding behaviors over practical time scales. Not only is the answer to this question of scientific importance, but also has potential ramifications regarding the interpretation of experimental binding data. For example, human polyclonal IgG (hIgG), which has broad molecular diversity, is often used in breakthrough studies to characterize ProA resins. Non-binding IgG_3 species present in hIgG are easily removed prior to testing, but the question remains as to whether the presence of multiple, distinct antibody species affects the experimental results and whether using a polyclonal mixture is predictive of the binding behavior of a mAb.

Additionally, the answer to this question has ramifications regarding the possibility of operating ProA chromatography processes to resolve antibody heterogeneity by taking advantage of competitive binding effects.

The principal objective of this work is to compare the adsorption behaviors of a highly purified mAb against that of hIgG using three commercial ProA resins. We first study the chromatographic behavior of each resin with regards to static binding capacity, uptake kinetics, and elution pH for hIgG and for the mAb independently. Next, we conduct pH gradient elution experiments with fractions collected from a polyclonal IgG breakthrough curve to assess binding strength. Finally, we use confocal laser scanning microscopy (CLSM) to visualize the spatial and temporal distribution of different protein species within individual ProA particles during transient adsorption.

3.3. Materials and methods

3.3.1. Materials

Three commercial ProA resins, CaptivA PriMAB (Repligen, Waltham, MA), MabSelect and MabSelect SuRe (GE Healthcare, Piscataway, NJ), were used in this work. The resins were packed in 1.2-cm diameter OPUS columns with bed lengths from 4.2 to 4.7 cm by Repligen. The mAb used in this work is an industrially purified IgG_1 antibody (~10 ppm host cell protein) with a pI ~ 8.2 and an extinction coefficient at 280 nm of 1.48 AU•mL•mg^{-1}•cm^{-1}. Based on size exclusion chromatography with a Superdex 200 column from GE Healthcare (Piscataway, NJ, USA), the highly purified mAb used is essentially 100% monomer (aggregate content below detection limit). The hIgG used is a lyophilized powder from Lee BioSolutions (Maryland Heights, MO); an extinction coefficient of 1.36 AU•mL•mg hIgG^{-1}•cm^{-1} was used [11]. The

particular lot of hIgG used in this study was reported by certificate of analysis to have an IgG purity level of $\geq$99% by protein electrophoresis. The hIgG did contain IgG_3 species. Based on absorbance levels produced by species that flowed through the column during breakthrough experiments, we determined this content to be low ($\sim$3.5% of total absorbance at 280 nm). Rhodamine Red™-X and Rhodamine Green™-X succinimidyl ester amine-reactive dyes were from Invitrogen Corporation (Carlsbad, CA). All other chemicals were from Sigma-Aldrich (St. Louis, MO) or Fisher Scientific (Pittsburgh, PA).

hIgG solutions were prepared by dissolving known weights of the lyophilized powder in the desired buffer and passed through a 0.2 μm filter. The dissolved protein concentration was determined from the UV absorbance at 280 nm and was measured with a Cary Bio 300 UV-Vis spectrophotometer (Agilent Technologies, Santa Clara, CA). Either a BioTek plate reader (Winooski, VT) or a NanoDrop 2000 spectrophotometer (Thermo Fisher Scientific, Waltham, MA) were subsequently used for routine measurements. The mAb sample was buffer-exchanged using Amicon Ultra-15 filters with a 100 kDa nominal molecular weight cut-off (EMD Millipore, Billerica, MA) or with PD-10 desalting columns (GE Healthcare, Piscataway, NJ). mAb concentrations were determined using the known extinction coefficient with the NanoDrop 2000 spectrophotometer.

All adsorption experiments were conducted at 22$\pm$2 °C in phosphate buffered saline (PBS) containing 137 mM NaCl, 2.7 mM KCl, 10 mM Na_2HPO_4, and 1.8 mM KH_2PO_4 adjusted to pH 7.0 with 1 M NaOH.

3.3.2. Resin properties

Table 3.1 summarizes the relevant properties of the resins used. All three are based on an agarose backbone, but have different agarose content, ligand chemistry, ligand density, and particle diameter. CaptivA PriMAB is based on 4% cross-linked agarose (Sepharose 4FF) with an average particle diameter of 90 μm and on a recombinant version of Staphylococcal Protein A that has wild type binding domains E, D A, B, and C with multi-point attachment to the agarose backbone via a truncated, lysine-enriched X domain. MabSelect is based on highly cross-linked agarose with an average particle diameter of 85 μm and with a recombinant ProA that contains the same five wild type binding domains and a C-terminal cysteine to enable a directed, single-point attachment to the resin backbone via a thiol linkage. MabSelect SuRe is based on the same backbone as MabSelect, but employs an engineered ligand, which is a tetramer of the so-called Z-domain.

Resin	Base Matrix	Average Particle Diameter (μm)	Protein A Ligand	Ligand Attachment	Ligand Density (mg/mL)
CaptivA PriMAB	4% cross-linked agarose	90	Recombinant Staphylococcal Protein A (rSPA)	Multi-point attachment	10
MabSelect	Highly cross-linked agarose	85	rProtein A	Single-point attachment	5
MabSelect SuRe	Highly cross-linked agarose	85	Alkali-stabilized Protein A	Single-point attachment	6

Table 3.1. Properties of the ProA resins used in this work [2,12-14].

The hydrated resin particle density was measured by first preparing a ~50 % v/v resin slurry in PBS buffer, then separating the hydrated particles from the supernatant by centrifuging the slurry in 0.2 μm centrifugal filters (VWR, Radnor, PA) at 3000×g for 45 min, and finally determining the particle volume with a 10 mL pycnometer. Resin densities were 1.042 ± 0.003 g/mL for CaptivA PriMAB and 1.055 ± 0.001 g/mL for MabSelect and MabSelect SuRe; errors reported represent 95% confidence limits based on triplicate measurements.

3.3.3. Batch adsorption isotherms

The static protein binding capacity was determined by equilibrating samples of each resin with protein solutions of various concentrations and calculating the amount of protein bound by material balance based on the final and initial protein concentrations in solution. For hIgG, known weights of hydrated resin particles (3 to 35 mg) were added to protein solutions (1 to 4.5 mL) in microcentrifuge tubes at initial concentrations ranging from 0.1 to 3.0 mg/mL. The tubes were rotated end-over-end at 18 rpm for 24 h, then centrifuged at 800 rpm for 5 min. The supernatant concentration was measured with the BioTek plate reader. Resin weights and solution volumes were chosen to reduce the supernatant concentration of hIgG to 30-35% of its original value to reduce measurement error. The resin densities were used to convert the weight of hydrated particles to units of volume. Experiments were done in triplicate for each resin.

For hIgG, the data were well described by the Langmuir isotherm, given by:

$$q = \frac{q_{max}KC}{1+KC} \qquad (3.1)$$

where q is the binding capacity in mg per mL hydrated particle, C is the protein concentration in solution at equilibrium, q_{max} the maximum binding capacity, and K the affinity constant. For the

mAb, the static binding capacities were determined using a similar procedure but via a single-point measurement conducted at an initial protein concentration of 3.0 mg/mL in triplicate.

3.3.4. Batch adsorption kinetics

Batch uptake measurements were conducted in a 50 mL beaker with an overhead mixer at 300 rpm. For each measurement, 30 mL of a 2 mg/mL protein solution were placed in the vessel and recirculated through a flow cell in a Cary Bio 300 spectrophotometer at ~20 mL/min with a peristaltic pump. The dead volume of the pump tubing and flow cell was measured from the volume of displaced liquid when purging the system with air. After reaching signal baseline, a known weight of hydrated resin was added to the vessel and mixed for 2 hr. The protein concentration of the recirculating supernatant was continuously measured by UV absorbance at 280 nm and used to calculate the protein bound at each time point. All experiments were repeated in duplicate.

3.3.5. pH gradient experiments

The pH at which the protein elutes from a Pro A column was determined for each resin with a linear pH elution gradient. In these experiments, conducted at a flow rate of 1 mL/min, 100 μL injections of 15 mg/mL protein in PBS were made on an Akta Explorer 10, followed by washing with 3 column volumes (CV) of 25 mM citrate at pH 5.5, and elution with a 10 CV pH gradient from pH 5.5 to pH 2.5 with a constant citrate concentration. Extra-column volume corrections of the UV and pH detectors were obtained by making pulse injections with inlet and outlet lines connected by a low-volume union in place of the column. The Akta system pH detector was calibrated using buffered standards at pH 7.00 and 4.01.

3.3.6. Elution pH of breakthrough fractions

Breakthrough curves for hIgG were obtained for a CaptivA PriMAB column. For this purpose, 300 mL of PBS buffer containing 2.0 mg hIgG/mL were loaded onto the column with the Akta Explorer 10 system at a flow rate of 1.0 mL/min (residence time ~ 5 min). Subsequently, the IgG was eluted using 50 mM glycine, 100 mM NaCl buffer at pH 3.0. The outlet protein concentration was determined by absorbance at 280 nm and the presence of non-binding IgG_3 species was accounted for by subtracting the UV absorbance produced by the flow through protein.

Ten 20-mL fractions were collected along the breakthrough curve and the elution pH of the protein within each fraction was determined. Fraction collection was initiated at 4% breakthrough and continued for a total of 200 mL. Each fraction was concentrated by reducing the volume to about 1 mL with Amicon Ultra-15 centrifugal filters. 500 µL of each of these concentrated fractions was then re-injected into the regenerated ProA column and eluted using the same pH gradient elution protocol described above.

3.3.7. Confocal laser scanning microscopy (CLSM)

Confocal laser scanning microscopy (CLSM) was used to obtain the spatial and temporal distribution of protein species within the ProA resin particles during transient adsorption following the procedure described in Tao et al. and Zhang et al. [15,16]. For the individual adsorption of hIgG and the mAb, both proteins were labeled with Rhodamine Red™-X reactive dye while for the two-component adsorption experiments the mAb was labeled with Rhodamine Green™-X and hIgG was labeled with Rhodamine Red™-X. In both cases, labeling was performed by mixing each protein with the dye in a 3:1 dye:protein molar ratio in 500 mM

sodium bicarbonate buffer at pH 8.5 and incubating in the dark for 1 hour. The unreacted dye was removed by SEC and the labeled protein buffer-exchanged into PBS using Econo-Pac 10DG desalting columns (BioRad Laboratories, Hercules, CA). The molar labeling ratio was calculated using the dye extinction coefficients (120,000 AU•M^{-1}•cm^{-}1 for Rhodamine Red™-X, 68,000 AU•M^{-1}•cm^{-}1 for Rhodamine Green™-X, provided by Invitrogen) and absorbances at 280, 503, and 570 nm for protein, Rhodamine Green™-X, and Rhodamine Red™-X, respectively. The absorbance at 280 nm was adjusted by a correction factor ($0.17 \times A_{570}$ for Red, $0.19 \times A_{503}$ for green) supplied by the manufacturer to account for UV absorption of the dye.Dye/protein labeling ratios ranged from 0.19 to 0.28 depending on the protein and dye used. The labeled protein mixture was further diluted with unlabeled protein to achieve a 1:200 labeled to unlabeled ratio. CLSM experiments were performed with a Zeiss LSM 510 microscope with a Plan-Apochromat 64 x/1.4 NA oil objective (Carl Zeiss MicroImaging, LLC, Thornwood, NY). Due to different binding capacities and particles sizes, incident laser intensities were adjusted for different resins and proteins to optimize the CLSM image and avoid saturating the detector.

The individual transient adsorption CLSM experiments for hIgG and the mAb were conducted by adding less than 1 mg of hydrated resin particles to 5 mL of each labeled protein sample with a 2.0 mg/mL protein concentration, periodically pipetting out 300 μL of the mixture, and rapidly filtering the sample with a microcentrifuge filter to remove the interstitial liquid. The resin particles were then re-suspended in PBS and imaged. To determine whether higher molecular weight species in the polyclonal IgG sample affected the result, similar experiments were conducted with hIgG purified by SEC with a Superdex 200 column (10 mm x 300 mm) at 0.5 mL/min.

Sequential adsorption experiments were conducted by adding less than 1 mg of hydrated resin particles to 0.4 mL of the Rhodamine Green-labeled mAb sample with a 2.0 mg/mL protein concentration, allowing the resin to incubate for 15 min, and rapidly filtering the sample with a microcentrifuge filter to remove the interstitial liquid. The particles were then washed with PBS to remove any free mAb and filtered again to remove the buffer. The partially mAb saturated resin was then transferred with a spatula to a solution containing the Rhodamine Red-labeled hIgG also at a 2.0 mg/mL protein concentration and periodically imaged as described above.

The radial fluorescence intensity profiles from the confocal images were obtained by radially averaging the intensity values within the resin particle. Briefly, the center of each particle was determined by finding the circle of best fit using a digital overlay in MATLAB. A dataset was generated of all pixel intensity values as a function of distance from the center coordinate. Each resulting dataset was binned in steps of 1 pixel and the averaged to complete the averaging for the corresponding radial distance. Units of pixels were converted into length given the resolution of the microscope: 3.584 µm/pixel.

3.4. Results and discussion

3.4.1. Adsorption isotherms

Full adsorption isotherms were obtained for the three resins with hIgG (results in section 2.6). These isotherms were essentially rectangular and reached the maximum binding capacity, q_m, at a protein concentration of ~1 mg/mL for all three resins. For the mAb, the binding capacity was measured in triplicate experiments using an initial concentration of 3 mg/mL. As seen in the Supplementary Materials, all isotherms with hIgG were clearly saturated for all resins well at equilibrium solution concentrations of 1 mg/mL or less. This isotherm behavior is

consistent with that for IgG class antibodies in other ProA characterizations in the literature [13,17-19]. Based on these observations and the previous literature, we considered this single point measurement to be a good approximation for the maximum binding capacity of the mAb while conserving precious material. Table 3.2 shows the corresponding values of q_{max}. As seen from the data, capacities are consistently higher for hIgG compared to the particular mAb used on all resins but follow the same trend in terms of relative capacity among the different resins.

Resin	$q_{max,hIgG}$ (mg hIgG/mL)	$q_{max,mAb}$ (mg mAb/mL)
CaptivA PriMAB	85 ± 1	61
MabSelect	98 ± 3	80
MabSelect SuRe	111 ± 3	86

Table 3.2. Maximum binding capacities, q_{max}, for hIgG and the mAb. Reported error values represent a 95% confidence interval of the fit to multiple repeats of the isotherm points. mAb values were determined via single point measurements at an initial solution concentration of 3 mg/mL.

3.4.2. Batch uptake kinetics

Figure 3.1a shows the batch uptake curves of hIgG on the three resins while Fig. 3.1b shows the mAb uptake results on the CaptivA PriMAB resin, all at an initial protein concentration of 2 mg/mL. The results are shown over a period of 7000 s as percentages of the resins' respective q_m values. As seen from Fig. 3.1a, following a fairly rapid initial uptake, the hIgG curves become very shallow at longer times, reaching only about 73-89% of the static capacity. In contrast, as shown in Fig. 3.1b, essentially 100% of the static capacity was obtained in 2 hr for the mAb on CaptivA PriMAB. The mAb behavior is consistent with the results for another mAb on MabSelect reported by Zhang et al. [19]. The hIgG behavior is consistent with the results of Perez-Almodovar and Carta [18] for adsorption on the UNOsphere SuPrA resin.

However, this behavior is not consistent with the hIgG results of Hahn et al. [17]. These authors reported achievement of the static capacity in about 1 hr, but their maximum capacity was determined with an 8-hour incubation time which may not have been sufficient to attain equilibrium. Combined, these results suggest that adsorption of hIgG on ProA requires a much longer time to achieve saturation as compared to the time required for a mAb.
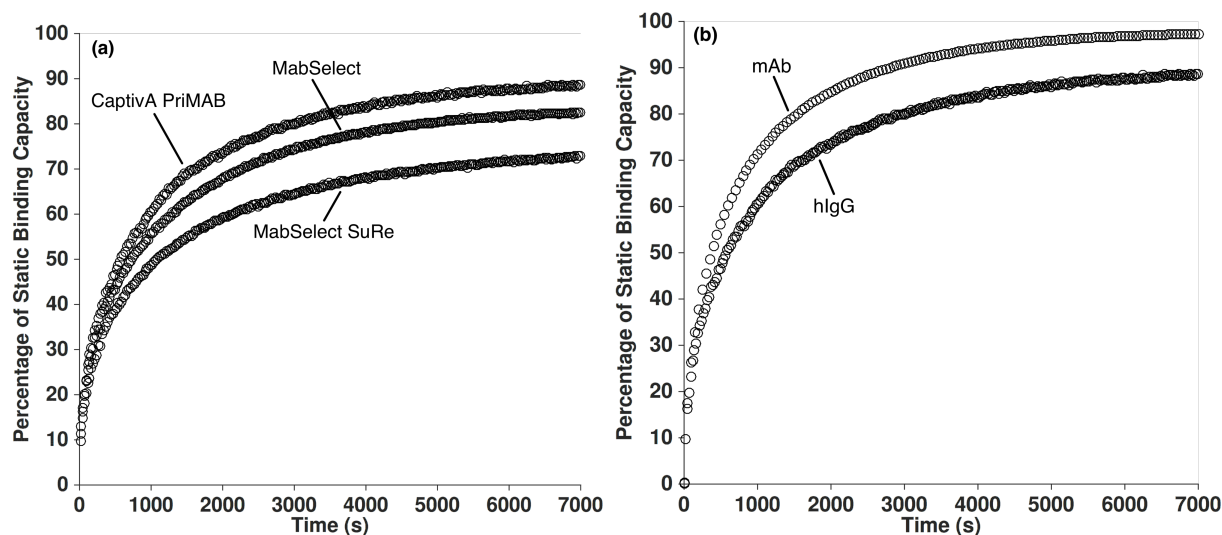
Figure 3.1. (a) Batch uptake curves for hIgG on CaptivA PriMAB, MabSelect, and MabSelect SuRe resins at an initial solution concentration of 2 mg/mL. (b) Batch uptake curves for 2 mg/mL mAb and for 2 mg/mL hIgG on CaptivA PriMAB.

3.4.3. pH gradient elution

Figure 3.2 shows the pH gradient elution profiles for hIgG and for the mAb on the three resins. The profiles are normalized by their respective peak maxima for ease of comparison. As seen in this figure, while the mAb elutes mainly as a single fairly sharp peak, a broader peak with distinct shoulders is evident for the hIgG on all three resins. The elution pH of the main peak (3.6 $\pm$ 0.1) is the same as that of the mAb in all three cases. Both early and late eluting species are evident for both the CaptivA PriMAB and MabSelect resins, while only early eluting species are evident with MabSelect SuRe. The elution similarities between CaptivA PriMAB and MabSelect

75

are consistent with their respective ligand chemistry since both contain a recombinantly produced ProA ligand with the five native binding domains. The ligand attachment chemistry is, however, different for the two resins, which could explain the apparent differences between the two resins in terms of resolution of the early and late eluting species from the main peak. The paucity of low pH eluting species seen for MabSelect SuRe may be attributed the nature of the SuRe ligand that minimizes secondary interactions with the IgG variable region, thus reducing the heterogeneity of binding strengths from hIgG. Ghose et al. [6] have also reported different elution pH values for different mAbs, but attributed this effect to variable region interactions with the ligand.
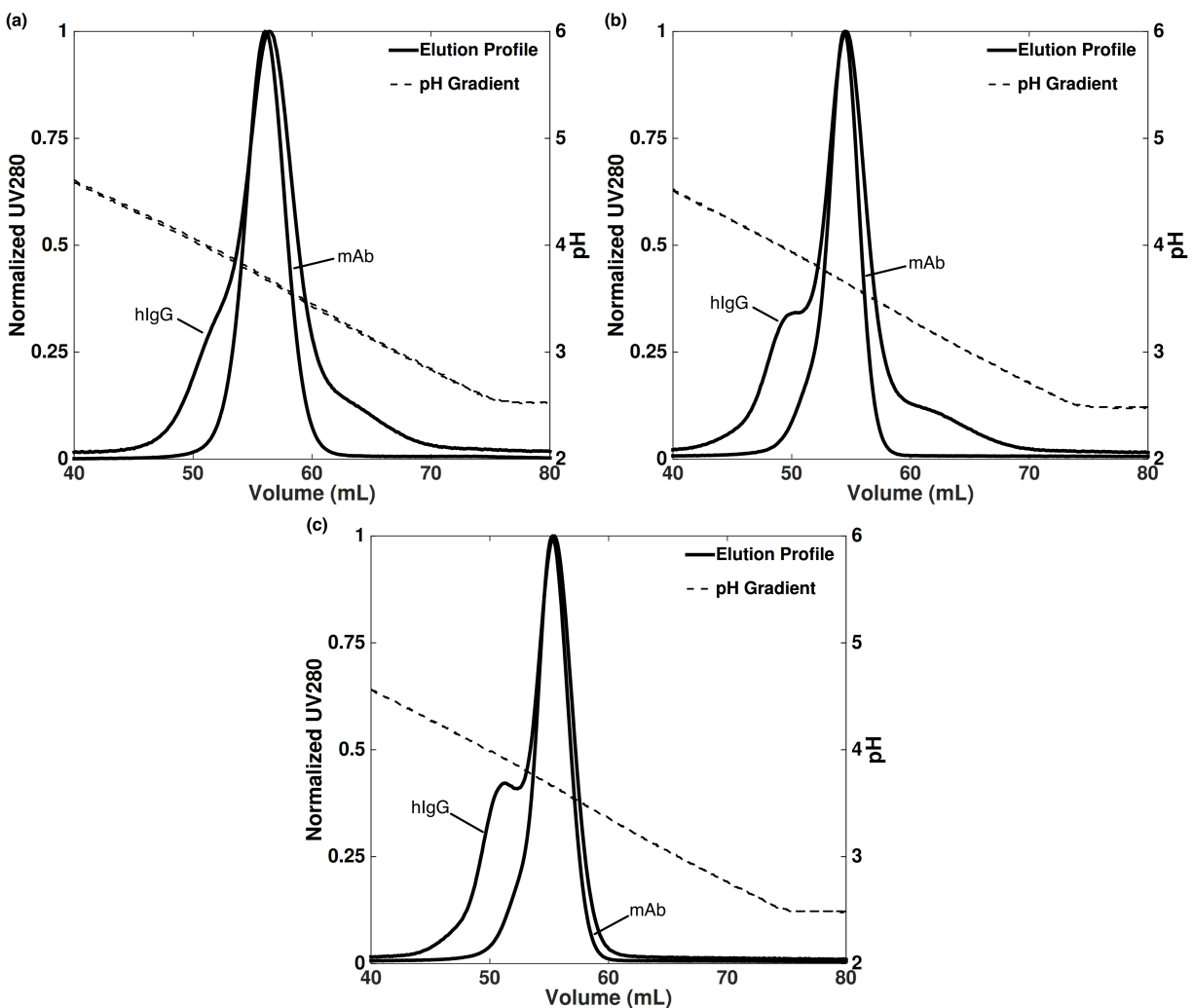
Figure 3.2. Normalized pH gradient elution profiles of polyclonal IgG and the mAb on (a) CaptivA PriMAB, (b) MabSelect, and (c) MabSelect SuRe.

The similarity of the hIgG elution profiles for CaptivA PriMAB and MabSelect suggests that three main groupings of binding strength exist in the polyclonal IgG sample, perhaps associated with the three IgG sub-classes IgG_1, IgG_2, and IgG_4 that are known to bind to ProA. This explanation is consistent with the work of Ey et al. [20] and Duhamel et al. [21] who successfully fractionated sub-classes of mouse and human IgG from serum on ProA-Sepharose with pH gradient elution. Papadea and Check [22] reported an IgG sub-class distribution in human serum of 66%, 23%, and 4% by mass for IgG_1, IgG_2, and IgG_4, respectively, which is

consistent with similar measurements by Duhamel et al. [21] upon analysis of collected fractions. Duhamel et al. [21] obtained profiles similar to Figs. 3.2a-b upon fractionation of human serum. Here, Duhamel et al. [21] determined that the high pH eluting species (first peak) was 95% IgG_2 while the remaining fraction of species was predominantly IgG_1. While the profile obtained by Duhamel et al. [21] also included a low pH shoulder seen in Figs. 3.2a-b, a sub-fraction that isolated this shoulder was also predominantly IgG_1 species. IgG_4 species were found to be evenly distributed among all peaks. With this considered, the mAb used in this work, which is an IgG_1, falls within expectations by aligning well with the predominantly IgG_1 main peak of hIgG. Finally, given that the low pH shoulder is not present in the hIgG elution profiles generated on MabSelect SuRe, it is likely that the species in that peak are predominantly IgG_1 that have a stronger binding strength due to secondary Fab interactions. While additional analysis is required to confirm that the species in the low pH shoulder have these secondary interactions, this work suggests IgG elution pH from ProA is dependent on both variable region interactions and IgG sub-class.

Figure 3.3 shows the breakthrough curve obtained by loading the CaptivA PriMAB column with hIgG (Fig. 3.3a) along with the pH gradient elution behavior of the 10 fractions collected along this curve (Fig. 3.3b). As seen in Fig. 3.3a, the breakthrough curve is initially relatively steep, but becomes very shallow as time goes on. This behavior is consistent with the batch uptake curve behavior shown in Fig. 3.1a and is similar to the behavior reported by Perez-Almodovar and Carta [18] for a different ProA resin. This article attributed the observed behavior to the potential existence of multiple ligand orientations, resulting in slow and fast binding kinetics. However, in our case, the pH gradient elution behavior of the fractions collected along the breakthrough curve suggests that different IgG species emerge from the

column at different times. As seen in Fig. 3.3b, the early fractions contain predominately species that elute at higher pH (which we call "weaker binding") while the later fractions contain mainly species that elute at lower pH (which we call "stronger binding"). Combined, these results suggest that the tailing behavior of the breakthrough curve is associated with the different binding strengths of the IgG species present in the polyclonal sample. The weaker binding species emerge early from the column, likely being displaced by the stronger binding species. Interestingly, this explanation is analogous to that provided by Hunter and Carta [23] for the tailing behavior observed when a mixture of bovine serum albumin (BSA) monomer and dimers is loaded on an anion-exchange resin. There, Hunter and Carta [23] demonstrated that the tailing of the breakthrough curve results from the displacement of BSA monomers by BSA dimers. While such competitive binding of monomer and dimer species is expected given the mechanisms governing anion-exchange chromatography, it is indeed surprising to see this behavior reprised in the competitive binding of antibody species on ProA resins, given the strong binding indicated by the rectangular isotherms.
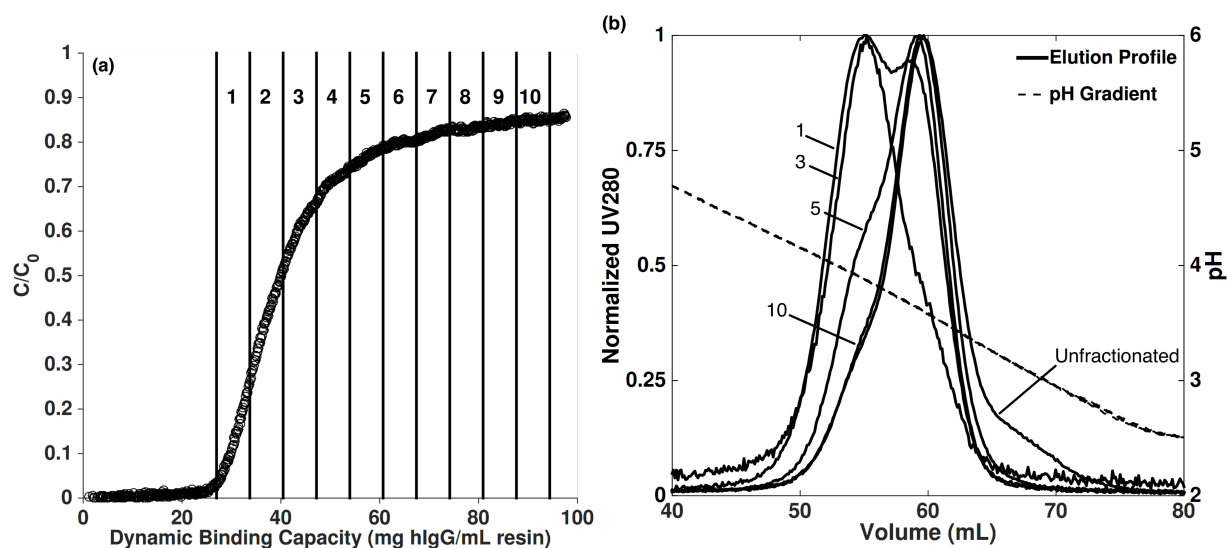
Figure 3.3. (a) hIgG breakthrough curve on CaptivA PriMAB shown along with fraction collection windows. (b) Normalized pH gradient elution profiles of Fractions 1, 3, 5, and 10 from the breakthrough curve in (a) reinjected on CaptivA PriMAB overlaid with the peak obtained for the unfractionated hIgG sample.

It should be noted that severely restricted pore diffusion was also considered as an explanation for the long saturation times observed in the batch uptake and breakthrough curves with hIgG. However, values of effective diffusivity for hIgG in CaptivA PriMAB attained from HETP experiments conducted under non-binding conditions and subsequent van Deemter analysis (see section 3.6) suggested that antibody diffusion was not severely restricted in the pores. Thus, the significant tailing in the breakthrough curve suggests a very slow approach to saturation and that the displacement process is likely affected by kinetic resistances.

3.4.4. CLSM adsorption experiments

Figure 3.4 compares the hIgG and mAb adsorption results on the CaptivA PriMAB resin. Although images were obtained for up to 24 hours, representative images are shown only at 15 and 30 min for resin particles of comparable size (Fig. 3.4a). As seen in this figure, hIgG gave a much more diffuse and slower moving front compared to the sharp front obtained with the mAb.

80

These differences are better appreciated with reference to Figs. 3.4b and 3.4c, which show the corresponding digitized intensity profiles. For hIgG, it is evident that a certain amount of protein reaches the center well before the particle is completely saturated. This behavior is consistent with the presence of weaker and stronger binding species that compete for binding sites [15,24]. On the other hand, the sharp front observed for the mAb is consistent with the highly favorable binding of a single species by a pore diffusion controlled mechanism [25]. CLSM experiments repeated with SEC purified hIgG monomer gave the same results, confirming that the observed transient adsorption behavior is not affected by the presence of aggregates (see section 2.6).
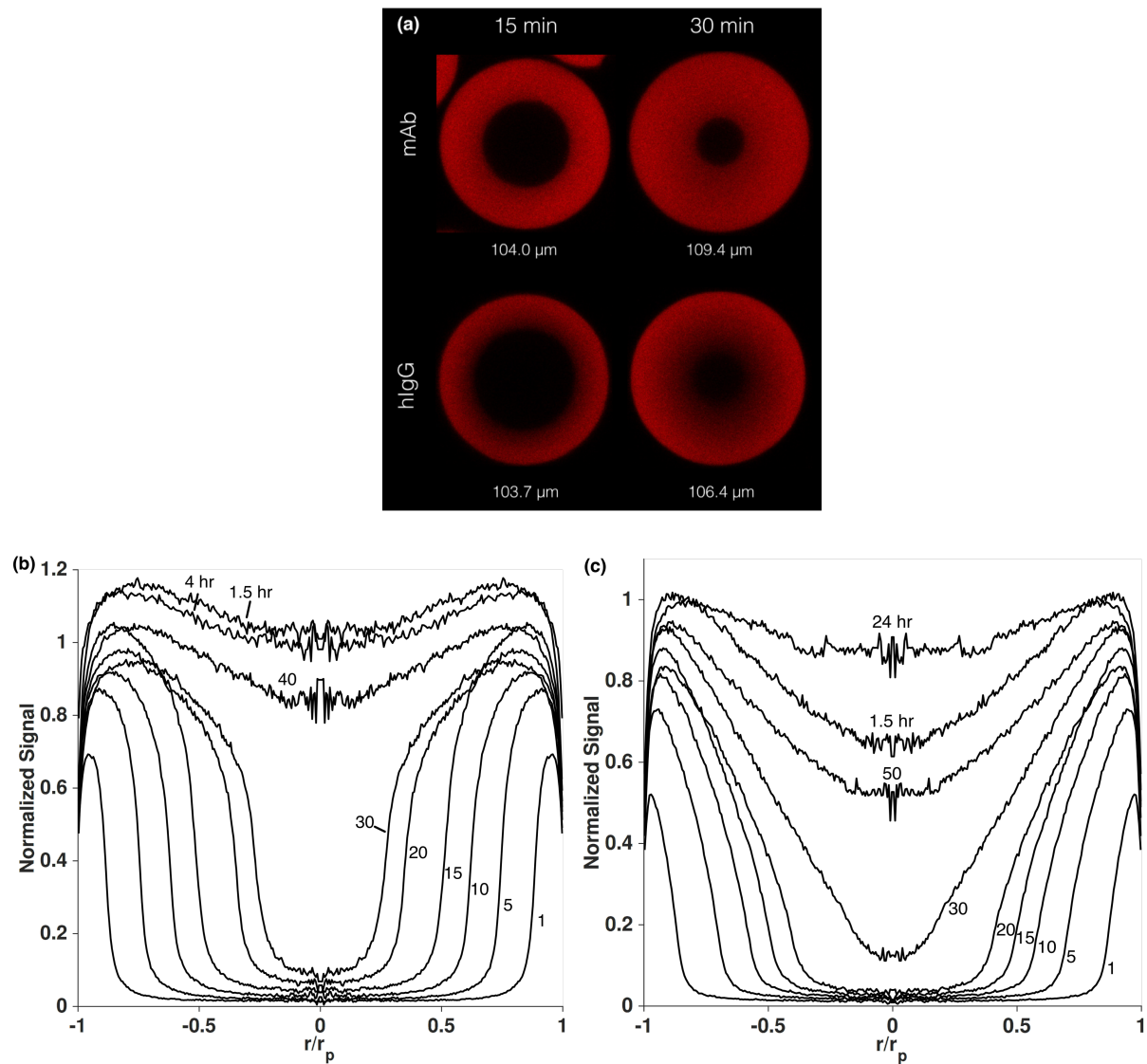
Figure 3.4. (a) Representative CLSM images of the mAb (top row) and hIgG (bottom row) adsorbing onto CaptivA PriMAB resin particles with similar diameters at 15 min (left column) and 30 min (right column). Normalized, radially averaged intensity profiles obtained from the CLSM images are shown for the mAb in (b) and for hIgG in (c) hIgG. Time labels without specified units on (b) and (c) represent minutes.

Sequential adsorption experiments were performed with Rhodamine Green-X™ labeled mAb and Rhodamine Red-X™ labeled hIgG. In this case, the mAb was first loaded onto the resin for 15 min at 2.0 mg/mL. The mAb-loaded resin was then washed with PBS and thereafter exposed to 2 mg/mL hIgG for up to 4 hr. Here, it was hypothesized that the fraction of hIgG

species that had a lower elution pH, or higher binding strength, (see Fig. 3.4a-c) would compete with and ultimately displace the pre-bound mAb. Figures 3.5a-c shows the corresponding CLSM images for the three resins. Times shown are counted from the beginning of resin exposure to hIgG. Figures 3.6a-c display the corresponding intensity profiles. It was assumed that the integrated fluorescence intensity was proportional to the adsorbed IgG concentration in the resin (q_t). mAb integrated intensities were normalized to initial values (at t = 0) while hIgG integrated intensities were normalized to final values (at t = 4 h), where they achieved their respective maxima. The radial intensity profiles were integrated over the particle surface area via:

$$\frac{q_t}{q_{t,max}} = \frac{\int_0^1 I_t(\rho)\rho^2 d\rho}{\int_0^1 I_{t,max}(\rho)\rho^2 d\rho} \tag{3.2}$$

where $I_t(\rho)$ is the fluorescence intensity at dimensionless radial position, $\rho = r/r_p$.

As seen in Figs. 3.5a and 3.6a for CaptivA PriMAB, the hIgG quickly displaced a substantial portion of the pre-bound mAb. In turn, the displaced mAb initially diffused from the outer shell, where it was initially bound, into the core of the particle while the hIgG continued to increase in intensity from the surface of the particle towards the core. After 4 hr, both the mAb and hIgG had nearly uniform intensities throughout the particle with only about $33 \pm 3\%$ of the initially bound mAb still present in the resin. These observations are consistent with the pH gradient elution results for the fractions collected along the hIgG breakthrough curve (Fig. 3.5b), which suggested that stronger binding hIgG species displaced weaker binding species resulting a distribution of binding strengths along the breakthrough curve.

Figures 3.5b and 3.6b display the sequential adsorption results on MabSelect. As seen in Fig. 3.5b, sequential adsorption of mAb followed by hIgG produced two distinct regions in the resin particles. In this case, the mAb mostly remained mostly in its initially adsorbed position

and was not quickly displaced into the inner core of the resin particles. While it can be seen that there was in fact competition and desorption of the mAb, which was reduced to $57 \pm 3\%$ of its initial bound concentration after 4 hr of incubation, the competition was clearly occurring over longer time scales. hIgG diffused through the mAb-saturated outer shell and occupied the free binding sites in the core of the particle. The adsorbed hIgG concentration intensified in the outer shell of the particles over time due to displacement of the mAb, but did not reach uniformity across the particle at 4 hr likely due to the slower binding kinetics.

Sequential adsorption behavior on MabSelect SuRe was consistent with that on MabSelect, as seen in Figs. 3.5c and 3.6c. This is a particularly interesting result as this resin did not resolve lower pH eluting species compared to CaptivA PriMAB and MabSelect. Since the extent of desorption of the mAb was similar from MabSelect and MabSelect SuRe at 4 hr ($57 \pm$ 7%), these results suggest that species of equivalent or near equivalent elution pH were also capable of displacing each other on the resin. The competition was slower in both MabSelect resins compared to that in CaptivA PriMAB, which is consistent with the batch uptake curves shown in Fig. 3.1a, since both MabSelect resins achieved a smaller proportion of static binding capacity after 7000 s of incubation. Combined, these results suggest that the speed of the displacement phenomena depends on the ProA ligand attachment chemistry. A possible explanation for this is that the single-point attachment of the ProA on the MabSelect resins allows for more ligand flexibility, resulting in multiple binding events for a given IgG molecule per ligand, and thus a higher binding strength, rather than in displacement from the ProA. This explanation is consistent with the fact that IgG_1, IgG_2, and IgG_4 species contain two functional ProA binding sites on the Fc region of the antibody [26,27]. In fact, Tustian et al. [28] recently demonstrated that removing one of these Fc binding sites via protein engineering resulted in

higher elution pHs, and thus lower binding strengths, for multiple ProA resins due to reduced ligand avidity.

(c) | 1 min | 15 min | 30 min | 60 min | 4 hr

mAb

hIgG

96.9 µm | 96.1 µm | 97.6 µm | 99.7 µm | 96.5 µm
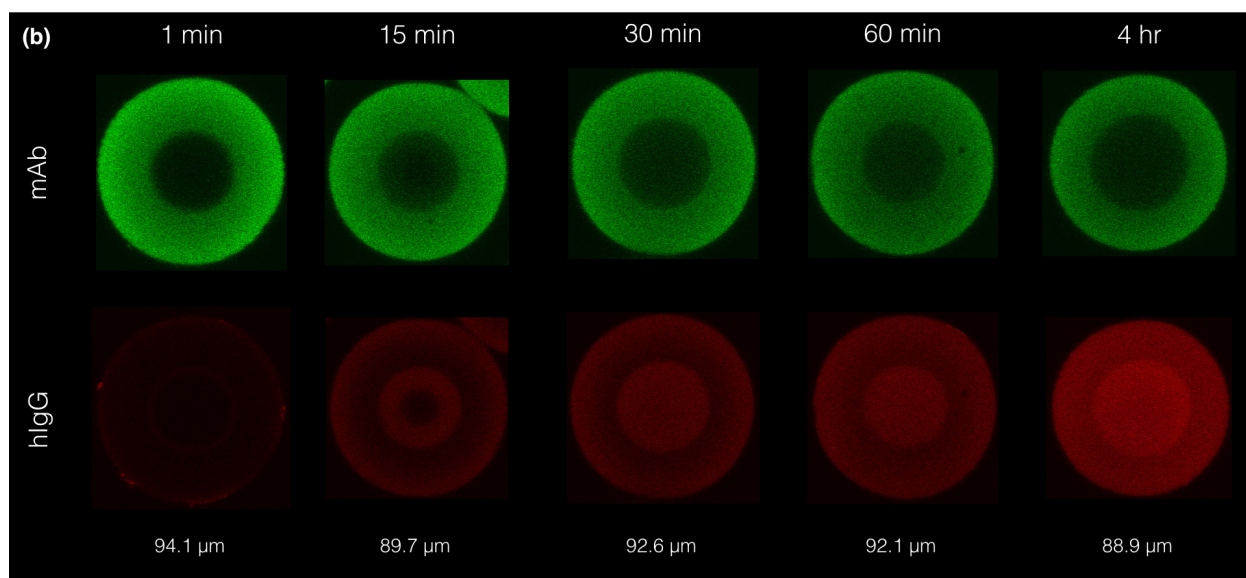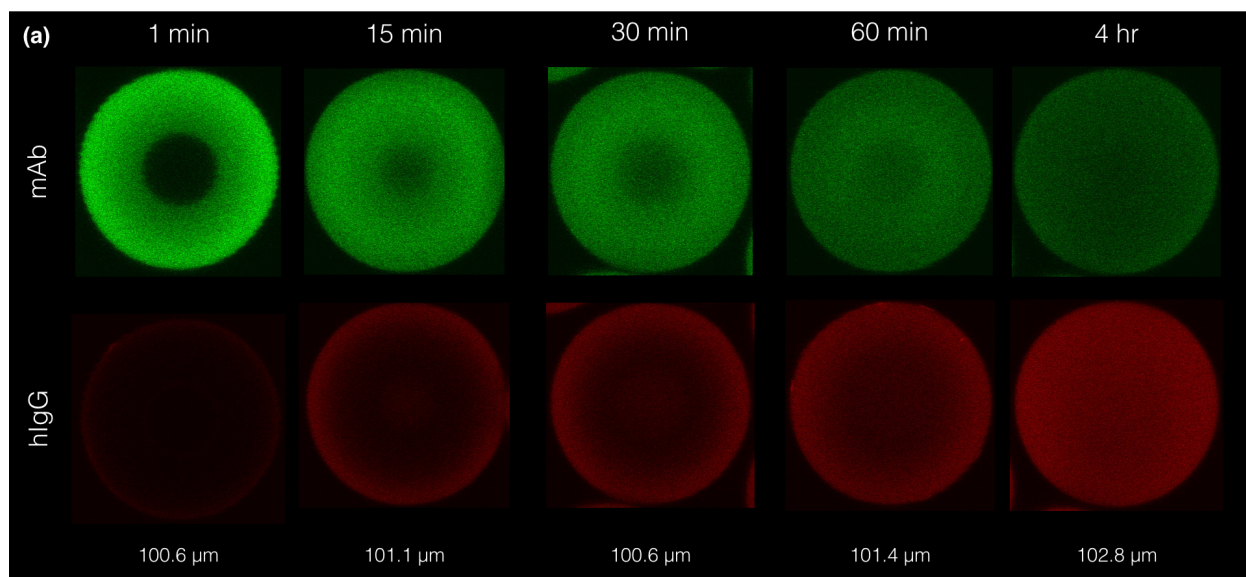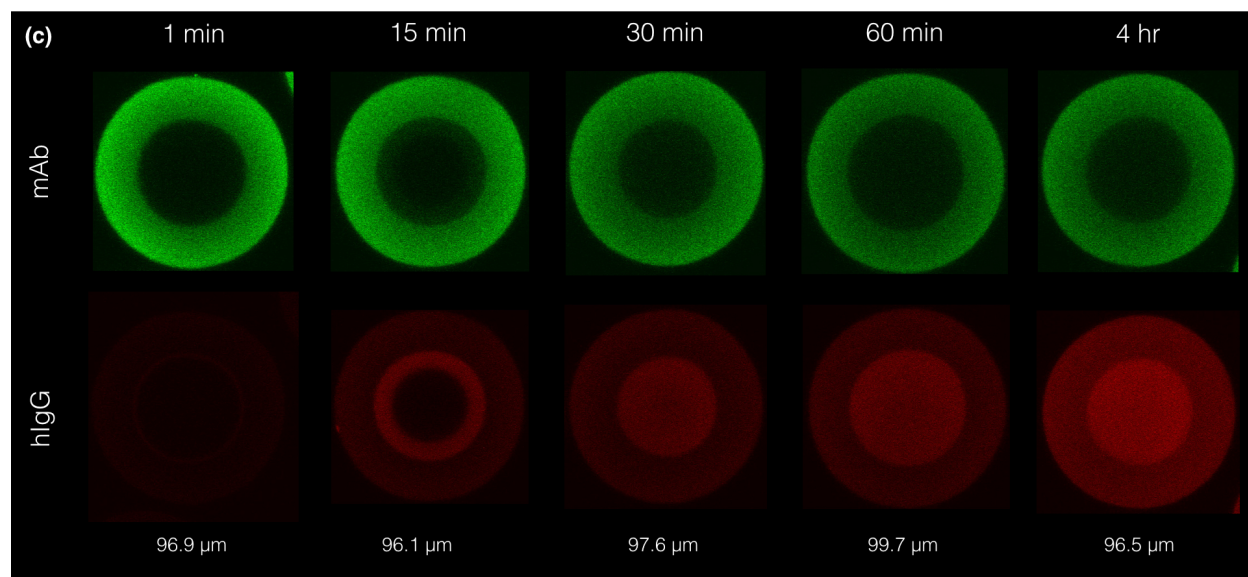
Figure 3.5. Representative CLSM images of sequential mAb-hIgG adsorption experiments showing mAb (top row, green dye) and hIgG (bottom row, red dye) at time periods of 1, 15, 30, 60, and 240 min incubation with hIgG solution for (a) CaptivA PriMAB, (b) MabSelect, and (c) MabSelect SuRe.
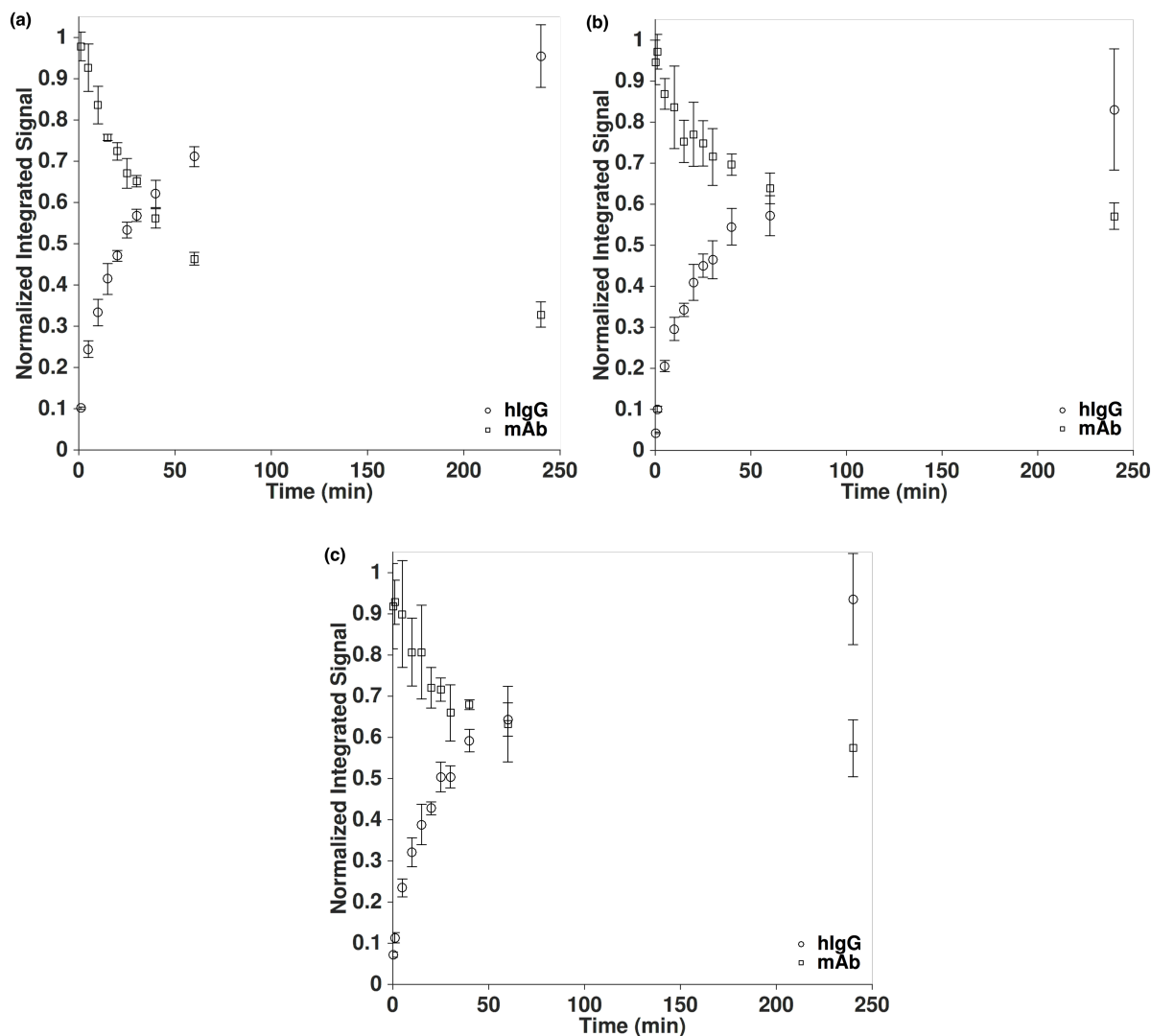
Figure 3.6. Normalized integrated fluorescence signal of CLSM images over 240 min of incubation with hIgG solution for hIgG and the mAb during sequential mAb-hIgG adsorption experiments on (a) CaptivA PriMAB, (b) MabSelect, and (c) MabSelect SuRe. mAb integrated intensities were normalized to initial values (at t = 0) while hIgG integrated intensities were normalized to final values (at t = 4 h).

3.5. Conclusions

Our results demonstrate that IgG molecules of varying binding strength and elution pH, compete for binding sites during simultaneous and sequential adsorption on typical ProA resins. Due to the many species and sub-species present in hIgG, there is a distribution of elution pH and, thus, binding strengths that is evident in pH gradient elution experiments. For recombinant

ligands with the five native ProA binding domains, the three main groups of binding strength point to IgG_2, IgG_1, and IgG with secondary Fab interactions as the underlying cause of this behavior. For the SuRe ligand, there are two main groups of binding strength due to reduced heterogeneity from minimization of Fab interactions.

Competitive binding during adsorption of hIgG was confirmed on the CaptivA PriMAB resin by the shifting pH gradient elution profiles of fractions sampled along the breakthrough curve. This result shows that IgG species of low elution pH, or higher binding strength, displace species of higher elution pH, or weaker binding strength. This competition results in long saturation times and a diffuse adsorption front compared to a single-component mAb. Sequential adsorption of a mAb followed by hIgG monitored by CLSM reveal that competition among species exists in all three resins studied. However, quantitative differences suggests that the competitive adsorption and displacement kinetics are slower in resins with a single-point ligand attachment as compared to a multi-point ligand attachment due to the increased avidity permitted by the more flexible attachment chemistry.

Given the clear differences in adsorption behavior between hIgG and mAbs, care should be taken when setting expectations for resin performance for mAbs based on resin performance characterizations produced with hIgG. In this work, it was determined that the particular lot of hIgG used had consistently and significantly higher values of q_{max} and a different adsorption kinetic profile compared to the particular mAb used.

3.6. Appendix

3.6.1. Evaluation of adsorption equilibrium via static binding isotherms

Static binding isotherms for each resin were performed to determine static binding capacities, q_{max}, and equilibrium affinities, K, for hIgG at neutral pH. Briefly, a known weight of hydrated resin particles was added to set volumes of hIgG solution in centrifuge tubes at known initial solution concentrations, C, ranging from 0.1 to 3.0 mg lyophilized hIgG powder/mL. The hIgG was dissolved in PBS adjusted to pH 7.0, which was used as an IgG loading buffer for all experiments. Every concentration was measured in triplicate for each isotherm and every isotherm was completed in duplicate on separate days for each resin. Resin weights ranged from 3 to 35 mg and hIgG volumes ranged from 1 to 4.5 mL depending on the particular IgG concentration used. The resin weights and solution volumes for each experiment were chosen to reduce the supernatant concentration of hIgG to 30-35% of its original value at equilibrium to reduce measurement error. After adding the resin, the tubes were allowed to rotate end-to-end at 18 rpm for 24 hours to achieve equilibrium. After incubation, the tubes were gently centrifuged at 800 rpm for 5 min and the supernatant concentration was measured on a BioTek plate reader. Subsequently, a mass balance was performed to determine the adsorbed protein concentration, q. The resin densities were used in the mass balance to convert the weight of the hydrated resin particles to units of volume. The static binding capacities and equilibrium affinities for each isotherm were determined via fits of the data to the Langmuir isotherm. Values of q_{max} are reported in Table 3.2 while values of K ranged from 83 ± 27 to 110 ± 39 mL/mg, which are consistent with the rectangular shape of the isotherm.

Figure 3.7 displays the full adsorption isotherms for CaptivA PriMAB, MabSelect, and MabSelect SuRe resins along with the associated Langmuir fits used to determine values of q_{max} as reported in Table 3.1.
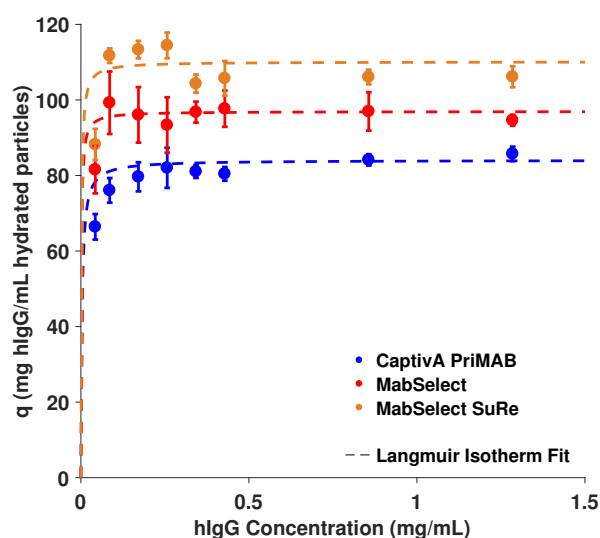
Figure 3.7. Static binding isotherms of hIgG on CaptivA PriMAB (blue), MabSelect (red), and MabSelect SuRe (orange) resins. Dotted lines represent fits of the Langmuir isotherm. Error bars represent 95% confidence intervals of triplicate measurements.

3.6.2 Evaluation of mass transfer resistance via HETP and van Deemter analysis

The mass transfer resistance of the CaptivA PriMAB resin was evaluated from the effective hIgG pore diffusivity, D_e, determined by HETP and subsequent van Deemter analysis under non-binding conditions. Triplicate injections of 100 µL of 2.0 mg lyophilized hIgG powder/mL were performed on each column at flow velocities ranging from 37 to 106 cm/hr using a Waters 2690 HPLC monitored by a Waters 996 PDA detector at 280 nm. The hIgG was dissolved in a 50 mM glycine, 100 mM NaCl buffer at pH 3.0, which was also used as the mobile phase during these experiments. The non-binding peaks produced by the injections were baseline corrected and fit to an exponentially-modified Gaussian (EMG) function to determine

90

the normalized first and second central statistical moments, μ_1 and μ'_2. The retention volume of each injection was determined from μ_1. The EMG function is given by:

$$EMG(t) = \frac{A}{2\tau} \exp\left\{\frac{\sigma^2}{2\tau^2} + \frac{t_g - t}{\tau}\right\} \left[\text{erf}\left\{\frac{t - t_g}{\sigma\sqrt{2}} - \frac{\sigma}{\tau\sqrt{2}}\right\} + 1\right] \qquad (3.3)$$

with moments

$$\mu_0 = A, \quad \mu_1 = t_g + \tau, \text{ and } \mu'_2 = \sigma^2 + \tau^2 \qquad (3.4)$$

In equations 3.3 and 3.4, A is the peak area, t_g is the retention time of the Gaussian component, σ^2 is the variance of the Gaussian component and τ is the time constant for the exponential decay component. The EMG function represents an approximation of the effect of back–mixing on a translating and diffusing one-dimensional point source. Figure 3.8 shows a representative fit of the EMG function to a non-binding IgG pulse injection peak produced a flow rate of 1.25 mL/min on Captiva PriMAB.
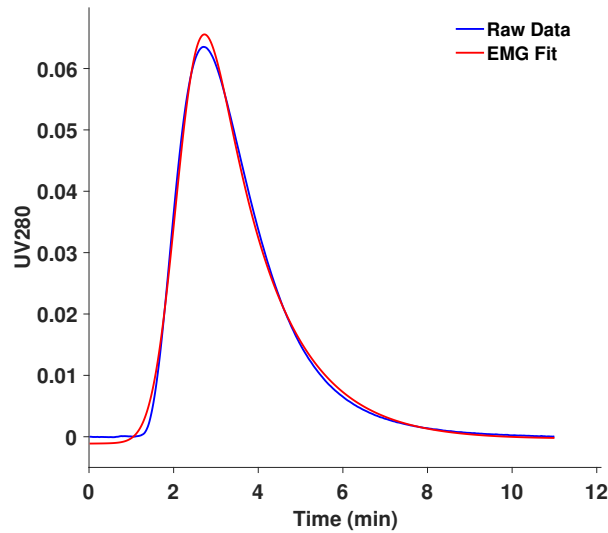
Figure 3.8. Representative fit of the EMG function to a non-binding IgG pulse injection peak produced a flow rate of 1.25 mL/min on Captiva PriMAB.

The experiments were repeated by replacing the column with a union fitting to correct for the extra-column contributions to the moments. Additionally, 0.22 mL was subtracted from the

retention volume to account for the column frit dead volume contribution, as determined by Repligen. These experiments provided the corrected retention volume, V_R.

The height equivalent to a theoretical plate, $HETP$, for each flow rate was determined by

$$HETP = \frac{\mu_2' L}{\mu_1^2} \tag{3.5}$$

where L is the column bed length.

The effective pore diffusivity of hIgG was determined from the corresponding van Deemter plot of reduced plate height, $h = HETP/d_p$, versus the reduced velocity, $v' = u_s d_p / D_0$. Here, d_p is the average particle diameter of the resin reported in Table 3.1, u_s is the superficial mobile phase velocity, and D_0 is the bulk diffusivity of IgG, estimated to be 3.7×10^{-7} cm^2/s from the correlation described by Tyn and Gusek [29]. The moment solution of the general rate model of chromatography under non-binding conditions, and with mass transfer resistances resulting from both film and pore diffusion, provides the connection between the linear slope of the van Deemter plot and D_e [30],

$$h = a + \frac{1}{30}\left(\frac{\varepsilon}{1-\varepsilon}\right)\left(\frac{V_R - V_0}{V_R}\right)^2 \left(\frac{10}{Sh} + \frac{D_0}{D_e}\right) v' \tag{3.6}$$

where a is a constant approximating axial diffusion and dispersion contributions to h, ε is the column interstitial porosity, V_0 is the interparticle void volume, and Sh is the Sherwood number. The column interstitial porosity, ε, was determined from the corrected retention volume of 100 μL injections of a 10 μg/mL solution of lambda DNA onto the columns (V_0) as monitored by a Waters 996 PDA detector at 260 nm, $\varepsilon = V_0/V_C$. V_C is the column bed volume based on the given column dimensions. Lambda DNA, with a molecular weight of 31.5 MDa, was excluded

from all pores of the resin [31]. The Sherwood number was estimated from a correlation expression developed for mass transfer in packed beds [30].

$$Sh = \frac{1.09}{\varepsilon} Re_p^{0.33} Sc^{0.33} = \frac{1.09}{\varepsilon} \left(\frac{\rho u d_p}{\eta} \right)^{0.33} \left(\frac{\eta}{\rho D_0} \right)^{0.33},$$ (3.7)

where Re_p is the particle Reynolds number, Sc is the Schmidt number, ρ is the density of the mobile phase fluid, $u = u_s/\varepsilon$ is the linear velocity of the mobile phase, η is the viscosity of the mobile phase fluid, d_p is the resin average particle diameter from Table 3.1, and D_0 is the IgG free solution diffusivity.

The accessible particle porosity for IgG molecules, β_{IgG}, for the resin was determined using [32]:

$$\beta_{IgG} = \frac{V_{hIgG} - V_0}{V_C - V_0}$$ (3.8)

where V_{hIgG} is the corrected retention volume of non-binding hIgG species.

Figure 3.9a shows representative non-binding IgG pulse injections over a series of increasing flowrates. Figure 3.9b shows a van Deemter plot for hIgG on the CaptivA PriMAB column. As seen from Figure 3.9a, the peaks become broader and asymmetrical as the flow rate is increased due to the smaller particle residence time [18]. As seen from the Figure 3.9b, the HETP data fit well to a straight line as expected from the van Deemter equation. The slope of the linear fit, along with a β_{IgG} value of 0.65 ± 0.01, was used to determine the final D_e value of 7.5 $\pm 0.5 \times 10^{-8}$ cm^2/s.
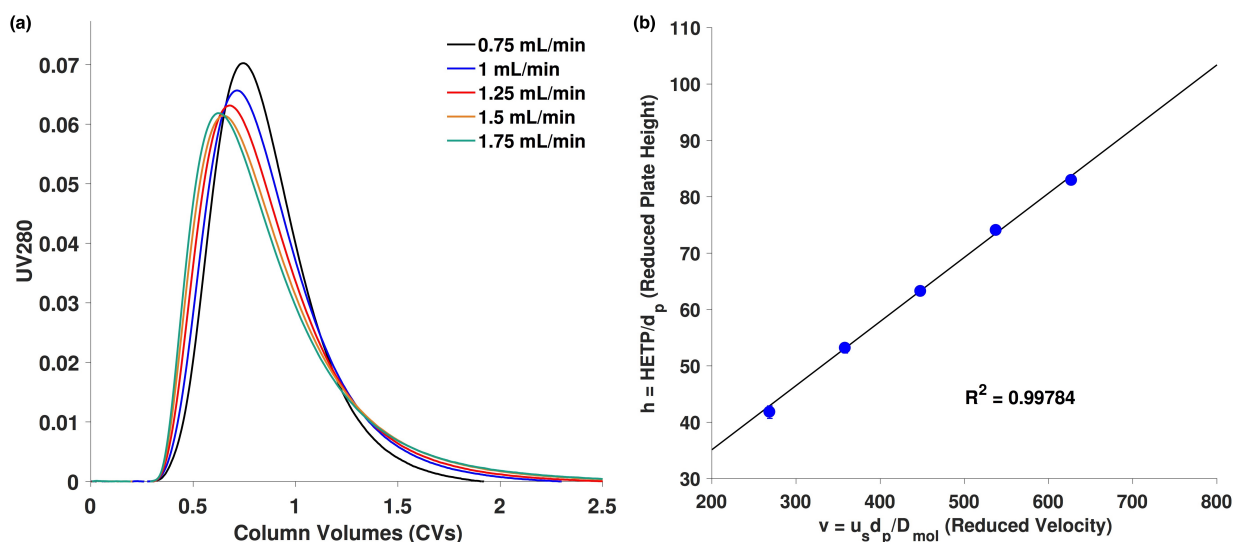
Figure 3.9. Dimensionless plate height (blue) data for CaptivA PriMAB as a function of dimensionless column velocity. The solid black line represents a linear fit of the data. Error bars represent 95% confidence intervals of triplicate measurements. Error bars are the same size or smaller than the size of the data symbols.

3.6.3. Visualizing adsorption behaviors of hIgG monomer via CLSM

To determine if there was any dependence of the observed hIgG adsorption behavior on the presence of a significant amount of IgG dimers and higher aggregates (~10% of total SEC peak area) in the sample, similar experiments were conducted, as described in the main text, with hIgG monomer labeled with Rhodamine Red™-X on CaptivA PriMAB. The hIgG monomer was generated via size exclusion chromatography, SEC, purification of hIgG on a Superdex 200 column (10 mm x 300 mm) at 0.5 mL/min.

Figure 3.10 displays an overlay of the chromatograms for unpurified hIgG on the Superdex 200 column along with a reinjection of the purified monomer peak. As seen in the figure, a very small amount of aggregate remains after SEC purification.

Figure 3.11 displays representative confocal microscopy images of the hIgG and purified hIgG monomer adsorbing on CaptivA PriMAB at 10, 15, and 30 min. As seen by comparing the images across the same time periods, both hIgG and purified hIgG monomer had the same

diffuse adsorption front as well as similar front progression kinetics. This served as evidence that the observed differences in adsorption behavior between hIgG and the mAb were not due to the presence of aggregates in the hIgG sample.
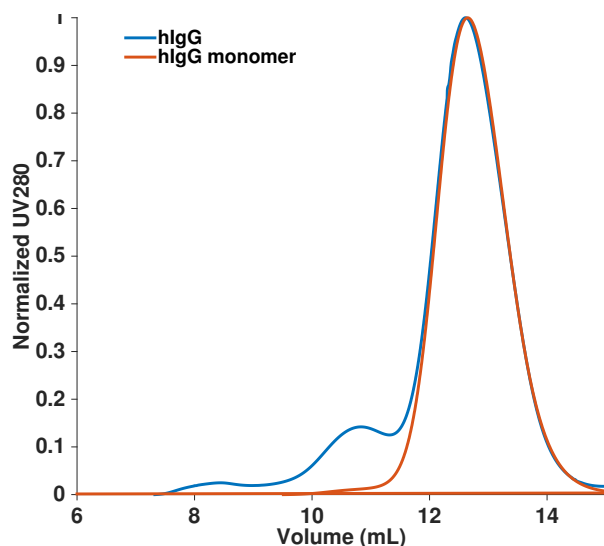
Figure 3.10. Chromatograms of 100 µL injections of hIgG (blue) and purified hIgG monomer (red) on a Superdex 200 column.
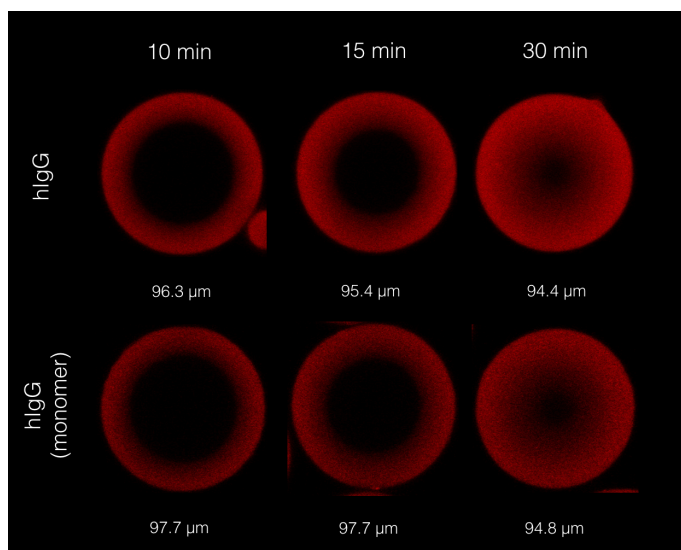
Figure 3.11. Representative CLSM images of hIgG (top row) and hIgG monomer (bottom row) adsorbing onto CaptivA PriMAB resin particles with similar diameters at 10 min (left column), 15 min (center column), and 30 min (right column).

3.7 References

[1] S. Hober, K. Nord, M. Linhult, Protein A chromatography for antibody purification, J Chromatogr B. 848 (2007) 40-47.

[2] R.D.R. Tarrant, M.L. Velez-Suberbie, A.S. Tait, C.M., Smales, D.G. Bracewell, Host cell protein adsorption characteristics during protein a chromatography, Biotechnol Progr. 28 (2012) 1037-1044.

[3] S. Ghose, J. Zhang, L. Conley, R. Caple, K. Williams, D. Cecchini, Maximizing binding capacity for protein A chromatography, Biotechnol Progr. 30 (2014) 1335-1340.

[4] L. Jendeberg, P. Nilsson, A. Larsson, P. Denker, M. Uhlén, B. Nilsson, P.Å. Nygren, Engineering of Fc(1) and Fc(3) from human immunoglobulin G to analyze subclass specificity for staphylococcal protein A, J Immunol Methods. 201 (1997) 25-34.

[5] S. Ghose, B. Hubbard, S.M. Cramer, Binding capacity differences for antibodies and Fc-fusion proteins on protein A chromatographic materials, Biotechnol Bioeng. 96 (2007) 768-779.

[6] S. Ghose, M. Allen, B. Hubbard, C. Brooks, S.M Cramer, Antibody variable region interactions with Protein A: Implications for the development of generic purification processes, Biotechnol Bioeng. 92 (2005) 665-673.

[7] J. Bach, N. Lewis, K. Maggiora, A. Gillespie A, L. Connell-Crowley, Differential binding of heavy chain variable domain 3 antigen binding fragments to protein a chromatography resins, J Chromatogr A. 1409 (2015) 60-69.

[8] S. Bottomley, B. Sutton, M. Gore, Elution of human IgG from affinity columns containing immobilised variants of protein A, J Immunol Meth. 182 (1995) 185-192.

[9] S. Gulich S, Protein engineering of an IgG-binding domain allows milder elution conditions during affinity chromatography, Biotechnol. 76 (2000) 233-243.

[10] T. Pabst, R. Palmgren, A. Forss, J. Vasic, M. Fonseca, C. Thompson, W.K. Wang, X. Wang, A.K. Hunter, Engineering of novel Staphylococcal Protein A ligands to enable milder elution pH and high dynamic binding capacity, J Chromatogr A. 1362 (2014) 180-185.

[11] G. Howard, M. Kaser, Making And Using Antibodies, Taylor & Francis/CRC Press, Boca Raton, FL, 2003.

[12] K.M Jones, J.L. Lewis, W.Y.G. Ma, A.C. Dumetz, D.N. Paolella, K.E. Göklen, Investigation of Protein Binding Capacity Observed for mAb and mAb Fragments on Protein A and Protein L Affinity Resins, ACS National Meeting Spring 2014 (Dallas, TX, USA).

[13] Z. Liu, S. Mostafa, A. Shukla, A comparison of Protein A chromatographic stationary phases: Performance characteristics for monoclonal antibody purification, Biotechnol Appl Biochem. 62 (2014) 37-47.

[14] Repligen, Captiva Primab—Protein A affinity resin—Regulatory Support File RSF-1003201, March 2010.

[15] Y. Tao Y, E.X. Perez-Almodovar, G. Carta, G. Ferreira, D. Robbins, Adsorption kinetics of deamidated antibody variants on macroporous and dextran-grafted cation exchangers. III. Microscopic studies, J Chromatogr A. 1218 (2011) 8027-8035.

[16] S. Zhang, W. Daniels, J. Salm, J. Glynn, J. Martin, C. Gallo, R. Godavarti, G. Carta, Nature of foulants and fouling mechanism in the Protein A MabSelect resin cycled in a monoclonal antibody purification process, Biotechnol Bioeng. 113 (2016) 141-149.

[17] R. Hahn, P. Bauerhansl, K. Shimahara, C. Wizniewski, A. Tscheliessnig, A. Jungbauer, Comparison of protein A affinity sorbents II. Mass transfer properties, J Chromatogr A. 1093 (2005) 98-110.

[18] E.X. Perez-Almodovar, G. Carta, IgG adsorption on a new protein A adsorbent based on macroporous hydrophilic polymers. I. Adsorption equilibrium and kinetics, J Chromatogr A 1216 (2009) 8339-8347.

[19] S. Zhang, K. Xu, W. Daniels, J. Salm, J. Glynn, J. Martin, C. Gallo, R. Godavarti, G. Carta, Structural and functional characteristics of virgin and fouled Protein A MabSelect resin cycled in a monoclonal antibody purification process, Biotechnol Bioeng. 113 (2016) 367-375.

[20] P. Ey, S. Prowse, C. Jenkin, Isolation of pure IgG1, IgG2a and IgG2b immunoglobulins from mouse serum using protein A-Sepharose, Immunochem. 15 (1978) 429-436.

[21] R. Duhamel, P. Schur, K. Brendel, E. Meezan E, pH gradient elution of human IgG1, IgG2 and IgG4 from protein A-Sepharose, J Immunol Meth. 31 (1979) 211-217.

[22] C. Papadea, I.J. Check, Human immunoglobulin G and immunoglobulin G subclasses: biochemical, genetic, and clinical aspects, Crit Rev Clin Lab Sci. 27 (1989) 27–58.

[23] A.K. Hunter, G. Carta, Effects of bovine serum albumin heterogeneity on frontal analysis with anion-exchange media, J Chromatogr A. 937 (2001) 13-19.

[24] T. Linden, A. Ljunglöf, M.R. Kula, J. Thömmes, Visualizing two-component protein diffusion in porous adsorbents by confocal scanning laser microscopy, Biotech Bioeng. 65 (1999) 622.

[25] M. Stone, G. Carta, Patterns of protein adsorption in chromatographic particles visualized by optical microscopy, J Chromatogr A. 1160 (2007) 206-214.

[26] J. Sjöquist, B. Meloun, H. Hjelm, Protein A isolated from Staphylococcus aureus after digestion with lysostaphin, Eur J Biochem. 29 (1972) 572-578.

[27] T. Moks, L. Abrahmsén, B. Nilsson, U. Hellman, J. Sjöquist, M. Uhlén, Staphylococcal protein A consists of five IgG-binding domains, Eur J Biochem. 156 (1986) 637-643.

[28] A.D. Tustian, C. Edicott, B. Adams, J. Mattila, H. Bak, Development of purification processes for fully human bispecific antibodies based upon modification of protein A binding avidity, MAbs. 8 (2016) 828-838.

[29] M.Y. Tyn, T.W. Gusek, Prediction of diffusion coefficients of proteins, Biotechnol Bioeng. 35 (1990) 327-328.

[30] M.D. LeVan, G. Carta G, Perry's Chemical Engineers' Handbook, Section 16: Adsorption and Ion Exchange, eighth ed, New York, NY. McGraw-Hill 2007.

[31] L.G. Caro, The molecular weight of lambda DNA, Virology. 25 (1965) 226-236.

[32] P. DePhillips, A. Lenhoff, Pore size distributions of cation-exchange adsorbents determined by inverse size-exclusion chromatography, J Chromatogr A. 883 (200) 39-54.

4

Chemical Modification of Protein A Chromatography Ligands with Polyethylene Glycol: Effects on IgG Adsorption Equilibrium, Kinetics, and Transport

This chapter of the thesis was adapted from the manuscript, "Chemical Modification of Protein A Chromatography Ligands with Polyethylene Glycol. I: Effects on IgG Adsorption Equilibrium, Kinetics, and Transport", authored by Justin Weinberg, Shaojie Zhang, Gillian Crews, Giorgio Carta, and Todd Przybycien. The manuscript was submitted for review to the Journal of Chromatography A on September 5th, 2017.

4.1 Chapter abstract

Chemical modification of Protein A (ProA) chromatography ligands with polyethylene glycol (PEGylation) has been proposed as a strategy to increase the process selectivity and resin robustness by providing the ligand with a steric repulsion barrier against non-specific binding. This article comprises a comprehensive study of IgG adsorption and transport in Repligen CaptivA PriMAB resin with PEGylated ProA ligands that are modified using 5.2 and 21.5 kDa PEG chains. We studied the impact of PEG chain molecular weight as well as the extent of PEGylation for the 5.2 kDa PEG modification. In all cases, PEGylation of ProA ligands decreases the resin average pore size, particle porosity, and static binding capacity for IgG in proportion to the volume of conjugated PEG in the resin. Resin batch uptake experiments

conducted in bulk via a stirred-tank system and with individual resin particles under confocal laser scanning microscopy confirm that PEGylation introduces heterogeneity into IgG adsorption kinetics: a fraction of the IgG binding sites are transformed from typical fast association kinetic behavior to slow kinetic behavior. pH gradient elution experiments of an IgG molecule on the modified resins show an increase in IgG elution pH for all modified resins, implying a decrease in IgG-ProA binding affinity on modification. Despite losses in static binding capacity for all resins with PEGylated ligands, the loss of 10% dynamic binding capacity ($DBC_{10\%}$) ranged more broadly from almost 0 to 47% depending on the PEG molecular weight and the extent of PEGylation. Minimal losses in $DBC_{10\%}$ were observed with a low extent of PEGylation with a smaller molecular weight PEG, while higher losses were observed at higher extents of PEGylation and with higher molecular weight PEG due to decreased static binding capacity and increased mass transfer resistance. This work provides insight into the practical implications for resin performance if PEGylation is considered as a strategy for selectivity enhancement in affinity chromatography with macromolecular ligands.

4.2. Introduction

Protein A (ProA) chromatography is used extensively throughout the biopharmaceutical industry for the selective capture of monoclonal antibodies (mAbs) and Fc-fusion proteins. Due to its general applicability, ProA has been widely adopted as the "platform" capture step for mAb downstream processing, typically achieving single step target purities in excess of 98% [1-3].

While the earliest resins were based on wild-type ProA ligands from *Staphylococcus aureus* immobilized on cross-linked agarose supports [4], multiple generations of ProA resins have entered the market over the past two decades that have improved binding capacity, ligand

stability, and mechanical strength. While some of the resin improvements have focused on base matrix modifications to enhance IgG transport and resin rigidity, others have focused on engineering the ProA ligand to enhance its chemical stability and accessibility. Notable among these improvements are the SuRe ligand from GE Healthcare, engineered through selective substitution of asparagine residues in order to increase stability under the alkaline conditions used for clean-in-place (CIP) operations, and ligands with C-termini enriched in lysine content from Repligen to enable multiple covalent attachments to the base matrix per ligand to reduce ProA leakage [2,5,6].

Recently, Gonzalez-Valdez et al. [7] explored the direct chemical modification of ProA ligands with polyethylene glycol (PEG), a neutral and hydrophilic polymer, as a way to introduce a steric barrier that reduces non-specific binding and resin fouling as well as the proteolytic degradation of the ProA ligand. Evidence for the protective effects of PEGylation on proteins in solution is well known. For example, PEGylation has been adopted to shield pharmaceutical proteins from immune agents and proteases *in vivo*, as well as to increase its size, thus increasing the drug's half-life and effectiveness in the body [8,9]. Additionally, PEGylation has been shown to improve the stability of concanavalin A affinity chromatography ligands against thermal and organic solvent denaturation [10].

In the Gonzalez-Valdez et al. [7] work, the recombinant staphylococcal ProA ligands (rSPA) of Repligen CaptivA PriMAB resin were PEGylated *in situ* using a methoxy-PEG-propionaldehyde (mPEG-PA) chemistry with either 5.0 or 20.7 kDa molecular weight polymer chains. The rSPA structure consists of the five wild type Fc binding domains (E, D, A, B, and C) together with the aforementioned lysine-rich anchoring domain, X [11]. The base matrix of CaptivA PriMAB is Sepharose 4FF, which comprises 45–165 μm particles (90 μm mean particle

diameter) of 4% crosslinked agarose [12]. With these modified resins, Gonzalez-Valdez et al. [10] demonstrated a promising 2- to 3-fold reduction in non-specific protein binding for PEGylated rSPA resins versus the unmodified commercial resin using yeast extract and fetal bovine serum as mock contaminants.

Despite these selectivity advantages, there are concerns about the effect of PEGylation on other key resin performance characteristics such as IgG binding capacity and transport within the pores of the modified resin. For example, it would be expected that while PEGylation may reduce non-specific binding, the steric barrier provided by the PEG molecule may also block some of the desired, specific binding of IgG molecules to the ProA ligand, thus reducing binding capacity. Additionally, PEGylation is expected to increase the size of the ProA ligand, which would be expected to reduce the free pore volume and increase diffusional hindrance within the resin beads. A detailed understanding and quantification of potential tradeoffs that exist between improvements in selectivity or robustness and decreases in IgG binding capacity and/or increased mass transport or kinetic resistance are key to the future development of optimized PEGylation conditions and to the possible commercial viability of PEGylated ProA chromatography resins in downstream bioprocessing.

Gonzalez-Valdez et al. [10] have provided nascent answers to some of these questions. In particular, a 20-40% reduction in the dynamic binding capacity at 10% breakthrough ($DBC_{10\%}$) of human polyclonal IgG (hIgG) on CaptivA PriMAB resin modified with a 20.7 kDa PEG was reported compared to the unmodified resin. A subsequent physical characterization of the unmodified resins and resins with PEGylated ligands demonstrated small reductions in average pore size and effective IgG diffusivity in the modified resins, as expected due to the reduction in accessible pore volume accompanying PEGylation. However, pore diffusion-limited transport

model simulations suggested that the small increase in mass transfer resistance in the resin modified with 20.7 kDa PEG chains was not significant enough to explain the associated reduction in $DBC_{10\%}$, suggesting that other factors contributed to this decline. Understanding these factors is critical in order to design optimized PEGylation strategies.

In this work, we have comprehensively characterized the behavior of ProA chromatography resins with PEGylated ligands with respect to IgG adsorption, transport, robustness, and selectivity. Here in Part I (this chapter), we investigate the IgG binding capacity, elution pH, binding kinetics, and transport in the modified resins. In addition to comparing differences between PEGylation with large and small PEG chains, we compare differences between two resins modified with the same 5.2 kDa PEG but with varying extents of modification. In Part II (Chapter 5) [13], we report on the selectivity and robustness properties of the modified resins.

4.3. Materials and methods

4.3.1. Materials

Loose CaptivA PriMAB and Sepharose 4FF resins were donated by Repligen (Waltham, MA) and GE Healthcare (Piscataway, NJ), respectively. Chromatographic experiments were conducted with CaptivA PriMAB and modified variants packed into OPUS columns (internal diameter 1.2 cm) by Repligen. Bed lengths varied from 4.4 to 4.6 cm. rSPA ligand in free solution was provided by Repligen at a concentration of 52 mg/mL in deionized water.

The mAb used in this work was a purified, glycosylated IgG_1 antibody (~10 ppm host cell protein content) with a pI ~8.2, and an extinction coefficient of 1.48 AU•mL•mg^{-1}•cm^{-1}. Based on size exclusion chromatography with a Superdex 200 column from GE Healthcare

(Piscataway, NJ), the mAb was found to be essentially 100% monomer (aggregate content below detection limit). hIgG was obtained as a lyophilized powder from Lee BioSolutions (Maryland Heights, MO) with a reported purity of 99% as established by electrophoresis. The polyclonal hIgG included about 3.5% of IgG_3 species, which do not bind to ProA, and about 10% aggregate species according to size exclusion chromatography analysis.

Rhodamine Red™-X succinimidyl ester amine-reactive dye was obtained from Invitrogen Corporation (Carlsbad, CA). Technical-grade dextrans of various average molecular weights (3.5 to 2000 kDa) were obtained from Pharmacosmos (Holbaek, Denmark). Phage lambda DNA was obtained from New England BioLabs (Ipswich, MA). Activated mPEG-PAs were obtained from NOF America Corporation (White Plains, NY) in powder form with average molecular weights of 5,215 and 21,514 Da, respectively, as reported by certificates of analysis. In addition, the certificates of analysis reported polydispersities of 1.01 and 1, PEG mass percentages of 99.5% and 99.6%, and activated percentages of 93.3% and 92.9% for the nominal 5.2 kDa and 21.5 kDa mPEG-PAs, respectively. Coomassie Plus (Bradford) assay reagent was obtained from Pierce Biotechnology (Rockford, IL). All other chemicals and assay components were obtained from Sigma-Aldrich (St. Louis, MO) or Fisher Scientific (Pittsburgh, PA). All water was purified by reverse osmosis followed by treatment to 18 MΩ·cm resistivity using a Barnstead NANOpure Diamond system from Barnstead International (Dubuque, IA). All experiments were conducted at room temperature (maintained at 22±2 ºC in our laboratories).

Polyclonal hIgG solutions were prepared by dissolving known weights of the lyophilized powder in the desired buffer followed by filtration through a 0.2 μm membrane. Since the lyophilized powder contained some amount of associated water and salts, the dissolved protein concentration was determined by measuring the UV absorbance at 280 nm on a Cary 300 UV-

Vis spectrophotometer (Agilent Technologies, Santa Clara, CA) using an extinction coefficient of 1.36 AU•mL•mg hIgG^{-1}•cm^{-1} [14]. Linearity in accordance with Beer-Lambert's law was verified by measuring the absorbance of solutions containing 0 to 3 mg lyophilized powder/mL. Either a BioTek plate reader (Winooski, VT) or a NanoDrop 2000 spectrophotometer (Thermo Fisher Scientific, Waltham, MA) were subsequently used for UV-Vis absorbance measurements. For the plate reader, a separate calibration was performed based on prepared standards due to the unknown path length. The mAb sample was buffer exchanged as needed via Amicon Ultra-15 centrifugal filters with a 100 kDa molecular weight cutoff (EMD Millipore, Billerica, MA) or PD-10 desalting columns (GE Healthcare, Piscataway, NJ). mAb sample concentrations were determined exclusively with the NanoDrop 2000 spectrophotometer using the known extinction coefficient.

All adsorption experiments were conducted in phosphate buffered saline (PBS) containing 137 mM NaCl, 2.7 mM KCl, 10 mM Na$_2$HPO$_4$, and 1.8 mM KH$_2$PO$_4$ adjusted to pH 7.0 with 1 M HCl.

4.3.2. Resin hydrated particle densities and ligand densities

The hydrated particle densities of the CaptivA PriMAB and Sepharose 4FF resins were measured at room temperature by first preparing ~50% resin slurries in PBS buffer, then separating the hydrated particles from the supernatant by centrifuging the slurry in 0.2 µm centrifugal filters at 3000×g for 45 min, and finally determining the particle volume with a KIMAX 10 mL pycnometer. The density of the PBS buffer was measured separately to be 1.005 $\pm$ 0.001 g/mL. The hydrated particle density of CaptivA PriMAB and Sepharose 4FF were determined to be 1.042 $\pm$ 0.003 g/mL and 1.033 $\pm$ 0.003 g/mL, respectively. Unless stated

otherwise, experimental errors are reported throughout as 95% confidence limits based on triplicate measurements.

The rSPA ligand density on the CaptivA PriMAB resin was determined by a Bradford dye depletion assay. For this purpose, 52.1 mg of CaptivA PriMAB hydrated resin particles, or 50 µL of hydrated particle volume, were added to microcentrifuge tubes in triplicate followed by 1.25 mL of Coomassie Plus assay reagent. This was repeated for 51.7 mg of Sepharose 4FF hydrated resin particles as a control for non-specific dye uptake. The resulting mixtures were then vortexed periodically for 5 minutes and then centrifuged at 1500×g for 2 minutes. This entire procedure was repeated, with the exception of centrifugation, for 50 µL of diluted rSPA standards in a range of 5 to 15 mg/mL in triplicate. The absorbance of the supernatants and resulting standard mixtures was measured at 465 nm on a Biotek plate reader. This absorbance was corrected by subtracting the Sepharose 4FF control measurements and used to calculate the rSPA ligand content of the resin based on a standard curve generated using rSPA in solution. Using this method, the rSPA ligand content was determined to be 14 ± 1 mg/mL hydrated resin particles.

4.3.3. PEGylation reactions

The immobilized rSPA ligands on the CaptivA PriMAB resin were PEGylated in a batch reaction using the mPEG-PA chemistry with polymer molecular weights of either 5.2 or 21.5 kDa. A ~50% resin slurry in PBS buffer was prepared and then separated by centrifuging in 0.2 µm centrifugal filters at 3000×g for 45 min to obtain hydrated resin particles. For each reaction, ~10 g of hydrated resin particles were then transferred to 50 mL conical centrifuge tubes. Solutions of mPEG-PA were prepared by dissolving known weights of the powder in a buffer

consisting of 100 mM sodium phosphate and 20 mM sodium cyanoborohydride at pH 5.1. This chemistry has been reported in the literature to be selective towards the N-terminus of the target protein [15-17]. A small amount (~1 mL) of the resulting solutions was withdrawn and used to prepare mPEG-PA standards consisting of 12.5%, 25%, and 50% of the initial concentration, respectively. A known volume of the remaining mPEG-PA solution was then transferred to the conical tubes containing the hydrated resin particles and was immediately mixed by end-to-end rotation. Volumes and concentrations used for the mPEG-PA solution were determined based on the amount of hydrated resin, the desired initial PEG:rSPA molar ratio, and the need to ensure that the resin was well suspended during the reaction. After one minute of mixing, 500 µL of the resulting slurry were withdrawn and centrifuged at 1500×g for 2 minutes to extract the supernatant. The conical tube containing the slurry was then placed on a rotator and allowed to mix end-to-end at 18 rpm for 24 hours at room temperature. At 24 hours, another 500 µL of the reaction slurry was withdrawn and centrifuged to extract the supernatant. The remaining slurry was then immediately and thoroughly washed into a solution of 20% ethanol to stop the PEGylation reaction.

The extent of PEGylation was determined by the depletion of free mPEG-PA in the supernatant. The free mPEG-PA concentrations before and after reaction were determined using an HPLC-SEC assay. The assay was performed on a Waters Alliance 2690 HPLC system (Milford, MA) with a Waters Xbridge BEH SEC 200Å column and Waters 2414 refractive index detector. Briefly, 100 µL injections of the mPEG-PA standards and the initial reaction supernatant were performed at a flow rate of 1 mL/min in triplicate. PBS loading buffer was used as the mobile phase for the assay. The procedure was then repeated for the final reaction supernatant. Due the high sensitivity of the refractive index detector, the standards were injected

both times to calibrate the response and account for any room temperature fluctuations or slight changes in buffer preparation. The peak areas of the standards were found to be highly linear with respect to concentration ($R^2 \geq 0.999$) for all samples. The calibration curves from the standard injections were used to determine the free mPEG-PA concentrations at the initial and final times of reaction, which were then used in tandem with a mass balance to determine the PEGylation extent of the rSPA ligands for each batch reaction.

4.3.4. Inverse size exclusion chromatography

Inverse size exclusion chromatography (iSEC) was performed to determine the apparent average pore radius (r_{pore}) and pore size distribution of the modified and unmodified resins. One hundred microliter injections of 5 mg/mL glucose and technical grade dextrans dissolved in PBS loading buffer were introduced into packed columns of each resin in triplicate. The injections were performed on a Waters Alliance 2690 HPLC system (Milford, MA) operating at a mobile phase flow rate of 1 mL/min and monitored with a Waters 2414 refractive index detector. The retention volume of each probe was determined from the baseline-corrected first statistical moment (μ) of each peak produced by injection. Extra column volumes were determined from blank injections (without the column). Additionally, 0.22 mL was subtracted from the retention volume to account for dead volumes in the OPUS column hardware, as determined by Repligen. The distribution coefficient (K_D) for each probe in the particle pores was then calculated as:

$$K_D = \frac{\mu - V_0}{V_T - V_0} \tag{4.1}$$

where V_T is the total column void volume, determined from the retention of glucose, and V_0 is the interstitial (or extraparticle) void volume. The latter was determined from the corrected retention volume of 100 µL injections of a 10 µg/mL solution of lambda DNA onto the columns

at mobile phase flow rate of 1 mL/min and monitored with a Waters 996 PDA detector at 260 nm. Lambda DNA, with a molecular weight of 31.5 MDa [18], should be fully excluded from all pores of the resin. Values of interstitial porosity ($\varepsilon = V_0/V_C$) were determined to be between 0.31 and 0.35 for the columns used, which are typical for packed beds in chromatography columns. The value of r_{pore} was determined by fitting the experimental K_D-values to a log-normal pore size distribution as described in DePhillips and Lenhoff [19], where the pore size distribution function is assumed to be:

$$f(r) = \frac{1}{r}\exp\left[-\frac{1}{2}\left(\frac{\log(r/r_{pore})}{s_{pore}}\right)^2\right] \tag{4.2}$$

Accordingly, K_D is given by:

$$K_D = \frac{\int_{r_{probe}}^{\infty} f(r)\left[1-(r_{probe}/r)\right]^2 dr}{\int_0^{\infty} f(r)dr} \tag{4.3}$$

where s_{pore} is the standard deviation of the pore size distribution, and r_{probe} is the probe radius, which was estimated via the correlation developed by Hagel [20]:

$$r_{probe} = 0.0271M^{0.498} \tag{4.4}$$

where M is the average molecular weight of the dextran sample in Da and r_{probe} is determined in nm. The radius of glucose was taken as 0.36 nm by extrapolating eq. 4.4 to a molecular weight of 180 Da.

4.3.5. IgG partitioning in the resin pores and HETP

The accessible porosity and effective pore diffusivity (D_e) of IgG in the pores of unmodified and PEGylated rSPA resins were evaluated from pulse IgG injection experiments conducted under non-binding conditions in a 50 mM glycine, 100 mM NaCl buffer at pH 3.0. Triplicate injections of 100 µL of the mAb at a concentration of 2.0 mg/mL were performed on

each column at flow velocities ranging from 37 to 106 cm/hr (0.75 to 1.75 mL/min) using a Waters 2690 HPLC monitored by a Waters 996 PDA detector at 280 nm. The ensuing peaks were baseline corrected and fitted to an exponentially-modified Gaussian (EMG) function to determine their first moment and second central moment, μ and σ^2, respectively. Dead volume corrections were made in a manner similar to those made for the iSEC experiments described above. The particle porosity accessible to the IgG molecules (β_{IgG}) and the corresponding $HETP$ values were calculated from the following equations:

$$\beta_{IgG} = \frac{\mu_{IgG} - V_0}{V_C - V_0}$$

(4.5)

$$HETP = \frac{\sigma^2 L}{\mu^2}$$

(4.6)

where μ_{IgG} is the baseline-corrected first statistical moment for the non-binding IgG injections, V_C is the column volume, and L is the column bed length. The $HETP$ values were used to estimate D_e of IgG in the different resins by comparing them with those predicted by the general rate model of chromatography according to the following equation [21]:

$$h = a + \frac{1}{30}\left(\frac{\varepsilon}{1-\varepsilon}\right)\left(\frac{\mu - V_0}{\mu}\right)^2 \left(\frac{10}{Sh} + \frac{D_0}{D_e}\right)v'$$

(4.7)

where $h = HETP/d_p$ is the reduced $HETP$ and $v' = u_s d_p / D_0$ is the reduced velocity. Here, d_p is the average particle diameter of the resin, u_s is the interstitial mobile phase velocity, D_0 is the bulk diffusivity of IgG (estimated to be 3.7×10^{-7} cm^2/s according to Tyn and Gusek [22]), and $Sh = k_f d_p / D_0$ is the Sherwood number. The latter was estimated from the following correlation [23]:

$$Sh = \frac{1.09}{\varepsilon} Re_p^{0.33} Sc^{0.33} = \frac{1.09}{\varepsilon}\left(\frac{\rho_L u d_p}{\eta}\right)^{0.33}\left(\frac{\eta}{\rho_L D_0}\right)^{0.33}$$

(4.8)

where Re_p is the particle Reynolds number, Sc is the Schmidt number, and ρ_L, $u_s = u/\varepsilon$, and η are the density, superficial velocity, and viscosity of the mobile phase, respectively.

4.3.6. Adsorption capacity

Static binding capacities were obtained by equilibrating samples of each resin with protein solutions of various concentrations and calculating the amount of protein bound by material balance based on the final and initial protein concentrations in solution. For hIgG, known weights of hydrated resin particles (3 to 35 mg) were added to set volumes of protein solution (1 to 4.5 mL) in microcentrifuge tubes at initial protein concentrations ranging from 0.1 to 3.0 mg/mL. The tubes were then rotated end-over-end at 18 rpm for 24 hours. After this period, the tubes were centrifuged at 800 rpm for 5 min and the supernatant protein concentration was measured on the BioTek plate reader. Subsequently, a mass balance was performed to determine the adsorbed protein concentration. The weights and volumes for each experiment were chosen to reduce the supernatant concentration of hIgG to 40-50% of its original value at equilibrium to reduce measurement error. The CaptivA PriMAB resin density was used to convert the weight of the hydrated resin particles to units of volume of hydrated particles. Experiments were performed in triplicate for each resin.

For hIgG, the data were well correlated by the Langmuir isotherm, given by:

$$q = \frac{q_{max}KC}{1+KC} \tag{4.9}$$

were q is the binding capacity in mg antibody per mL hydrated particle, C is the equilibrium protein concentration in solution, q_{max}, the maximum binding capacity, and K the affinity constant.

For the mAb, in order to conserve material, the equilibrium binding capacity was determined by a single point isotherm at an equilibrium concentration ~1.3 mg/mL mAb in triplicate.

4.3.7. pH gradient elution

The pH values at which mAb elution occurs when a linearly decreasing pH gradient is applied to mAb-loaded columns were determined for both unmodified and PEGylated variants of CaptivA PriMAB. In these experiments, 100 μL injections of 15 mg/mL mAb in PBS buffer were made on an Akta Explorer 100 chromatography system, followed by washing with 3 column volumes (CV) of 25 mM citrate buffer at pH 5.5 at flow rate of 1 mL/min, and elution, also at a flow rate of 1 mL/min, with a 10 CV pH gradient from pH 5.5 to pH 2.5 with a constant concentration of the citrate buffer. The UV absorbance of the column outlet was monitored at 280 nm. Extra-column volume corrections for the UV and pH detectors on the Akta system used were obtained as described before. The outlet pH profile was obtained from the trace generated by the Akta system pH detector that was calibrated using buffer standards at pH 7.00 and 4.01. Experiments were performed in triplicate.

4.3.8. Breakthrough curves

Breakthrough curves were generated using hIgG to evaluate the dynamic binding capacity of CaptivA PriMAB and modified variants. For this purpose, 300 mL of PBS buffer containing 2.0 mg lyophilized powder hIgG/mL were loaded onto resin columns on the Akta Explorer 100 system at flow rates of 0.5, 0.75, 1.0, 1.25, and 2 mL/min, which corresponded to residence times of between 2 and 11 minutes depending on the exact column volume. The

breakthrough curve was monitored by measuring the UV absorbance of the column outlet stream at 280 nm. After loading, the protein was allowed to bypass the column to determine the 100% breakthrough absorbance value. Subsequently, the IgG was eluted using 50 mM glycine buffer, pH 3.0 with 100 mM NaCl and the column was regenerated using PBS loading buffer. The experiment was repeated without the column inline to correct for the extra-column dead volume in the Akta system. The presence of non-binding IgG_3 species was accounted and corrected for by subtracting the shift in the UV absorbance baseline produced by flow through protein after the initial hIgG front reached the column outlet and the detector. The mass of hIgG loaded per unit column bed volume at 10% breakthrough, after correction for the contribution of IgG_3, was used to determine the value of $DBC_{10\%}$.

4.3.9. Batch uptake kinetics

The adsorption kinetics were obtained from batch uptake measurements performed in a 50 mL beaker continuously stirred by an overhead mixer at 300 rpm. Briefly, for each measurement, a 30 mL sample of a solution containing 2.0 mg/mL protein in PBS was placed in the vessel and allowed to recirculate through a Cary 300 UV-Vis spectrophotometer equipped with a flow-through cuvette. The recirculation flow rate was set at ~20 mL/min using a peristaltic pump with a Waters 10 μm solvent reservoir filter (Milford, MA) at the inlet to prevent uptake of suspended media. The dead volume of the pump tubing and flow cell was measured from the volume of displaced liquid when thoroughly flushing the system with air. After reaching signal baseline, a known weight of hydrated resin particles was added into the protein solution and allowed to mix for 2 hours. The resulting protein concentration in the vessel was continuously measured from the UV absorbance at 280 nm of the recirculating supernatant.

113

The supernatant protein concentration was then used in a mass balance to determine the adsorbed protein concentration over time. All experiments were repeated in duplicate.

4.3.10. Confocal laser scanning microscopy (CLSM)

Confocal laser scanning microscopy (CLSM) was used to obtain the spatial and temporal distribution of the mAb within the resin particles during transient adsorption, following the procedure described in Tao et al. and Zhang et al. [24,25]. For this purpose, the mAb was labeled with Rhodamine Red™-X reactive dye. Labeling was performed by mixing the mAb and dye in a 3:1 molar ratio in 500 mM sodium bicarbonate buffer at pH 8.5 with slow rotation in the dark for 1 hour. The protein was then separated from the unreacted dye by SEC and buffer exchanged into PBS loading buffer using BioRad Econo-Pac 10DG desalting columns (Hercules, CA). The molar labeling ratio was calculated from the molar concentrations of dye and protein, which, in turn, were determined from the dye extinction coefficient (120,000 AU•M^{-1}•cm^{-1}) and UV absorbances at 280 nm and 570 nm for protein and Rhodamine Red™-X, respectively. The absorbance at 280 nm was adjusted by a correction factor ($0.17 \times A_{570}$) supplied by the manufacturer to account for UV absorption of the dye. The UV absorbances were measured on a Nanovue instrument from GE Healthcare (Piscataway, NJ) and the extinction coefficient of the dye was provided by Invitrogen documentation. The labeling ratio was determined to be 0.19 labels per protein molecule. The labeled protein mixture was then further diluted with unlabeled protein to achieve a 1:200 labeled-to-unlabeled protein molar ratio. CLSM experiments were conducted with a Zeiss LSM 510 microscope with a Plan-Apochromat 64 x/1.4 NA oil objective (Carl Zeiss MicroImaging, LLC, Thornwood, NY).

The CLSM experiments were conducted in batch mode by adding less than 1 mg of hydrated resin particles to 5 mL of each labeled protein sample with a 2.0 mg/mL total mAb concentration, periodically pipetting out 300 μL of the mixture, and rapidly filtering the withdrawn slurry in a 0.2 μm microcentrifuge filter to remove the interstitial liquid. The hydrated resin particles were then re-suspended in PBS loading buffer and subsequently imaged.

The radial fluorescence intensity profiles from each confocal image were determined from a radial averaging of the intensity values within the resin particle. Briefly, the center of each particle was determined by finding the circle of best fit using a digital overlay in MATLAB. A dataset was generated of all pixel intensity values with their corresponding distance from the central pixel. The dataset was binned in distance in steps of 1 pixel from the center to the particle radius and an average intensity within each distance bin was computed to produce the radially averaged intensity profile. Each resulting dataset was averaged to complete the averaging for the corresponding radial distance. Units of pixels were converted into length given the resolution of the microscope: 3.584 μm/pixel. The optical slice thickness of the images was 1 μm.

4.4. Results and discussion

4.4.1. Physical properties of PEGylated rSPA resins

Table 4.1 shows the results of PEGylations with 5.2 and 21.5 kDa PEG polymers. For the 5.2 kDa PEG, the extent of PEGylation increased with the initial ratio of PEG to rSPA from a little over 100% using a low value of this ratio, to nearly 300% with a high value of this ratio. The former indicates an average of one PEG molecule conjugated per rSPA ligand while the latter indicates an average of about three PEG molecules conjugated per rSPA ligand. The lower PEGylation extent for the 21.5 kDa PEG is likely due to significant steric hindrance that made it

difficult for more than one of the large PEG chains to covalently attach to the rSPA ligand. To compare the different modifications on a consistent scale, the immobilized PEG volume per mole of rSPA in each resin was calculated assuming that the PEG chains occupy a spherical, random coil domain adjacent to the anchored rSPA ligand. The viscosity radius of PEG (r_{PEG}) was determined via the correlation by Kuga [26]: $r_{PEG} = 0.01912 M_{PEG}^{0.559}$ where M_{PEG} is the PEG molecular mass in Da and r_{PEG} is determined in nm.

Resin	PEG MW (kDa)	PEG:rSPA Initial Molar Ratio	PEGylation Extent (%)	Volume of PEG conjugated per mole of rSPA (nm³ PEG/mol rSPA)
rSPA + 1×5 kDa PEG	5.2	2.79:1	111 ± 8	56 ± 4
rSPA + 3×5 kDa PEG	5.2	7.32:1	285 ± 11	143 ± 6
rSPA + 20 kDa PEG	21.5	3.25:1	66 ± 24	325 ± 118

Table 4.1. Results of PEGylation reactions performed on immobilized rSPA ligands on CaptivA PriMAB resin. Error ranges given represent 95% confidence limits based on PEGylations performed in triplicate.

Figure 4.1a shows the K_D values of the dextran probes obtained for the unmodified and PEGylated rSPA resins while Figure 4.1b shows the van Deemter plots (h vs. v') obtained for IgG from pulse injections under non-binding conditions. Table 4.2 shows the corresponding values of r_{pore}, s_{pore}, β_{IgG} and D_e determined from these measurements. As seen in Fig. 4.1a, the dextran K_D data are consistent with the assumed log-normal cylindrical pore size distribution with a mean pore radius that, as seen in Table 4.2, decreases with the extent of PEGylation. The corresponding values of β_{IgG} also decrease with the introduction of PEG chains indicating increasingly restricted access to the particle pores by the IgG molecules. Figure 4.1a displays corresponding values of K_D for the mAb with a hydrodynamic radius of 5.75 nm [27], which

show excellent agreement between the dextran data, model predictions, and actual partitioning of

the IgG molecules.
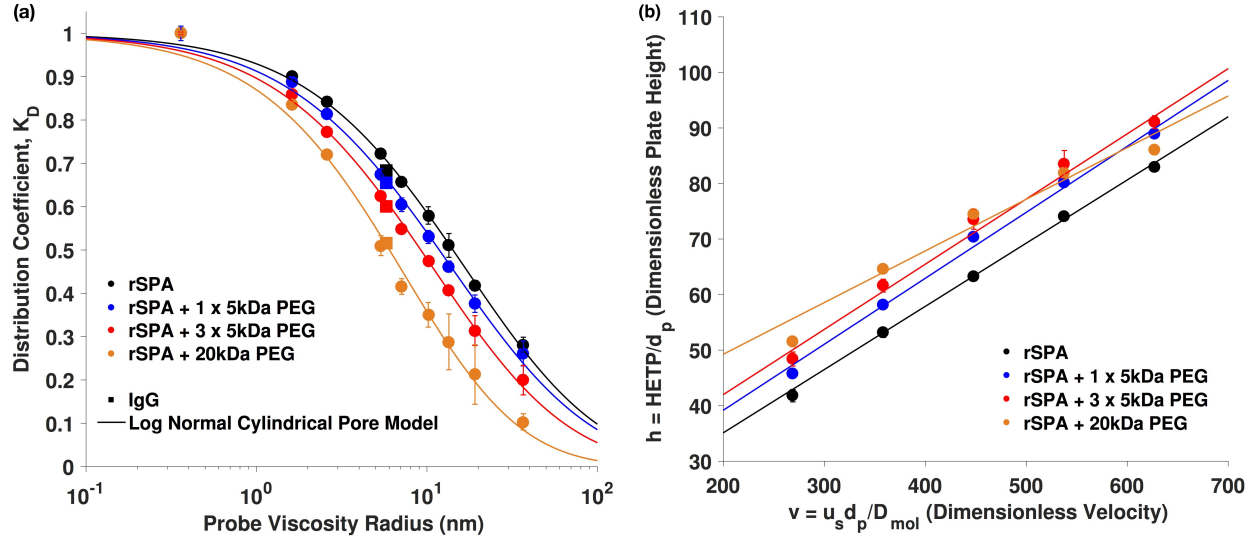
Figure 4.1. (a) Plot of K_D versus iSEC dextran probe viscosity radius for unmodified and PEGylated rSPA resins. Square data points represent experimental K_D values for the mAb (IgG molecule). IgG error bars are smaller than the symbol size. Solid lines represent fits according to eqs. 4.2-4.3. (b) Dimensionless van Deemter plots for unmodified and PEGylated rSPA resins. Solid lines represent fits according to eq. 4.7. Error bars in both figures represent 95% confidence limits based on triplicate measurements.

Resin	r_{pore} (nm)	s_{pore}	β_{IgG}	D_e (10^{-8} cm^2/s) from HETP	D_e (10^{-8} cm^2/s) from SCM
rSPA	57.3 ± 1.6	1.26 ± 0.07	0.65 ± 0.01	7.5 ± 0.5	7.5 ± 0.5
rSPA + 1×5 kDa PEG	47.8 ± 1.8	1.32 ± 0.10	0.61 ± 0.01	6.2 ± 0.2	12 ± 2
rSPA + 3×5 kDa PEG	37.1 ± 1.3	1.26 ± 0.09	0.56 ± 0.01	6.9 ± 0.2	7.0 ± 0.6
rSPA + 20 kDa PEG	23.8 ± 1.3	1.05 ± 0.13	0.48 ± 0.01	5.9 ± 0.8	7.9 ± 0.9

Table 4.2. Summary of the physical and mass transfer characteristics of the unmodified and PEGylated rSPA resins determined by analysis of iSEC and HETP experiments. Error ranges for all values, with the exception of D_e estimated from the shrinking core model (SCM), represent 95% confidence limits based on triplicate measurements. Errors for the SCM values represent 95% confidence limits based of the slope for the linear fit of the CLSM data (shown in Fig. 4.7).

As seen in Table 4.2, the decreases in β_{IgG} and r_{pore} are approximately inversely proportional to the volume of conjugated PEG suggesting that the assumption of a random coil PEG domain adjacent to the rSPA protein domain is appropriate for these conjugates as also noted previously for other PEGylated proteins [28]. Interestingly, the standard deviation of the pore size distribution, s_{pore}, remained roughly unchanged on PEGylation, with the exception of the rSPA + 20 kDa resin. This suggests, albeit indirectly, that the PEGylation is fairly uniform throughout the resin particles: the entire distribution of pore sizes shifted to smaller radii on PEGylation preserving the original width of the distribution, suggesting that all pores experienced similar immobilized PEG volumes; if just a subset of the pores contained immobilized PEG, such as those in an outer shell of the particle, or only the larger pores, the pore size distribution would tend to broaden or sharpen, respectively. While the changes in rSPA + 1×5 kDa PEG and rSPA + 3×5 kDa pore size distributions compared to that of the unmodified resin are small, a significant decrease in s_{pore} is seen for rSPA + 20 kDa PEG, which suggests a tightening of the pore size distribution for this resin. This result also suggests that the larger PEG chains in rSPA + 20 kDa PEG resin might be found, preferentially, in the larger pores of the starting unmodified resin. As with any iSEC analysis, due to the highly complex nature of the pore network structure, the pore dimensions and distributions shown in Table 4.2 cannot be considered as absolute but rather as relative to facilitate a functional comparison between resins [19,20].

As also seen in Table 4.2, the D_e values for IgG determined from the HETP data decrease significantly for all PEGylated rSPA resins compared to the unmodified resin. This decrease is approximately linearly correlated with the lower values of β_{IgG} observed with the introduction of

immobilized PEG chains. For diffusional transport in a porous network, the effective diffusivity is expected to be given by [21]:

$$D_e = \frac{\beta_{IgG} D_0}{\tau} \qquad (4.10)$$

where τ is the network tortuosity factor. The approximate linear relationship between D_e and β_{IgG} observed for the PEGylated rSPA resins suggests that the main effect on D_e is a reduction in accessible porosity with τ remaining essentially constant.

4.4.2. Static binding capacities and IgG average binding affinities

The hIgG adsorption isotherms for the unmodified and PEGylated rSPA resins are shown in Figure 4.2. The dashed lines represent fits of the Langmuir isotherm, which were used to determine values of the affinity constant K and the maximum binding capacity q_{max}. The isotherms for all four resins are sharp, which is a result of the highly favorable interaction between IgG and the ProA ligand. The K-values ranged from 78 ± 24 to 103 ± 36 mL/mg hIgG and are consistent with the values reported in Perez-Almodovar and Carta [21] for hIgH adsorption on another commercial ProA resin on a hydrated particle volume basis. Due to the uncertainties caused by the steepness of the isotherms, it was not possible to draw any specific conclusions about the effects of PEGylation on IgG binding affinity based on the K-values other than the fact that PEGylation did not seem to disrupt the highly favorable interaction. On the other hand, as seen in Table 4.3, PEGylation does affect the hIgG binding capacity, which declined from about 19% to about 37% as the volume of PEG conjugated to the rSPA ligand increased. As also seen in Table 4.3, this trend is similarly exhibited by the mAb adsorption capacity at an equilibrium solution concentration of ~1.3 mg/mL, which shows a decline ranging

from about 26% to about 33% from the capacity observed for the unmodified resin. The reasons for this decline are not precisely known but it is likely that a portion of the conjugated PEG chain occludes one or more ProA binding domains for IgG, reducing or even eliminating their ability to interact with IgG molecules. This behavior is also consistent with the results of Wen and Niemeyer [10], who obsereved reduced static binding capacity of glucose oxidase on PEGylated concanavalin A resins. Similarly to PEGylated rSPA resins, the binding capacity of PEGylated concanavalin A resins was inversely proportional to the volume of conjugated PEG in the resin.
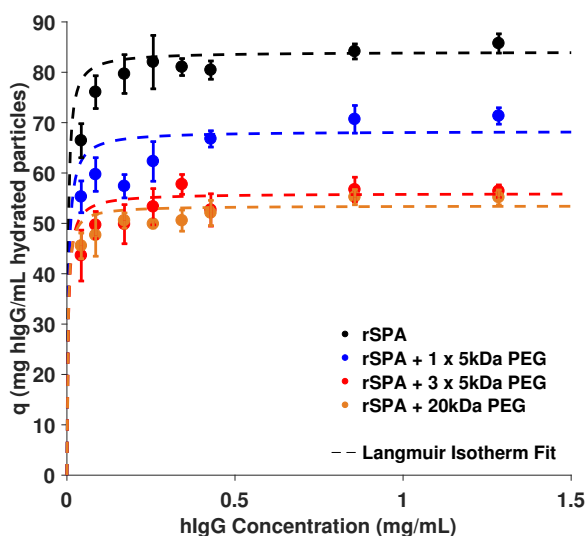
Figure 4.2. Adsorption isotherms for hIgG for the unmodified and PEGylated rSPA resins. Dashed lines represent fits of the Langmuir isotherm to the data. Error bars in both figures represent 95% confidence limits based on triplicate measurements.

Resin	hIgG q_{max} (mg hIgG/mL hydrated resin particles)	mAb q_{max} (mg mAb/mL hydrated resin particles)	Elution pH (mAb)
rSPA	84 ± 1	61 ± 3	3.70 ± 0.02
rSPA + 1×5 kDa PEG	68 ± 2	45 ± 3	3.80 ± 0.02
rSPA + 3×5 kDa PEG	56 ± 1	45 ± 3	3.93 ± 0.02
rSPA + 20 kDa PEG	53 ± 1	41 ± 3	3.88 ± 0.02

Table 4.3. Summary of q_{max} values for the unmodified and PEGylated rSPA resins determined for hIgG and the mAb. Values of q_{max} for hIgG were obtained from a Langmuir fit of the isotherms while values for the mAb are at an equilibrium concentration of ~1.3 mg/mL. Additionally, a summary of the mAb elution pH for the unmodified and PEGylated rSPA resins. Errors in all cases represent 95% confidence limits based on triplicate experiments.

To obtain a more precise comparison of the IgG binding affinities on the modified resins, the elution pH of the mAb was determined from pH gradient elution experiments. Figure 4.3 displays the pH gradient elution profiles for pulse injections of the mAb on columns packed with the unmodified and PEGylated rSPA resins. The corresponding elution pH values, determined by the pH corresponding to the peak apex, are summarized in Table 4.3. As seen from both of these results, the elution pH of the mAb increased for all PEGylated rSPA resins compared to that of the unmodified resin. Such an increase can be regarded as a decrease in average binding affinity or binding strength between the IgG and the ProA ligand due to the lower degree of electrostatic repulsion forces necessary to dissociate the two proteins [29]. These results are consistent with the presence of the steric repulsion barrier provided by the PEG, which likely lowers the stability of the IgG-ProA complex.
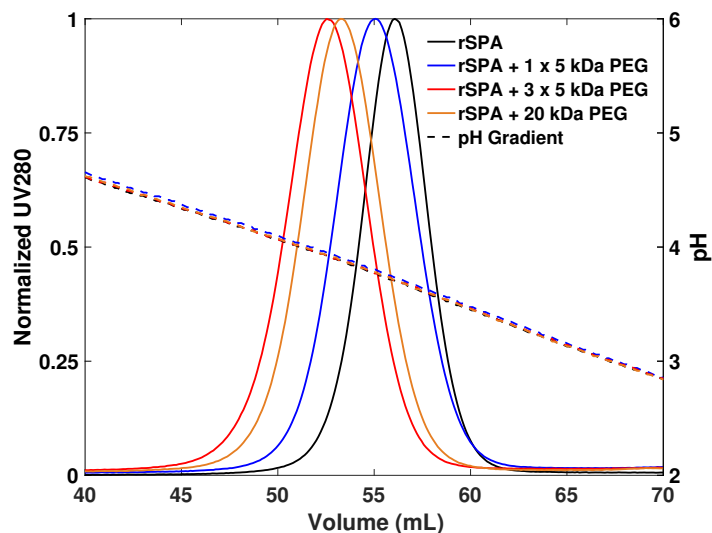
Figure 4.3. pH gradient elution profiles of the mAb on the unmodified and PEGylated rSPA resins. The four essentially coincident dashed lines represent the pH gradient for each of the elution experiments.

4.4.3. Dynamic binding capacities

The dynamic binding capacities of hIgG on the unmodified and the PEGylated rSPA resins were evaluated via breakthrough experiments conducted at a mobile phase concentration of 2 mg hIgG/mL and with residence times ranging between 2 and 11 minutes. Figure 4.4 displays values of $DBC_{10\%}$ for all four resins as a function of residence time. As expected, the $DBC_{10\%}$ increased with residence time for all resins since more time becomes available for the IgG molecules to diffuse and bind within the particles. Based on the static binding capacity values described above, it was also expected to see proportional losses in $DBC_{10\%}$ for the PEGylated rSPA resins compared to the unmodified resin. While this expectation held true for the rSPA + 3×5 kDa PEG and rSPA + 20 kDa PEG resins, there was negligible loss in $DBC_{10\%}$ for the rSPA + 1×5 kDa PEG resin relative to the unmodified resin. For a simple pore-diffusion limited transport model, decreases in values of both q_{max} and D_{eff}, which were measured for the

rSPA + 1×5 kDa PEG resin, will in tandem reduce $DBC_{10\%}$. Therefore, the $DBC_{10\%}$ values shown in Figure 4.3 for the rSPA + 1×5 kDa PEG resin provide further evidence that the attachment of PEG to the rSPA ligand results in additional complexity in the IgG adsorption kinetics that is not captured by a simple pore-diffusion limited model.
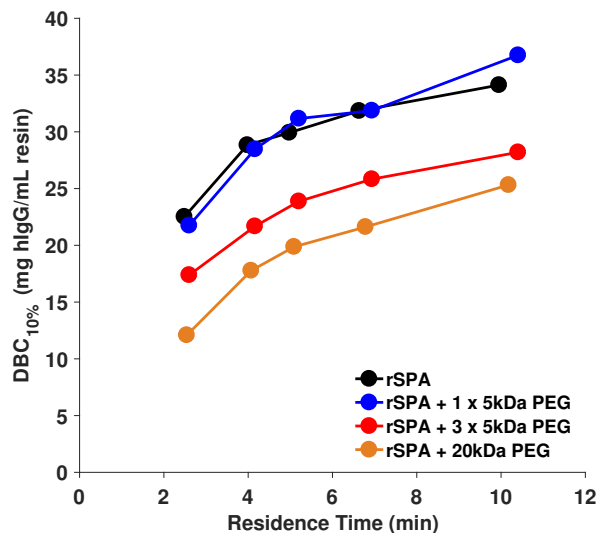
Figure 4.4. Plot of $DBC_{10\%}$ as a function of column residence time for the unmodified and PEGylated rSPA resins. Solid lines represent linear interpolations of the data points to highlight trends.

Unlike the values of β_{IgG}, r_{pore}, and q_{max}, which are correlated with the conjugated PEG volume within the resin pores, values of $DBC_{10\%}$ appear to have no direct or simple relationship with immobilized PEG volume. In addition, it is again shown that the covalent attachment of PEG to rSPA can significantly reduce values of $DBC_{10\%}$ for certain modification strategies. For example, $DBC_{10\%}$ values for the rSPA + 20 kDa PEG resin ranged from 12 to 25 mg hIgG/mL resin, which represents a 26 to 47% decrease in $DBC_{10\%}$ compared to the unmodified resin. This result is consistent with the previous findings of Gonzalez-Valdez et al. for a similar PEGylation chemistry [7].

4.4.4. Adsorption kinetics

Figure 4.5 shows the batch uptake curves for the mAb on the unmodified and PEGylated rSPA resins at an initial hIgG concentration of 2 mg/mL over a 7000 s period. To facilitate comparisons, the uptake curves for each resin were normalized by their respective values of q_{max} for the mAb as given in Table 4.3. The adsorption kinetics were exclusively studied with the mAb to remove the confounding effects of the competitive binding behavior of hIgG on ProA resins, as reported by Weinberg et al. [30]. As seen in Figure 4.5, essentially 100% of q_{max} was achieved for the unmodified resin over a period of 7000 s. However, for the PEGylated rSPA resins, while initially fast, the adsorption kinetics slow down dramatically for longer times, only achieving between 73 and 91% of q_{max} at 7000 s. These results suggest that PEGylation of the rSPA ligands results in heterogeneous binding kinetics with a fraction of the ligand binding domains binding IgG rapidly and another binding much more slowly. From a molecular perspective, it is likely that the steric hindrance of the PEG chains reduces the number of successful collisions between the IgG and some fraction of the ProA binding domains, thus resulting in a slower approach to equilibrium. Since these slow kinetics are apparent at longer times, it is also possible that the steric hindrance of the PEG is primarily disrupting the kinetics of secondary IgG binding events on the same ligand. Furthermore, the observed slow kinetics align with the apparent increase in elution pH, and decrease in average IgG binding affinity, for the PEGylated rSPA ligands. It is possible that a portion of ProA binding sites may have slower association kinetics due to a less thermodynamically stable IgG-(PEG)-ProA complex.
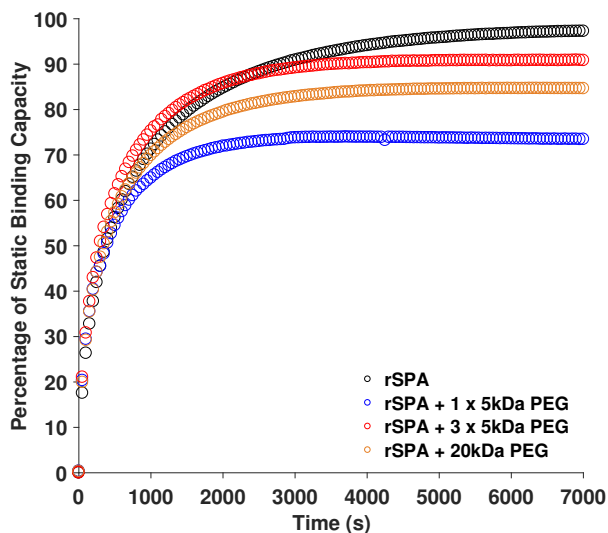
Figure 4.5. Normalized batch uptake curves for the unmodified and PEGylated rSPA resins for the mAb at an initial concentration of 2 mg/mL over 7000s.

It is interesting to note that the rSPA + 1×5 kDa PEG resin, which had the smallest volume of immobilized PEG per mole of rSPA, achieved the lowest percentage of q_{max} over the 7000 s period. This is counterintuitive since it was expected that increasing the amount of steric hindrance with the amount of PEG on the ligands would result in a higher fraction of binding events with slower kinetics.

4.4.5. CLSM results

Figure 4.6 shows the CLSM images obtained for the adsorption of mAb from a 2 mg/mL solution on the unmodified and the PEGylated rSPA resins as a function of incubation time. Figures 4.7a-d shows the corresponding radially averaged fluorescence intensity profiles for up to 4 hr of adsorption for the unmodified, rSPA + 1×5 kDa PEG, rSPA + 3×5 kDa PEG, and rSPA + 20 kDa PEG resins, respectively. As seen in Fig. 4.6, the adsorption front of the mAb is relatively sharp for both unmodified and PEGylated rSPA resins, which is the behavior expected for highly favorable and pore diffusion-limited adsorption. However, Fig. 4.6 also shows that

PEGylation affects the speed at which the adsorption front moves toward the center of the particle. For example, the mAb adsorption front in rSPA + 1×5 kDa PEG resin reaches the center of the particle between 10 and 15 min, which is well before the 30 to 40 min required for the unmodified resin. This is also evident when comparing the intraparticle intensity profiles over time in Fig. 4.7.
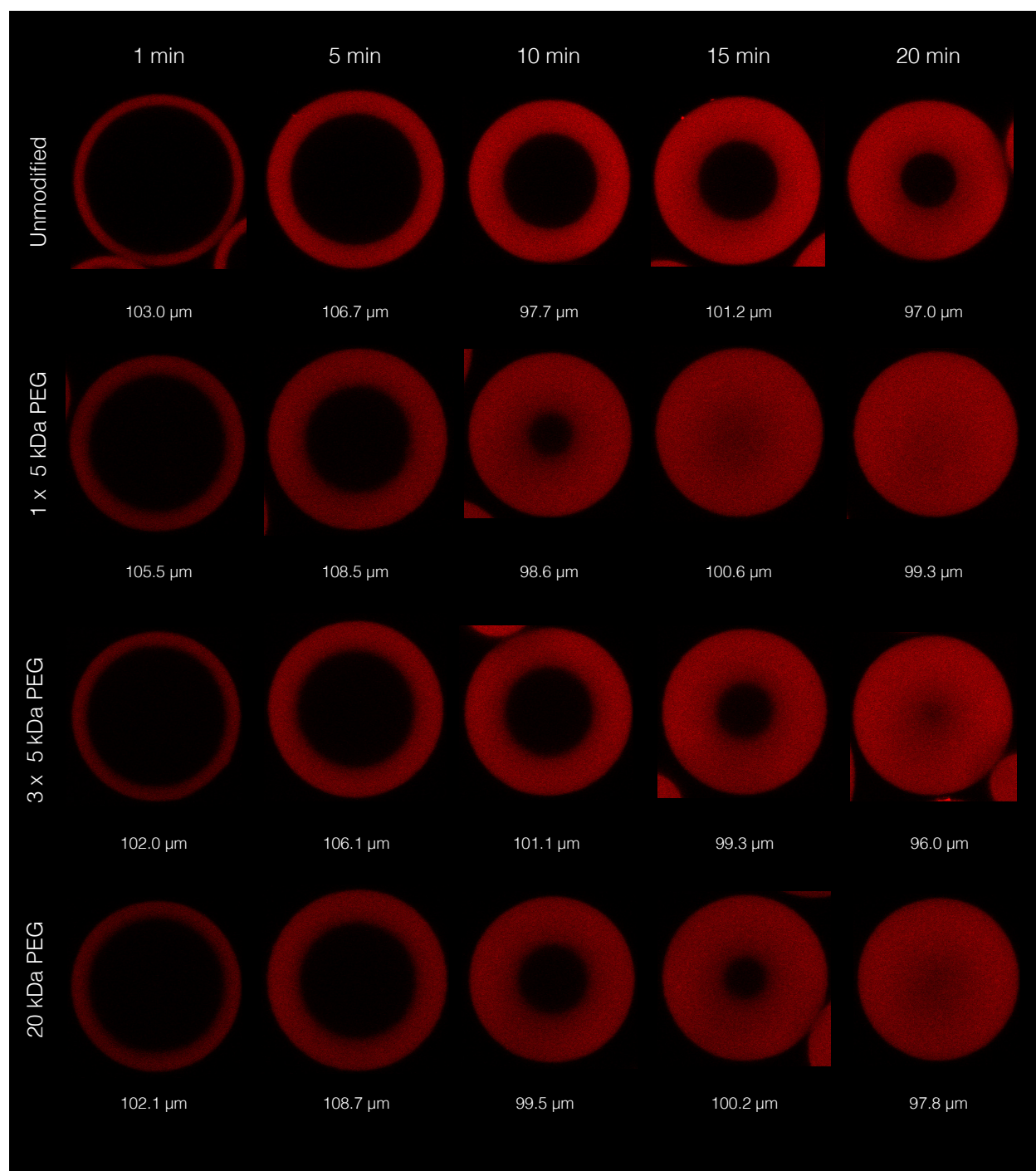
Figure 4.6. Representative CLSM images of adsorption of 2 mg/mL mAb for the unmodified and PEGylated rSPA resins for times up to 20 min. Data for longer times are given in Fig. 4.7. Actual particle diameters are shown below each image.
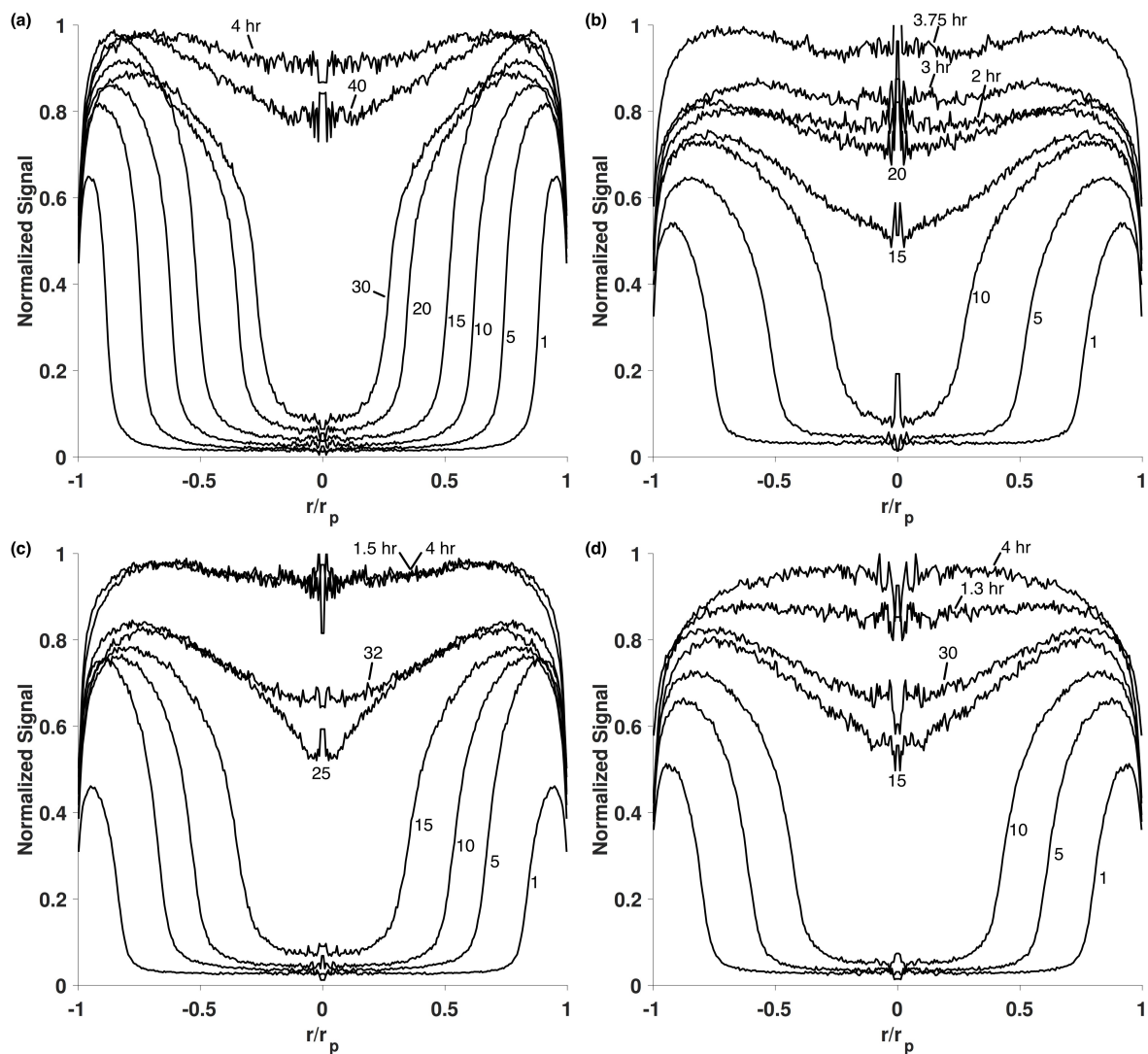
Figure 4.7. Radially averaged and normalized intensity profiles obtained from the CLSM batch images for times up to 4 hr for (a) the unmodified resin, (b) rSPA + 1×5 kDa PEG, (c) rSPA + 3×5 kDa PEG, and (d) rSPA + 20 kDa PEG resins. Time labels without specified units represent minutes.

The increase in the speed of the adsorption front for the rSPA + 1×5 kDa PEG resin is partially explained by its lower static binding capacity. However, when comparing the speed of the adsorption fronts of the rSPA + 1×5 kDa PEG and rSPA + 3×5 kDa PEG media, it is seen that the front slows down as additional PEG chains are added into the resin. Since both resins have similar values of q_{max} for the mAb, it is likely that the slower front speed is due to the fact

that a higher percentage of q_{max} is utilized for short times in the more heavily PEGylated rSPA resin (shown in Fig. 4.5) with the remaining capacity utilized only over longer time scales as a result of a higher kinetic resistance to binding. A similar comparison between rSPA + 3×5 kDa PEG and rSPA + 20 kDa PEG shows roughly equivalent adsorption front speeds. Furthermore, since the value of q_{max} for rSPA + 20 kDa PEG is even smaller, the similar adsorption front speed suggests additional mass transfer resistance exists compared to rSPA + 3×5 kDa PEG resin. This is consistent with the decrease in D_e for the rSPA + 20 kDa PEG resin shown in Table 4.2.

The increase in the speed of the mAb adsorption front for the rSPA + 1×5 kDa PEG resin also provides a likely explanation for the DBC$_{10\%}$ behaviors measured for the same resins (shown in Fig. 4.4). Despite losing a number of total active binding sites due to PEGylation, IgG molecules are able to utilize more of the resin particle interior surface area, and thus binding sites, over the same amount of time compared to the unmodified resin. When more PEG is added to the rSPA ligands, the increase in mass transfer resistance combined with the additional loss of active binding sites results in a loss in DBC$_{10\%}$.

When comparing the CLSM adsorption profiles over longer times in Fig. 4.7a-d, it is seen that while the unmodified resin follows the typical "shrinking core" behavior expected for diffusion-limited adsorption, the PEGylated rSPA resins do not. In the latter case, mAb molecules reach the center of the particle well before full saturation is attained. This is consistent with the batch uptake data in Fig. 4.5, which showed rapid initial adsorption kinetics followed by a very slow approach to saturation for the PEGylated rSPA resins. The radial profiles of the rSPA + 1×5 kDa PEG resin in Figure 4.7b show the most significant rise in intensity over longer

times, which is also consistent with the batch uptake data showing that the same resin achieved the lowest percentage of q_{max} over 2000 s of adsorption.

Figure 4.8 shows the dimensionless position of the adsorption front as a function of time for the unmodified and PEGylated rSPA resins. To validate that the mAb adsorption kinetics do not follow the typical shrinking core behavior in the PEGylated rSPA resins, the CLSM images were analyzed under the shrinking core model (SCM), which is given by [31]:

$$2\rho_s^3 - 3\rho_s^2 + 1 = \frac{6D_0 C_0 t}{q_{max} r_p^2} \frac{D_e}{D_0} \tag{4.11}$$

where ρ_s is the dimensionless front position within the resin particle, C_0 is the mAb concentration in the bulk solution, r_p is the particle radius, and t is the time of adsorption.
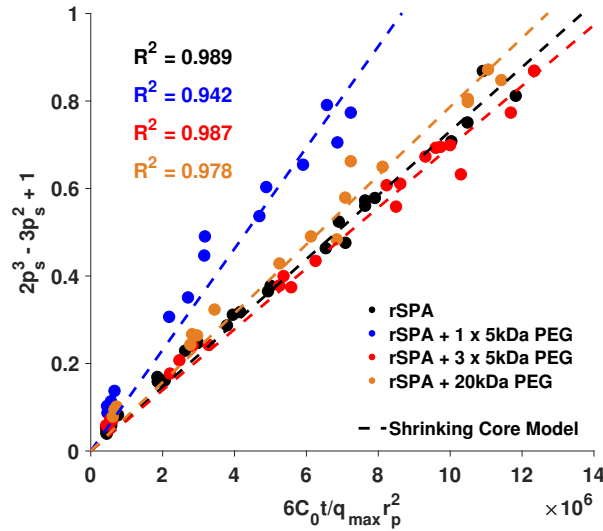
Figure 4.8. Plots of the dimensionless position of the adsorption front according to the shrinking core model versus $6C_0 t / q_{max} r_p^2$ for the unmodified and PEGylated rSPA resins.

As seen in Figure 4.8, both the unmodified and all PEGylated rSPA resins had excellent fits to the SCM. A comparison of D_e values obtained from the linear fits of the SCM via eq. 4.11 are

reported alongside the values obtained via non-binding HETP experiments in Table 4.2. Values of D_e for the unmodified and rSPA + 3×5 kDa PEG resins were in good agreement for both methods, but values for the rSPA + 1×5 kDa PEG and rSPA + 20 kDa PEG resins were significantly off. In particular, the values of D_e within these two resins were determined via the SCM to be greater than that within the unmodified resin. This result is seemingly physically impossible given that values of β_{IgG} and r_{pore} decreased for the rSPA + 1×5 kDa PEG and rSPA + 20 kDa PEG resins, which implies an increase in mass transfer resistance and decrease in D_e via eq. 10.

Although the adsorption behavior of the PEGylated rSPA resins appear to be shrinking core-like from a visual perspective in the CLSM images over short times, the heterogeneous binding kinetics in the modified systems add complexities that are not captured in the simple SCM. Since there is a percentage of capacity in the PEGylated rSPA resins that binds with fast kinetics under short times and another percentage with slow kinetics at long times, the single capacity parameter in SCM only accounts for the former. This explains why the values of D_e from the SCM and HETP experiments appear to converge as a function of the percentage of q_{max} that each resin achieves at the end of its respective stirred-tank batch uptake profile in Fig. 4.5. For example, the rSPA + 3×5 kDa PEG resin achieves 91% of q_{max}, which makes it the most "shrinking core-like", and thus explains the apparent qualitative agreement between the SCM and HETP methods.

Finally, as seen in Figures 4.7a-d, the level of mAb intensity at long times was fairly uniform throughout the resin particle space, which again suggested that there was an even spatial distribution of PEG within the PEGylated rSPA resins.

4.5. Conclusions

Our results elucidate important physical and performance characteristics of ProA chromatography ligands conjugated with PEG chains. We find that in all cases, PEGylation of ProA ligands decreases the resin particle porosity, apparent pore size, and static binding capacity for IgG to an extent that is proportional to the volume of conjugated PEG in the resin. Additionally, we find that PEGylation induces heterogeneous adsorption kinetics; transforming a fraction of IgG binding sites with typical fast association kinetics to slow kinetics. This heterogeneity is displayed in batch adsorption profiles where a slow tailing behavior is observed for long-time binding events. An increase in IgG elution pH for all PEGylated rSPA resins signals an average decrease in IgG-ProA binding affinity post-modification, likely explaining the emergence of binding sites with slow association kinetics. Finally, we discover that the loss of resin $DBC_{10\%}$ for hIgG is dependent on both the PEG molecular weight and the extent of modification. In lighter modifications with a small molecular weight, it is possible to retain $DBC_{10\%}$, but heavier modifications result in a loss of dynamic capacity due to decreased static binding capacity and increased mass transfer resistance.

Commercial adoption of a ProA resin with lower values of $DBC_{10\%}$, and thus lower productivity, would be a significant challenge for downstream processing due to the need for additional, expensive resin or longer processing times to meet the same throughput. However, the loss in productivity would need to be considered in the context of tradeoffs with the benefits of increased selectivity or and/or increased resin lifetime, which are discussed in Part II of this work. The retention of $DBC_{10\%}$ in the rSPA + 1×5 kDa PEG resin is an important and promising result as it points towards the potential to optimize the PEGylation strategy for maximizing $DBC_{10\%}$ and productivity.

In the context of bioprocessing, the increase in elution pH for the PEGylated rSPA resins is also significant when purifying mAbs or related drug products, such as Fc-fusion proteins, that may be pH sensitive. In this case, it is beneficial for the pH of elution to be higher so that protein denaturation at low pH values is avoided. As a result, this work points to another path for commercial viability of the modified resins in the case of pH sensitive targets where binding capacity is not a primary concern.

While our results increase the general understanding of ProA resins with PEGylated ligands, the specific approach of modifying ProA used in this work remains "naïve". Moving forward, an approach where the modification strategy can be engineered to optimize performance characteristics such as binding capacity, selectivity, robustness, or elution pH will be preferred. Developing mechanistic models to describe the complex adsorption kinetics or experimental methods that allow for high throughput screening of many different modification strategies are two steps that can be taken towards achieving this goal. In addition, adding a level of control to where and how many PEG molecules are covalently attached to the ProA ligand will also allow the performance of the resin to be optimized. In the current "naïve" approach, it is extremely difficult to determine which residues, most likely lysines, of the ProA participate in the covalent attachment of the PEG chains since the ligand is already immobilized within a cross-linked network. PEGylating ProA molecules in free solution and then immobilizing the modified protein onto the base matrix might allow for better control of the ligand properties. In this case, care would need to be taken to prevent the PEGylation from hindering the ability for the ligand to be immobilized to the resin. Additional techniques such as masking the ProA ligand with a mAb or Fc fragment prior to modification may preserve IgG binding capacity by avoiding hindrance with binding sites.

4.6. References

[1] A. Shukla, J. Thommes, Recent advances in large-scale production of monoclonal antibodies and related proteins, Trends Biotechnol. 28 (2010) 253-261.

[2] S. Hober, K. Nord, M. Linhult, Protein A chromatography for antibody purification, J Chromatogr B. 848 (2007) 40-47.

[3] R.D.R. Tarrant, M.L. Velez-Suberbie, A.S. Tait, C.M. Smales, D.G. Bracewell, Host cell protein adsorption characteristics during protein a chromatography, Biotechnol Prog. 28 (2012) 1037-1044.

[4] H. Hjelm, K. Hjelm, J. Sjöquist. Protein a from Staphylococcus aureus. Its isolation by affinity chromatography and its use as an immunosorbent for isolation of immunoglobulins, FEBS Lett. 28 (1972) 73-76.

[5] R. Hahn, K. Shimahara, F. Steindl, A. Jungbauer, Comparison of protein A affinity sorbents III. Life time study, J Chromatogr A. 1102 (2006) 224-231.

[6] Repligen, Captiva Primab—Protein A affinity resin—Regulatory Support File RSF-1003201. (2010).

[7] J. González-Valdez, A. Yoshikawa, J. Weinberg, J. Benavides, M. Rito-Palomares, T. Przybycien, Toward improving selectivity in affinity chromatography with PEGylated affinity ligands: The performance of PEGylated protein A, Biotechnol Prog. 30 (2014) 1364-1379.

[8] M. Michaelis, J. Cinatl, P. Pouckova, K. Langer, J. Kreuler, J. Matousek, Coupling of the antitumoral enzyme bovine seminal ribonuclease to polyethylene glycol chains increases its systemic efficacy in mice, Anti-Cancer Drugs. 13 (2002) 149-154.

[9] J.M. Harris, N.E. Martin, M. Modi, Pegylation: a novel process for modifying pharmacokinetics, Clin Pharmacokinet. 40 (2001) 539-551.

[10] Z. Wen, B. Niemeyer, Preparation and characterization of PEGylated Concanavalin A for affinity chromatography with improved stability, J Chromatogr B. 879 (2011) 1732–1740.

[11] J.R. Peyser, Nucleic acids encoding recombinant protein A, US Patent no. 7,691,698 B2., 2010.

[12] GE Healthcare Life Sciences, Sepharose 4 Fast Flow Sepharose 6 Fast Flow, Data File 18-1020-52 AD, 2013.

[13] J. Weinberg, S. Zhang, A. Kirkby, E. Shachar, G. Carta, T. Przybycien, Chemical Modification of Protein A Chromatography Ligands with Polyethylene Glycol. II: Effects on Resin Robustness and Process Selectivity, J Chromatogr A. (2017) *in review.*

[14] G. Howard, M. Kaser, Making And Using Antibodies, Taylor & Francis/CRC Press, Boca Raton, FL, 2003.

[15] O. Kinstler, N. Gabriel, C. Farrar, R. DePrince, N-terminally chemically modified protein compositions and methods, US Patent no. 5,824,784 A, 1998.

[16] M. Cisneros-Ruiz, K. Mayolo-Deloisa, T.M. Przybycien, M.A. Rito-Palomares, Separation of PEGylated from unmodified ribonuclease A using sepharose media, Sep Purif Technol. 65 (2009) 105–109.

[17] S.M. Daly, T.M. Przybycien, R.D. Tilton, Adsorption of poly(ethylene glycol)-modified lysozyme to silica, Langmuir. 21 (2005) 1328–1337.

[18] L.G. Caro, The molecular weight of lambda DNA. Virol J. 25 (1965) 226-236.

[19] P. DePhillips, A. Lenhoff, Pore size distributions of cation-exchange adsorbents determined by inverse size-exclusion chromatography. J Chromatogr A. 883 (2000) 39-54.

[20] L. Hagel, Ö Magnus, A. Torvald, Apparent pore size distributions of chromatography media, J Chromatogr A. 743 (1996) 33-42.

[21] E.X. Perez-Almodovar, G. Carta, IgG adsorption on a new protein A adsorbent based on macroporous hydrophilic polymers. I. Adsorption equilibrium and kinetics, J Chromatogr A. 1216 (2009) 8339-8347.

[22] M.T. Tyn, T.W. Gusek, Prediction of diffusion coefficients of proteins, Biotechnol Bioeng. 35 (1990) 327-338.

[23] M.D. LeVan, G. Carta, D.W. Green, R.H. Perry, Perry's Chemical Engineers' Handbook, Section 16: Adsorption and Ion Exchange, eighth ed., McGraw-Hill, New York, 2007.

[24] Y. Tao, E. Perez-Almodovar, G. Carta, G. Ferreira, D. Robbins, Adsorption kinetics of deamidated antibody variants on macroporous and dextran-grafted cation exchangers. III. Microscopic studies. J Chromatogr A. 1218 (2011) 8027-8035.

[25] S. Zhang, W. Daniels, J. Salm, J. Glynn, J. Martin, C. Gallo, R. Godavarti, G. Carta, Nature of foulants and fouling mechanism in the Protein A MabSelect resin cycled in a monoclonal antibody purification process, Biotechnol Bioeng. 113 (2016) 141-149.

[26] S. Kuga, Pore size distribution analysis of gel substances by size exclusion chromatography, J Chromatogr. 206 (1981) 449-61.

[27] P. Gagnon, R. Nian, D. Leong, A. Hoi, Transient conformational modification of immunoglobulin G during purification by protein A affinity chromatography, J Chromatogr A. 1395 (2015) 136-142.

[28] S.S. Pai, B. Hammouda, K. Hong, D.C. Pozzo, T.M. Przybycien, R.D. Tilton, The conformation of the poly (ethylene glycol) chain in mono-PEGylated lysozyme and mono-PEGylated human growth hormone, Bioconjugate Chem. 22 (2011) 2317–2323.

[29] P. Gagnon, Purification Tools for Monoclonal Antibodies, Validated Biosystems, Inc., Tucson, 1996.

[30] J. Weinberg, S. Zhang, G. Crews, E. Healy, G. Carta, T. Przybycien, Polyclonal and monoclonal IgG binding on protein A resins—Evidence of competitive binding effects, Biotechnol Bioeng. 114 (2017) 1803–1812.

[31] C. Martin, G. Iberer, A. Ubiera, G. Carta, Protein Mass Transfer Kinetics in Ion Exchange Media: Measurements and Interpretations, J. Chromatogr. A 1079 (2005) 105.

5

Chemical Modification of Protein A Chromatography Ligands with Polyethylene Glycol: Effects on Resin Robustness and Process Selectivity

This chapter of the thesis was adapted from the manuscript, "Chemical Modification of Protein A Chromatography Ligands with Polyethylene Glycol. II: Effects on Resin Robustness and Process Selectivity", authored by Justin Weinberg, Shaojie Zhang, Allison Kirkby, Enosh Shachar, Giorgio Carta, and Todd Przybycien. The manuscript was submitted for review to the Journal of Chromatography A on September 5th, 2017.

5.1. Chapter abstract

We have proposed chemical modification of Protein A (ProA) chromatography ligands with polyethylene glycol (PEGylation) as a strategy to increase the resin selectivity and robustness by providing the ligand with a steric repulsion barrier against non-specific binding. Here, we report on robustness and selectivity benefits for Repligen CaptivA PriMAB resin with ligands modified with 5.2 kDa and 21.5 kDa PEG chains, respectively. PEGylation of ProA ligands allowed the resin to retain a higher percentage of static binding capacity relative to the unmodified resin upon digestion with chymotrypsin, a representative serine protease. The level of protection against digestion was independent of the PEG molecular weight or modification extent for the PEGylation chemistry used. Additionally, PEGylation of the ligands was found to

decrease the level of non-specific binding of fluorescently labeled bovine serum albumin (BSA) aggregates to the surface of the resin particles as visualized via confocal laser scanning microscopy (CLSM). The level of aggregate binding decreased as the PEG molecular weight increased, but increasing the extent of modification with 5.2 kDa PEG chains had no effect. Further examination of resin particles via CLSM confirmed that the PEG chains on the modified ligands were capable of blocking the "hitchhiking" association of BSA, a mock contaminant, to an adsorbed mAb that is prone to BSA binding. Ligands modified with 21.5 kDa PEG chains were effective at blocking the association, while ligands modified with 5.2 kDa PEG chains were not. Finally, ligands with 21.5 kDa PEG chains increased the selectivity of the resin against host cell proteins (HCPs) produced by Chinese Hamster Ovary (CHO) cells by up to 37% during purification of a monoclonal antibody (mAb) from harvested cell culture fluid (HCCF) using a standard ProA chromatography protocol. The combined work suggests that PEGylating ProA chromatography media is a viable pathway for increasing both resin lifetime and host cell impurity clearance in downstream bioprocessing.

5.2. Introduction

Protein A (ProA) chromatography is well established as the gold standard in downstream bioprocessing for the selective capture and purification of IgG-class monoclonal antibodies (mAbs) and Fc-fusion proteins [1]. In a ProA chromatography-based capture step, harvested cell culture fluid (HCCF) containing the expressed drug product, typically using Chinese Hamster Ovary (CHO) cells as the host, is loaded onto a column packed with ProA chromatography resin at neutral pH. After diffusing into the pores of the resin, the IgG molecules interact and bind selectively via the Fc region to immobilized ProA ligands, which enables the broad and

practically universal applicability of ProA chromatography for this class of biomolecules [2]. Contaminants from the HCCF such as host cell proteins (HCPs), host DNA, and host virus mostly pass through the column. Following a series of wash steps, the IgG molecules are eluted from the column at low pH and are collected at purity levels typically above 98% by mass [3].

While ProA chromatography intrinsically provides a high level of clearance for host cell impurities, strict requirements on contaminant content in final drug product formulations set by the FDA and other regulatory authorities require the addition of multiple, subsequent "polishing" processing steps to achieve desired purity levels [1]. Amongst the various classes of impurities, clearance of HCPs in downstream processing is often challenging due to their wide range of physiochemical properties, the possibility of association with IgG molecules, and concerns about their immunogenicity [4]. In recent years, as upstream technology has advanced and the number of mAbs (and related products) in development and on the market have accelerated, purification processes have become the bottleneck for production [5]. This has driven numerous studies of the nature of impurity interactions in the context of ProA chromatography as well as best practices, such as improved wash steps and low pH cell culture harvest treatments, for increasing HCP and other impurity clearances [3,5-10].

Another significant concern with ProA chromatography is resin lifetime due to fouling. Recent studies have estimated that downstream purification represents 50-80% of total mAb manufacturing costs; a large portion of this cost is from consumables such as chromatography resins [11]. ProA resins, in particular, are significant costs with a price tag of $5,000-15,000/L resin and with industrial columns requiring volumes of up to 1000 L [12-14]. As a result, it is typically desired to reuse ProA resins over multiple process cycles, but this has to be balanced against declining resin performance. Several factors can affect this decline, including cleavage or

denaturation of the ProA ligand by host cell proteases or under CIP conditions, leakage of the ligand from the resin base matrix, fouling due to irreversible binding of large biomolecules that block binding sites or normally accessible pores, or physical failures of the resin particle structure or packed bed [13-17]. As a result, resin lifetime is a significant consideration during process development and has spurred development of more rigid base matrices as well as alkali-stabilized and protease-resistant ProA ligands such as the SuRe ligand from GE Healthcare [2,18-20]. Recent presentations suggest that a new generation of even more alkali-stable ProA ligands are in development [21].

In this work, we investigate the performance of ProA chromatography resins with ligands that have been chemically modified with polyethylene glycol (PEGylated) to provide a steric barrier against proteolytic degradation of the ligand as well as against non-specific binding from process contaminants and foulants. This approach was motivated by the extensive prior literature that had shown that PEGylation can reduce proteolytic and immunogenic attack of protein drugs *in vivo*, improve the fouling resistance of surfaces, and improve the stability of the affinity chromatography ligand, concanavalin A [22-27]. The basic idea of PEGylating ProA ligands to improve affinity resins was introduced by the initial study of Gonzalez-Valdez et al. [28]. In Part I of this work (Chapter 4) [29], we investigated the IgG adsorption and transport characteristics on Repligen CaptivA PriMAB resins with recombinant Staphylococcal Protein A (rSPA) ligands that had been PEGylated with either 5.2 or 21.5 kDa PEG to determine the extent to which PEGylation impacts IgG binding capacity, affinity, and kinetics. Here in Part II (this chapter), we utilize the same modified resins to investigate resulting enhancements to resin robustness and selectivity. In combination, the two parts of this study provide the means for developing

optimized PEGylation strategies that achieve a desired balance of process performance characteristics.

Three aspects related to resin robustness are considered in this work. The first is the ability of PEGylation to improve resistance to proteolytic degradation. For this purpose, we subjected the PEGylated rSPA resins to accelerated proteolytic digestion using a representative serine protease, chymotrypsin, to determine lifetime trajectories of resin static binding capacity. The second is the ability of PEGylation to reduce non-specific binding leading to resin fouling. For this purpose, we exposed the resins to fluorescently labeled bovine serum albumin (BSA) aggregates and studied their accumulation in the resin beads by confocal laser scanning microscopy (CLSM). The third is the ability of PEGylation to reduce association of impurities with the bound IgG. With regards to the latter aspect, studies have confirmed that the vast majority of residual impurities in ProA chromatography are from species that associate with the bound IgG molecules and the level of carryover is dependent on the particular IgG molecule used [4,8,9,20]. In fact, recent work by Zhang et al. [30] suggested that this "hitchhiking" occurs due to structural perturbation that IgG undergoes when bound to ProA, allowing for impurities to associate with the bound IgG even when no association occurs in free solution. This effect was demonstrated using a particular mAb that associated with fluorescently labeled BSA when bound to a ProA resin but did not in free solution nor when bound to a cation exchange resin. In order to test whether PEGylation of the ProA ligand can also reduce this association effect, we exposed the PEG-modified resins saturated with the same mAb used by Zhang et al. [30] to fluorescently labeled BSA. We hypothesized that PEGylation of the ligand would create a "size exclusion effect" where the excluded volume and low protein-binding tendency of the polymer [31] would

141

make it more difficult for an additional host impurity to associate with the mAb-(PEG)-ProA complex.

The original study of PEGylated ProA chromatography ligands by Gonzalez-Valdez et al. [28] reported up to an order of magnitude increase in process selectivity when the modified resins were subjected to pulse injections of rabbit polyclonal IgG spiked with yeast extract and fetal bovine serum as mock contaminants. While promising, these experiments did not include typical process contaminants, particularly those found in CHO HCCF. Additionally, the pulse IgG injections used represented a small fraction of the typical ProA chromatography process loads of 20-40 g mAb/L resin [5,15,32,33]. To test the selectivity of the PEGylated rSPA resins under more realistic conditions, we loaded CHO HCCF containing an expressed mAb to 30 g/L in order to determine HCP clearance and mAb yield.

5.3. Materials and methods

5.3.1. Materials

CaptivA PriMAB and the PEGylated rSPA resins in both loose and packed column formats, described and characterized in Part I (Chapter 4) [29], were used in this work. The PEGylated rSPA resins are denoted rSPA + 1×5 kDa PEG, rSPA + 3×5 kDa PEG, and rSPA + 20 kDa PEG to specify the molecular weight and average number of PEG chains per ProA ligand. Loose MabSelect SuRe resin was donated by GE Healthcare (Piscataway, NJ) and packed into an OPUS column for our use by Repligen (Waltham, MA). Two mAbs were used in Part II of this work (this chapter), identified as mAb A and mAb B. mAb A was provided by Pfizer (St. Louis, MO) and was an industrially purified, glycosylated IgG_2 antibody (with ~10 ppm HCP content) with a pI of ~8.1 and an extinction coefficient of 1.51 AU•mL•mg^{-1}•cm^{-1}.

mAb B was provided by Biogen (Cambridge, MA) and was a glycosylated IgG_1 antibody with a pI of 8.45 and an extinction coefficient of 1.5 AU•mL•mg^{-1}•cm^{-1}. mAb B was provided in two forms: as expressed in CHO HCCF that was produced at Biogen and as a neutralized ProA chromatography column eluate with <100 ppm HCP content. Based on size exclusion chromatography, both mAbs were essentially 100% monomer; aggregate levels were below the detection limit. Both mAb samples were buffer exchanged as needed via Amicon Ultra-15 centrifugal filter units with a 100 kDa molecular weight cutoff (EMD Millipore, Billerica, MA) or with PD-10 desalting columns (GE Healthcare, Piscataway, NJ). Human polyclonal IgG antibody (hIgG) was obtained from Lee Biosolutions (Maryland Heights, MO) and was prepared as described in Part I of this work (Chapter 4) [29].

α-Chymotrypsin from bovine pancreas was obtained as a lyophilized powder with an activity level of 40 units/mg from Sigma-Aldrich (St. Louis, MO). BSA was also obtained as a lyophilized powder (purity $\geq$ 95%) from Sigma-Aldrich (Catalog No. A2058, St. Louis, MO). Rhodamine Red™-X and Rhodamine Green™-X succinimidyl ester amine-reactive dyes were obtained from Invitrogen Corporation (Carlsbad, CA). CHO HCP third-generation ELISA kits were obtained from Cygnus Technologies (Southport, NC). All other chemicals and assay components were obtained from Sigma-Aldrich (St. Louis, MO) or Fisher Scientific (Pittsburgh, PA). All water was purified by reverse osmosis followed by treatment to 18 M$\Omega \cdot$ cm resistivity using a Barnstead NANOpure Diamond system from Barnstead International (Dubuque, IA). All experiments were conducted at room temperature (22$\pm$2 ºC in this work).

5.3.2. Chymotrypsin digestion experiments

The ligands on unmodified CaptivA PriMAB resin and the PEGylated rSPA resins were digested using the model protease, chymotrypsin, in order to simulate lifetime trajectories of each resin's maximum static binding capacity (q_{max}) over multiple process cycles. Hydrated particles of each resin variant were first synthesized as described in Part I of this work (Chapter 4) [29]. Roughly 100 mg of hydrated resin particles were added to microcentrifuge tubes followed by 1 mL of a 1 mg/mL (40 units/mL) chymotrypsin solution in phosphate buffered saline (PBS) buffer. The chymotrypsin solutions were prepared immediately before resin digestion experiments to prevent losses in protease activity from autolysis. The PBS buffer used contained 137 mM NaCl, 2.7 mM KCl, 10 mM Na_2HPO_4, and 1.8 mM KH_2PO_4 and was adjusted to pH 7.0 with 1 M HCl. The microcentrifuge tubes were then allowed to rotate end-to-end at 18 rpm for a set period of time after which the entire contents of the tube were immediately filtered and washed 2 times with PBS buffer in 0.2 μm centrifugal filters at 1500×g for 2 minutes. This removed the chymotrypsin from the pores of the resin and stopped the digestion. The resin was washed a final time with PBS buffer and centrifuged at 3000×g for 45 min to regenerate hydrated resin particles. A single-point adsorption assay was performed by adding known weights of the digested, hydrated resin particles to a solution of 3.0 mg/mL hIgG (equilibrium concentration of ~1.3 mg/mL hIgG) in triplicate to estimate the value of q_{max} for each resin. The single-point adsorption isotherm measurement was conducted as described in Part I of this work (Chapter 4) [29]. This entire procedure was repeated for each resin and for time points ranging from 15 min to 3 hours. A single-point adsorption isotherm on each undigested resin was also performed in triplicate to serve as a time zero data point.

5.3.3. Non-specific BSA binding experiments

Non-specific binding of BSA as a model contaminant was tested by exposing CaptivA PriMAB and the PEGylated rSPA resins to fluorescently labeled BSA and quantifying the ensuing binding using CLSM. For this purpose, BSA, which was obtained as a lyophilized powder, was dissolved in PBS buffer and purified by size exclusion chromatography on a Superdex 200 column (GE Healthcare, Piscataway, NJ) to remove aggregates. The purified BSA was then labeled with Rhodamine Green™-X reactive dye using the procedure described in Part I of this work (Chapter 4) [29]. The dye extinction coefficient used was 68,000 AU•M^{-1}•cm^{-1} at 503 nm per Invitrogen documentation and absorbance values at 280 and 503 nm were used to determine the BSA:dye molar labeling ratio. The absorbance at 280 nm was adjusted by a correction factor supplied by the manufacturer ($0.17 \times A_{570}$ for Red, $0.19 \times A_{503}$ for green) to account for UV absorption of the dye. A literature BSA extinction coefficient value of 0.667 AU•mL•mg^{-1}•cm^{-1} at 280 nm was used [34]. The labeling ratio was determined to be 0.18 labels per protein molecule. The labeled BSA mixture was then diluted with unlabeled protein to achieve a final concentration of 0.2 mg/mL with a 1:20 labeled-to-unlabeled protein molar ratio. Less than 1 mg of each resin variant was then added to 0.4 mL of the labeled BSA mixture in 0.2 μm microcentrifugal filters, which were allowed to rotate end-to-end in the dark for 24 hours. After mixing, the slurries were filtered and then rapidly washed three times with PBS buffer. The hydrated resin particles were then re-suspended in PBS and subsequently imaged and analyzed under CLSM as described in Part I of this work (Chapter 4) [29].

5.3.4. BSA-mAb A association experiments

The selectivity of CaptivA PriMAB and the PEGylated rSPA resins during simultaneous adsorption of BSA, which served as a model "hitchhiking" contaminant, and mAb A was examined using CLSM. mAb A was labeled with Rhodamine Red™-X reactive dye using the procedure described in Part I of this work (Chapter 4) [29]. The labeling ratio was determined to be 0.25 labels per protein molecule. The labeled mAb A mixture was then diluted with the labeled BSA mixture and unlabeled mAb to achieve final concentrations of 2 mg/mL and 0.2 mg/mL, and labeled to-unlabeled protein molar ratios of 1:200 and 1:20, for mAb A and BSA, respectively. Several milligrams of each resin variant were first soaked in a labeled BSA mixture with a protein concentration of 0.2 mg/mL and a 1:20 labeled-to-unlabeled protein molar ratio for 5 minutes. This was performed to fill the resin pores with BSA and simulate real-world process conditions where contaminants first flow through the ProA resin before interacting with the mAb. The soaked resins were then filtered to remove the interstitial liquid and then less than 1 mg of hydrated resin particles were added to 5 mL of the BSA-mAb A mixture. The suspension was then mixed followed by periodically pipetting out 300 µL, rapidly filtering, and then suspending the particles in PBS buffer for imaging. This procedure was repeated for each resin variant for time points from 1 minute to 2 hours. CLSM imaging and analysis was performed as described in Part I of this work (Chapter 4) [29].

5.3.5. HCP clearance and resin selectivity with CHO HCCF purification experiments

The HCP clearance and selectivities of CaptivA PriMAB and the rSPA + 20 kDa PEG modified resin were determined by purifying mAb B from CHO HCCF. A mAb B concentration calibration curve was first generated from the neutralized mAb B ProA eluate provided by

Biogen. The concentration of mAb B in the eluate was determined to be 6.6 mg/mL using a Nanodrop 2000 spectrophotometer (Thermo Fisher Scientific, Waltham, MA) and the known protein extinction coefficient. mAb B concentrations in complex mixtures were assayed via ProA chromatography conducted in an analytical mode with a MabSelect SuRe column. Pulse injections of 5 mL for a series of diluted mAb B standards were performed with an Akta Explorer 100 system (GE Healthcare, Piscataway, NJ) in triplicate. The injections were performed by equilibrating, loading, and washing the column with a total of 6 column volumes (CVs) of PBS buffer as the mobile phase and then eluting the protein with 4 CVs of 25 mM sodium acetate buffer at pH 3.5. Strongly bound species were stripped from the column using 4 CVs of 100 mM sodium citrate buffer at pH 2.0, however, negligible protein was removed during this step for the purified standards. The experiments were conducted at a constant flow rate of 1 mL/min. The calibration curve was generated from the areas under the absorbance curve at 280 nm during mAb elution versus the known standard concentrations. As expected, this relationship was highly linear ($R^2 \geq 0.999$). Subsequently, 5 mL pulse injections of the HCCF on the MabSelect SuRe column were performed in triplicate using the same load-wash-elute-strip method. The area under the absorbance curve generated during the elution step was used in conjunction with the calibration curve to determine the concentration of mAb B in the CHO HCCF. The CHO HCCF material was thawed from frozen aliquots and minor fluctuations were noted in the mAb B concentration depending on the particular aliquot used. mAb B concentrations in the HCCF ranged from 1.5-1.6 mg/mL.

After determining the concentration of mAb B in the CHO HCCF, a set volume (~100 mL) of the CHO HCCF was loaded onto columns of CaptivA PriMAB and the rSPA + 20 kDa PEG resin to achieve 30 g mAb/L resin. Briefly, the columns were equilibrated with 1 CV of

PBS buffer, loaded with the set volume of HCCF, washed with 5 CVs of PBS, eluted with 7 CVs of 25 mM sodium acetate at pH 3.5, stripped with 3 CVs of 100 mM sodium citrate at pH 2.0, regenerated with 4 CVs of 50 mM NaOH, 1 M NaCl solution, and finally washed with 10 CVs of PBS. The column eluate fraction for each experiment was collected and then immediately neutralized to pH 5.5 with a 50 mM Tris, 100 mM NaCl buffer at pH 8.0. All experiments were performed at a flow rate corresponding to a residence time of 6 minutes and in triplicate for each column.

To determine the mAb B yield for each purification, 5 mL pulse injections of the neutralized eluate fractions were performed on the MabSelect SuRe column using the load-wash-elute-strip method in triplicate. The area under the absorbance curve generated during the elution step was used in conjunction with the calibration curve to determine the concentration of mAb B in the eluate. A mass balance was performed to determine the final yield values. The HCP content in the neutralized eluate samples was determined using the CHO HCP ELISA kit according to the protocol provided by Cygnus Technologies. Eluate samples were diluted as appropriate with the assay diluent provided by the manufacturer in order to obtain absorbance readings which fell within the range of the provided CHO HCP standards. Analysis of the HCP content in the initial CHO HCCF suggested levels of $142,000 \pm 7,000$ ppm.

5.4. Results and discussion

5.4.1. Proteolytic degradation results

Figure 5.1 shows the residual IgG binding capacity of the unmodified and PEGylated rSPA resins after incubation with chymotrypsin plotted as the percentage of the initial binding capacity as a function of incubation time. Chymotrypsin is known to hydrolyze amide bonds

where the carboxyl side of the bond comprises one of four hydrophobic amino acids (Tyr, Trp, Phe, and Leu) [35]. Based on its sequence, rSPA has 49 possible chymotrypsin cleavage sites [36]. As seen from the figure, despite a sharp initial drop, all three PEGylated resins retained a higher percentage of their respective original binding capacity compared to the unmodified resin regardless of the PEG molecular weight or extent of PEGylation. This suggested that the PEG on the modified ligands was protecting a common cleavage site on the protein that would normally be accessible to chymotrypsin. Along the same lines, this also suggested that the PEG chains were covalently attached to the ligand in a similar location; likely the N-terminus based on the PEGylation chemistry used [37-39]. As also seen in the figure, following the initial drop, the rate of loss of binding capacity remained roughly unchanged for the modified resins. Combined, this suggested that the PEG was effective at blocking certain, likely proximal, cleavage sites but was ineffective at slowing the rate of attack for others. The results provide a promising sign that PEGylation may provide increased resin robustness under normal process conditions against serine proteases, which are a major class of proteinases produced by the CHO cell [40].
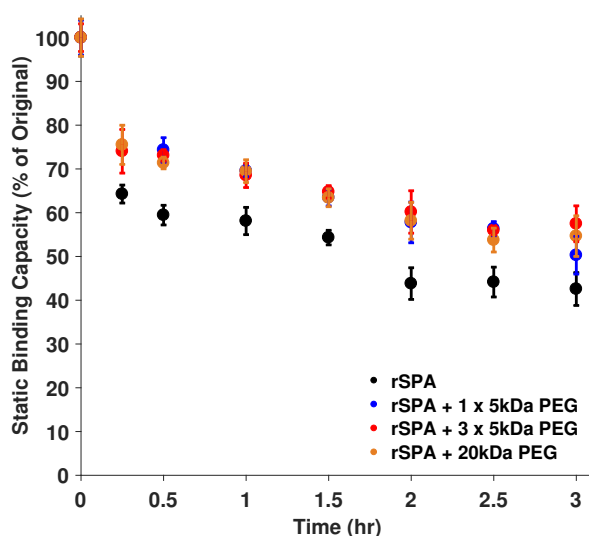
Figure 5.1. Plots of percentage of original IgG binding capacity of the unmodified and PEGylated rSPA resins after digestion with chymotrypsin for up to 3 hours. Error bars represent 95% confidence intervals based on triplicate measurements.

149

5.4.2. Non-specific BSA binding

Figure 5.2 displays a set of confocal images of similarly-sized particles from all four resins samples after incubation with fluorescently labeled BSA for 24 hr. As seen from the images, in all four cases binding of fluorescently labeled BSA occurred primarily near the bead outer surface suggesting that the labeled BSA aggregated on the surface or aggregated in solution and then bound to the surface; forming species that were too large to enter the pores of the resin. As seen from Figure 5.2, the fluorescence intensity was much fainter for the PEGylated rSPA resins than for the unmodified resin. The average intensities were calculated by averaging and normalizing the digitized intensity profiles over image surface areas according to the following equation (given constant optical slice thickness):

$$\bar{q}_{BSA} \approx \frac{\int_0^1 I_{BSA}(r)r^2 d\rho}{r_p^2} \tag{5.1}$$

where $\bar{q}_{BSA}$ is proportional to the amount of BSA bound per unit bead volume, I_{BSA} is the radially averaged local fluorescence intensity, r is the radial position, and r_p is the particle radius in μm.
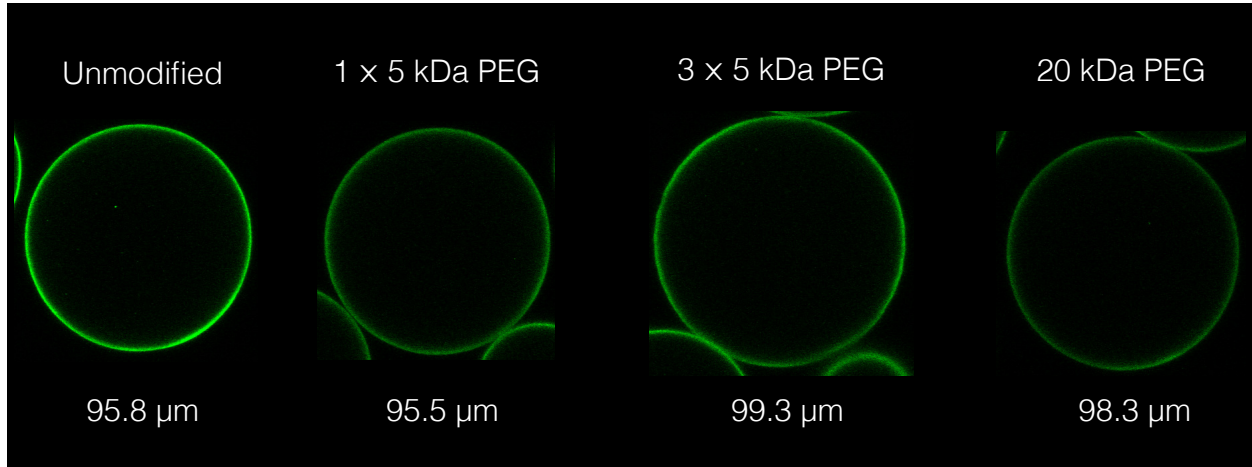
Figure 5.2. Representative CLSM images of unmodified and PEGylated rSPA resin particles showing surface aggregation of BSA molecules after 24 hours of incubation.

As seen in Fig. 5.3, the differences in $\bar{q}_{BSA}$ between unmodified and PEGylated resins were not significant for rSPA + 1×5 kDa PEG and rSPA + 3×5 kDa PEG but became significant for rSPA + 20 kDa PEG, which exhibited much less BSA binding (45% smaller on average) compared to the unmodified resin. These results suggest that the effectiveness of PEG to block non-specific BSA aggregate binding is dependent on the molecular weight of the polymer rather than on the extent of the PEGylation.
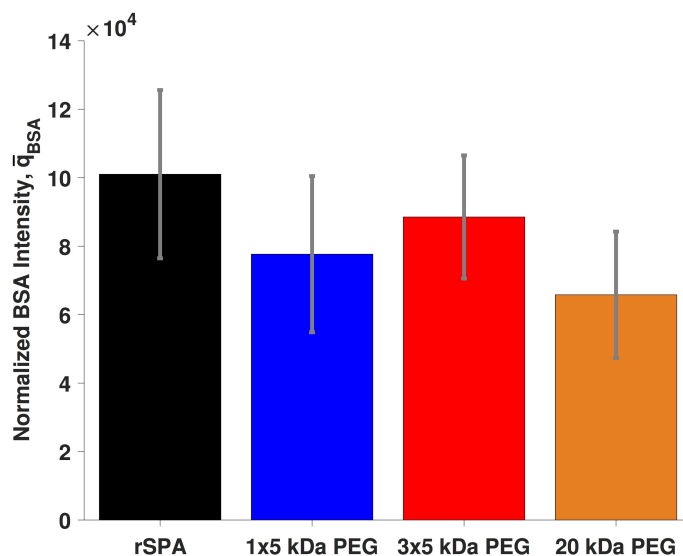
Figure 5.3. Plot of $\bar{q}_{BSA}$ for the unmodified and PEGylated rSPA resins. Error bars represent 95% confidence intervals based on the number of particle images (at least three) obtained for each resin.

5.4.3. BSA-mAb association

Figures 5.4a and b display a set of CLSM images for similarly-sized particles incubated in mixtures of Rhodamine Red-labeled mAb (diluted with native mAb at a total concentration of 2 mg/mL) and Rhodamine Green-labeled BSA (diluted with native BSA at a total concentration of 0.2 mg/mL) for the unmodified and rSPA + 20 kDa PEG resins over a 2 hr period. Both resin samples had been pre-incubated in BSA alone to simulate the exposure to flow-through species in an actual capture step. As seen from these figures, BSA appears to associate with the mAb

151

when it adsorbed to both unmodified and the rSPA + 20 kDa resin with the green fluorescence intensity obviously tracking the rise in red fluorescence, which is due to the bound mAb. Similar results, not shown for brevity, were also observed for rSPA + 1×5 kDa PEG and rSPA + 3×5 kDa PEG. As seen in Fig. 5.4, the red mAb fluorescence intensity is obviously much lower for the PEGylated resin compared to the unmodified resin, since, as shown in Part I of this work (Chapter 4) [29], the mAb binding capacities are different for the different resins. The concentrations of BSA and mAb A were compared by:

$$\frac{q_{BSA}(t)}{q_{mAb\ A}(t)} \approx \frac{\int_0^1 I_{BSA}(\rho,t)\rho^2 d\rho}{\int_0^1 I_{mAb\ A}(\rho,t)\rho^2 d\rho} \tag{5.2}$$

where $q_{mAb\ A}$ and q_{BSA} are the corresponding adsorbed concentrations of mAb A and BSA, respectively. $I_{mAb\ A}$ and I_{BSA} are the radially averaged local fluorescence intensities of mAb A and BSA, respectively.
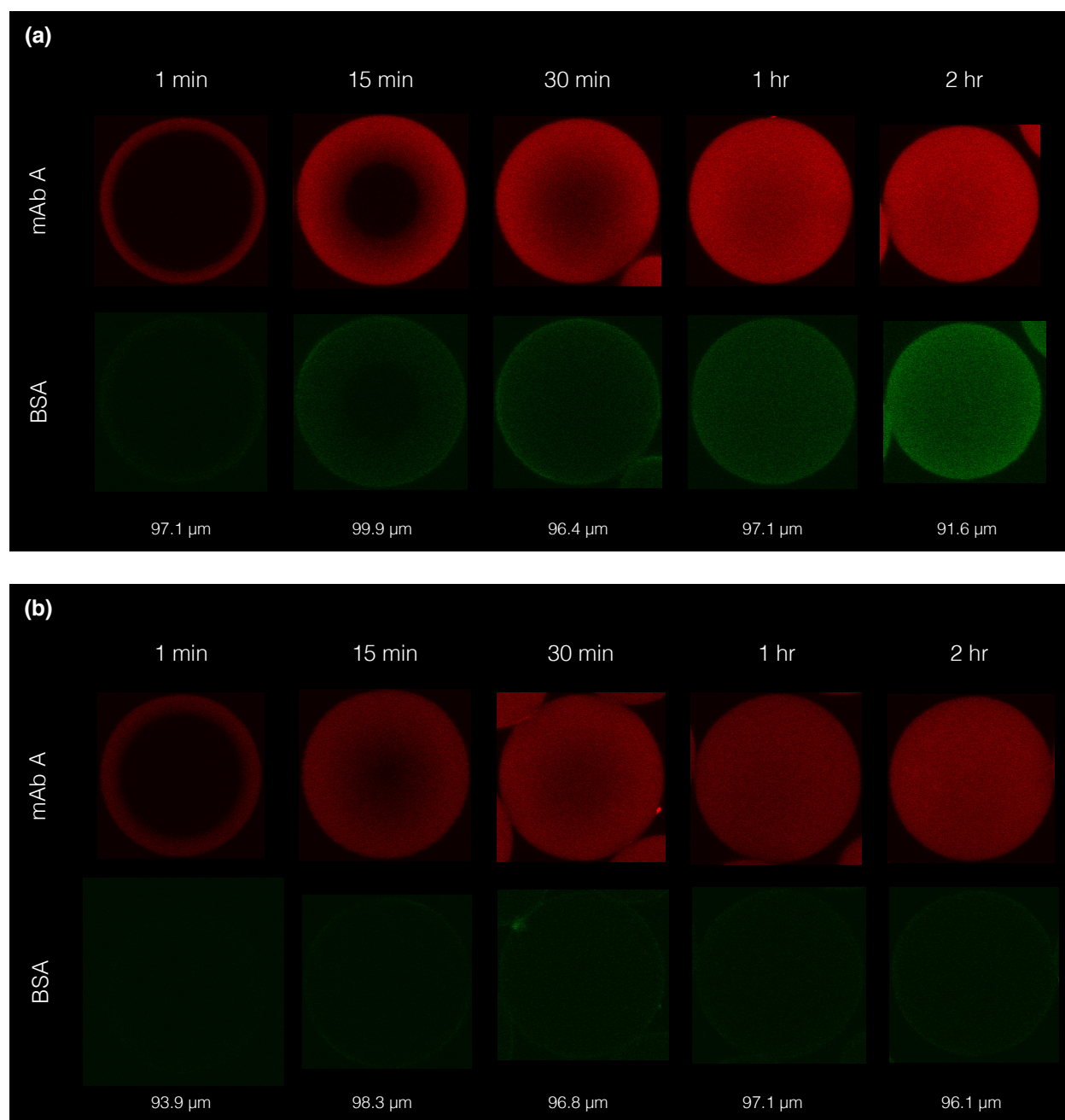
Figure 5.4. Representative CLSM images for simultaneous adsorption of mAb A (top rows) and BSA (bottom rows) for (a) the unmodified resin and (b) the rSPA + 20 kDa PEG resin over a period of 2 hr.

The ratio of BSA to mAb, shown in Fig. 5.5, for all four resins suggests that the extent of BSA-mAb association is similar for the rSPA + 1×5 kDa PEG and rSPA + 3×5 kDa PEG resins and the unmodified resin but is much smaller for the rSPA + 20 kDa PEG resin. This result

indicates that long PEG chains attached to the rSPA ligand are needed to significantly reduce association of BSA with the bound mAb. It is likely that as the size of the PEG increases, it becomes more difficult for BSA to associate with the bound mAb due to the increased steric hindrance. Finally, it is apparent from Fig. 5.5 that the ratio of $\bar{q}_{BSA}$ to $\bar{q}_{mAb\,A}$ increased over time for all four resins, which suggest that the BSA association with the bound mAb is to some extent kinetically limited, but more so for the PEGylated reins and, in particular for the rSPA + 20 kDa PEG.
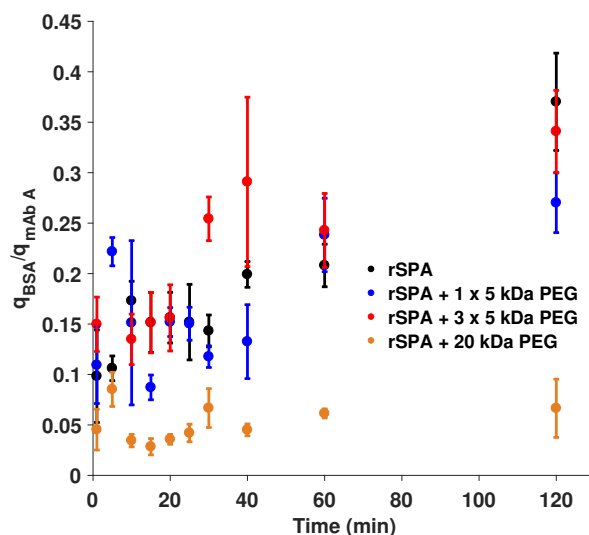
Figure 5.5. Plots of $q_{BSA}/q_{mAb\,A}$ as a function of time for the unmodified and PEGylated rSPA resins. Error bars represent 95% confidence intervals based on the number of particle images (at least three) obtained for each resin.

5.4.4. Evaluating PEGylated rSPA resin selectivity against CHO HCPs

The real-world resin selectivities of the unmodified and rSPA + 20 kDa PEG resins against CHO HCPs were determined by purification of CHO HCCF containing expressed mAb B. The selectivities of the rSPA + 1×5 kDa PEG and rSPA + 3×5 kDa PEG resins were not evaluated due to the limited supply of CHO HCCF material. The rSPA + 20 kDa PEG resin was

chosen due to the promising results of the CLSM selectivity experiments. Both resins were loaded to 30 g mAb/L, which falls within the range of typical industrial process loads for ProA chromatography [5,15,32,33]. Here, an effective selectivity (α_{HCCF}) was defined by:

$$\alpha_{HCCF} = \frac{q_{mAb\,B}}{q_{HCP}} \frac{c_{HCP}}{c_{mAb\,B}} \tag{5.3}$$

where $q_{mAb\,B}$ and q_{HCP} are the adsorbed concentrations of mAb B and CHO HCPs, respectively, which were determined from the concentration of the mAb and HCPs in the eluate fractions; $c_{mAb\,B}$ and c_{HCP} are the free concentrations of mAb B and CHO HCPs, respectively, where $c_{mAb\,B}$ was determined from the initial concentration of mAb in the CHO HCCF and c_{HCP} was taken as 142,000 $\pm$ 7,000 ppm based on the ELISA analysis of the raw HCCF.

Table 5.1 reports the mAb B percentage yields, CHO HCP content in the eluate fractions, and values of α_{HCCF} for the two resins. As seen from Table 5.1, HCP content in the eluate fraction was significantly lower for the rSPA + 20 kDa PEG resin compared to the unmodified resin with equivalent mAb loads. It should be noted that while the particular ELISA assay used to determine CHO HCP content has been reported to be essentially blind to histone HCPs [41], and possibly other proteins, the comparison does confirm lower contaminant binding. Surprisingly, there was also no appreciable loss in mAb yield for the rSPA + 20 kDa PEG resin compared to the unmodified resin. This contrasts sharply with the values of 10% dynamic binding capacity (DBC$_{10\%}$) for hIgG on the same resins, which are discussed in Part I of this work (Chapter 4) [29]. We had reported DBC$_{10\%}$ values of ~30 and ~20 g hIgG/L for the unmodified rSPA and rSPA + 20 kDa PEG resins at a residence time of 6 minutes, respectively. A simple explanation for this discrepancy is that mAb B has a significantly higher value of DBC$_{10\%}$ for the rSPA + 20 kDa PEG resins compared to the particular lot of hIgG used for the

155

dynamic binding capacity study. This explanation is consistent with the work of Ghose et al. [32] who demonstrated that various mAbs can have significantly different values of $DBC_{10\%}$ on the same resin. However, the original $DBC_{10\%}$ values still point towards a comparative loss in mAb yield for the rSPA + 20 kDa PEG resin if the loading concentration is increased to approach breakthrough.

Resin	mAb B Yield (%)	HCP (ppm)	α_{HCCF}
rSPA	99.3 ± 0.9	566 ± 47	165 ± 20
rSPA + 20 kDa PEG	99.2 ± 0.7	399 ± 31	230 ± 14

Table 5.1. Values of mAb yield percent, CHO HCP content in eluate fractions, and α_{HCCF} for the unmodified and rSPA + 20 kDa PEG resin. Error represents 95% confidence intervals based on triplicate measurements.

As a result of the increase in HCP clearance and retention of mAb yield, the value of α_{HCCF} increased 37% for the rSPA + 20 kDa PEG resin compared to the unmodified resin. This result confirmed that the PEGylated ligand was able to selectively block association of HCPs during chromatography and is consistent with the results of the CLSM experiments. As such, the combined results suggest that ProA resins with PEGylated ligands are a viable pathway to improve selectivity, particularly towards HCPs, in downstream processing if mAb yields are maintained.

5.5. Conclusions

Our results describe the benefits of PEGylating ProA chromatography ligands for increased resin robustness and process selectivity. We find that PEGylation of ProA ligands

allows the resin to retain a higher percentage of q_{max} after digestion with the model protease, chymotrypsin. The level of protection against digestion appears to be independent of the PEG molecular weight or modification extent. Additionally, we find that PEGylating the ligands decreases the level of non-specific binding of BSA aggregates to the surface of the resin particles. The decrease in level of aggregation appears to be dependent on the PEG molecular weight rather than the modification extent. We demonstrate that the PEG on the modified ligand is mechanistically capable of blocking non-specific association of BSA, as a mock contaminant, to adsorbed mAbs. In the particular experimental system used, ProA ligands with 21.5 kDa PEG chains were effective at blocking the association while ligands with 5.2 kDa PEG chains were not. Finally, we find that ligands with 21.5 kDa PEG chains are able to increase the real-world selectivity of the resin against CHO HCPs by up to 37% during purification of a mAb expressed in HCCF.

PEGylation of ProA ligands clearly offers valuable benefits that deserve consideration and future investigation in the context of downstream bioprocessing. The results presented in Part I (Chapter 4) and II (this chapter) of this work provide a foundational understanding of PEGylation's effect on common ProA chromatography process parameters. However, as discussed in Part I (Chapter 4) of this work, the current "naïve" approach to PEGylation of ProA is not optimized and high-throughput resin screening methods are necessary to aid future development in a time and cost-efficient manner. In addition to PEGylation parameters such as molecular weight and modification extent, it is also apparent the particular IgG system used is a significant factor in the results and conclusions. For example, it was possible to load the unmodified and rSPA + 20 kDa PEG resins to 30 g mAb B/L without losses in yield, however, this result is not expected for all mAbs or at higher loading concentrations. In these cases, a

tradeoff between binding capacity and selectivity would exist. Additionally, it has been shown in the literature that the level of residual host cell impurities is dependent on the expressed IgG molecule. Testing PEGylation's effect on selectivity with various IgG molecules will demonstrate its broader effectiveness and provide more information about the types of non-specific interactions it is responsible for removing. Additional performance testing of the PEGylated ProA resins for other impurities such as host DNA, virus particles, and leached ProA are of interest for industrial applications.

It should be noted that PEGylated ProA resins would inevitably be more expensive as the cost to produce the material would increase due to the additional reaction and modification processes involved. Utilizing a resin with lower productivity due to lower dynamic binding capacity would also introduce the need for additional or larger columns (more resin) to meet the same process throughput. However, optimizing the PEGylated resin properties to significantly increase lifetime and/or increasing selectivity such that a subsequent downstream polishing step could be eliminated would offset the increased resin costs such that the net impact on the cost-of-goods for mAb production would be favorable.

5.6. References

[1] A. Shukla, J. Thommes, Recent advances in large-scale production of monoclonal antibodies and related proteins, Trends Biotechnol. 28 (2010) 253-261.

[2] S. Hober, K. Nord, M. Linhult, Protein A chromatography for antibody purification, Chromatogr B. 848 (2007) 40-47.

[3] R.D.R. Tarrant, M.L. Velez-Suberbie, A.S. Tait, C.M. Smales, D.G. Bracewell, Host cell protein adsorption characteristics during protein a chromatography, Biotechnol Prog. 28 (2012) 1037-1044.

[4] A.A. Shukla, P. Hinckley, Host cell protein clearance during protein A chromatography: development of an improved column wash step, Biotechnol Prog. 24 (2008) 1115-1121.

[5] S. Ghose, J. Zhang, L. Conley, R. Caple, K. Williams, D. Cecchini, Maximizing binding capacity for protein A chromatography, Biotechnol Progress. 30 (2014) 1335-1340.

[6] X. Wang, A.K. Hunter, N.M. Mozier, Host Cell Proteins in Biologics Development: Identification, Quantitation and Risk Assessment, Biotechnol Bioeng. 103 (2009) 446-458.

[7] A.A. Shukla, C. Jiang, J. Ma, M. Rubacha, L. Flansburg, S.S. Lee, Demonstration of Robust Host Cell Protein Clearance in Biopharmaceutical Downstream Processes, Biotechnol Prog. 24 (2008) 615−622.

[8] N. Levy, K. Valente, L. Choe, K. Lee, A. Lenhoff, Identification and characterization of host cell protein product-associated impurities in monoclonal antibody bioprocessing, Biotechnol Bioeng. 111 (2013) 904-912.

[9] B. Nogal, K. Chhiba, J.C. Emery, Select host cell proteins coelute with monoclonal antibodies in protein a chromatography, Biotechnol Prog. 28 (2012) 454-458.

[10] P. Gagnon, R. Nian, Y. Yang, Q. Yang, C.L. Lim, Non-immunospecific association of immunoglobulin G with chromatin during elution from protein A inflates host contamination, aggregate content, and antibody loss, J Chromatogr A. 1408 (2015) 151−160.

[11] G. Guiochon, L.A. Beaver, Separation science is the key to successful biopharmaceuticals, J Chromatogr A. 1218 (2011) 8836−8858.

[12] J.R. Ryland, Process Development, Manufacturing Strategies and Costs, Recovery of Biological Products XIV, 2010.

[13] C. Jiang C, J. Liu, M. Rubacha, A.A. Shukla, A mechanistic study of Protein A chromatography resin lifetime, J Chromatogr A. 1216 (2009) 5849-5855.

[14] B. Kelley, Very large scale monoclonal antibody purification: The case for conventional unit operations, Biotechnol Prog. 23 (2007) 995-1008.

[15] S. Zhang, W. Daniels, J. Salm, J. Glynn, J. Martin, C. Gallo, R. Godavarti, G. Carta, Nature of foulants and fouling mechanism in the Protein A MabSelect resin cycled in a monoclonal antibody purification process, Biotechnol Bioeng. 113 (2016) 141-149.

[16] T.T. Ngo, S. Jogie-Brahim, D. Narinesingh, Affinity chromatographic purification of antibodies, Anal Lett. 40 (2007) 2799-2820.

[17] A.C.A. Roque, C.R. Lowe, M.A. Taipa, Antibodies and Genetically Engineered Related Molecules: Production and Purification, Biotechnol Prog. 20 (2004) 639-654.

[18] R. Hahn, K. Shimahara, F. Steindl, A. Jungbauer, Comparison of protein A affinity sorbents III. Life time study, J Chromatogr A. 1102 (2006) 224-231.

[19] GE Healthcare Life Sciences. MabSelect SuRe, Data File 11-0011-65 AC, 2011.

[20] Z. Liu, S. Mostafa, A. Shukla, A comparison of Protein A chromatographic stationary phases: Performance characteristics for monoclonal antibody purification, Biotechnol Appl Biochem. 62 (2014) 37-47.

[21] T. Bjorkman, F. Berqvist, M. Wetterhall, Molecular study on the MabSelect SuRe ligand after treatment under alkaline conditions, 249th ACS National Meeting, 2015.

[22] M. Michaelis, J. Cinatl, P. Pouckova, K. Langer, J. Kreuler, J. Matousek, Coupling of the antitumoral enzyme bovine seminal ribonuclease to polyethylene glycol chains increases its systemic efficacy in mice, Anti-Cancer Drugs. 13 (2002) 149-154.

[23] J.M. Harris, N.E. Martin, M. Modi, Pegylation: a novel process for modifying pharmacokinetics, Clin Pharmacokinet. 40 (2001) 539-551.

[24] Z. Wen, B. Niemeyer, Preparation and characterization of PEGylated Concanavalin A for affinity chromatography with improved stability, J Chromatogr B. 879 (2011) 1732–1740.

[25] R. Gref, A. Domb, P. Quellec, T. Blunk, R.H. Muller, J.M. Verbavatz, R. Langer, The Controlled Intravenous Delivery of Drugs using PEG-Coated Sterically Stabilized Nanospheres, Adv Drug Deliv Rev. 16 (1995) 215-233.

[26] I. Szleifer, M.A. Carignano, Tethered polymer layers: phase transitions and reduction of protein adsorption, Macromol Rapid Commun. 21 (2000) 423-448.

[27] J. Wei, D.B. Ravn, L. Gram, P. Kingshott, Stainless steel modified with poly(ethylene glycol) can prevent protein adsorption but not bacterial adhesion, Colloids Surf B Biointerfaces 32 (2003) 275-291.

[28] J. González-Valdez, A. Yoshikawa, J. Weinberg, J. Benavides, M. Rito-Palomares, T. Przybycien, Toward improving selectivity in affinity chromatography with PEGylated affinity ligands: The performance of PEGylated protein A, Biotechnol Prog. 30 (2014) 1364-1379.

[29] J. Weinberg, S. Zhang, G. Crews, G. Carta, T. Przybycien, Chemical Modification of Protein A Chromatography Ligands with Polyethylene Glycol. I: Effects on IgG Adsorption Equilibrium, Kinetics, and Transport, J Chromatogr A. (2017) *in review*.

[30] S. Zhang, K. Xu, W. Daniels, J. Salm, J. Glynn, J. Martin, C. Gallo, R. Godavarti, G. Carta, Structural and functional characteristics of virgin and fouled Protein A MabSelect resin cycled in a monoclonal antibody purification process, Biotechnol Bioeng. 113 (2016) 367-375.

[31] S.S. Pai, B. Hammouda, K. Hong, D.C. Pozzo, T.M. Przybycien, R.D. Tilton, The conformation of the poly (ethylene glycol) chain in mono-PEGylated lysozyme and mono-PEGylated human growth hormone, Bioconjugate Chem. 22 (2011) 2317–2323.

[32] S. Ghose, B. Hubbard, S.M. Cramer, Binding capacity differences for antibodies and Fc-fusion proteins on protein A chromatographic materials, Biotechnol Bioeng. 96 (2007) 768-779.

[33] R. Hahn, P. Bauerhansl, K. Shimahara, C. Wizniewski, A. Tscheliessnig, A. Jungbauer, Comparison of protein A affinity sorbents II. Mass transfer properties, J Chromatogr A 1093 (2005) 98-110.

[34] T. Peters, The Plasma Proteins, Putman FW, ed., Academic Press pp. 133–181.

[35] L. Gráf, L. Szilágyi, I. Venekei, Handbook of Proteolytic Enzymes Chapter 582 - Chymotrypsin, Academic Press, 2013.

[36] J.R. Peyser, Nucleic acids encoding recombinant protein A, US Patent no. 7,691,698 B2., 2010.

[37] O. Kinstler, N. Gabriel, C. Farrar, R. DePrince, N-terminally chemically modified protein compositions and methods, US Patent no. 5,824,784 A, 1998.

[38] M. Cisneros-Ruiz, K. Mayolo-Deloisa, T.M. Przybycien, M.A. Rito-Palomares, Separation of PEGylated from unmodified ribonuclease A using sepharose media, Sep Purif Technol. 65 (2009) 105–109.

[39] S.M. Daly, T.M. Przybycien, R.D. Tilton, Adsorption of poly(ethylene glycol)-modified lysozyme to silica, Langmuir. 21 (2005) 1328–1337.

[40] M.F. Clincke, E. Guedon, F.T. Yen, V. Ogier, J.L. Goergen, Characterization of metalloprotease and serine protease activities in batch CHO cell cultures: control of human recombinant IFN-γ proteolysis by addition of iron citrate, BMC Proceedings. 5 (2011) 115.

[41] P. Gagnon, R. Nian, J. Lee, L. Tan, S.M.A. Latiff, C.L. Lim, C. Chuah, X. Bi, Y. Yang, W. Zhang, H.T. Gan, Nonspecific interactions of chromatin with immunoglobulin G and protein A, and their impact on purification performance, J Chromatogr A. 1340 (2014) 68–78.

6

Additional Resin Characterization

Chapters 3-5 were adapted from publications or manuscripts that were submitted for publication. This chapter of the thesis summarizes research that was conducted within the scope of Chapters 3-5, which but was not included in publications for brevity or because it was tangential to the main conclusions of the articles.

6.1. Utilizing iSEC and HETP analysis to determine effective IgG diffusivity under binding conditions

As seen in Chapters 3 and 4, height equivalent to a theoretical plate (*HETP*) experiments and subsequent van Deemter analysis is a powerful tool to characterize the mass transfer characteristics of chromatography resins. In particular, this technique was used in Chapters 3 and 4 to obtain values of effective IgG diffusivity (D_e) in both the unmodified CaptivA PriMAB and PEGylated rSPA resin variants under non-binding conditions.

As discussed in Chapter 3, upon observation of the batch uptake kinetics and breakthrough profiles for the unmodified CaptivA PriMAB resin using human polyclonal IgG (hIgG) antibodies, there was a slow approach to equilibrium that resulted in very shallow uptake curves at long-times (seen in Figures 3.1b and 3.3a). Through pH gradient elution analysis of hIgG breakthrough fractions, the slow approach to equilibrium was determined to be a result of competitive binding behavior between the different IgG sub-species and sub-classes present within the hIgG sample.

However, before this result was elucidated, severely hindered pore diffusion at long-times was considered as a possible explanation for the shallow uptake at long-times. Here, it was hypothesized that the reduced pore volume from previously adsorbed IgG molecules made it increasingly difficult for new IgG molecules to transport and bind within the resin. Since the value of D_e from the HETP analysis was obtained under non-binding conditions, this did not reflect any potential hindrances that might occur when the resin was loaded with significant concentrations of IgG. As discussed in Chapter 4, it is possible to use the shrinking core model (SCM), given confocal images of fluorescently labeled IgG adsorption on resin particles, to determine a value of D_e under binding conditions. In Table 4.2, it is shown that excellent agreement is obtained between non-binding HETP and SCM values of D_e when the protein adsorption follows shrinking core behavior. However, it is not always the case that adsorption follows shrinking core behavior, as seen with hIgG adsorption on ProA resins in Chapter 3, mAb adsorption on PEGylated rSPA resins in Chapter 4, and IgG adsorbed on other chromatography resins in the literature such as ion exchange resins [1].

As an alternative method to obtain the value of D_e under binding conditions for unmodified CaptivA PriMAB, and theoretically for any ProA resin, HETP experiments were performed after loading a column of the unmodified resin to ~85% breakthrough with hIgG. Here, pulse injections of non-binding IgG_3 species were performed to determine the HETP; where the IgG_3 was collected from the initial flowthrough of the same breakthrough experiment used to load the column. The collection method is illustrated in Figure 6.1 where it is seen that during the period before breakthrough occurs, there is flowthrough of non-binding species: notably IgG_3 species which do not bind to ProA and large IgG aggregates that are too large to diffuse into the pores of the resin. During this period, the column outlet was collected, filtered using a 0.2 μm membrane, and

subsequently concentrated to ~1 mg/mL in Amicon Ultra-15 centrifugal filters with a 100 kDa molecular weight cutoff (EMD Millipore, Billerica, MA). The breakthrough experiment with hIgG itself was conducted as described in both Chapters 3 and 4.
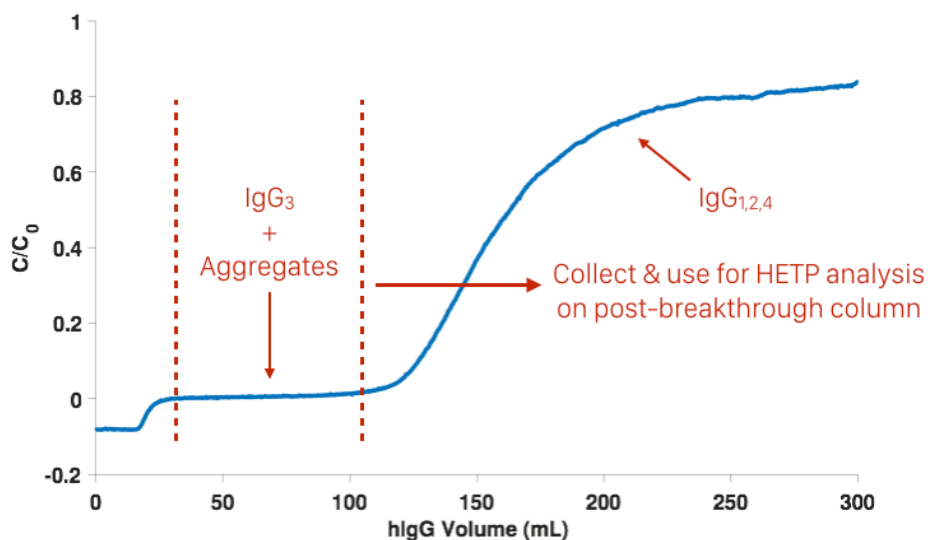
Figure 6.1. Breakthrough curve of hIgG on CaptivA PriMAB at a column residence time of 5 min showing the flowthrough of IgG_3 and large aggregate species before breakthrough of $IgG_{1,2,4}$ species.

After loading the column to ~85% breakthrough, which corresponded to a load of 300 mL of hIgG solution at a concentration of 2 mg/mL, the loaded CaptivA PriMAB column was transferred to a Waters Alliance 2690 system and equilibrated for 3 hours with PBS loading buffer at a flow rate of 1 mL/min. This long equilibration time was implemented to remove any free IgG in the resin pores and remove any loosely bound IgG. The long equilibration time also ensured a relatively stable baseline for subsequent analytical experiments.

To determine values of average pore radius (r_{pore}) and accessible IgG particle porosity (β_{IgG}) after loading to ~85% breakthrough, inverse size exclusion chromatography (iSEC) experiments were first performed on the column as described in Chapter 4. Figure 6.2a displays the K_D values of the dextran probes obtained for the clean and loaded CaptivA PriMAB resins,

respectively, while Figure 6.2b shows the van Deemter plots (dimensionless plate height (h) vs. dimensionless velocity, (v')) obtained from pulse injections of the IgG$_3$ species. Table 6.1 reports the corresponding values of r_{pore}, the standard deviation of the log-normal cylindrical pore distribution (s_{pore}), and the β_{IgG} and D_e values determined from these measurements.
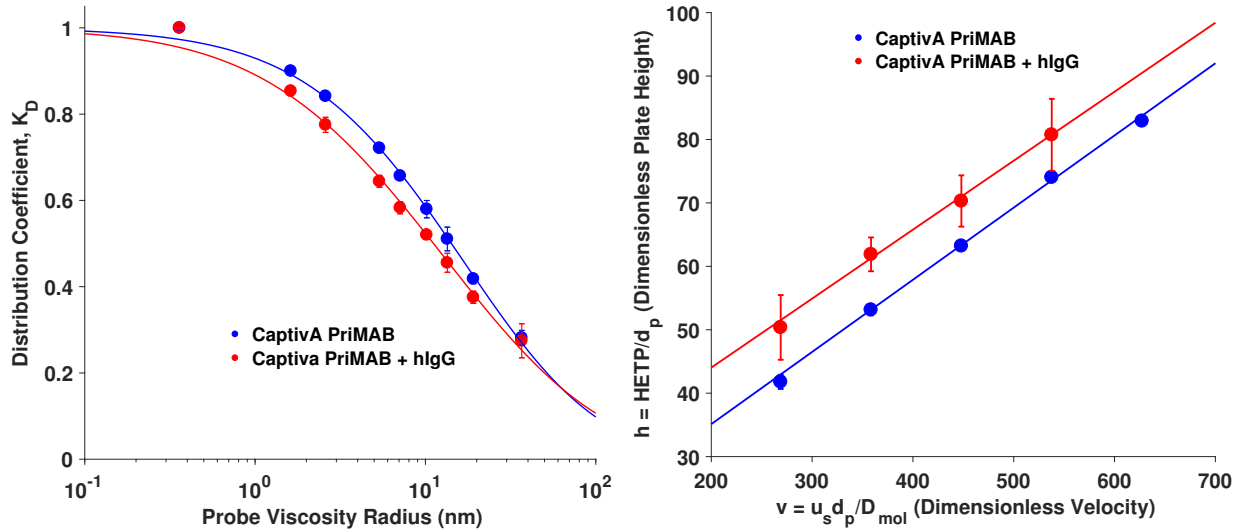
Figure 6.2. (a) Plot of K_D versus iSEC dextran probe viscosity radius for the clean and loaded CaptivA PriMAB resins. Solid lines represent fits according to eqs. 3.2 and 3.3. (b) Dimensionless van Deemter plots for the clean and loaded CaptivA PriMAB resins. Solid lines represent fits according to eq. 3.7. Error bars in both figures represent 95% confidence limits based on triplicate measurements.

Resin	r_{pore} (nm)	s_{pore}	β_{IgG}	D_e (10^{-8} cm^2/s) from HETP
CaptivA PriMAB	57.3 ± 1.6	1.26 ± 0.07	0.65 ± 0.01	7.5 ± 0.5
CaptivA PriMAB + hIgG	45.9 ± 2.1	1.53 ± 0.12	0.58 ± 0.01	5.6 ± 1.3

Table 6.1. Values of r_{pore}, s_{pore}, β_{IgG}, and D_e for the clean and loaded CaptivA PriMAB resins. Error represents 95% confidence intervals for triplicate measurements.

As seen in Figure 6.2a, the dextran K_D values remain consistent with the log-normal cylindrical pore size distribution model (discussed in Chapter 4) after loading the column with IgG. Unsurprisingly, values of r_{pore} and β_{IgG} decreased after loading the column with hIgG due to the reduced pore volume. When comparing the values in Table 6.1 to those in Table 4.2 after PEGylation of the rSPA ligands, it is seen that both the rSPA + 3×5 kDa PEG and rSPA + 20 kDa PEG resins had lower values of r_{pore} and β_{IgG} compared to the CaptivA PriMAB column pre-loaded with significant concentrations of IgG. Interestingly, the value of s_{pore} increased after loading. This is consistent with IgG's apparent preference for smaller pores given that the values of K_D between the two resins converge as the probe viscosity radius increases in Figure 6.2a. Thus, the results suggest that loading the resin with IgG increases the relative amount of smaller pores and increases the variance of the distribution.

Along expectations, the value of D_e decreased after loading the resin with IgG. However, the value of D_e remained within the same order of magnitude and within the expected range of values for IgG on agarose-based ProA resins [2-4]. As seen in Figure 6.2b and Table 6.1, the size of the 95% confidence interval for the loaded resin also significantly increased for the HETP experimental data points and for value of D_e compared to the clean resin. The increased size of the confidence interval was due to deviation in the measured second central moment (μ'_2) of the peaks produced by the IgG_3 pulse injections, which is required to determine values of HETP. Since the value of μ_2' has a squared dependence on time, it is highly sensitive to slight shifts in the peak baseline. During the experiments, shifts in the pulse injection peak baseline were experienced due to small amounts of IgG exiting the column that were previously bound to ProA. Additionally, small amounts of non-binding aggregates in the pulse injection also interfered with the peak baseline. Thus, it was not possible to obtain value of D_e with the same precision as seen with the

clean HETP experiments. However, the results did suggest that mass transfer resistance increased, as expected, but not to an extent where diffusion was severely hindered during or after loading of IgG. This conclusion is consistent with the mass transfer resistance analysis of the PEGylated rSPA resins in Chapter 4, which had similar or lower values of r_{pore}, β_{IgG}, and D_e.

In the future, the post-loading HETP experiment may be improved by obtaining a purified source of non-binding human IgG$_3$ species to prevent aggregates from interfering with the peak baseline. Alternatively, a purified and engineered version of an IgG mAb with ProA binding residues removed, as described in Tustian et al. [5], may be used in a non-binding pulse injection. In the latter, the experiment would not be limited to IgG$_3$ species. With improved precision, the loaded HETP experiment described above is a viable method for comparing values of D_e before, during, and after loading for ProA chromatography resins.

6.2. Lot-to-lot variability in hIgG dynamic binding capacity

Chapter 4 reports values of 10% dynamic binding capacity for hIgG (DBC$_{10\%}$) on unmodified CaptivA PriMAB and the PEGylated rSPA resin variants, which were determined from a series of hIgG breakthrough experiments conducted at various column residence times. In these experiments, and in all hIgG breakthrough experiments conducted in Chapters 3-5, a single lot/batch of hIgG was used for consistency. Figure 6.3 displays values of DBC$_{10\%}$ for the Captiva PriMAB resin as a function of residence time for a second lot of hIgG (Lot #2) overlaid with values from the lot used in Chapters 3-5 (Lot #1) for residence times between 2.5 and 10 min. As seen by comparing the two data sets, Lot #2 had similar DBC$_{10\%}$ to Lot #1 for residence times of 2.5 and 4 min followed by significantly higher DBC$_{10\%}$ for residence times greater than 4 min. It has been reported in the literature that different IgG antibodies can have significantly different static and

dynamic binding capacities on the same ProA resin [6]. The behavior of the two lots of hIgG is consistent with the literature considering that hIgG contains a large variety of IgG species. In this case, the significantly different values of $DBC_{10\%}$ suggest that the IgG composition between the two lots is also different. Since the values of $DBC_{10\%}$ are higher in Lot #2, this indicates that breakthrough occurs later than in Lot #1 and suggests that the IgG molecules Lot #2 had slower competitive binding kinetics compared to those in Lot #1. This may perhaps suggest the presence of more "weaker" species compared to "strong" species in Lot #2 than Lot #1 on a per mass basis.

Since ProA resin manufacturers often use $DBC_{10\%}$ of hIgG to market general resin capacities for mAbs, the data in Figure 6.3 suggests that care should be taken before setting mAb performance expectations based on characterizations with hIgG. In the future, performing pH gradient elution experiments of hIgG lots with significant differences in performance on ProA resins may elucidate a relationship between IgG binding strength or sub-class with binding capacity.
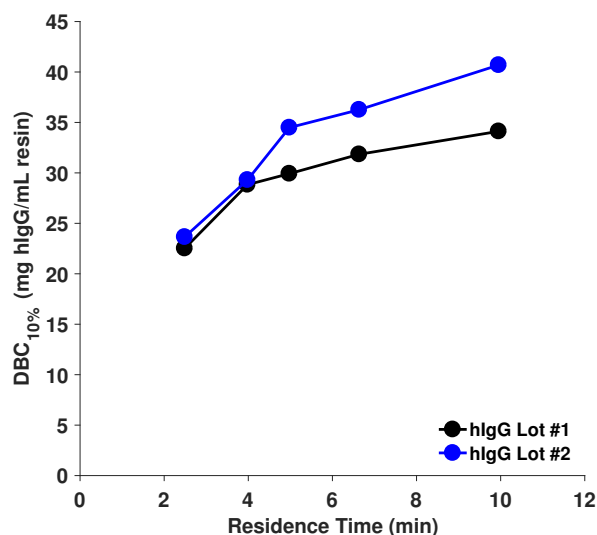
Figure 6.3. $DBC_{10\%}$ with hIgG Lot #1 (black) and Lot #2 (blue) on CaptivA PriMAB as a function of column residence time Data points represent single measurements. It should be noted that in the context of this research, breakthrough experiments were highly reproducible with $DBC_{10\%}$ values within ± 1 mg/mL.

6.3. Modeling breakthrough of hIgG on CaptivA PriMAB

In Chapter 3, non-binding HETP experiments and subsequent van Deemter analysis on the CaptivA PriMAB resin determined a value of $7.5 \pm 0.5 \times 10^8$ cm^2/s for D_e, which is consistent in the literature for IgG molecules diffusing within the pores of agarose-based ProA resins [2-4].

Using the determined value of D_e, the breakthrough behavior was simulated and compared to experimental results with a pore diffusion model for breakthrough described by Perez-Almodovar and Carta [2]. This particular pore diffusion model neglects kinetic resistances to binding and is typically used to describe the transport and simultaneous fast, highly favorable binding of IgG to ProA [3,4]. The pore mobile phase mass balance for antibody and associated boundary conditions at the resin particle center and outer surfaces and the bulk mobile phase mass balance for antibody and associated boundary and initial conditions for the model are as follows:

$$\left[\beta_{IgG} + \frac{q_{max}K}{(1+Kc)^2} \right] \frac{\partial c}{\partial t} = \frac{D_e}{r^2} \frac{\partial}{\partial r} \left(r^2 \frac{\partial c}{\partial r} \right) \tag{6.1}$$

$$r = 0, \quad \frac{\partial c}{\partial r} = 0 \tag{6.2}$$

$$r = r_p, \quad D_e \frac{\partial c}{\partial r} = k_f (C - c|_{z,r=r_p}) \tag{6.3}$$

$$\varepsilon \frac{\partial C}{\partial t} + (1 - \varepsilon) \frac{\partial \bar{q}}{\partial t} + u \frac{\partial C}{\partial z} = 0 \tag{6.4}$$

$$\frac{\partial \bar{q}}{\partial t} = \frac{3}{r_p} k_f (C - c|_{z,r=r_p}) \tag{6.5}$$

$$t = 0, \ z > 0, \ C = 0 \tag{6.6}$$

$$z = 0, \quad C = C_0 \tag{6.7}$$

where c is the IgG concentration in the particle pores, C is the IgG concentration in the interstitial particle fluid, C_0 is the initial front concentration, r_p is the average particle radius, k_f is the film

mass transfer coefficient determined from the dimensionless Sherwood (Sh) number, $Sh = k_f d_p / D_0$. Values of β_{IgG}, ε, q_{max}, and K were determined for the CaptivA PriMAB resin to be 0.65 ± 0.01, 0.34 ± 0.01, 84 ± 1 mg/mL, and 78 ± 24 mL/mg, respectively, via iSEC, HETP, and static binding isotherm determinations as reported in Chapters 3 and 4.

Equations 6.1-7 were discretized by finite differences in the radial (r) and axial (z) coordinates to reduce the partial differential equations to a series of ordinary differential equations, which, in turn, were solved numerically via subroutine ode15s in MATLAB.

Figures 6.4a-e compares an experimental breakthrough curve for hIgG Lot #1 on the CaptivA PriMAB at a residence times from 2.5 to 10 minutes with corresponding predictions using the pore diffusion-limited mass transport model. As seen in Figures 6.4a-e, the pore diffusion model significantly over predicts the dynamic binding capacity compared to the experimental curve at all residence times. In the 5 min residence time case, the model predicts the value of DBC$_{10\%}$ to be ~20 mg/mL higher than the corresponding experimental curve. Additionally, the model does not account for the tailing behavior of the hIgG breakthrough due to competitive binding observed in the experimental system and instead predicts full saturation of the resin given the same load volume. Given that the simulations were based on independently measured mass transfer parameters, the model-data comparison serves as additional evidence to show that the low DBC$_{10\%}$ and long-time tailing behavior for hIgG are due to factors outside of typical pore diffusion limitations for ProA resins. These results are once again consistent with the work of Perez-Almodovar and Carta, McCue et al., and Hanh et al. [2-4] who were unable to generate reasonable predictions of breakthrough behavior of hIgG with the pore diffusion model without artificially changing values of q_{max} or allowing the values of D_e to depend on batch concentration or column residence time which is not consistent for pore diffusion controlled mass transfer.
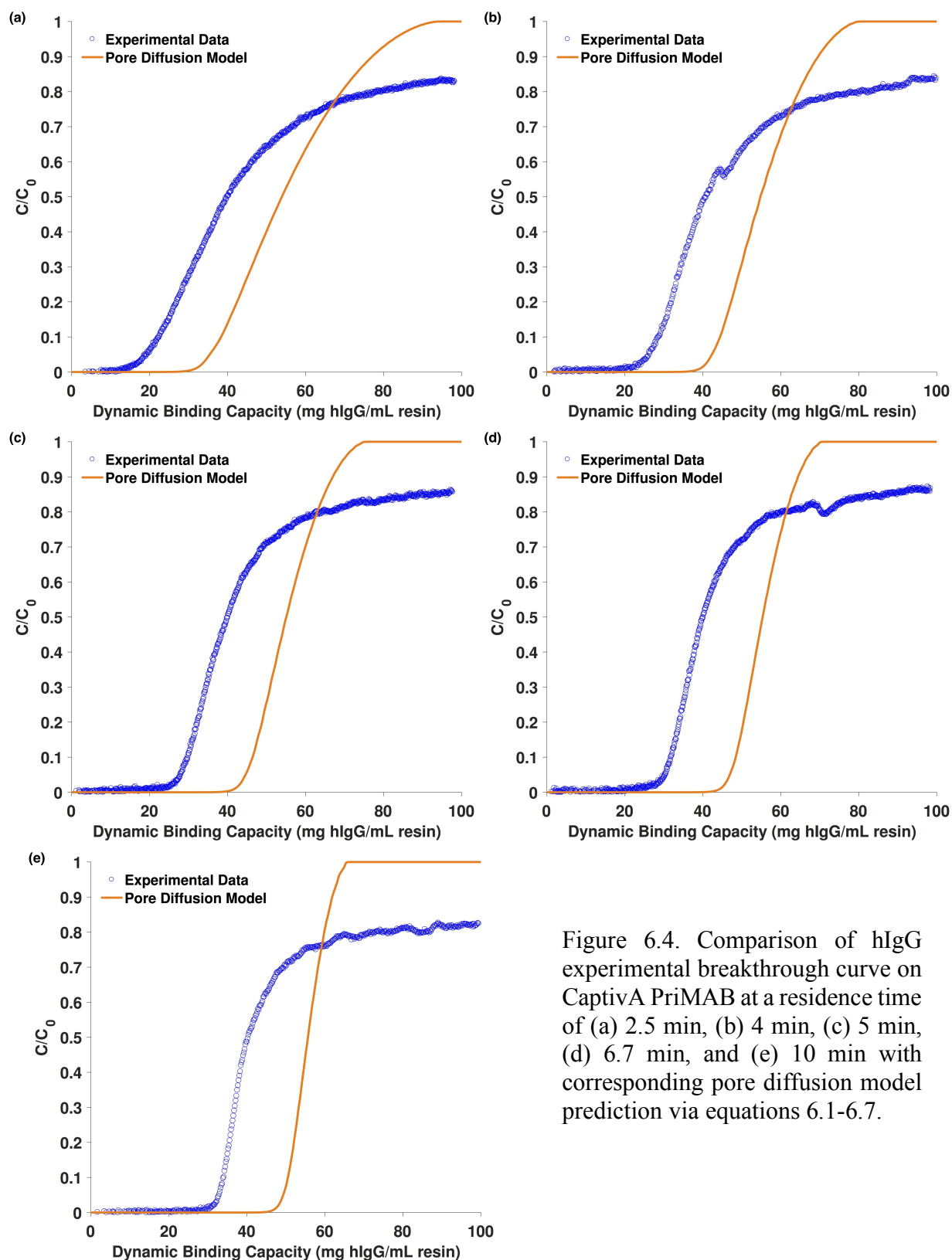
Figure 6.4. Comparison of hIgG experimental breakthrough curve on CaptivA PriMAB at a residence time of (a) 2.5 min, (b) 4 min, (c) 5 min, (d) 6.7 min, and (e) 10 min with corresponding pore diffusion model prediction via equations 6.1-6.7.

6.4. Additional PEGylated rSPA resins and characterization

Chapters 3 and 4 describe the physical and performance characterization of three PEGylated rSPA resins, notably the rSPA + 1×5 kDa PEG, the rSPA + 3×5 kDa PEG, and the rSPA + 20 kDa PEG resins. In addition to these three resins, a total of six PEGylated rSPA resin variants were generated, which are summarized in Table 6.2. The remaining PEGylated rSPA resins were not included in Chapters 3 and 4 (the publications) because they lacked complete characterization, such as CLSM adsorption images, in order to generate a full comparison and appropriate conclusions.

As seen in Table 6.2, four (Reactions #1-4) and two (Reactions #5-6) PEGylation reactions were performed using the 5.2 kDa and 21.5 kDa methoxy-PEG-propionaldehyde (mPEG-PA) chemistries, respectively. The extents of each reaction were determined to be directly proportional to the initial PEG:rSPA molar reaction ratio used. Reactions 1, 2, 5, and 6 resulted in PEGylation extents below or near 100%, which is consistent with the expectation that the aldehyde-activated PEG would be selective towards the N-terminus of rSPA under low PEG:protein molar ratios [7]. However, as seen in Reactions 3 and 4, increasing the PEG:rSPA initial molar ratio resulted in PEGylation extents significantly above 100%, which suggested that more than one PEG molecule (on average) became covalently attached to the rSPA ligand. The resins resulting from Reactions 2, 3, 4, and 6 (denoted rSPA + 1×5 kDa PEG, rSPA + 1.8×5 kDa PEG, rSPA + 3×5 kDa PEG, and rSPA + 20 kDa PEG, respectively) were translated to a packed column format for appropriate characterization.

Reaction #	Reference Name	PEG MW (kDa)	PEG:rSPA Initial Molar Reaction Ratio	PEGylation Extent (%)	Volume of PEG conjugated per mole of rSPA (nm^3 PEG/mol rSPA)
1	Reaction 1	5.2	2.76	103 ± 6	52 ± 3
2	rSPA + 1×5 kDa PEG	5.2	2.79	111 ± 8	56 ± 4
3	rSPA + 1.8×5 kDa PEG	5.2	2.97	177 ± 6	89 ± 3
4	rSPA + 3×5 kDa PEG	5.2	7.32	285 ± 11	143 ± 6
5	Reaction 5	21.5	2.95	34 ± 5	185 ± 27
6	rSPA + 20 kDa PEG	21.5	3.25	66 ± 24	325 ± 118

Table 6.2. Results of all PEGylation reactions performed on immobilized rSPA ligands on CaptivA PriMAB resin. Error ranges given represent 95% confidence limits based on PEGylations performed in triplicate.

Figure 6.5a is a modified version of Figure 4.2, which includes the static binding isotherm for hIgG on the rSPA + 1.8×5 kDa PEG resin. Values of q_{max} determined from fits of the Langmuir isotherm for all five resins are summarized in Table 6.3. Static binding isotherms and Langmuir isotherm model analysis were conducted as described in Chapter 4. The static binding isotherm for the rSPA + 1.8×5 kDa PEG resin follow the trends established and discussed for the other PEGylated rSPA resins in Chapter 4. Given that the value of q_{max} is directly proportional to the volume of conjugated PEG in the resin, the value for the rSPA + 1.8×5 kDa PEG resin fell in between the rSPA + 1×5 kDa PEG and rSPA + 3×5 kDa PEG resins, as expected. Figure 6.5b displays the relationship between q_{max} for hIgG in the unmodified and all six PEGylated rSPA resins with respect to the conjugated PEG volume per mole of rSPA as reported in Table 6.2. As seen in the figure, there is an overall negative correlation between q_{max} and PEG volume in the resin, which visualizes the trend between these variables discussed in Chapter 4.
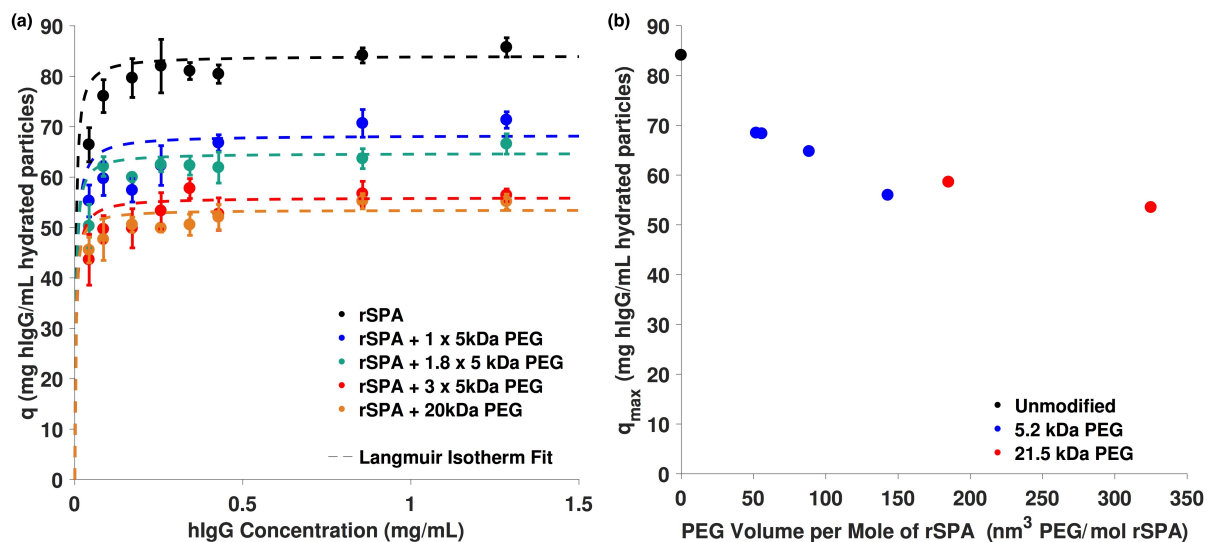
Figure 6.5. (a) Static binding isotherms of hIgG for the unmodified and four PEGylated rSPA resins. Dashed lines represent fits of the Langmuir isotherm to the data. (b) Plot of q_{max} for hIgG determined in the unmodified and all six PEGylated rSPA resins as a function of the conjugated PEG volume per mole of rSPA in each resin. Error bars in both figures represent 95% confidence limits based on triplicate measurements. All isotherms were measured at room temperature ($20 \pm 2°C$ for our laboratories).

The remainder of this section discusses additional column characterization performed on the rSPA + 1.8×5 kDa PEG resin that was not reported in Chapter 4. Experimental materials, methods, and analysis were used and conducted exactly as described in Chapter 4.

Figure 6.6a is a modified version of Figure 4.1a, which includes a plot of K_D versus iSEC dextran probe viscosity radius for the rSPA + 1.8×5 kDa PEG resin. Values of r_{pore}, s_{pore}, and β_{IgG} for all five resins are summarized in Table 6.3. The results for the rSPA + 1.8×5 kDa PEG resin again follow the trends established and discussed for the other PEGylated rSPA resins in Chapter 4. Values of r_{pore} and β_{IgG} decrease in proportion with the volume of conjugated PEG per mole of rSPA as reported in Table 6.2. There was no significant change in the value of s_{pore} compared to the unmodified resin, which is consistent with other two PEGylated rSPA resins with

the 5.2 kDa mPEG-PA chemistry. As discussed in Chapter 4, the consistent value of s_{pore} suggests that the 5.2 kDa PEG was evenly distributed within the pore distribution.

Figure 6.6b is a modified version of Figure 4.1b, which includes a dimensionless van Deemter plot for the rSPA + 1.8×5 kDa PEG resin. Values of D_e determined by the van Deemter analysis for all five resins are summarized in Table 6.3. The results for the rSPA + 1.8×5 kDa PEG resin again follow the trends established and discussed for the other PEGylated rSPA resins in Chapter 4. Values of D_e decreased approximately linearly with respect to the values of β_{IgG} observed with the introduction of immobilized PEG chains.

Figure 6.6c is a modified version of Figure 4.3, which includes a pH gradient elution profile of a mAb on the rSPA + 1.8×5 kDa PEG resin. The mAb used to generate Figure 6.6c was the same as in Figure 4.3. Values of elution pH, which were determined from the pH corresponding to the elution peak maximum, are summarized in Table 6.3 for all five resins. As expected, the elution pH of the mAb bound on the rSPA + 1.8×5 kDa PEG resin increased compared to that of the unmodified resin and was in between the values for the rSPA + 1×5 kDa PEG and rSPA + 3×5 kDa PEG resins. As discussed in Chapter 4, the increase in elution pH suggests a decrease in relative IgG binding affinity compared to the unmodified resin.

Figure 6.6d is a modified version of Figure 4.4, which includes values of $DBC_{10\%}$ for hIgG on the rSPA + 1.8×5 kDa PEG resin as a function of column residence time. As seen in Figure 6.6, and consistent with expectations, values of $DBC_{10\%}$ fell in between the rSPA + 1×5 kDa PEG and rSPA + 3×5 kDa PEG resins. This is consistent with the conclusion made in Chapter 4 where it was shown that significantly increasing the conjugated PEG volume leads to decreases in static binding capacity and increases in mass transfer resistance that ultimately results in a reduction in $DBC_{10\%}$.
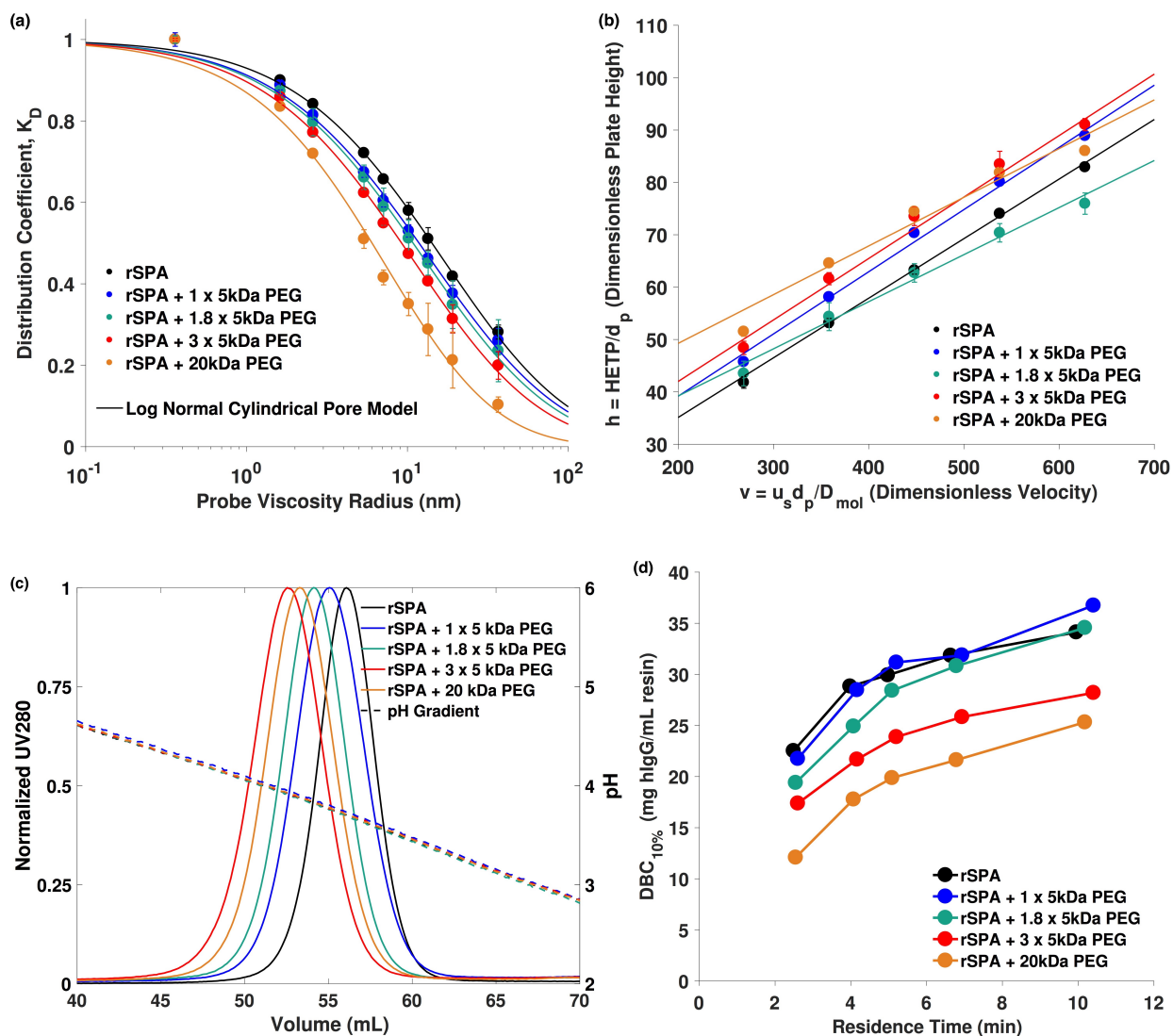
Figure 6.6. (a) Plot of K_D versus iSEC dextran probe viscosity radius for unmodified and four PEGylated rSPA resins. Solid lines represent fits according to eqs. 3.2-3.3. (b) Dimensionless van Deemter plots for unmodified and PEGylated rSPA resins. Solid lines represent fits according to eq. 3.7. (c) pH gradient elution profiles of the mAb on the unmodified and four PEGylated rSPA resins. The five essentially coincident dashed lines represent the pH gradient for each of the elution experiments. (d) Plot of $DBC_{10\%}$ for hIgG as a function of column residence time for the unmodified and four PEGylated rSPA resins. Solid lines represent linear interpolations of the data points to highlight trends. Error bars in all figures represent 95% confidence limits based on triplicate measurements.

176

Resin	r_{pore} (nm)	s_{pore}	β_{IgG}	D_e (10^{-8} cm^2/s) from HETP	q_{max} (mg hIgG/mL hydrated resin particles)	Elution pH (mAb)
rSPA	57.3 ± 1.6	1.26 ± 0.07	0.65 ± 0.01	7.5 ± 0.5	84 ± 1	3.70 ± 0.02
rSPA + 1×5 kDa PEG	47.8 ± 1.8	1.32 ± 0.10	0.61 ± 0.01	6.2 ± 0.2	68 ± 2	3.80 ± 0.02
rSPA + 1.8×5 kDa PEG	43.8 ± 1.9	1.29 ± 0.11	0.57 ± 0.01	5.9 ± 0.7	65 ± 2	3.82 ± 0.02
rSPA + 3×5 kDa PEG	37.1 ± 1.3	1.26 ± 0.09	0.56 ± 0.01	6.9 ± 0.2	56 ± 1	3.93 ± 0.02
rSPA + 20 kDa PEG	23.8 ± 1.3	1.05 ± 0.13	0.48 ± 0.01	5.9 ± 0.8	53 ± 1	3.88 ± 0.02

Table 6.3. Summary of physical, mass transfer, capacity, and elution characteristics for unmodified and four PEGylated rSPA resins. Error for all values represents 95% confidence limits based on triplicate measurements.

6.5. Binding of hIgG to PEGylated rSPA resins

In Chapter 3, it is shown that upon adsorption of hIgG on multiple commercial ProA resins, the sub-species within the polyclonal sample exhibit competitive binding behavior. As such, the PEGylated rSPA resins in Chapters 3 and 4 were characterized with single-component mAbs wherever possible to avoid the confounding effects of the competitive binding behavior. This section reports additional characterization experiments that were conducted on the PEGylated rSPA resins with hIgG. Experimental materials, methods, and analysis were used and conducted as described in Chapters 3 and 4.

Figure 6.7 is an analgous plot to Figure 6.6c, which displays the pH gradient elution profiles for hIgG on the unmodified and four PEGylated rSPA resins. As seen in Figure 6.7, all four curves displayed the same broad profile with distinct shoulders as did the unmodified resin. As discussed in Chapter 3, this broad profile is due to the different sub-classes and secondary binding events that result in a range of antibody binding strengths and elution pHs. The fact that

177

the profiles for the PEGylated rSPA resins retain the same overall shape and distribution suggests that the modification of rSPA does not disrupt the relative binding strengths within the sample. As also seen in Figure 6.7, all four PEGylated rSPA resin curves shift to the left compared to the unmodified resin curve, which indicates higher elution pHs for all hIgG sub-species. The curves shift such that their peak maxima are in the same order of increasing elution pH as for the mAb in Figure 6.6c. This particular result is consistent with the fact that the mAb used to generate the profiles in Figure 6.6c was an IgG_1 while the main peak in hIgG pH gradient elution profiles has been shown to be predominantly IgG_1 species [8].
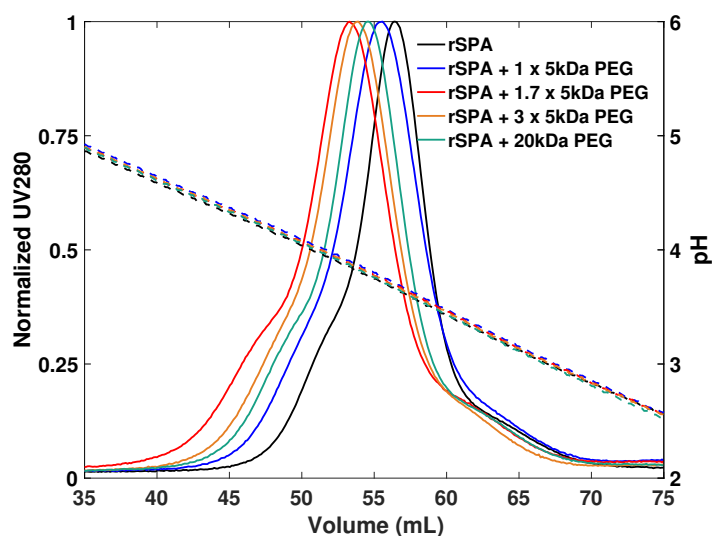
Figure 6.7. pH gradient elution profiles of hIgG on the unmodified and four PEGylated rSPA resins. The five essentially coincident dashed lines represent the pH gradient for each of the elution experiments.

Figure 6.8 is an analogous plot to Figure 4.5, which displays normalized batch uptake curves for the unmodified and four PEGylated rSPA resins for hIgG at an initial concentration of 2 mg/mL over 7000s. The curves were normalized to each resin's respective value of q_{max} for hIgG, which is reported in Table 6.3. As seen Figure 6.8, all resins, with the exception of the rSPA + 20 kDa PEG resin, displayed a slow approach to equilibrium that is consistent with the competitive binding behavior for hIgG discussed in Chapter 3 and with the heterogeneous binding

kinetics for PEGylated rSPA resins discussed in Chapter 4. Here, it is difficult to draw specific conclusions about these batch uptake profiles since there are two complex kinetic phenomena occurring simultaneously. However, it is expected that the fact that the rSPA + 20 kDa PEG resin approaches saturation at 7000s is due to the combination of the competitive binding behavior arising from the hIgG population and heterogeneous binding kinetics arising from the PEGylation of the rSPA ligand.
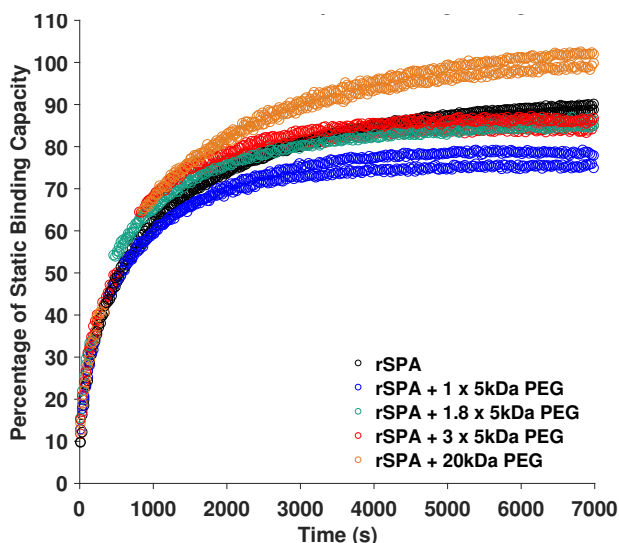
Figure 6.8. Normalized batch uptake curves for the unmodified and four PEGylated rSPA resins for hIgG at an initial concentration of 2 mg/mL over 7000s.

Figures 6.9a-e display the individual batch uptake profiles at initial hIgG concentrations of 2.0, 1.0, 0.5, and 0.2 mg/mL for the unmodified, rSPA + 1×5 kDa PEG, rSPA + 1.8×5 kDa PEG, rSPA + 3×5 kDa PEG, and rSPA + 20 kDa PEG resins, respectively. As seen by comparing the profiles amongst the resin variants, the PEGylated rSPA resin variant uptake curves were depressed due to the loss in static binding capacity compared to the unmodified resin. As also seen by comparing the profiles, the PEGylated rSPA resins appear to have a slower approach to equilibrium compared to the unmodified resin; the slope of the uptake curve at long times is flatter. This long-time behavior is similar to that of the uptake profiles of the mAb on the same resins

shown in Figure 4.5. For all resins, both the 2.0 and 1.0 mg/mL uptake curves converge towards the end of the profile at 7000s. This is consistent with the fact that the static binding isotherms for all of the resins were fully saturated at concentrations below 1.0 mg/mL. Thus, it is expected that both of these curves reach the same adsorbed concentration of IgG as they approach equilibrium at long times.
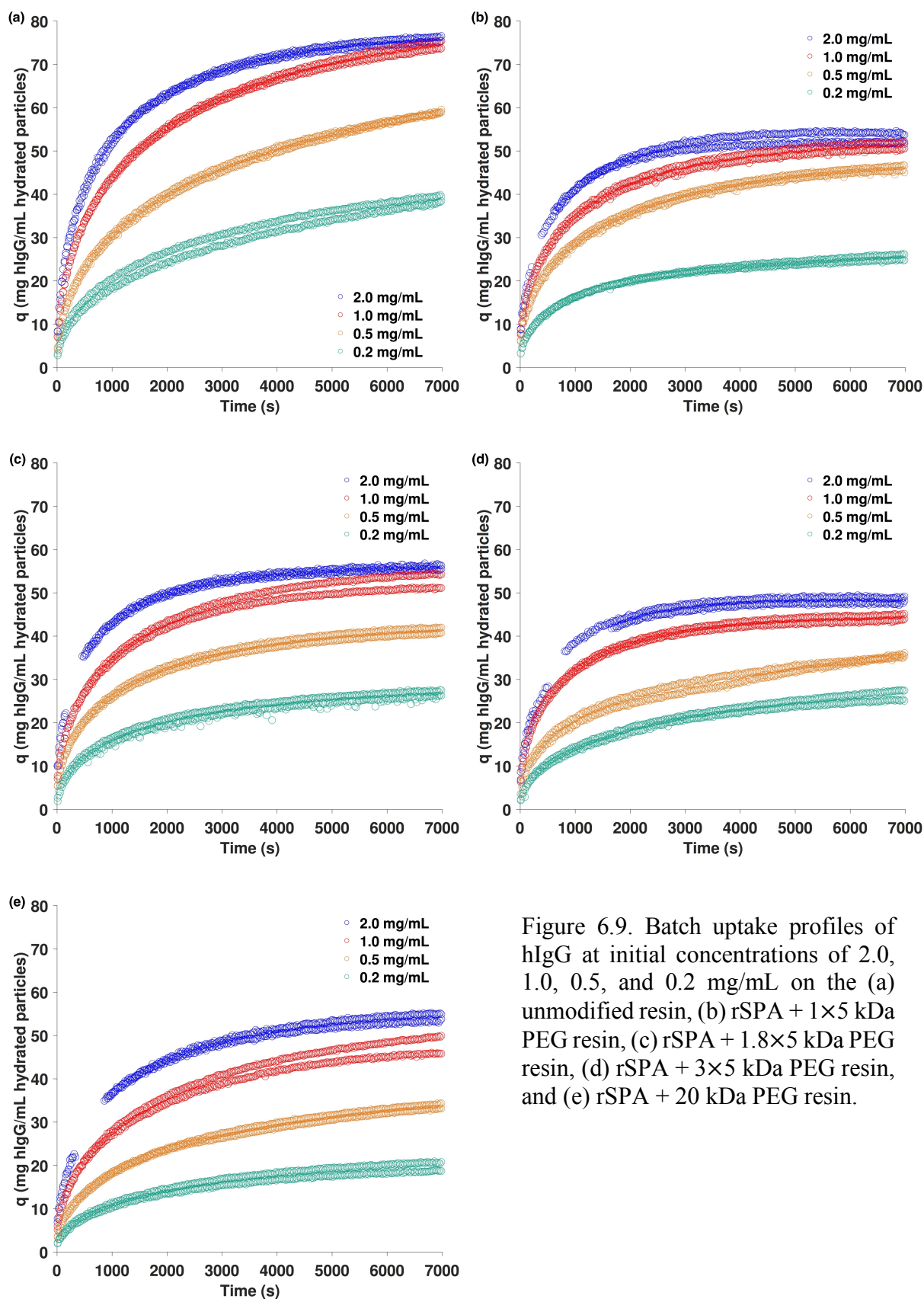
Figure 6.9. Batch uptake profiles of hIgG at initial concentrations of 2.0, 1.0, 0.5, and 0.2 mg/mL on the (a) unmodified resin, (b) rSPA + 1×5 kDa PEG resin, (c) rSPA + 1.8×5 kDa PEG resin, (d) rSPA + 3×5 kDa PEG resin, and (e) rSPA + 20 kDa PEG resin.

Figure 6.10 is analogous to Figure 4.6, which displays CLSM images of batch adsorption of fluorescently labeled hIgG at 2.0 mg/mL on the unmodified, rSPA + 1×5 kDa PEG, rSPA + 3×5 kDa PEG, and rSPA + 20 kDa PEG resins. As seen in Figure 6.10, the adsorption front of hIgG on all resins was broad and diffuse, which is consistent with the competitive binding behavior discussed in Chapter 3. When comparing the CLSM images of the PEGylated rSPA resin variants to the unmodified resin, it is seen that the adsorption fronts are even more diffuse, which is possibly due to the decrease in IgG binding strength upon PEGylation of rSPA as discussed in Chapter 4. Similar to the adsorption fronts of the mAb in Figure 4.6, the speed of the hIgG adsorption front traversing the resin particles increases for the rSPA + 1×5 kDa PEG resin compared to the unmodified resin; the speed then decreases for the rSPA + 3×5 kDa PEG and rSPA + 20 kDa PEG resins. Also similar to the movement of the adsorption fronts of the mAb, the speeds of the adsorption fronts for the rSPA + 3×5 kDa PEG and rSPA + 20 kDa PEG resins are roughly equivalent. As discussed in Chapter 4, the change in adsorption front speeds is due to a combination of a loss in static binding capacity and increase in mass transfer resistance when conjugated PEG is present in the resin. The fact that these same phenomena are observed for hIgG on the PEGylated rSPA resins suggests that this trend is not limited to the particular mAb used in Chapter 4. These observations also validate the link between the CLSM images for the mAb and the trends and values of $DBC_{10\%}$ generated with hIgG.
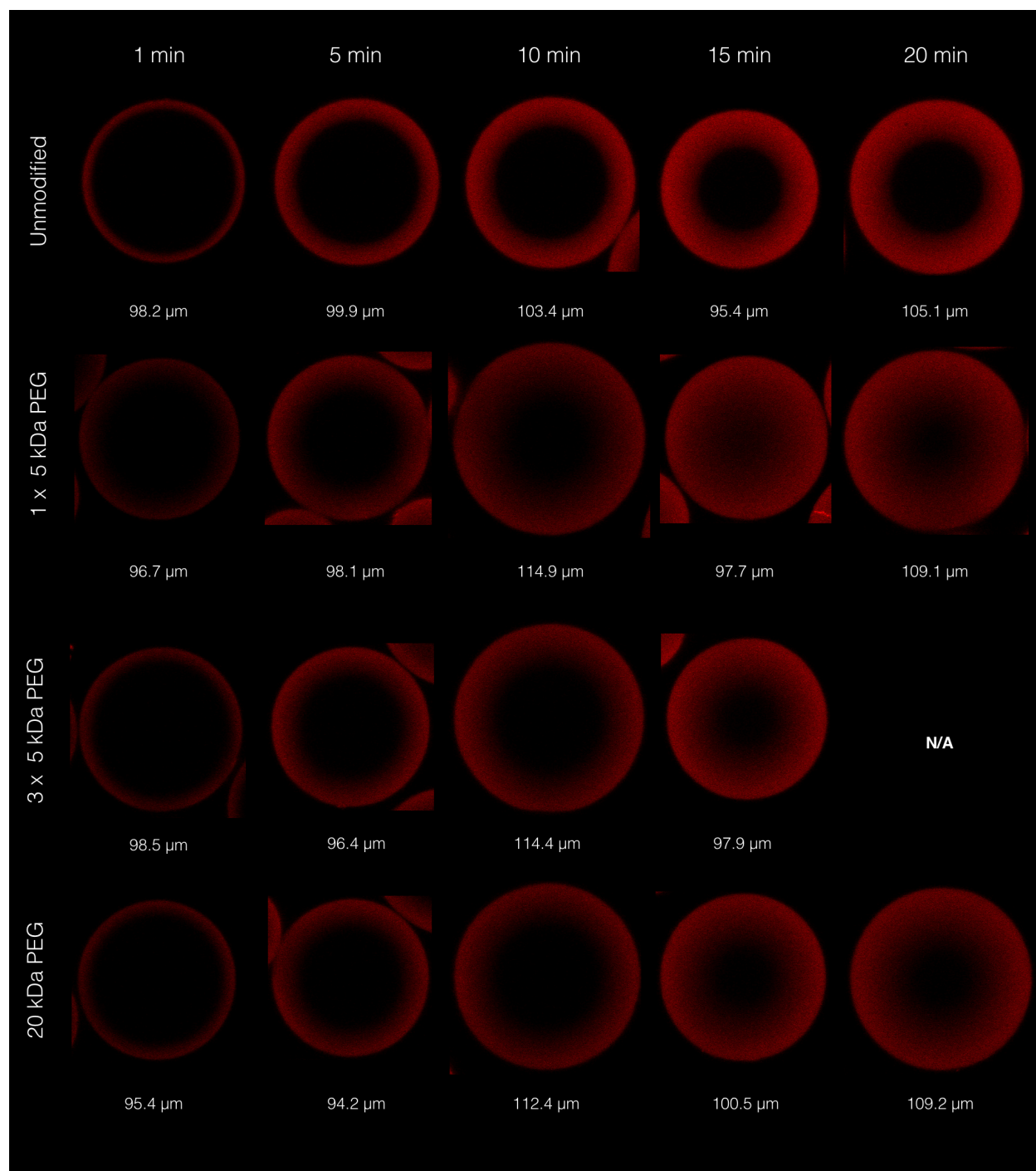
Figure 6.10. Representative CLSM images of adsorption of 2 mg/mL hIgG for the unmodified and three PEGylated rSPA resins for times up to 20 min. The 20 min time point for the rSPA + 3×5 kDa PEG resin was not available. Actual particle diameters are shown below each image.

6.6. Breakthrough curves for hIgG on PEGylated rSPA resins

Figures 6.11a-e display the hIgG breakthrough curves at column residence times of 2.5, 4, 5, 6.7, and 10 min that were generated on the unmodified, rSPA + 1×5 kDa PEG, rSPA + 1.8×5 kDa PEG, rSPA + 3×5 kDa PEG, and rSPA + 20 kDa PEG resins, respectively. All breakthrough curves were generated using a hIgG front concentration of 2.0 mg/mL and were conducted as described in Chapter 4. Each breakthrough curve was used to determine values of $DBC_{10\%}$ for each resin shown in Figures 4.4 and 6.6. As seen by comparing the breakthrough curves amongst the resin variants, all curves experienced a very slow approach to saturation at long-times, which is a consequence of the hIgG competitive binding behavior discussed at length in Chapter 3.
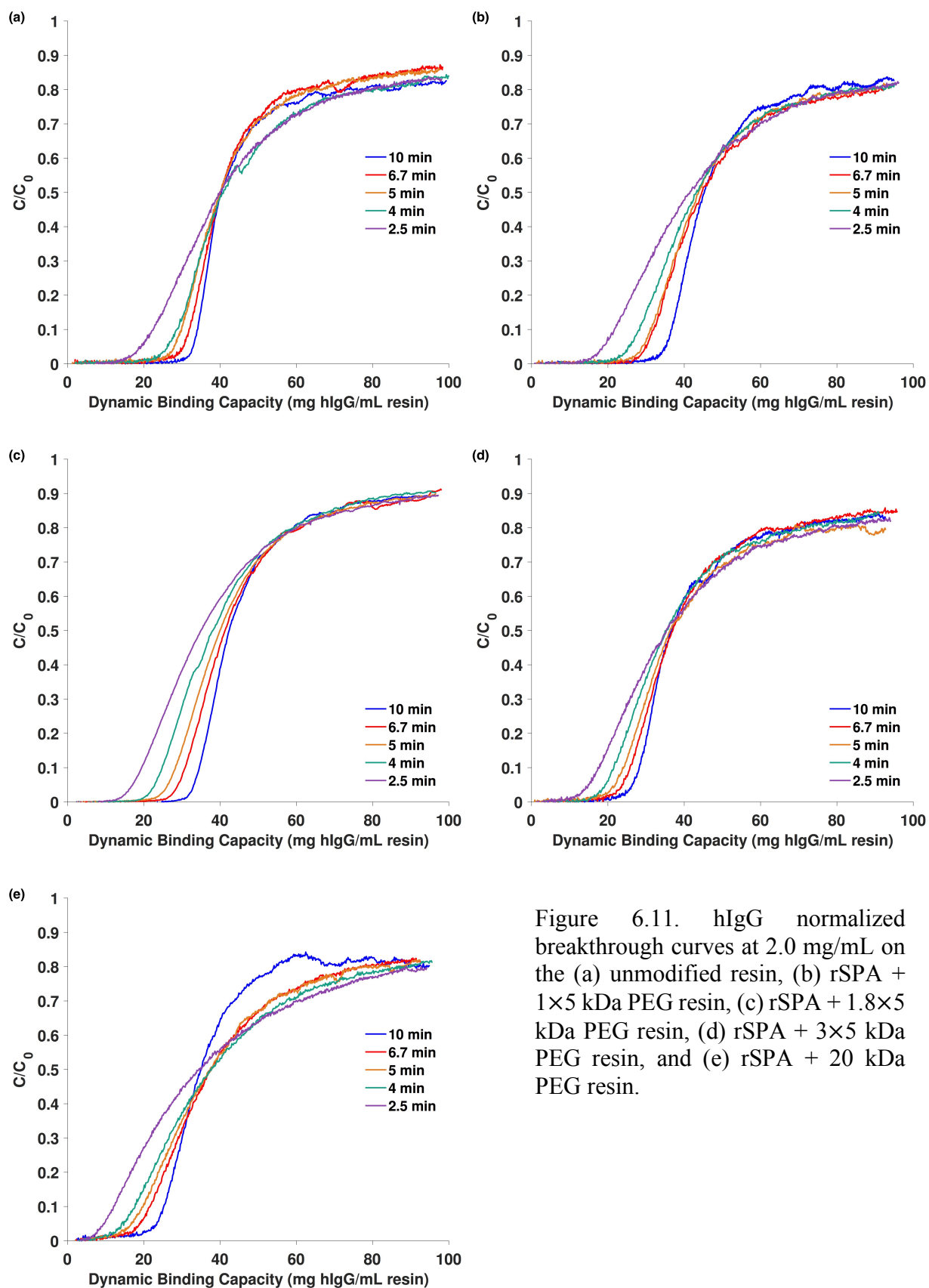
Figure 6.11. hIgG normalized breakthrough curves at 2.0 mg/mL on the (a) unmodified resin, (b) rSPA + 1×5 kDa PEG resin, (c) rSPA + 1.8×5 kDa PEG resin, (d) rSPA + 3×5 kDa PEG resin, and (e) rSPA + 20 kDa PEG resin.

185

6.7. BSA-mAb A association on other PEGylated rSPA resins

Figures 6.4a and b display CLSM images for the simultaneous adsorption of BSA and mAb A on the unmodified and rSPA + 20 kDa PEG resins, respectively. Images of the same adsorption process on the rSPA + 1×5 kDa PEG and rSPA + 3×5 kDa PEG resins were excluded from Chapter 5 for brevity. Figures 6.12a and b display the aforementioned CLSM images. As seen in Figure 6.12a and b, there is a decrease in the intensity of the BSA signal for the two PEGylated rSPA resins compared to the unmodified resin, however, the ratio of BSA to mAb A integrated intensity remains roughly equivalent. This trend is quantified Figure 5.5 and discussed in Chapter 5. In these particular images, the BSA intensity is decreased due to the loss in mAb binding capacity that results in less protein for the BSA to bind to. Because the ratio of BSA to mAb A signal intensity remains the same, the rSPA + 1×5 kDa PEG and rSPA + 3×5 kDa PEG resins do not seem to offer the apparent 'selectivity' advantages that are observed for the rSPA + 20 kDa PEG resin in this assessment. As discussed in Chapter 5, the likely explanation for these observations is the significant increase in excluded volume that is present when the rSPA ligand is modified with the 21.5 kDa PEG.
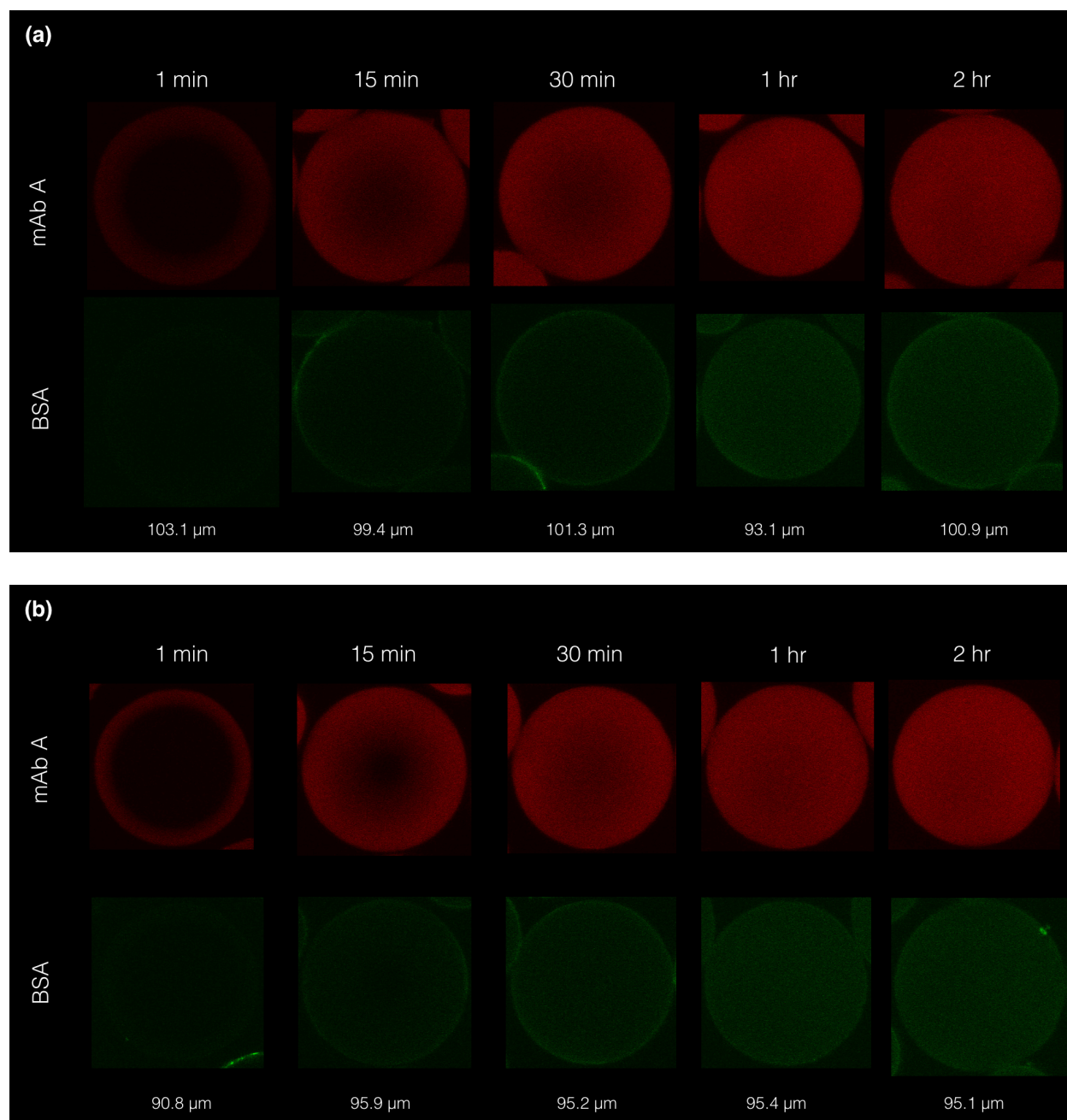
Figure 6.12. Representative CLSM images for simultaneous adsorption of mAb A (top rows) and BSA (bottom rows) for (a) the rSPA + 1×5 kDa PEG resin and (b) the rSPA + 3×5 kDa PEG resin over a period of 2 hr.

6.8. Alkaline stability of PEGylated rSPA resins

As discussed in Chapter 5, one of the main sources of fouling and loss of binding capacity in ProA resins is exposure to harsh, alkaline clean-in-place (CIP) conditions. To clean ProA resins,

caustic solutions, such as 0.1-1M NaOH, are typically used to regenerate the column for multiple

process cycles [9]. Studies in the literature have shown that the high pH conditions cause chemical

denaturation of the ProA ligand and irreversible binding of large aggregate species that block pores

and binding sites [10-13]. As a result, alkali-stabilized ProA ligands have been developed, such as

the SuRe ligand from GE Healthcare, to mitigate these effects [14].

To test the relative alkaline stability of the rSPA + 1×5 kDa PEG and rSPA + 20 kDa PEG

resins relative to the unmodified resin, all three resins were exposed to a solution of 0.1M aqueous

NaOH to simulate lifetime trajectories of each resin's q_{max} over multiple process cycles.

Additionally, the three resins were compared to a Repligen "IPA700 resin", which is a prototype

and proprietary alkali-stabilized Pro A ligand based resin. Briefly, hydrated resin particles were

generated for each resin as described in Chapters 3 and 4. Roughly 100 mg of hydrated resin

particles were added to microcentrifuge tubes followed by 1 mL of the 0.1M NaOH solution. The

microcentrifuge tubes were then allowed to rotate end-to-end at 18 rpm for a set period of time

after which the entire contents of the tube were immediately filtered and washed 2 times with PBS

buffer in 0.2 μm centrifugal filters at 1500×g for 2 minutes. This removed the NaOH from the

pores of the resin and brought the pH down to neutral conditions. The resins were washed a final

time with PBS buffer and centrifuged at 3000×g for 45 min to regenerate hydrated resin particles.

A single-point adsorption assay was performed by adding known weights of the alkali-exposed,

hydrated resin particles to a solution of 3.0 mg/mL hIgG (resulting in an equilibrium concentration

of ~1.3 mg/mL hIgG) in triplicate to estimate the resin's value of q_{max}. The single-point

adsorption isotherm measurement was conducted as described in Chapters 3 and 4. This entire

procedure was repeated for each resin and for time points ranging from 1 hour to 48 hours. A

single-point adsorption isotherm on each unexposed resin was also performed in triplicate to serve as a time zero data point.

Figure 6.13 displays the residual IgG binding capacity of the unmodified resin, the two PEGylated rSPA resins, and IPA700 after exposure to 0.1M NaOH plotted as the percentage of the initial binding capacity as a function of exposure time. The values of binding capacity over time were fit to a first order decay model:

$$q_{max}(t) = q_{max}(0) \exp(-k_{decay}t) \tag{6.8}$$

where k_{decay} is the first order decay rate constant. Table 6.4 summarizes the values of k_{decay} obtained for each resin.

As seen in Figure 6.13 and from the values of k_{decay} in Table 6.4, PEGylation of rSPA had no significant effect on the alkaline stability of the ProA ligand. This is not surprising considering that PEG is a neutral macromolecule that would not be expected to hinder the accessibility of small hydroxide ions to the ligand. The results for the unmodified and PEGylated rSPA resins are in stark contrast to the IPA700 resin, which had a value of k_{decay} that was an order of magnitude lower than that for the CaptivA PriMAB based resins. The IPA700 resin employs direct protein engineering to stabilize the ligand rather than an external chemical modification, which clearly is more effective than PEGylation with respect to increasing alkaline stability.
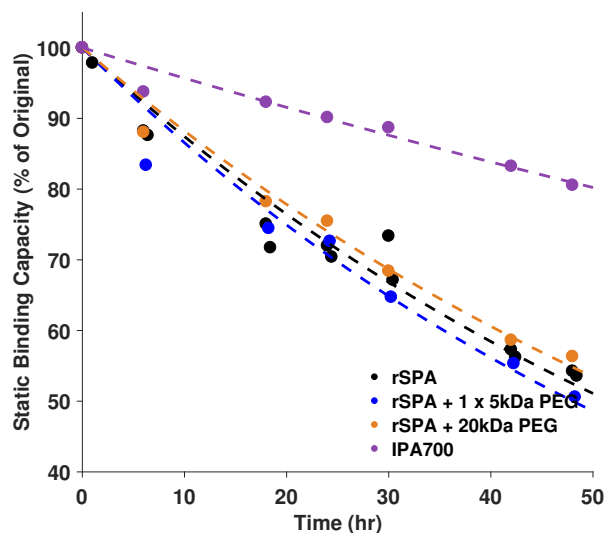
Figure 6.13. Plots of percentage of original IgG binding capacity of the unmodified and PEGylated rSPA resins after exposure to 0.1M NaOH for up to 48 hours. Dashed lines represent fits to equation 6.8.

Resin	k_{decay} (hr^{-1})
rSPA	0.013 ± 0.001
rSPA + 1 × 5kDa PEG	0.014 ± 0.002
rSPA + 20 kDa PEG	0.012 ± 0.001
Repligen IPA700	0.0044 ± 0.0005

Table 6.4. Values of k_{decay} for the unmodified resin, PEGylated rSPA resins, and Repligen IPA700 resin. Error represents 95% confidence limits of the non-linear regression of the dataset.

6.9. ^{1}H NMR of immobilized rSPA and PEGylated rSPA

^{1}H NMR was employed to confirm the presence of conjugated PEG in the modified rSPA resins and to evaluate the mobility of the polymer when it is chemically bonded to rSPA. Briefly, both the unmodified and rSPA + 1×5 kDa PEG resins were washed into D$_2$O to remove the majority of water. Roughly ~50 mg of the washed resin were then allowed to settle in a suspension of D$_2$O in the bottom of separate NMR tubes. NMR data were then acquired at 25 ºC for both resins on Bruker spectrometers operating at 600 MHz per Sinha et al. [14].

Figure 6.14 displays ^{1}H NMR spectra for the unmodified and rSPA + 1×5 kDa PEG resins. As seen from Figure 6.14, both resins had a large and sharp peak at δ ~4.8 ppm with respect to

DSS, which is consistent for literature values of H_2O [16]. The rSPA + 1×5 kDa PEG resin spectrum also had a smaller peak between 3.5 and 4 ppm, which is consistent with the chemical shift of hydrogens adjacent to ether functional groups (R-CH$_2$-O-R, δ 3.3-4.9 ppm) that are present in PEG molecules [16]. The fact that PEG produces a peak in an ^{1}H NMR spectrum suggests that the polymer retains some amount of mobility when chemically bonded to rSPA. As expected, since the rSPA ligand is immobilized to the resin base matrix, there is no obvious peak corresponding to the protein in either spectra.

The NMR spectra proved to be a relatively facile method of directly confirming PEGylation of rSPA. In the future, extending measurements to include internal PEG standards may be used as an *in situ* method for determine PEGylation extent.
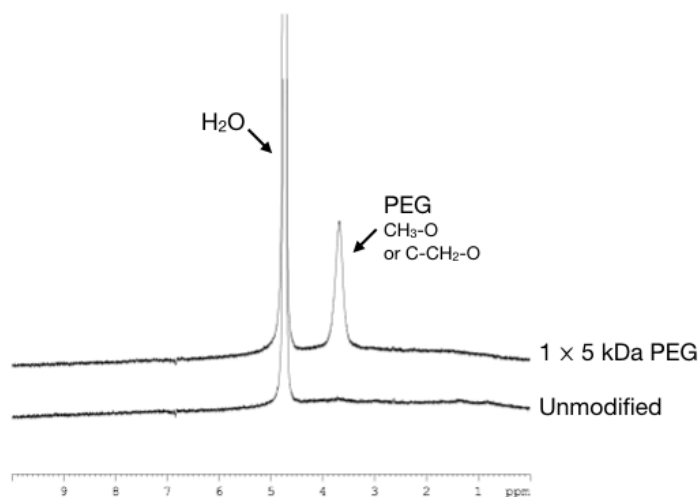
Figure 6.14. ^{1}H NMR spectra for the unmodified and rSPA + 1×5 kDa PEG resins.

6.10. References

[1] Y. Tao, E. Perez-Almodovar, G. Carta, G. Ferreira, D. Robbins, Adsorption kinetics of deamidated antibody variants on macroporous and dextran-grafted cation exchangers. III. Microscopic studies. J Chromatogr A. 1218 (2011) 8027-8035.

[2] E.X. Perez-Almodovar, G. Carta, IgG adsorption on a new protein A adsorbent based on macroporous hydrophilic polymers. I. Adsorption equilibrium and kinetics, J Chromatogr A. 1216 (2009) 8339-8347.

[3] R. Hahn, P. Bauerhansl, K. Shimahara, C. Wizniewski, A. Tscheliessnig, A. Jungbauer, Comparison of protein A affinity sorbents II. Mass transfer properties, J Chromatogr A. 1093 (2005) 98-110.

[4] J.T. McCue, G. Kemp, D. Low, I. Quiñones-García, Evaluation of protein-A chromatography media, J Chromatogr A. 989 (2003) 139-153.

[5] A.D. Tustian, C. Edicott, B. Adams, J. Mattila, H. Bak, Development of purification processes for fully human bispecific antibodies based upon modification of protein A binding avidity. MAbs 8 (2016) 828-838.

[6] S. Ghose, B. Hubbard, S.M. Cramer, Binding capacity differences for antibodies and Fc-fusion proteins on protein A chromatographic materials, Biotechnol. Bioeng. 96 (2007) 768-779.

[7] O. Kinstler, N. Gabriel, C. Farrar, R. DePrince, N-terminally chemically modified protein compositions and methods, US Patent no. 5,824,784 A, 1998.

[8] Duhamel R, Schur P, Brendel K, Meezan E. 1979. pH gradient elution of human IgG1, IgG2 and IgG4 from protein A-Sepharose. J. Immunol. Meth. 31:211-217.

[9] C. Jiang C, J. Liu, M. Rubacha, A.A. Shukla, A mechanistic study of Protein A chromatography resin lifetime, J Chromatogr A. 1216 (2009) 5849-5855.

[10] B. Kelley, Very large scale monoclonal antibody purification: The case for conventional unit operations, Biotechnol Prog. 23 (2007) 995-1008.

[11] S. Zhang, W. Daniels, J. Salm, J. Glynn, J. Martin, C. Gallo, R. Godavarti, G. Carta, Nature of foulants and fouling mechanism in the Protein A MabSelect resin cycled in a monoclonal antibody purification process, Biotechnol Bioeng. 113 (2016) 141-149.

[12] A.C.A. Roque, C.R. Lowe, M.A. Taipa, Antibodies and Genetically Engineered Related Molecules: Production and Purification, Biotechnol Prog. 20 (2004) 639-654.

[13] R. Hahn, K. Shimahara, F. Steindl, A. Jungbauer, Comparison of protein A affinity sorbents III. Life time study, J Chromatogr A. 1102 (2006) 224-231.

[14] GE Healthcare Life Sciences. MabSelect SuRe, Data File 11-0011-65 AC, 2011.

[15] S. Sinha, S.S. Sangani, A.D. Kehr, G.S. Rule, L. Jen-Jacobson, Metal Ion Binding at the Catalytic Site Induces Widely Distributed Changes in a Sequence Specific Protein–DNA Complex, Biochemistry. 55 (2016) 6115-6132.

[16] H.G. Gottlieb, V. Kotlyar, A. Nudelman, NMR Chemical Shifts of Common Laboratory Solvents as Trace Impurities, J Org Chem. 65 (1997) 7512-7515.

7

Conclusions and Future Directions

7.1. Thesis outcomes

The overall objectives of this thesis were to 1) increase the scientific community's understanding of IgG adsorption behavior on Protein A (ProA) chromatography resins and 2) improve the performance of ProA chromatography through the use of PEGylated ligands.

The work presented in this thesis suggests that IgG molecules of varying binding strength, or varying elution pH, are capable of competing for binding sites on ProA chromatography resins in simultaneous or sequential adsorption. Competitive binding behavior in protein chromatography or other forms of affinity chromatography has been well documented [1], however, this is the first report of IgG competition on ProA chromatography resins since ProA was first reported as an affinity chromatography ligand in 1972 [2]. It is particularly unexpected since ProA has shown to have essentially equal, strong, and highly specific binding to all human IgG_1, IgG_2, and IgG_4 species [3]. Based on the results of Chapter 3, the competitive phenomena, differences in IgG binding strength, and differences in IgG elution pH appear to derive from differences in sub-class behavior as well as secondary binding interactions with the ProA ligand. It is readily apparent in the adsorption of human polyclonal IgG (hIgG), which has a wide variety of IgG sub-classes and binding epitopes. The results also explain lingering questions in the literature about abnormalities in the adsorption profiles of hIgG on ProA resins. The competitive binding phenomenon is

193

demonstrated to occur on at least three commercial ProA resins, suggesting universality, with kinetics that appear to be faster on resins that have less ligand accessibility, and hence, less expected binding avidity.

Additionally, the work presented in this thesis suggests that ProA chromatography resins with PEGylated ligands are a viable path to increase resin robustness and real-world process selectivity. It is demonstrated that ligand PEGylation can increase resistance to proteolytic digestion, mitigate impurity interactions with monoclonal antibodies (mAbs) that are bound to ProA (so-called "hitchhiker" impurities), and increase process selectivity against Chinese Hamster Ovary (CHO) host cell proteins (HCPs) by up to 37%. However, ligand PEGylation must be carefully considered against potential tradeoffs in decreased binding capacity and increased mass transfer resistance that are associated with the modification. It is demonstrated that PEGylation universally decreases IgG static binding capacity to an extent that is proportional to the volume of conjugated PEG in the resin. Heavier modifications with large volumes of conjugated PEG significantly decrease static binding capacity and decrease the available pore space for IgG diffusion, resulting in losses in dynamic binding capacity and resin productivity. Lighter modifications appear to avoid losses in dynamic binding capacity, however, they do not appear to be effective at mitigating impurity interactions with mAbs that are bound to ProA, which is key to increasing process selectivity. ProA PEGylation also universally increases the elution pH of IgG molecules: the excluded volume of the conjugated PEG chains disfavors ligand binding, leading to weaker binding interactions between IgG and the PEG-ProA ligand. This last result opens another path of viability for ProA resins with PEGylated ligands for purification of mAbs of Fc-fusion proteins that are sensitive to low pH environments.

7.2. Original contributions

The following is a list of the notable and original contributions of this work in the order that they are presented in this thesis:

- Demonstrated that IgG molecules of varying binding strength, or varying elution pH, are capable of competing for binding sites on ProA chromatography resins in simultaneous or sequential adsorption on three commercial ProA resins. A phenomenon that has gone unnoted in the literature since ProA was first reported as an affinity chromatography ligand in 1972 [2].

- Answered lingering literature questions in Perez-Almodovar and Carta, Hahn et al., and McCue et al. [4-6] about the adsorption profile of hIgG on ProA resins. Specifically, demonstrating that the slow approach to equilibrium upon adsorption of hIgG on ProA resins is due to competitive binding behavior.

- Developed a reliable PEG depletion assay using HPLC with RI detection determine the extent of ProA ligand PEGylation. This assay may be easily extended to other chromatography ligands, matrices, or other polymer modifications.

- Performed inverse size exclusion chromatography, HETP experiments, and van Deemter analysis on an unmodified ProA resin and several resins with PEGylated ProA ligands to demonstrate that ligand PEGylation decreases available pore space and increases IgG mass transfer resistance.

- Generated static binding isotherms and determined maximum static binding capacities for an unmodified ProA resin and several resins with PEGylated ProA ligands with hIgG and a mAb to demonstrate that ligand PEGylation universally decreases static binding capacity of IgG to an extent that is proportional to the volume of conjugated PEG in the resin.

- Generated pH gradient elution curves for hIgG and a mAb on an unmodified ProA resin and several resins with PEGylated ProA ligands to demonstrate that ligand PEGylation universally weakens the binding interaction between antibodies and ProA and, hence, increases IgG elution pH.

- Generated hIgG breakthrough curves over a series of residence times on an unmodified ProA resin and several resins with PEGylated ProA ligands to demonstrate the relationship between IgG dynamic binding capacity, residence time, and ligand PEGylation extent.

- Generated batch uptake curves of a mAb on an unmodified ProA resin and several resins with PEGylated ProA ligands to demonstrate that ligand PEGylation can introduce heterogeneous binding kinetics. In this case, a fraction of traditionally fast binding sites in the unmodified resin are transformed to slow binding sites.

- Performed batch uptake experiments with a fluorescently labeled mAb monitored by confocal laser scanning microscopy (CLSM) on an unmodified ProA resin and several resins with PEGylated ProA ligands to show the relationship between IgG adsorption front speed and ligand PEGylation extent. Analysis and subsequent modeling of the CLSM images were also used as orthogonal confirmation of the heterogeneous binding kinetics described above.

- Demonstrated that PEGylation of ProA ligands can decrease resin degradation due to proteolytic digestion from a model protease, chymotrypsin.

- Used CLSM to demonstrate that PEGylation of ProA ligands can decrease the fouling of the resin surface by large, fluorescently labeled bovine serum album (BSA) aggregates.

- Performed simultaneous adsorption of a differentially labeled mAb and BSA on an unmodified ProA resin and several resins with PEGylated ProA ligands monitored by

CLSM to demonstrate that ligand PEGylation can mitigate the binding of BSA, as a mock hitchhiking contaminant, to the mAb when it is bound to ProA.

- Purified CHO harvested cell culture fluid (HCCF) containing an expressed mAb on an unmodified ProA resin and one resin with PEGylated ligands to demonstrate that ligand PEGylation can increase process selectivity against CHO HCPs by 37%.

- Proposed and demonstrated using non-binding IgG$_3$ species as a probe in HETP experiments to evaluate mass transfer resistance during loading conditions after a ProA resin has been partially or fully saturated with IgG.

7.3. Broader impacts

The work presented in this thesis is expected to have several impacts on the scientific community, and in particular, the bioprocessing community.

Many literature studies and resin manufactures have routinely used hIgG as a stand in for mAbs to characterize ProA resins. It is expected that the work discussed in Chapter 3 will promote discussion about the continued use of hIgG to characterize resins given the competitive binding behavior that is not present in single-component mAbs. Additionally, the discovery of IgG competitive binding behavior on ProA resins may open the possibility for ProA chromatography to be used in a displacement mode or other unforeseen applications.

This thesis demonstrates ProA ligand PEGylation as a viable pathway to increase the important performance aspects of the resin. Although this is not the first report of benefits of affinity ligand PEGylation [7], the aspect of external chemical modification of affinity chromatography ligands remains relatively unexplored. Given the importance of ProA chromatography to the bioprocessing and biopharmaceutical industries, the work presented in

Chapters 4 and 5 may spur additional investigations into PEGylation of other ProA ligands/resins, PEGylation of other affinity ligands, or even other polymer modifications to affinity ligands.

It is also important to note the impacts of this work outside of the results demonstrated. The work presented in this thesis has resulted in one publication in the journal of *Biotechnology and Bioengineering* and two manuscripts in review for the *Journal of Chromatography A*; both premier journals for bioprocessing and separation science literature. This work has been presented in various forms in at least 8 conferences, including three international conferences, and including the Recovery of Biological Products series, which is the premier conference for bioprocessing research.

This work has also initiated or intensified several collaborations between Carnegie Mellon University and the academic and bioprocessing communities. Notable amongst these is a new collaboration with Professor Giorgio Carta's laboratory at the University of Virginia, which was the platform for a significant fraction of the results presented in this thesis. Other collaborations have included Repligen (supply of chromatography resins and resin column packing), GE Healthcare (supply of chromatography resins), and Biogen (supply of CHO HCCF with expressed mAbs).

The research conducted in this thesis also included significant participation of undergraduates. A total of six undergraduate researchers were trained and mentored in various aspects of chromatographic techniques and analysis. Four of these undergraduates were included as co-authors on resulting publications and submitted manuscripts. Additionally, at least four of the undergraduates have expressed interest in career opportunities in the biotechnology industry; two of which have taken full-time positions in the industry after graduation from Carnegie Mellon University and one who has fulfilled a summer internship at a large biopharmaceutical company.

7.4. Future directions

7.4.1. Further investigation of IgG competitive binding mechanism

Chapter 3 discusses the discovery of IgG competitive binding behavior on ProA resins. It was noted that the competitive binding kinetics were faster on the CaptivA PriMAB resin than on the MabSelect and MabSelect SuRe resins. These results suggested that the difference in the competitive kinetics were due to ProA ligand accessibility where the ligand on CaptivA PriMAB has a multi-point covalent attachment to the resin (less accessible) compared to the MabSelect ligands that have a single-point attachment to the resin (more accessible). One hypothesis for this observation is that the increased accessibility of the MabSelect ligand allows more ligands to bind twice to the same IgG molecule, increasing the avidity, thus making it more difficult for another incoming IgG to displace the bound IgG.

One potential method to test this hypothesis is to repeat the sequential binding experiments of a mAb and hIgG in Chapter 3 with a mAb that is engineered with one ProA binding site on the Fc region removed. In fact, Tustian et al. [8] recently demonstrated that removing one of these Fc binding sites via protein engineering resulted in higher elution pHs, and thus lower binding strengths, for a mAb on multiple ProA resins due to reduced ligand avidity. In future experiments, the same mAb used in Tustian et al. [8] or a similar one can be used to directly test the ligand accessibility hypothesis. If the hypothesis is correct, the repeated sequential binding experiments of the mAb and hIgG will show faster displacement of the new mAb on MabSelect and MabSelect SuRe compared to the original mAb used in Chapter 3.

Another possibility for the observed differences in competitive binding kinetics is due to differences in resin ligand density. CaptivA PriMAB has a ligand density of 10 mg/mL while MabSelect and MabSelect SuRe have ligand densities of 5 and 6 mg/mL, respectively [9-13]. Since

the ligand density of the CaptivA PriMAB resin is significantly higher, the ligands are also physically closer together within the resin. With this considered, it is possible that there is a 'network' effect where IgG molecules are capable of transferring from one ligand to another more easily than in a resin where the ligands are not as closely packed. This hypothesis can be tested by once again repeating the sequential binding experiments of the mAb and hIgG on MabSelect SuRe LX resin, which uses the same base matrix and ligand as MabSelect SuRe resin but at a higher ligand density of 10 mg/mL [9]. If the hypothesis is correct, the repeated sequential binding experiments of the mAb and hIgG will show faster displacement of the mAb on MabSelect SuRe LX compared to the mAb on MabSelect or MabSelect SuRe shown in Chapter 3.

7.4.2. Modeling heterogeneous binding kinetics in ProA resins with PEGylated ligands

Chapter 4 discusses the observation of heterogeneous binding kinetics of a mAb on ProA resins with PEGylated ligands. The heterogeneous binding kinetics can possibly be described using the Heterogeneous Binding Model (HBM) described in Perez-Almodovar and Carta [4]:

$$\left[\beta_{IgG}\frac{\partial c}{\partial t} + \frac{\partial(q_1+q_2)}{\partial t}\right]\frac{\partial c}{\partial t} = \frac{D_e}{r^2}\frac{\partial}{\partial r}\left(r^2\frac{\partial c}{\partial r}\right) \tag{7.1}$$

$$r = 0, \quad \frac{\partial c}{\partial r} = 0 \tag{7.2}$$

$$r = r_p, \quad D_e\frac{\partial c}{\partial r} = k_f(C - c|_{z,r=r_p}) \tag{7.3}$$

$$\frac{\partial q_1}{\partial t} = k_1\left[\left(q_{max,1} - q_1\right)c - \frac{q_1}{K}\right] \tag{7.4}$$

$$\frac{\partial q_2}{\partial t} = k_2\left[\left(q_{max,2} - q_2\right)c - \frac{q_2}{K}\right] \tag{7.5}$$

$$\varepsilon \frac{\partial C}{\partial t} + (1 - \varepsilon) \frac{\partial \bar{q}}{\partial t} + u \frac{\partial C}{\partial z} = 0 \qquad (7.6)$$

$$\frac{\partial \bar{q}}{\partial t} = \frac{3}{r_p} k_f (C - c|_{z,r=r_p}) \qquad (7.7)$$

$$t = 0, \; z > 0, \; C = 0 \qquad (7.8)$$

$$z = 0, \quad C = C_0 \qquad (7.9)$$

As per the standard pore diffusion model, c is the IgG concentration in the particle pores, C is the IgG concentration in the interstitial particle fluid, C_0 is the initial front concentration, r_p is the average particle radius, k_f is the film mass transfer coefficient determined from the dimensionless Sherwood (Sh) number, $Sh = k_f d_p/D_0$, ε is the column interstitial porosity, β_{IgG} is the particle porosity accessible to IgG molecules, K is the IgG affinity constant, D_e is effective IgG diffusivity, and $\bar{q}$ is the average adsorbed IgG concentration.

The HBM introduces the concept that a fraction of the ProA binding capacity (q_1) is fast and binds with kinetic constant (k_1) while the remaining fraction of binding capacity (q_2) is slow and binds with a slow kinetic constant (k_2). It assumes that the dissociation rate constant is the same for both binding types. Since the q_1 is fast binding capacity that is only limited by diffusion, the value of k_1 is set to a large value such as 10 mL/mg•s.

With additional data generated for mAb adsorption on ProA resins with PEGylated ligands such as batch adsorption profiles at various concentrations (such as those in Figures 6.9a-e), the HBM can be used to fit the parameters k_2 and q_2. The parameters of the batch model can then be translated to a column model and be validated against experimentally generated breakthrough curves with a mAb. However, it is to be noted that these experiments will be expensive due to the need to large amounts of mAb to generate the full breakthrough curves.

7.4.3. Comprehensive selectivity study of PEGylated ProA resins

Chapter 5 demonstrates that CaptivA PriMAB resin modified with a 21.5 kDa PEG increases process selectivity against CHO HCPs by up to 37%. While this is an important result, it is the first step in a more comprehensive study that may demonstrate the full potential of ligand PEGylation to increase resin selectivity. The following is a list of experiments and studies that may provide additional value and insight:

- Determining process selectivity against CHO HCPs with resins that are modified with PEGs of smaller molecular weights (i.e. the 5.2 kDa PEG used in Chapters 4 and 5).

- Determining process selectivity with various modified resins against other process impurities from CHO HCCF including host DNA, virus particles, and mAb aggregates. An industrial collaborator may be relied on to assay DNA and virus content, which are typically expensive experiments to perform.

- Determining process selectivity with various modified resins against impurities at various column residence times.

- Determining process selectivity with various modified resins against impurities at various column loading concentrations.

- Determining process selectivity with various modified resins against impurities in CHO HCCF with different expressed mAbs. In particular, CHO HCCF with a mAb that is known to aggregate during ProA chromatography. The mAb from the CHO HCCF used in Chapter 5 was well behaved and did not aggregate.

- Performing 1-D or 2-D gel electrophoresis on the eluate pool collected from CHO HCCF purifications on various modified resins. The gel electrophoresis experiments will allow insights into the types of HCP impurities that the PEG is blocking (low vs. high molecular

weight, low vs. high pIs). Protocols for assaying CHO HCPs by 2-D gel electrophoresis are reported in the literature [13].

7.4.4. Effect of PEGylated ProA on intermediate washing steps

Shukla and Hinckley [14] demonstrated the use of intermediate wash steps during ProA chromatography to increase CHO HCP clearance. Amongst a variety of buffers and wash solutions, a combination of 1M urea and 10% isopropanol was found to optimize mAb yield and HCP clearance. These particular components were chosen due to their ability to mitigate protein-protein interactions (i.e. HCP-mAb interactions).

The CHO HCCF purification protocol used in Chapter 5 did not include an intermediate wash step. Washing was performed with loading buffer to clear the column of free impurities. In Chapter 4, ligand PEGylation was demonstrated to weaken IgG-ProA binding interactions via lowering elution pH. In Chapter 5, ligand PEGylation was demonstrated to mitigate impurity-IgG interactions. A study to determine the effect of ligand PEGylation on intermediate wash steps on HCP clearance would be a valuable addition to the selectivity work described in this thesis. It is possible that ligand PEGylation may weaken some HCP-mAb interactions, but not block them entirely. In this case, it might be possible for buffer components such as urea or propanol to be more effective at clearing these HCP interactions. Applying these techniques to ligands with smaller PEGylation extents may be a path to optimize IgG binding capacity and selectivity against HCPs.

7.4.5. PEGylation of ProA with succinimide activated PEGs

The aldehyde functionalized PEGs used in this thesis require a large total molar ratio of

PEG to target protein to achieve relatively small PEGylation extents. N-hydroxysuccinimide functionalized (NHS)-PEGs, on the other hand, are the most popular type of activated PEG species used for protein modification, are much more reactive due to the nature of the NHS-ester functional group, and are available for purchase in sizes ranging from 333 Da to 40 kDa [15]. NHS-PEGs will react with exposed primary amine groups on the protein including lysine side-chains and N-termini to form stable amide bonds between the two species. With this chemistry, it will be possible to modify ProA with small PEGs (< 5 kDa) and achieve higher modification extents. In particular, the rSPA ligand used in this thesis has a total of 55 lysine residues plus one N-terminus [16], thus it is theoretically possible to achieve higher PEGylation extents with the NHS-PEG chemistry. However, many of these sites may be inaccessible when immobilized on the resin; higher PEGylation extents with this chemistry are expected regardless. Due to the exponential relationship between PEG molecular weight and hydrodynamic radius, a higher PEGylation extent with a lower molecular weight NHS-PEG will result in a lower conjugated volume of PEG per mole of rSPA compared to the modified described in Chapters 4 and 5. The lower volume of conjugated PEG would be expected to retain the binding capacity of IgG. Additional studies will be required to determine if a more pervasive PEGylation chemistry with smaller molecular weight PEGs will offer similar benefits to selectivity and robustness.

With a higher PEGylation extent, another concern will be direct PEGylation of IgG binding sites on rSPA. This concern will be overcome with a 'masking' technique where IgG or IgG Fc fragments are first loaded onto the resin to sterically block the IgG binding site before the ligands are PEGylated; a similar technique was used by Wen and Niemeyer [7] in the PEGylation of immobilized Concanavalin A. IgG Fc fragments will be generated by digestion of IgG with papain; the use of IgG Fc fragments over intact IgG molecules is likely to reduce the number of side

PEGylation reactions on the protecting group. De-protection under typical IgG elution conditions will occur after PEGylation is complete. This technique can possibly minimize IgG binding capacity loss associated with modification.

7.4.6. PEGylation of ProA ligands on other commercial resins

The PEGylation of ProA ligands described in this thesis was only performed on one commercial ProA resin (CaptivA PriMAB). As discussed in Chapter 1 and throughout the thesis, there are a large variety of ProA resins that have unique properties and advantages. Evaluating the benefits of PEGylating ProA ligands on other resins would be valuable to further understanding the modification and exploring its commercial viability. In particular, applying PEGylation to the ligands on POROS MabCapture A resin, which has a more open pore network, may avoid mass transfer resistances incurred at heavier PEGylation extents.

7.4.7. High-throughput PEGylated ligand screening

As seen in Chapters 4 and 5, an extreme amount of time, effort, and resources are required to fully and properly characterize a limited number of resins. To truly optimize ProA ligand PEGylation for increased selectivity/robustness against retention in IgG binding capacity, a high throughput screening method must be implemented. Ligand screening platforms such as the FortéBio and techniques such as surface plasmon resonance exist but it can be difficult to directly translate the performance of trial ligands on these platforms to actual chromatography resins since they neglect the effects of hindered pore diffusion. Additionally, using these techniques/platforms will require PEGylation of ProA ligands in free solution, which are then immobilized on a typically flat surface. This creates further difficulties since much more of the ligand is accessible in free

solution than when it is immobilized within a resin. Hence, ligand PEGylation in free solution can modify the protein in areas that would normally be inaccessible in the resin and not be directly translatable. The rSPA ligand used in this thesis has a lysine enriched anchoring domain, which would be a prime target for PEGylation and thus hinder the ability for the protein to be properly immobilized in the resin. This effect can be mitigated in the future by using the MabSelect ligand, which does not have any anchoring domain and instead is directly linked to the resin via the C binding domain by a single thiol linkage. A particularly good use of the platforms mentioned above would be to study the mitigation of impurity interactions with mAbs that are bound to PEGylated ProA ligands. Here, a sequential experiment can be performed where the ligand is PEGylated in free solution, immobilized to the platform surface, exposed (loaded) with mAb, and then exposed to impurities to study the differences in interactions. Since this is essentially studying protein-protein interactions, the observations would be expected to translate when the ligand is immobilized within a resin. The aforementioned experiment may provide a viable pathway to perform high throughput screening for selectivity.

7.5. References

[1] N. Tugcu, Purification of proteins using displacement chromatography, Methos Mol Biol. 421 (2008) 71-89.

[2] H. Hjelm, K. Hjelm, J. Sjöquist. Protein a from Staphylococcus aureus. Its isolation by affinity chromatography and its use as an immunosorbent for isolation of immunoglobulins, FEBS Lett. 28 (1972) 73-76.

[3] L. Jendeberg, P. Nilsson, A. Larsson, P. Denker, M. Uhlén, B. Nilsson, P.Å. Nygren, Engineering of Fc(1) and Fc(3) from human immunoglobulin G to analyze subclass specificity for staphylococcal protein A, J Immunol Methods. 201 (1997) 25-34.

[4] E.X. Perez-Almodovar, G. Carta, IgG adsorption on a new protein A adsorbent based on macroporous hydrophilic polymers. I. Adsorption equilibrium and kinetics, J Chromatogr A 1216 (2009) 8339-8347.

[5] R. Hahn, P. Bauerhansl, K. Shimahara, C. Wizniewski, A. Tscheliessnig, A. Jungbauer, Comparison of protein A affinity sorbents II. Mass transfer properties, J Chromatogr A. 1093 (2005) 98-110.

[6] J.T. McCue, G. Kemp, D. Low, I. Quinones-Garcia, Evaluation of pro- tein-A chromatography media, J Chromatogr A. 2003989 (2003) 139–153.

[7] Z. Wen, B. Niemeyer, Preparation and characterization of PEGylated Concanavalin A for affinity chromatography with improved stability, J Chromatogr B. 879 (2011) 1732–1740.

[8] A.D. Tustian, C. Edicott, B. Adams, J. Mattila, H. Bak, Development of purification processes for fully human bispecific antibodies based upon modification of protein A binding avidity, MAbs. 8 (2016) 828-838.

[9] K.M Jones, J.L. Lewis, W.Y.G. Ma, A.C. Dumetz, D.N. Paolella, K.E. Göklen, Investigation of Protein Binding Capacity Observed for mAb and mAb Fragments on Protein A and Protein L Affinity Resins, ACS National Meeting Spring 2014 (Dallas, TX, USA).

[10] R.D.R. Tarrant, M.L. Velez-Suberbie, A.S. Tait, C.M., Smales, D.G. Bracewell, Host cell protein adsorption characteristics during protein a chromatography, Biotechnol Progr. 28 (2012) 1037-1044.

[11] Z. Liu, S. Mostafa, A. Shukla, A comparison of Protein A chromatographic stationary phases: Performance characteristics for monoclonal antibody purification, Biotechnol Appl Biochem. 62 (2014) 37-47.

[12] Repligen, Captiva Primab—Protein A affinity resin—Regulatory Support File RSF-1003201, March 2010.

[13] N. Levy, K. Valente, L. Choe, K. Lee, A. Lenhoff, Identification and characterization of host cell protein product-associated impurities in monoclonal antibody bioprocessing, Biotechnol Bioeng. 111 (2013) 904-912.

[14] A.A. Shukla, P. Hinckley, Host cell protein clearance during protein A chromatography: development of an improved column wash step, Biotechnol Prog. 24 (2008) 1115-1121.

[15] M. Roberts, M. Bentley, J. Harris J, Chemistry for peptide and protein PEGylation, Advanced Drug Delivery Reviews. 54 (2002) 459-476.

[16] J. González-Valdez, A. Yoshikawa, J. Weinberg, J. Benavides, M. Rito-Palomares, T. Przybycien, Toward improving selectivity in affinity chromatography with PEGylated affinity ligands: The performance of PEGylated protein A, Biotechnol Prog. 30 (2014) 1364-1379.

References

References are listed at the end of each chapter. Page numbers are listed below for convenience.